CRANFIELD UNIVERSITY

L. KIRKWOOD

CHARACTERISATION OF WEAR RESISTANCE OF NATURAL AND SYNTHETIC DIAMOND TOOLS DURING SINGLE POINT DIAMOND TURNING

SCHOOL OF APPLIED SCIENCES

PhD THESIS

Academic year: 2012-2013

Supervisors:

P. Shore

&

I. Durazo-Cardenas

February 2013

Cranfield University

Leigh Kirkwood

Characterisation of wear resistance of natural and synthetic diamond tools during single point diamond turning

School of Applied Sciences
PhD thesis

Supervisors:
Doctor I. Durazo-Cardenas
&
Professor P. Shore

This thesis is submitted in partial fulfilment of the requirements for the
Degree of Doctor of Philosophy

Abstract

Achievable cutting distance of a diamond tool during turning is finite and is a limiting factor in the size of component that can be turned. This limit is particularly problematic when attempting to turn brittle materials, such as those used in infra-red optics. Natural diamond tools have been used for this application. However natural diamond introduces problems: the gems can contain possible contamination with a range of impurities and strong residual stresses from formation. Cutting distance is therefore inconsistent when using natural diamond. Industry is keen to increase possible cutting distance and to increase the consistency of cutting distance.

One possible solution is synthetic diamond materials. New CVD single crystal synthetic diamonds possess high purity and consistent growth conditions and therefore have the potential to be a superior tool-material that provides longer achievable cutting distance and extremely consistent cutting behaviour. This new material is compared against natural and HPHT synthetic diamonds in machining tests against silicon workpieces in a selection of tool-orientations. Aluminium workpieces are machined with MCC and natural diamond tools to assess the performance of the new material against this commonly diamond turned material. While analysing the results from these cutting trials the failure modes of diamond tools were examined closely, resulting in discovering the existence of two separate failure modes and the development of a new wear-model. Natural diamond tools were carefully tested using a range of techniques hoping to find a root cause of the wide variability seen. FTIR offered a strong clue as to the defect within natural diamond tools that leads to occasional high cutting life.

Acknowledgements

Contents

List of figures

List of tables

Nomenclature

A	Contact area between diamond tool and workpiece
E	Young's Modulus
F_f	Flank force (Archard equation)
$F_{INITIAL}$	Cutting force generated when deforming material at the front of tool
F_T	Force acting in the thrust direction
H	Hardness
K_c	Material fracture toughness
K_p	Preston's constant
L	Load acting through the tool onto the workpiece
P_a	Arithmetical mean deviation of the primary profile
P_q	Root mean square of the primary profile
P_t	Total height of primary profile
R	radius of diamond tool
R_a	Arithmetical mean deviation of the roughness profile
V	Volume worn as predicted by Archard equation
d_s	Sliding distance
f	feed-rate
$f\{asyn\}$	Asynchronous spindle error
h	height of chipping damage on SPDT tool
k	Constant from the Waldorf cutting force model
k_a	Constant from Archard wear model
t_c	Critical chip thickness
ΔH	Difference in height caused by wear
Δs	Traverse distance during wear
Δt	Difference in time
δ	Geometrical minimum peak to valley value
Ψ	Process constant

Chapter 1- Introduction

Diamond turning is an ultra-precision machining method that has found application in the production of high accuracy infra-red (IR) optical components. There are several reasons for using diamond turning in this application; the high stiffness of diamond turning machines and the quality of the CNC control systems ensure that form accuracy is extremely good. However the primary reason for the move towards machining optics with diamond turning is the increasing geometrical complexity of optical components which makes polishing of these lenses impossible. This increased complexity is driven by the need to remove optical aberration effects from the component. Specifically, spherical aberration is compensated out by using an aspheric profile and chromatic aberration is corrected by machining a diffractive element into the workpiece.

Performance of hybrid lenses is also strongly dependent upon the quality of surface finish. Achieving a good quality surface finish is complicated when machining IR materials as many are extremely brittle and therefore exhibit a tendency to produce poor surfaces. Brittleness can lead to cracks propagating into the machined surface inducing so called sub-surface damage. However, good optical quality surfaces (with Ra values of a few nanometres) are possible in IR materials if specific machining criteria are met and the tool is in good condition. Keeping the tool in good condition is difficult when machining IR workpieces as the hardness of these materials is often high and attritious wear of the tool is fast. When producing IR lenses from such materials the accumulated wear damage to the tool-edge can very quickly result in the tool inducing damage to the surface of the workpiece. During literature searches the causal link between wear of a tool and the start of a tool to introduce brittle damage into the workpiece surface has not been found. The cause of brittle damage is therefore linked through unknown mechanisms to attritious wear of the diamond tool. This thesis addresses this lack of knowledge and introduces two different failure mechanisms into the discussion.

For many optical systems weight is an important factor therefore there is a continuous effort to develop methods for using lower density materials. For IR optics silicon offers

the greatest weight saving but the difficulty with using silicon is that it has extreme hardness and results in destructive tool-wear after a comparatively short cut-length. The short cut-life directly limits the maximum size of optic that can be manufactured (for example cutting a simple flat on a 120mm workpiece requires a working cut distance of 11.3 Km). Silicon is therefore a test material for the work presented here, with the hope that through this work larger workpieces can be successfully machined.

Even with softer materials, such as aluminium, tool-wear can result in a failure to machine the workpiece within tolerances. Aluminium does not suffer the brittle behaviour found among the IR crystalline materials but suffers different problems. Wear can make the tools finish rougher and this will directly "print-through" to the workpiece surface, potentially raising the Ra above tolerance. Additionally, wear of the tool can cause tool-geometry to change sufficiently that the tool cuts the incorrect form into the workpiece, (a particular problem with more complex geometries). Finally, it is possible for increased tool-wear to result in higher cutting forces, which on small or thin workpieces can easily result in distortion of the workpiece. On machines with lower loop stiffness high cutting forces can result in displacement of the axis and introduce form errors. Non-ferrous materials like aluminium are the larger market for diamond turning, and therefore reducing wear of diamond tools in this application is of interest.

Natural diamond tools have long shown inconsistent performance when machining a range of workpiece materials. For more than 30 years seemingly identical single crystal natural diamond tools have been known to have the potential to achieve very different cut distances, implying different tool-wear characteristics. At first this result might be unintuitive, however when the wide variety possible in natural diamond is considered (specifically the huge range in size, shape, stress-state, dopant materials and impurity arrangements), then the result is perhaps less surprising. Converting diamond tools away from the use of natural tools towards synthetic diamond material types would eliminate a lot of the inconsistency. The oldest synthetic diamond material is the high-pressure high-temperature (HPHT). Most diamond turning does not use this type of material as it has a reputation for performing poorly against most workpiece materials, (though some workpiece materials are preferentially machined with HPHT). This

relatively poor performance is largely thought to be due to the large quantity of nitrogen impurities within the crystal structure. A new single crystal chemical vapour deposition (CVD) synthetic diamond material (supplied by Element 6 under the trade name MCC) is of interest as a potential diamond turning tool material. The expectation is that a very pure, high crystallographic perfection, synthetic like MCC would be an exceptional tool material.

This project focuses on how various synthetic and natural diamond tool-materials wear. Experiments were performed testing the wear resistance of various natural and synthetic diamond materials, in various crystallographic orientations, against silicon and aluminium workpieces. Aluminium was selected as a representative soft non-ferrous material that is frequently diamond turned, while silicon was tested because of its strong commercial interest and ability to wear tools quickly. These trials were designed with the aim of describing their tool-wear characteristics and gaining an understanding of the mechanisms leading to tool failure. Furthermore these trials were designed to allow the development of models to describe wear, hopefully leading to predictions of useful tool-life.

1.1 Aims & objectives

To structure the research it is useful to define some research aims and the objectives that will help to achieve them. For this work three main aims need exploring:

Aim 1: Explore the effect of diamond quality on cutting tools during SPDT of silicon

Aim 2: Explore the effect of diamond quality on cutting tools during SPDT of aluminium

Aim 3: Explore the origins of the "supertool" effect

To start to approach the first aim we clearly need to define what "diamond quality" means. This can be done through a thorough literature review. Natural diamond and the two synthetic diamond materials could be expected to have different crystallographic properties. It is therefore possible to design experiments to explore the affect of diamond quality when diamond turning by using the three diamond materials.

The first three objectives can therefore be defined:

Objective 1: Test HPHT material against silicon workpieces

Objective 2: Test natural diamond tools against silicon workpieces

Objective 3: Test MCC material against silicon workpieces

These objectives should thoroughly test the behaviour of different types of tool when machining silicon workpieces. Combined with crystallographic knowledge about the three diamond materials from the literature review these tests should provide an understanding of which properties of a diamond lead to maximised cutting life during SPDT.

Tests against aluminium workpieces are sensible objectives towards completion of the second aim. A separate trial is needed as diamond properties that are positive during the turning of silicon workpieces can not be assumed to be positive factors for SPDT of aluminium.

Objective 4: Test natural diamond tools against aluminium workpieces

Objective 5: Test MCC material against aluminium workpieces

As the HPHT has been available for some time and is of limited use in the aluminium machining industry a trial with HPHT would be superfluous.

If the root cause of supertool behaviour is to be understood then an examination of the crystallographic properties of a known supertool and normal behaving tools will be required. Completing the following objectives should help find the cause of supertool behaviour.

Objective 6: Investigate crystallographic orientation as a cause of supertool behaviour

Objective 7: Investigate impurity content of natural diamond as a cause of supertool behaviour

Objective 8: Investigate other possible causes of supertool behaviour

The project therefore has eight objectives to complete leading to completion of three aims. Objective 8 is deliberately wide in scope, but the literature review should reduce this objective down to a small number of possible factors and provide enough information to decide if any are likely to be contributing to the supertool phenomena.

Chapter 2- Literature review

2.1 Background to diamond turning

The extreme hardness of diamond is one of its best known qualities and as such has found wide use as a cutting or abrasive material. Diamond turning is a process that generates extremely smooth surfaces for use in a number of industries, particularly demanding optical applications. Unlike traditional optical polishing techniques, the process of diamond turning can create complex forms because of precision control of the motions in the axes the machines used.
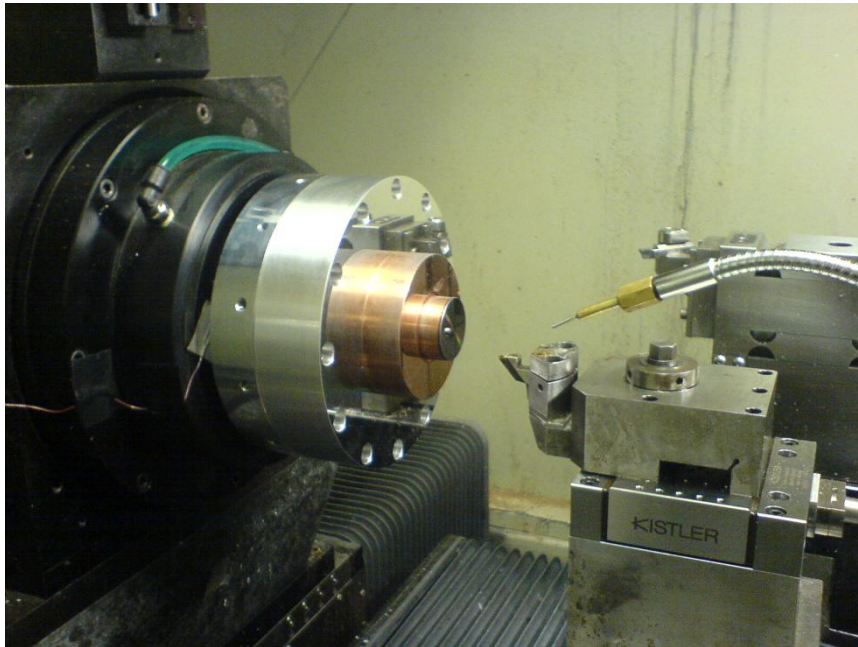
Figure 1: The Moore machine: principle diamond turning machine for this project.

The above image is of the Moore Nanotech 350 UPL diamond turning machine. This machine uses the design principles established by McKeown [1], which details the eleven design principles, establishing the criteria for any successful precision engineering machine.

The machine uses an airbearing spindle to rotate the workpiece; these are particularly suitable for ultra-precision diamond turning because of the very low error motion. Additionally the machines at Cranfield are operated within a temperature controlled

laboratory. This temperature control is necessary to minimise any thermal distortion that could affect machine tool accuracy.

Cranfield has an enviable record in ultra-precision engineering and a history of investigating single-point diamond turning. A recent investigation on machining of silicon for diffractive optics [2] examined the influence of various parameters upon the machining of complex forms, (hybrid refractive-diffractive optical components). There were two principal findings. The first dealt with which cutting fluid reduced tool-wear most effectively. The second was identifying that different diamonds that were made to the same specifications showed large variance in tool-life. Indeed, that *"the most noticeable influence on the results achieved, during the examination of tool life, whilst single point diamond turning single crystal silicon was the tool gem itself"* [2]. This result is extraordinary; that seemingly identical gems can give hugely varying tool lives is far from intuitive.

During the work of Jacklin [2] the term "supertool" was used to describe those rare tools that consistently display an ability to cut unusually long cutting distances before inducing brittle failure in the silicon workpieces. In contrast to the supertools there are "normal tools"; natural diamond tools which can not achieve the same cutting distance as supertools. Supertool diamonds are prepared to the same tolerances and specifications as normal diamond tools so the difference between normal tool and supertool performance was an unexpected result. It is noteworthy that a natural diamond tool will not change from being a supertool to a normal tool, or vice versa, after the reconditioning process [2]. As "supertool" and "normal tool" are convenient terms for natural diamond tools they will be used within this text.

2.2 Diamond turning of brittle materials

Simple refractive lenses are increasingly becoming unsuitable for many of the most demanding applications. These simple lenses lose too much image quality from aberrations, particularly chromatic aberration. Chromatic aberration is an error that has its root in dispersion; an optical effect where different wavelengths of light experience different refractive indices while travelling through the same material. This effect is

how a prism is able to separate white light into its constituent colours; in lenses it causes different wavelengths to come to different focal points. However, by combining a refractive surface with a diffractive surface, a single hybrid lens can be made which cancels the defects of the individual surfaces (see figure 2).

Refractive + Diffractive = Hybrid Achromat
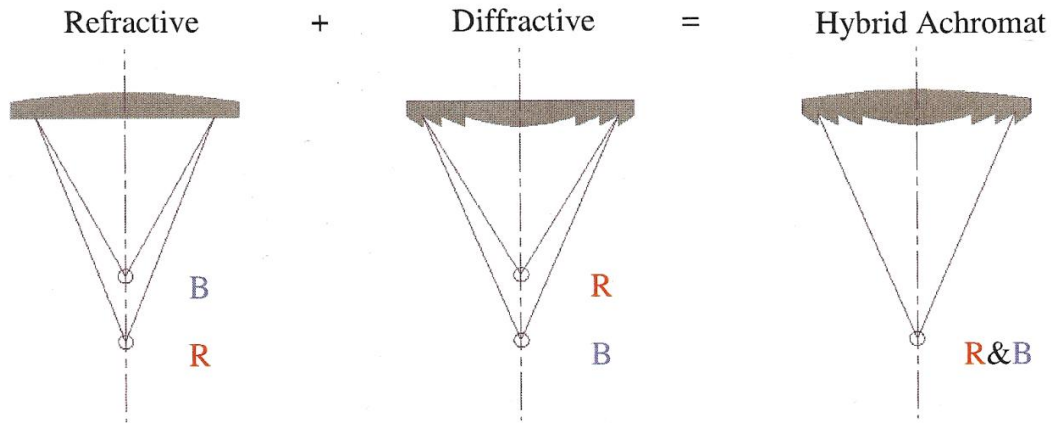
Figure 2: The refractive and diffractive lenses focus red and blue ends of the spectrum at different points, combining them into a single lens creates a single focus for the different ends of the spectrum [2]

These hybrid lenses are impossible to manufacture using traditional polishing methods the required form is just too difficult. Increased demand for diamond turning for producing IR-optics has grown as demand for higher quality optics increases.

Germanium is the material of choice for IR-optics as this is slightly easier to machine compared with silicon. However, germanium is denser and more expensive than silicon and therefore not ideal for weight sensitive applications. Despite the need for silicon to be made into IR-optics the diamond tools are currently displaying far too great a variability in tool-life, this is limiting the maximum diameter of the optics that are capable of manufacture. Using multiple tools is not an option because of the errors that will be introduced by replacing the tool. A silicon optic of 200mm diameter requires a tool-life of 31.4Km; this is a cut length that many natural diamond tools struggle to reach. Machining with a worn tool will ruin the optic that is being made and will result in a costly waste of a workpiece. Variability in diamond tool-life is poorly understood at this time. This project was instigated to investigate the variability of diamond tools and will investigate the latest synthetic diamond materials.
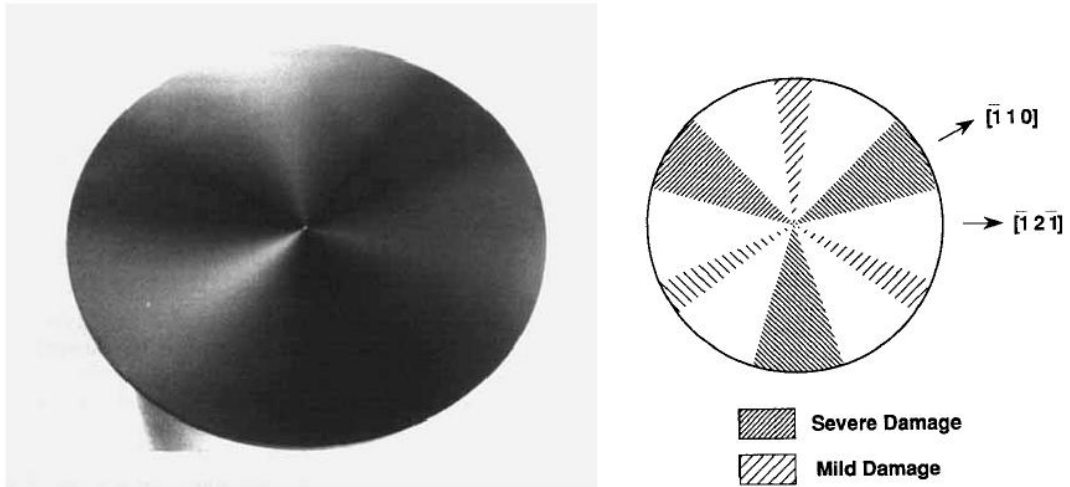
Figure 3: Damaged germanium on the (111) plane. [3] Left is a photograph of a turned surface and right is the mapping of the damage. This level of damage is extreme, and would certainly ruin an optical component.

For many early efforts the turning process was causing subsurface damage to the turned piece (figure 3). These micro-scale fractures that extended under the surface of the turned work piece make the workpiece unsuited for optical applications (figure 4).
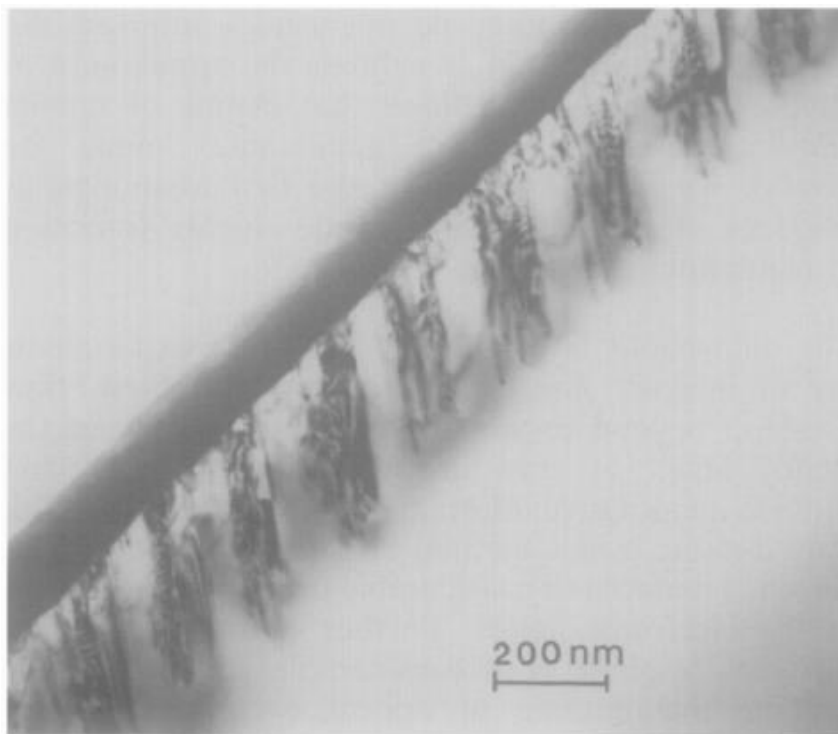
Figure 4: Cross section of subsurface damage from diamond turning of silicon [4]

Sometimes the turning successfully produced a damage free surface, and sometimes not. A theoretical understanding of why was presented in arguably the most important paper in the field of diamond turning, when the work of Blake and Scattergood managed to both formulate a reason for the subsurface damage and identify a method for eliminating it, back in 1990 [5]. Their work was developed using information gleaned from nano-indentation experiments and from fracture mechanics work developed by Lawn and Evans [6].

An idea central to their results was that of the critical depth for crack initiation. They knew that ductile removal was needed to keep the surface smooth and from the fracture mechanics knew that while ductile removal energy scales with volume, the energy of crack propagation scales with crack area. This has several consequences, firstly, that even extremely brittle and hard materials can be plastically deformed. Secondly, that there is a minimum crack size. Understanding this they could start to look at tool geometry and specifically, how this affects crack propagation and chip removal (figure 5).
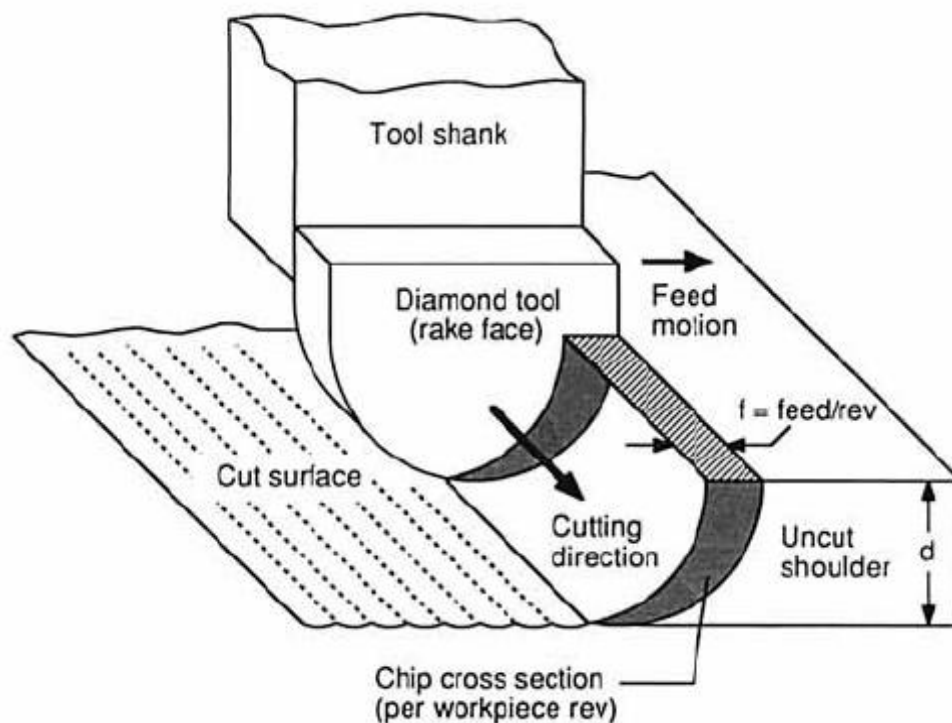
Figure 5: Schematic of the diamond-turning process. [5]

The diamond turning process creates a chip of increasing thickness up the lead-edge of the tool. The key to the turning of these very brittle materials is to make sure that any cracks are not long enough to reach the surface by ensuring that they start far enough up the lead-edge.
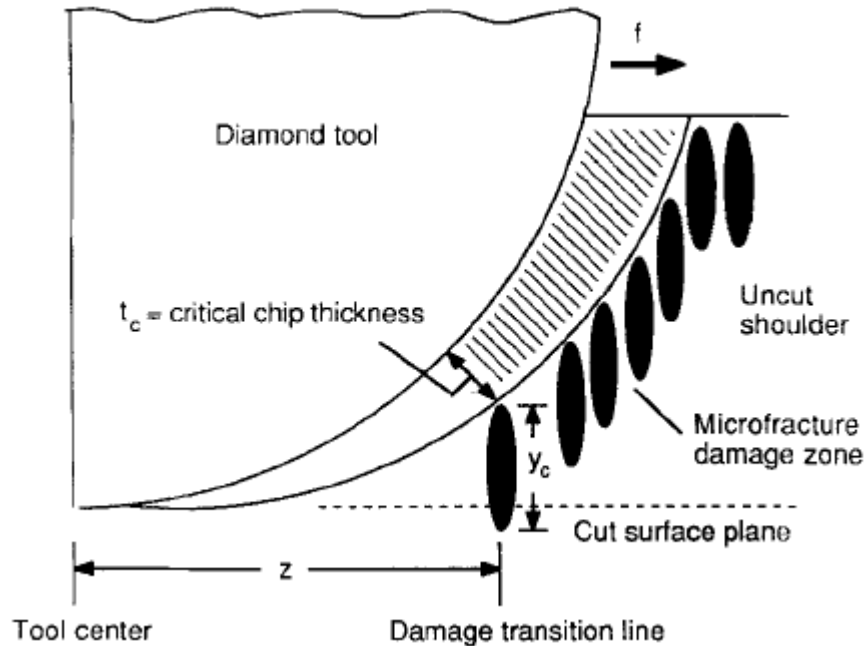
Figure 6: Brittle fracture occurring in ductile-regime turning [5]

Figure 6 clearly shows this crack propagation issue. As long as cracks form exclusively within the removed material, the surface will appear to have been machined in a ductile manner.

The tool geometry and the feed-rate both influence the chip thickness along the lead-edge. At the point at which the tool is removing more than the required amount of material to cause cracking is called the critical chip thickness, t_c. This critical chip thickness is the transition point; the point where the ductile removal (where energy requirement scales with volume) is no longer more favourable than the brittle chipping removal mechanism (which scales with surface area).

Measurement of the critical chip thickness is extremely difficult. There are two documented methods though; interrupted cutting of the turning process (Blake and Scattergood display this in their paper [5]). Via this method, the cut shoulder of the

workpiece material is made visible and the transition to brittle removal methods can be directly observed; though it should be noted that the transition requires some interpretation.
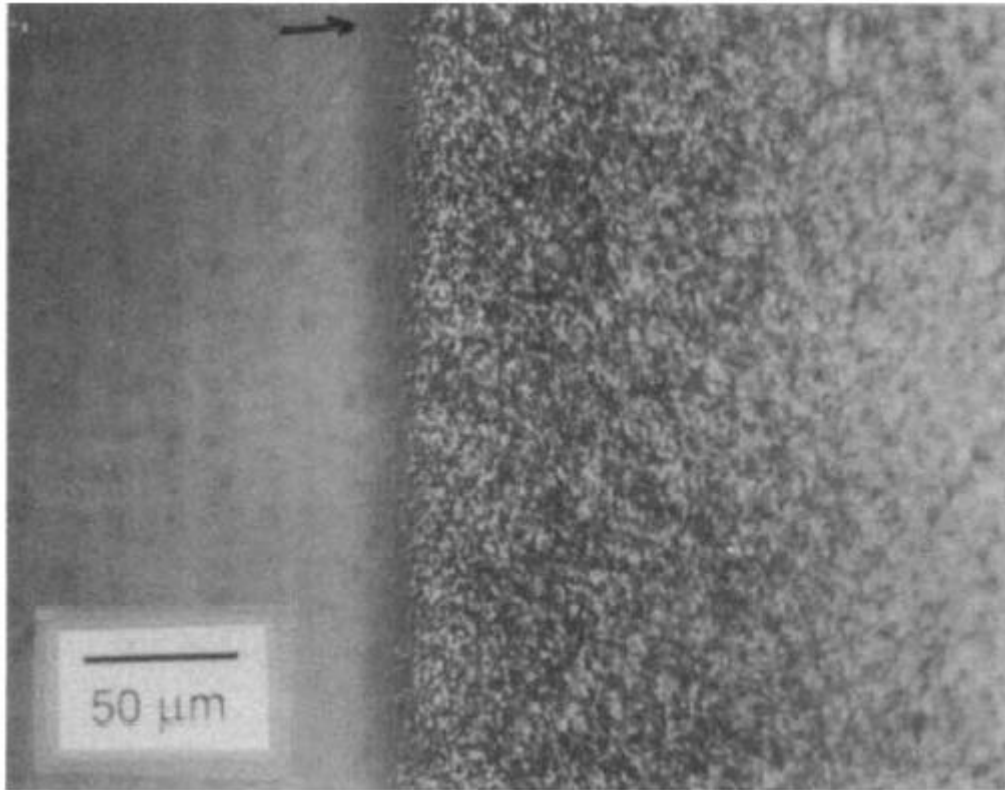
Figure 7: interrupted cutting has led to regions of both, ductile and brittle removal to be visible [5].

The second method of observing the critical chip thickness was displayed by O'Connor using a flycutting method. The issue with critical chip-thickness is further complicated by anisotropy within the workpiece material [7]. Silicon and germanium both display similar anisotropy (they are both bonded in the same configuration as diamond). This leads to directional variation within the material, with the critical chip thickness varying as the workpiece is rotated. Furthermore, there is a variation with which crystal plane is being turned.
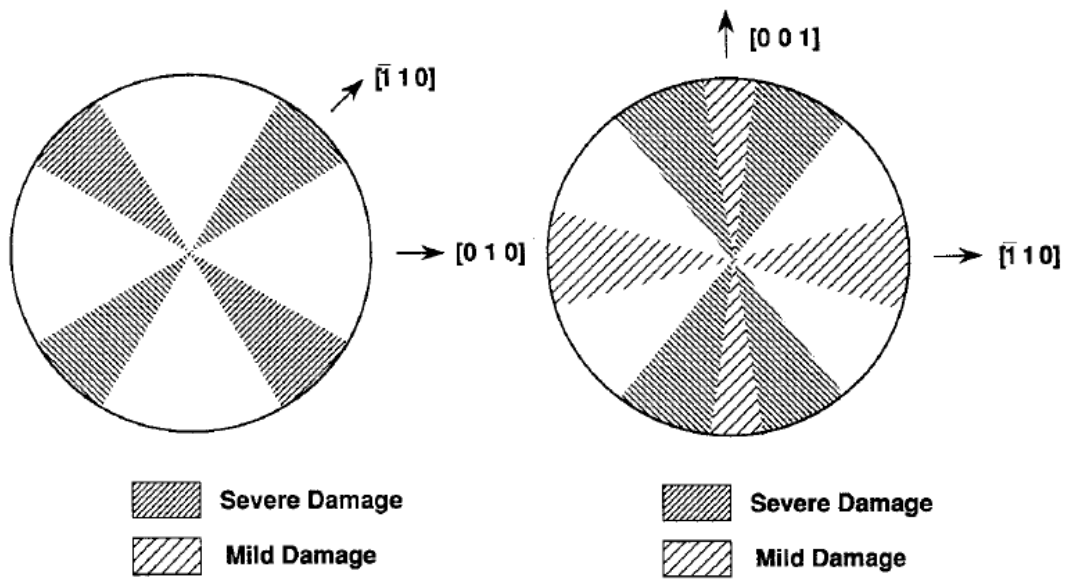
Figure 8: Variation in pitting damage with crystallographic direction for germanium. On the left the (100) plane has been turned, on the right the (110) plane. [3].

While turning a crack can propagate in any direction from the point of critical chip-thickness, possibly straight down into the workpiece material. This can result in subsurface damage and thus can ruin a potentially very valuable workpiece. Thus, predicting the length of crack will be extremely useful in combination with the critical chip-thickness as we can then start assessing if the surface of the workpiece will have subsurface cracks within it. The minimum crack length within silicon has been stated to be 0.4µm [8].

Putting this into a mathematical framework; the critical chip-thickness is defined as:

$$t_c = \Psi(E/H).(K_c/H)^2$$

Where Ψ is the "process constant"; a constant related to the indenter geometry (though the authors of the referenced paper also say that it will vary "in a complex fashion upon machining parameters and tool geometry" [5]. E is the materials Young's modulus, H is the Hardness of the material and K_c is the fracture toughness. The term K_c/H has been referred to as the brittleness index [8].

Surface finish in diamond turning is often of critical importance. Within an appendix to the same seminal paper [5] Blake and Scattergood detail the geometrical derivation of

the theoretical limit to the achievable peak-to-valley roughness parameter (defined as Rt in the ISO standard 4287:2000 [9]). The result of this derivation is displayed here:

$$\delta = \frac{f^2}{8R}$$

Where δ is the peak-to-valley measurement, f is the feed-rate and R is the radius of curvature of the tool. Despite having a geometrical minimum value for peak-to-valley roughness, (a "cusp" height), this ideal value is often not possible to achieve. (And indeed if the derivation is followed through they use an approximation that neglects another, admittedly very small, geometrical term). This ideal peak-to-valley value is often much smaller than real turned surfaces display. Thus often a corrected equation is quoted, which includes an extra error term.

$$\delta = \frac{f^2}{8R} + f\{Asyn\}$$

Where the *f{Asyn}* term is a result of asynchronous spindle error (as defined in ISO 230-7:2000 [10]). Any spindle error affects the z-position of the tool and thus form and roughness of the workpiece. The methodology for finding the critical chip-thickness displayed by O'Connor [7], makes a concerted effort to unravel the variation of critical chip-thickness with orientation angle. This method is shown in figure 9.
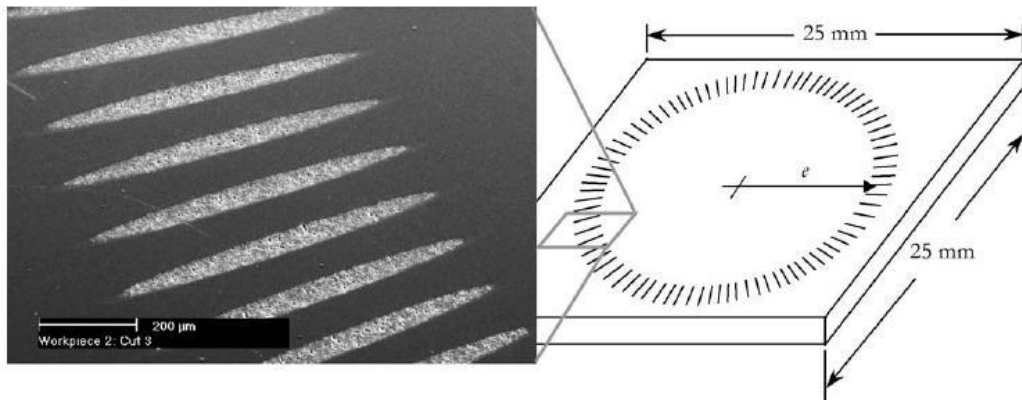
Figure 9: The scoring of the silicon workpiece material by a diamond flywheel cutter [7].

The method utilised a flywheel cutting process while rotating the workpiece. This results in numerous shallow cuts at a full circle of angles. The crystalline face is the (001) plane.
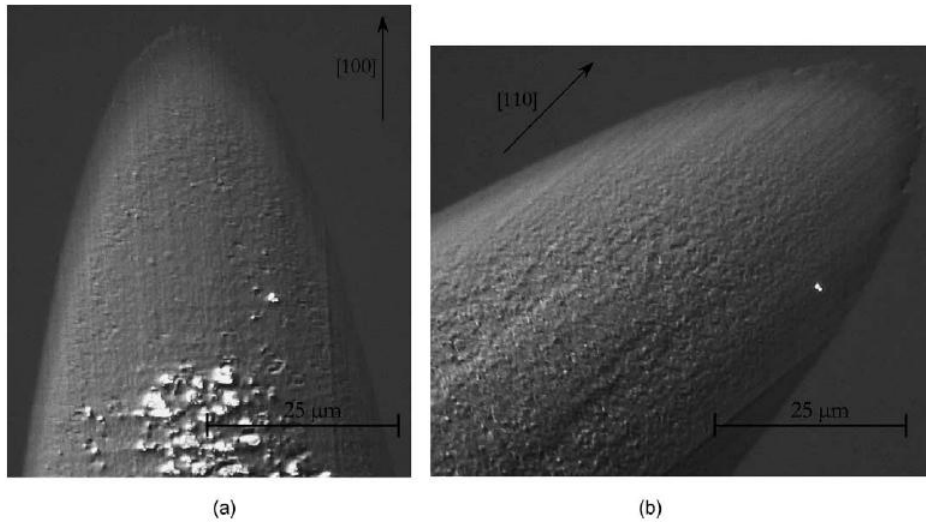
Figure 10: The SEM images from two different cuts. (a) A cut in the [100] direction. (b) A cut in the [110] direction. The pitting caused by brittle fracture removal mechanisms can clearly be seen to be closer to the surface in the [100] direction. [7].

The measurement by SEM of these cuts allowed the depth of the pitting to be calculated via geometry. The results displayed clear anisotropy of the pitting depth; with the depth ranging from 40nm in the most difficult direction to 120nm in the easiest to machine direction: as illustrated in figure 10.

A similar methodology was used by Leung et al. [11]. They examined a few variables, but significantly this time examining the effect of depth of cut.
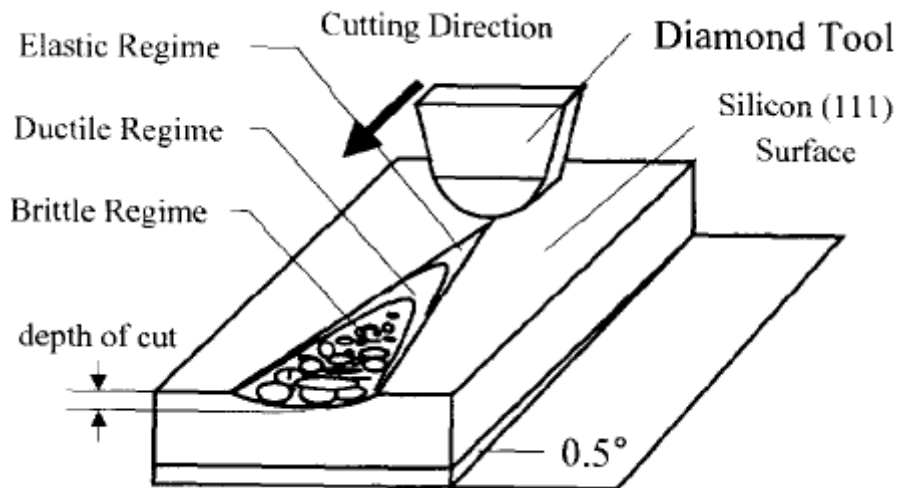
Figure 11: The increasing depth of cut experiment performed by Leung et al. [11].

The experimental set-up in figure 11 confirmed that the greater depths of cut result in larger pitting damage rather than their theories about depth of cut. The depth of cut is something that the "process constant" equation from Blake and Scattergood [5] does not factor. Implying that either it is not a factor of any great significance or that the equation is for those cases where depth of cut is constant. Leung states that depth of cut is a parameter that needs optimising for successful turning [11]. Later in the paper they also report "the surface finish became very smooth as the feed-rate or the depth of cut was decreased below particular values." This is interesting; while machining single crystal silicon on the (111) plane they found a depth of cut issue causing areas of brittle fracture to form. Initially this would appear to be a failure of Blake and Scattergoods' equation to predict machining behaviour, it is explainable. Their efforts at 2 μm/rev feed-rate seem particularly unwise considering the sensitivity to this parameter that turning has. Why they used this parameter while referencing a paper that clearly states this issue is unclear.

The trial uses tools with top-rakes of 0, -15 and -25 degrees (coincidentally supplied by Contour Fine Tooling) for some more traditional turning trials; finding that the 0 degree top-rake angle causes a higher RMS than the others. It is worth pointing out their roughness measurement technique using a Wyko interferometric device.
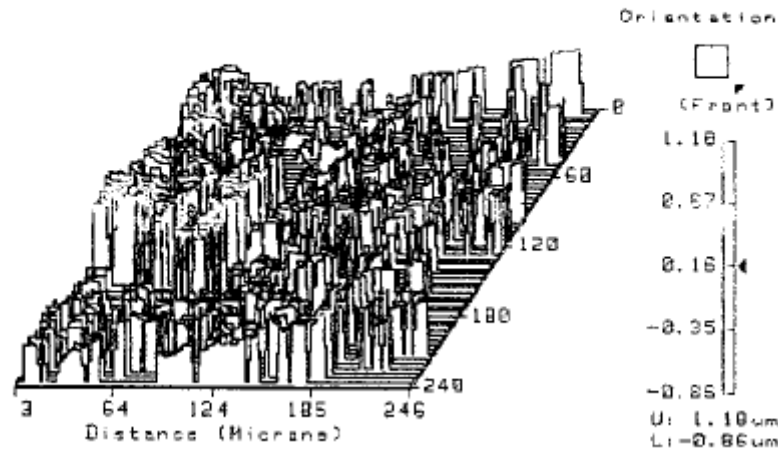
Figure 12: Unsurprisingly large Ra was recorded from this data. Questions about missing data seem not to have been asked [11].

Figure 12 appears to have large areas of missing data, further throwing doubts upon the results they have achieved. Most interesting is that we are able to use 10μm depths of cut with very similar machining parameters without such dramatic roughness.
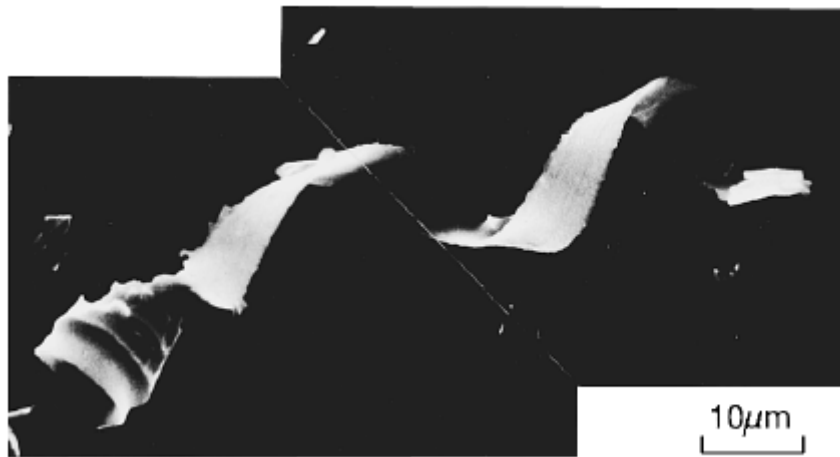
Figure 13: SEM image of continuous chips of silicon. [12]

Though not a unique methodology the work of Shibata, et al. [13], presents an interesting note upon the chips that are formed during diamond turning of silicon; it results in amorphous chips. Continuous chip formation, as shown in figure 13, has been

noted in silicon in several papers, (for example [5,12]). Analysis of these chips implies that they are composed of amorphous silicon [13-17], which clearly hints at a phase transformation during the plastic deformation of the silicon during diamond turning. A metallic phase may occur between the crystal and amorphous phases [18]. Under test conditions the transition to an amorphous phase requires significant pressure, 11.3-12.5 GPa has been reported [17] but that value can be lowered by using a shear force, to as low as 8 GPa. The conditions during diamond turning contain a shear force element in the direction of the tool motion, so should satisfy that criterian.

2.3 Properties of (natural and synthetic) diamond

2.3.1 Introduction to the diamond type structure

Diamond is made from covalently bonded carbon. The term "diamond structure" is sometimes used to describe structures formed not only of carbon, but also crystals of germanium and silicon that use the same bonding pattern. In the diamond structure a unit cell includes 8 atoms [19], thus with the limited number of bonds per atom, not all the atoms within the unit cell are bonded to every other. The interesting bonding within a diamond-type structure (specifically the tetrahedral arrangement) leads to an intriguing structural geometry.

The oldest synthetic diamond type, high-pressure high-temperature (often abbreviated to HPHT) is made in a process that seeks to re-create the geological conditions that create natural diamond. This simple principle can not match geological formation timescales and therefore the resulting stones tend to have high concentrations of unplanned inclusions. Most is in the form of nitrogen, which leads to a yellow colouration. Also notable is the boron and occasional transition metal inclusions [20]. For diamond turning applications this material is often made into tools that are used to cut softer materials (such as polymers) and are often orientated so that the tool is very wide (allowing for better surface roughness values).

Chemical vapour deposition (often abbreviated to CVD), is a method often used to form a crystalline layer upon a substrate. This process passes the methane reaction gas over

the substrate, where the carbon in the methane starts to form diamond. This is usually done at high temperature and low vacuum. Significant here is that the size of sample is suitable for making a turning tool, while reported CVD growth rates are historically prohibitively small [21]. Element 6 have managed to increase the growth rate to make growing millimetre scale single crystal samples possible [22].

2.3.2 Effect of crystallographic orientation

The image displayed in figure 14 displays the unit cell of silicon in that distinctive diamond-type structure. It is worth noting that the unit cell dimension of the silicon is 0.543nm which is longer than the unit cell of the carbon based diamond unit cell (which measures 0.3567nm [19]). This leads to the density differences between the materials; despite the lower atomic mass of carbon the shorter bond length makes it denser than the atomically heavier silicon structure.
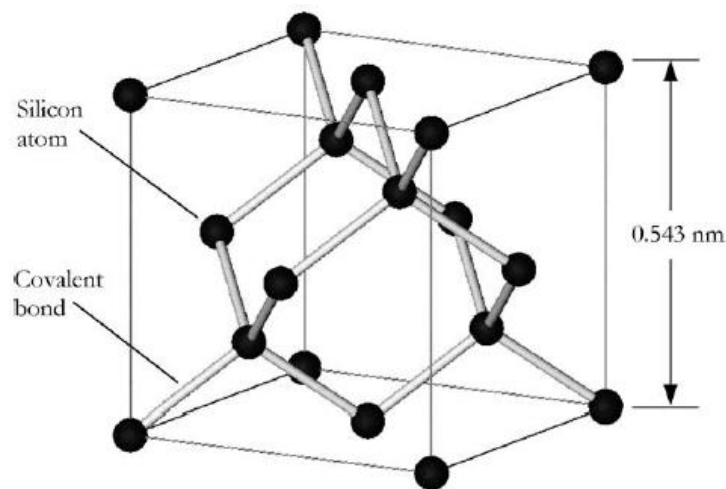
Figure 14: Detailing the complex bond structure in diamond type structures (silicon in this example). [7]

The structure of diamond leads to some strong direction dependency in material properties. The geometry of the bonding structure therefore leads to a directional variability of the material properties; particularly clearly shown in a figure showing 3D variation of the Young's modulus (figure 15).
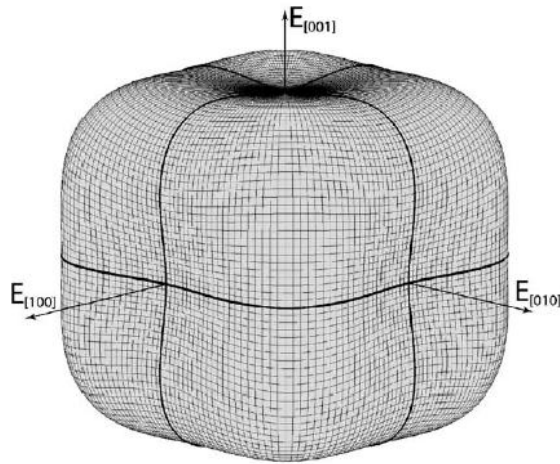
Figure 15: Detailing the differences in Young's modulus in different crystallographic directions for a diamond bonded material type: a perfectly isotropic material would appear spherical on this graph. [7]

A consideration to remember on the diamond structure outlined within this section is that it is an idealised model of what a diamond really is. Though a diamond is an arrangement of carbon atoms as described here, it also includes a lot of interesting variations away from this ideal. Internal strains within the material will cause variability in bond lengths and unit-cell size [23]. Material inclusions within diamond can range from small but visible specks of metallic materials [24], to the substitution replacement of individual carbon atoms with atoms of nitrogen [21].

Despite cubic crystal cells, diamond crystals grow in octahedral geometries (preferably, though not exclusively) [19]. M. Moore and others claim that the growth history of a diamond can be looked at in detail using X-ray topography techniques [19, 23, 25-31]; most natural diamonds exhibit residual stresses from their formation.

The point of the diamond tool is typically in the [100] direction, though slight variations have been observed (see Chapter 5), with the (110) orientation on the top face of the tool. Natural stones have a very different orientation than the synthetic HPHT tools, which have the crystal orientated in a different orientation. HPHT tools have the (100) plane on the top-face.
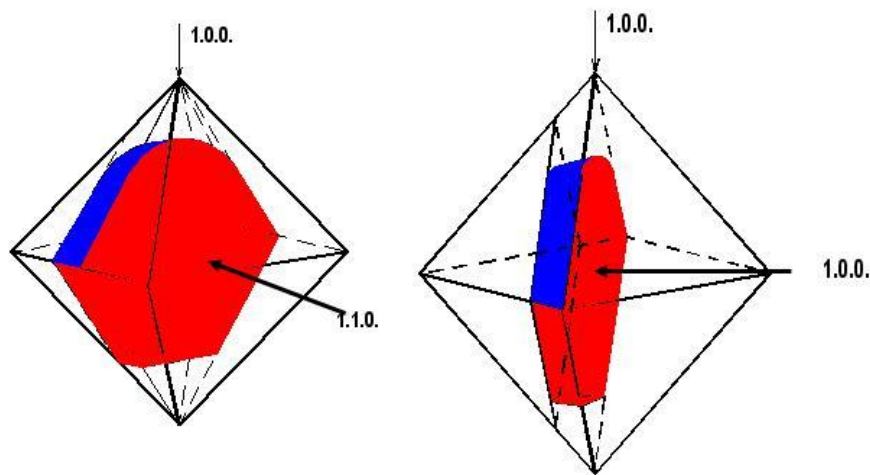
Figure 16: The orientations of the tools. The left image is of the natural tool, while on the right the situation is complicated by the orientation of the supplied synthetic material. [32]

Figure 16 displays the different orientation between the natural and the synthetic tools. (Denoted as (100/110) and (100/100) respectively). This is a consequence of the orientation the synthetic HTHP material grows in and causes complications for the grinding of the top-rake and results in a requirement to deliberately misalign the stone by angling how it sits upon the shank, as shown in figure 17.
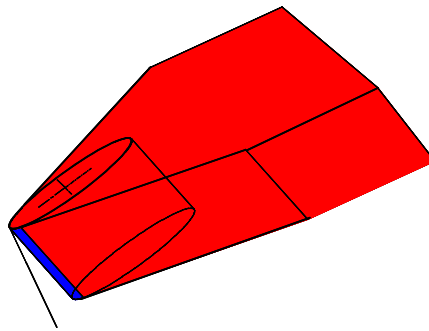
Figure 17: The orientation of the HTHP tools. [32]

This results in the top clearance of -25 degrees and from a crystallographic orientation point of view, the (100) direction is no longer going to be normal to the workpiece. This means that the crystallographic direction that will be in the same direction as the axis of workpiece rotation is now approximately [210] (rather than the [100] direction normally employed by natural tools). Obviously changing two things at once (tool material and

36

crystal orientation) complicates direct comparison between natural diamond tools and HPHT tools. Discussing diamond properties with Andrew Cox from Contour revealed that there is variation in wear-resistance whilst grinding in different crystallographic orientations. The literature is able to confirm the same for polishing [33,34,35] and is a macroscopic effect of the crystals' structure. The grinding result is important though as it obviously imposes limitations on the tools that are possible to make.

2.3.3 Impurity effect

Natural diamond is famous for being transparent but is also found in many different colours. Diamond, though often associated with purity, is frequently contaminated with traces of elements other than carbon. Roughly speaking, yellow stones arise from nitrogen content [36] while blue stones arise from boron content [37]. Brown and pink diamonds are due to the stone being stressed during its formation [38]. Other colours are possible too, but with increasing rarity.

The term dopant is used extensively within the semiconductor industry for inclusions into crystal structures (though in that industry the dopant materials are deliberately included and a great deal of effort goes to ensuring the right concentration of these materials throughout the materials). As diamond is a semiconducting material, (though with a very large band-gap), and is used frequently in the electronics industry it is reasonable to term unplanned elemental inclusions as dopants. Larger scale macroscopic inclusions of various materials are quite common, especially within synthetic diamonds created through high-temperature, high-pressure techniques [20].

Within diamond the most numerous inclusion is nitrogen, which has been linked to changes in mechanical properties, such as hardness (see figure 18).
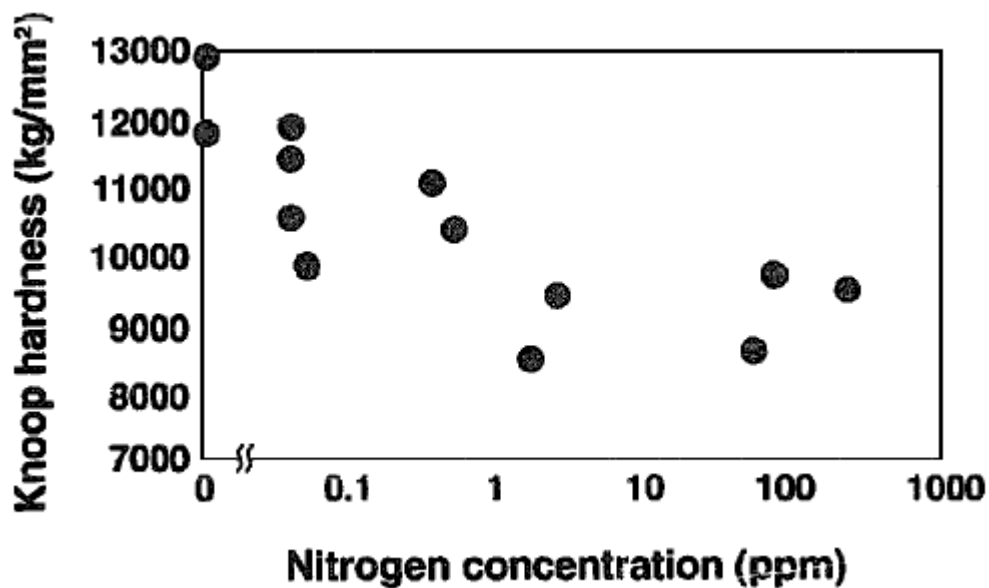
Figure 18: Nitrogen lowers the hardness of diamond [39].

Very small amounts of nitrogen will be found within clear gems, while yellow and brown stones will display progressively higher concentrations of nitrogen [38]. This crude visual method of establishing the nitrogen content is a clear indication that spectroscopy methods can be used to accurately establish concentrations within the material.

There is an established system of labelling diamonds by their nitrogen content. The majority of diamonds (~98%) have nitrogen impurity concentrations within the range of 0.003 to 0.3 percent nitrogen (percent by atomic constitution not weight). Such diamonds are labelled type I diamonds. Depending upon which form these type I nitrogen atoms coalesce together they can be further subdivided into type Ia and type Ib; where Ib has mostly substitutional positioning of the nitrogen content, while Ia type diamonds contain more advanced complexes of nitrogen [40]. It is worth noting that natural gems of type Ib are very rare (approximately 0.1% of natural gems are this type), but is much more common among HTHP synthetic diamond, where the nitrogen content is high and the synthesis time is too low to allow migration of the nitrogen into more complex optical centres.

Having stated the type I as the more numerous high nitrogen type of diamond it remains to explain that the type II diamond is composed of the very pure examples, (loosely defined as having lower than 0.003% diamond as a percentage). As can be easily imagined such pure gems are very rare and are thus very valuable.

Historically, the synthetic gems have included large quantities of nitrogen, (specifically, those crystals created via high-temperature, high-pressure methods). These inclusions are due to the manufacturing process trapping quantities of nitrogen within the mixing chamber. Under high temperature and pressure the carbon within the reaction chamber starts to crystallise into diamond, but without having any escape method for it, the nitrogen starts to become included within the structure. Nitrogen within synthetic diamond tends to be dispersed and isolated. A single nitrogen atom within a diamond unit cell will have to either substitute with a carbon (forming a substitutional defect) or will have to try and find space within the structure within the gaps (forming an interstitial defect) [21].

Nitrogen can also form more complicated defect centres, with various intricacy. These formations occur when multiple nitrogen atoms are close to each other within the structure. Their interaction causes shifts in the spectroscopy behaviours, thus allowing detection and classification. The simplest optical centre, is an aggregation of a pair of nitrogen atoms. Such a nitrogen pair have been identified by IR absorption spectra, and are known to strongly absorb at $1282cm^{-1}$ wavenumber. Commonly this defect is called an A-centre or an A-aggregate [21]. A more complex form of aggregate is the B-centre, formed when four nitrogen symmetrically surround a vacancy [41]. The B-centre is known to have an absorption peak at the $1175cm^{-1}$ wavenumber [21].

Aggregation into larger defects is a process that happens to diamond under geological conditions and over suitably large time scales. This is generally accepted as true, and is supported by the lack of aggregation within the rapidly formed synthetics. However, the exact reaction route to aggregation remains unclear and somewhat controversial [42], no aggregate being less controversial than the platelet. The "platelet" (also referred to as the B2-platelet in some literature [43]) is a source of great interest and contention within

the field of diamond study. This defect is said to form within the {100} equivalent planes [43]. The size of the platelet is far from clear. At least one source claims "smaller than several tens of nm" [43], while others claim up to a micrometre in length [43], while another claims its size is "varying between a few nanometres and a few micrometres" [42]. This is quite a staggering range of scale for one classification of defect, though all sources seem to agree the thickness does not exceed a single unit cell, the platelet is a comparatively huge defect structure. Frustratingly, little firm information is known about the platelet but may well be of critical importance for understanding variability in natural tools. The platelet is suspected to be critical because it has been suggested [44] that it can retard the propagation of a crack within diamond.

The significant difference between high nitrogen content synthetics and the high nitrogen content natural gems though is in the formation of aggregates. In the synthetic the formation of aggregates has not been observed [21], implying that the reaction time for crystallisation is a factor in aggregate formation. This has led some to speculate on the rates of aggregation however, as Collins [24] is quick to point out, calculations then imply that the formation of the concentration of aggregates within some measured samples would take longer than the age of the earth ($\sim 10^{11}$ years as opposed to $\sim 10^9$). So clearly, aggregation of nitrogen into optical centres is far from fully understood.

In general, high nitrogen content has been linked to lower attritious wear resistance within diamonds, while the platelet (also linked with nitrogen) has been linked to higher crack resistance [44]. Thus nitrogen appears a double-edged sword; wanting low overall nitrogen content to increase wear resistance, while simultaneously being extremely interested in the platelet defect which has so clearly been linked crack resistance. From this information an early prediction can be made about MCC: it may well resist the initial wear very well (most likely making the tool shaping more difficult), but by not including any platelets the critical failure of a tool due to crack formation may well be more likely compared to natural gems. This behaviour would arise solely as a consequence of MCC possessing extremely low nitrogen content.

Infra-red spectroscopy is a very well established technique for non-destructive testing, frequently used within chemistry to identify specific bonding behaviour. The technique basically has two experimental versions; absorption and reflection. In absorption IR-spectroscopy, infra-red light is passed through a sample of known thickness. (The thickness needs to be known as the transmitted light falls as an exponential decay of the product of length and the characteristic absorption co-efficient; as described by the Beer-Lambert absorption law). In reflection the spectra will be different from but related to the absorption spectra. However within the reflection arrangement alignment becomes more of an issue, as reflection varies with incident polarisation and incident angle. Often the specific variation used is dependent upon the transparency of the material.
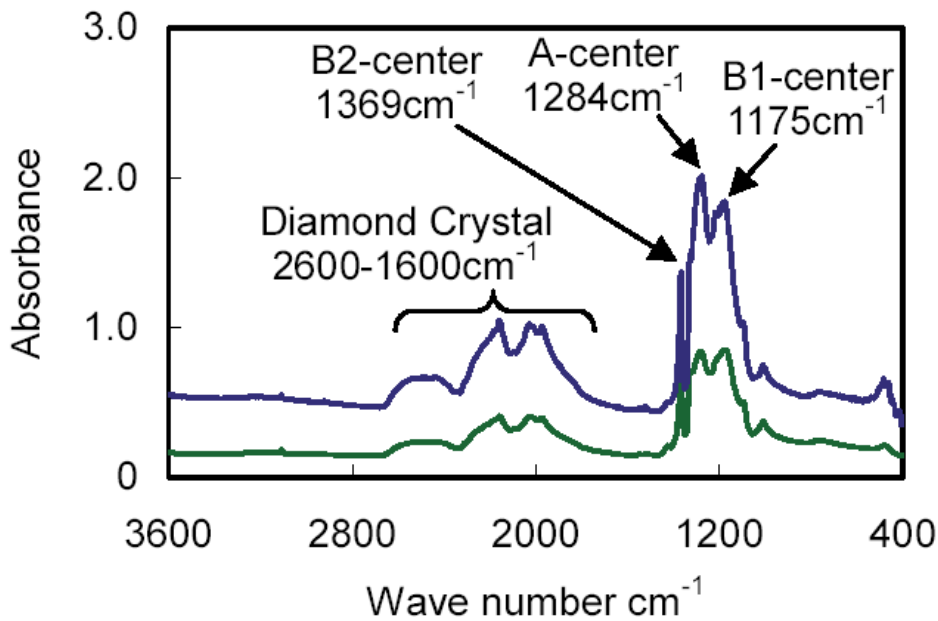
Figure 19: Infra-red absorption spectra of two diamond samples. [43].

Above (figure 19) are typical IR-spectra of two diamond samples, showing the peak lines at the higher end and the lower intensity broad absorption region from the diamond crystal structure.

One of the recurring names in IR-spectroscopy of diamond is Shimada. An early, but very useful, paper on IR-spectroscopy of diamond was published in 1985 [44]. In this paper IR-spectra of diamond tools were collected and then compared against the

hardness data collected via diamond indentation (a Hertzian fracture test). The qualitative finding of this paper is, "the higher the IRA coefficient at 7.3μm, the lower the microstrength". The 7.3μm absorption line is reported to be due to the "platelet" [44].

A difficulty comes with establishing how the 7.3 μm peak intensity corresponds to a given concentration of platelets. This sounds deceptively simple to work out but is greatly complicated by the inability to measure the concentration of platelets. The difficulty with the platelet is that it is far from an established idea. It is quite controversial, in part because direct observation is not possible. All the evidence of its existence is in the IR-spectroscopy and other indirect methods. Returning to the work of Shimada, it is clear from the papers since this early reporting that the issue is not resolved. In particular conclusions from his recent work [43,45] seem to complicate the conclusion from this earlier work. This paper backs up the previous statement by once more linking nitrogen content to a softening of the diamond, but then states that though lower nitrogen content tools are harder, this does not stop them from failure. Indeed, the B2-platelet (the optical centre responsible for absorbing at 7.3μm) that he has already reported as contributing to weakening the crystal, (*"the platelet is one of the defect highly detrimental to the micro-strength of diamond"* [44]) paradoxically is now reported to help impede fracture.
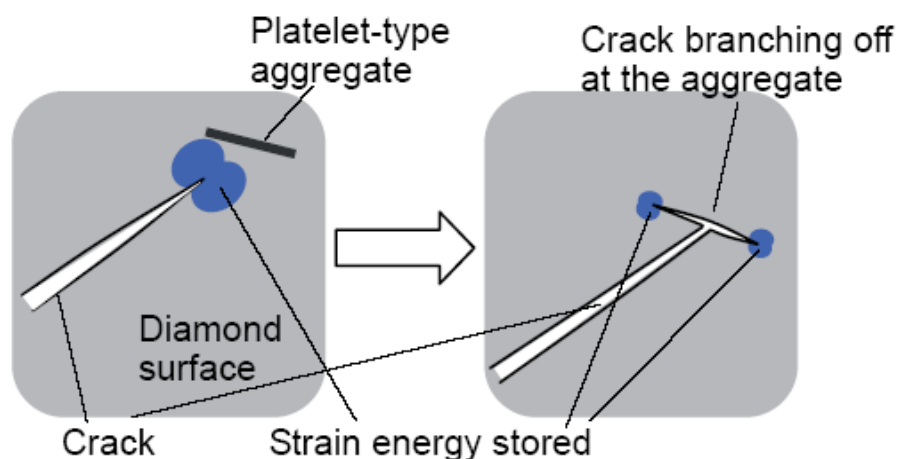
Figure 20: The progress of a crack being impeded by the platelet. [43]

The principle is quite attractively simple. The crack that propagates continues to do so until meeting the platelet. There, the platelet is able to disperse the energy of the fracture into a volumetric strain across and around the platelet which is below the critical strain for further cracking. This platelet as "shock absorber" idea is an elegant one; but does it stand up to any serious consideration? At the moment, there is no answer. There are no identified images of platelets having been sundered by proceeding crack fronts in the literature yet. So, the evidence is based upon the IR-absorption and the Hertzian strength data reported.

Shimada has developed an interest in acoustic emission (AE) to monitor tool-wear [43], and to predict tool failure [46]. Acoustic emission seems to be quite a popular processing topic at the moment. However, none of the data seems particularly convincing for the challenging silicon machining application. Furthermore, though monitoring for a tool break via this method would seem sensible, and, an advantage of using this process could be that it will allow more accurate determination of the distance cut by a tool before its failure. Potentially it is very helpful for trials using large workpieces.

Another, further, complication to the nitrogen debate is the report [47] of a series of diamonds from the Argyle mine which display the presence of two differently coloured areas within the same crystal.
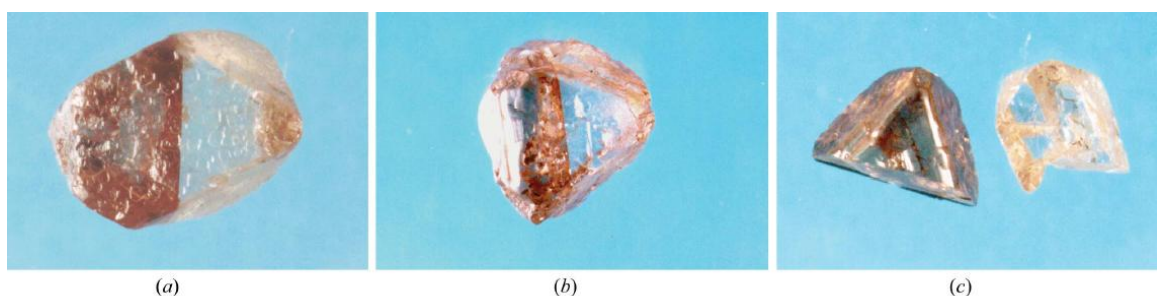
Figure 21: The three samples from the Argyle mine. The crystal in picture "c" was mechanically separated [47].

Brown diamonds are quite common, the surprising attribute of these stones is the fact that two regions with different colours have managed to maintain a single crystal

structure. These three diamonds (shown in figure 21) each displayed extreme stress when examined using X-ray topography rocking-curve analysis, particularly in the areas with the brown colouration. The different parts of the diamond both displayed large full-width half-maximum (FWHM) rocking-curves, particularly the brown section, which displayed a hugely stressed structure. The conclusion of that work was that nitrogen contributed towards preserving the integrity of the crystalline structures of these specimens. This result therefore greatly complicates the role that nitrogen plays within the structure of diamond.

Boron is another common impurity within diamond. Any boron within the material is often found in substitutional sites, causing p-type doping of the host diamond. This can make it useful for electronics applications, (and has been added deliberately to some synthetics in some cases [20,37]). The mechanical effect of including boron within the diamond structure does not appear to have been specifically studied at any point, though the optical properties arising from this dopant are clearly known. Boron-doped diamonds are known to absorb strongly in the red and infra-red regions and thus have a blue tint, (though this tint will appear black within samples of sufficient crystal thickness and/or boron concentration).
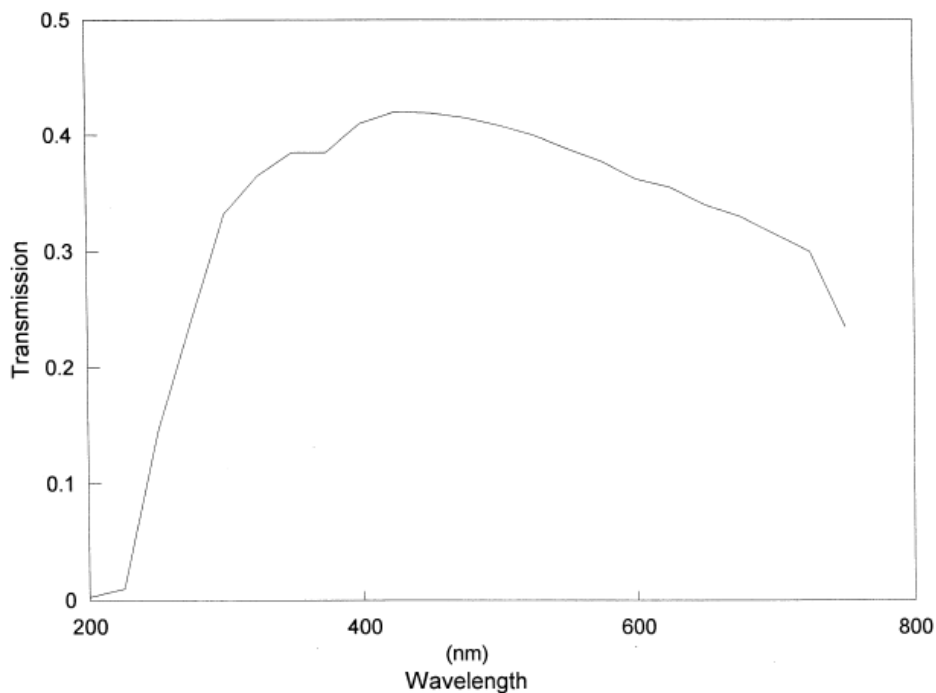
Figure 22: The visible absorption spectra of a boron-doped diamond [37].

IR-absorption spectra of boron are known to strongly absorb at 2,460 and 2,790cm^{-1} wavenumber [48]. It is therefore possible to search specifically for boron concentrations within diamonds and start examining their effect upon the mechanical properties. Though in the literature it is stated that *"although boron is one of the fundamental defects in diamond, we are still a long way from understanding the acceptor spectrum in detail"* [24]. Based upon the literature searched, the possibility of a dopant material other than nitrogen or boron having a strong effect upon tool-wear is looks unlikely as concentrations of materials other than nitrogen or boron are almost always negligible.

Finally, while discussing possible variation in composition of diamond the possibility of isotropic differences causing changes in material properties needs to be examined. From the literature it is known that samples containing larger quantities of ^{13}C have been found to have ~0.5% higher elastic moduli [49]. This is a relatively small effect compared with, for example, crystallographic orientation. The natural abundance of ^{13}C is low (only 1.1%), therefore naturally grown diamond crystals that contain large quantities of this isotope are extremely unlikely. In the paper a HPHT type of tool was prepared using an extremely high concentration of ^{13}C (99%).

2.3.4 Effect of crystallographic defects on crystal properties

Crystals are defined as having long range repeatable structure, and theoretically have very high fracture strength. However, the perfect crystal is a theoretical construct. In practice, despite the huge advances in crystal growth technology (mostly driven by the electronics industry), a range of structural defects will arise in even the highest quality crystals. Therefore even a perfectly compositionally pure crystalline material (i.e. no unplanned inclusion of unwanted elements) will hold structural defects and depending upon the number of these defects, exhibit lower fracture strength than the calculated theoretical maximums.

Defects within crystals are extremely small. Direct optical viewing of defects is impossible due to their scale: all are orders of magnitude lower than the diffraction limit. Even using extremely short wavelength X-rays does not allow direct viewing, but instead allows imaging of the effects such defects have upon the surrounding material. Using X-rays to examine crystalline structures is well established. When X-Rays interact with a crystal, the X-Ray wavelengths and the atomic separation are approximately the same, leading to strong diffraction effects. X-ray topography uses diffraction to effectively image information about one specific plane within the crystalline sample. The presence of a crystallographic defect disrupts the crystal plane it is on. The difference in lattice spacings will change the diffraction angle for X-rays travelling through that point, resulting in less X-rays propagating in the original Bragg angle (though there will be a different angle fulfilling the Bragg criteria). In short, different points across the diffraction spot will experience intensity differences from different parts of the crystal, depending upon the crystal perfection. Thus, if the diffraction spot is magnified we will see where the crystal quality is good (there'll be more photons delivered from these regions to the Bragg spot), but regions with poor lattice spacing behavior (due to defects) will send fewer photons in the Bragg angle direction, thus resulting in a darker spot.

The technological requirements for this experiment technique are extremely high as the required X-rays have to be well collimated in phase [50]. Thus, X-ray lasers or synchrotrons are the only method of truly performing this sort of work. Due to the spread of X-ray energies (so called "white" radiation) from a synchrotron source using white radiation allows much easier alignment of the sample. Thus in many cases it is preferable to use this type of source.

Analysis of X-ray topography results is extremely difficult. Telling the difference between surface scratches, and true defects is difficult, while differentiating between types of crystalline defect is even more challenging.
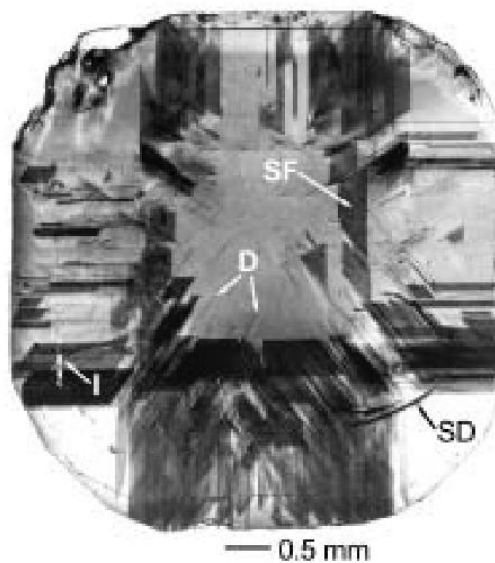
Figure 23: An XRT of a diamond (not a turning tool). This diagram shows four of the commonly observed crystal defects: (I) an inclusion, (SF) stacking faults, (D) dislocations and finally, (SD) surface damage. [50]

A particular difficulty is if the synchrotron optics have any artefact defects as these are displayed onto the results. Analysis of the gathered information is accomplished by either, great expertise and experience within the field or via use of complex numerical methods. [50]

A major contributor to the knowledge about XRT of diamond is Moore of Royal Holloway (University of London). He authored a very good review of the various techniques for XRT imaging of imperfections in single crystals [30].
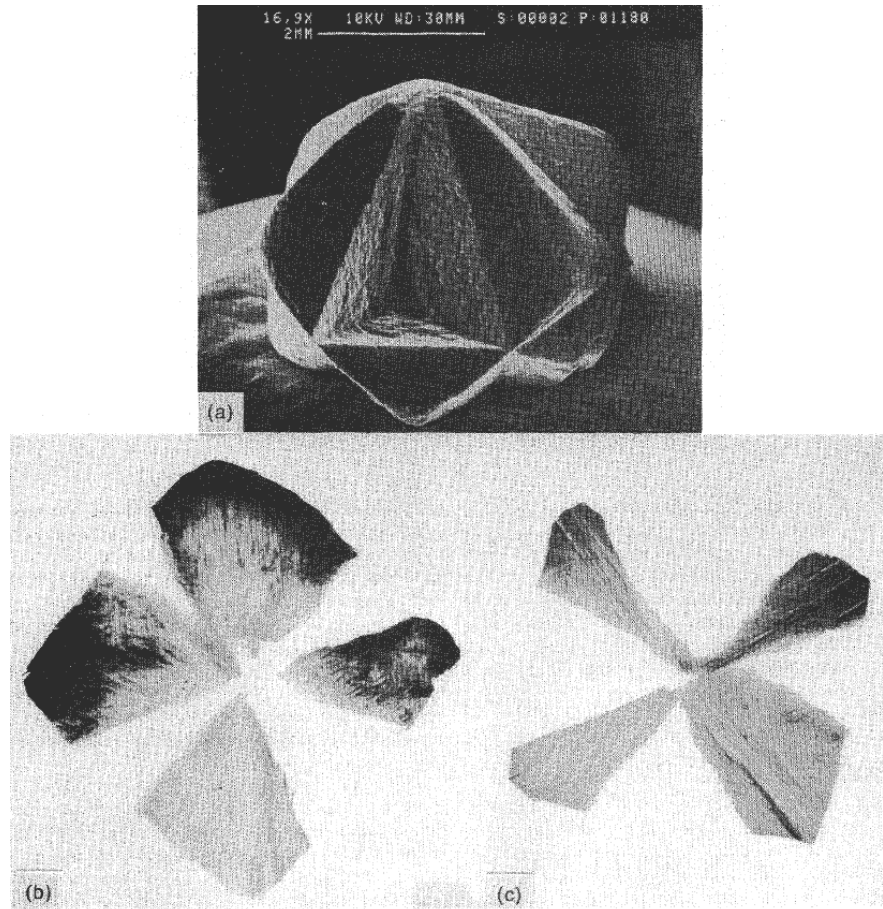
Figure 24: XRT has been used to investigate an unusual growth history. (a) SEM of the diamond in question. (b) and (c) the two intertwined structures [30].

The above figure clearly shows how complex diamond growth can be: here a single diamond has two distinct growth regions. Such twinning is the subject of many XRT related papers, (for example [28,29]), but such diamonds are unlikely to be used for diamond turning tools.

Detection of twinning is just one application of XRT. Another useful technique is the rocking curve. The rocking curve technique is a method for examining lattice spacings within a crystal. Rocking curves are gathered by tilting the crystal slightly away from the Bragg angle. Because the synchrotron generates highly correlated X-rays the detected intensity from a diffraction spot drops dramatically when the angle is changed away from the Bragg angle. Plotting intensity against angle gives the rocking curve. The rocking curve relates to the lattice spacings and therefore has a direct correlation to the strain within a crystal structure.
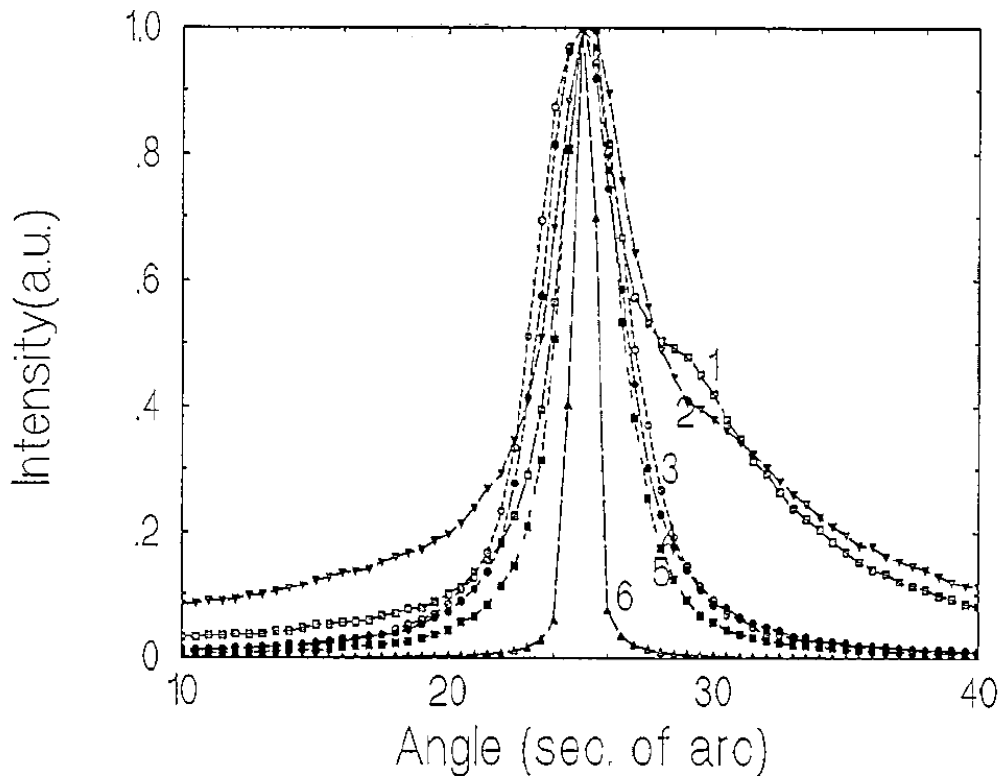
Figure 25: Rocking curve measurements of a HPHT synthetic diamond sample. [26].

The rocking curve shown in figure 25 is of a high-temperature high-pressure synthetic with different sections of the diamond being examined around an inclusion type defect.

Though crystallographic defects were considered a possible cause of the variation of tool-life characteristics, later on we were able to drop this as a possible hypothesis. The reported [2,51,52] wide deviation in tool-life is considered not to be due to crystallographic defects. Such defects have an exceedingly small scale and would be entirely removed when the tool was reconditioned. From earlier Cranfield work [2,52] it is known that superior performing diamond tools maintain their superiority despite a repair process that removes ~30 μm of material from the top-rake. Therefore we are clearly looking for a bulk property that is responsible for the variation of tool-wear behaviour between identical tools. Strain of the crystal or nitrogen impurities are examples of such a bulk property.

2.4 Tool-wear

Tool wear during single point diamond turning is strongly dependent upon the workpiece material. The definition of a worn tool is dependent upon workpiece material. Furthermore, the method in which the diamond experiences damage is workpiece material dependent. When machining some materials attritious wear is the dominant material removal mechanism experienced by the tool, however for other workpiece materials the removal mechanism is a chipping of the tool-edge.

2.4.1 Diamond turning soft materials

During diamond turning of soft materials (principally soft metals such as copper or aluminium) there is no well defined failure point for the tool, (unlike machining of brittle materials where it switches from ductile to brittle material removal). However attritious wear of a diamond tool can lead to problems for soft metals. For example, a given roughness tolerance which eventually will be exceeded by an excessively worn tool. The effect is primarily one of print through; attritious wear changes the shape of the tool and this changing profile is cut into the generated worksurface. The effect of a small chip upon the tool edge can in this way raise the roughness parameters quite markedly. It is common for machining with a worn tool to result in a marked change in the optical properties of a surface. Worn surfaces often diffract light, separating different parts of the spectrum. This colourful effect is a direct effect of tool wear increasing the roughness and helps machinists to determine when a tool is worn.

Conversely the effect of wear can have a positive effect upon a work surface. For example, a tool displaying a flat wear area at the nose of the tool will have a much larger effective radius than the tools' original radius value. This can be good for machining flat surfaces, but when the intended surface is something more complex the retreat of the tool point can lead to form errors.

Various studies upon the wear caused by soft metals are in the literature, with various metals and machining parameters being tested. One of the oldest wear-studies examined was that of Keen from 1971 [51]. In that study Al/Si piston skirt finishing is performed

using diamond tools. A particularly relevant quote is, "Though two tools might appear identical, one might produce ten or more times as many finished pistons as another." Interestingly this is the earliest found expression of a very pertinent problem with diamond tools: tool-life of similar tools varies widely and for an unknown reason. This effect would later be found to be very important in the diamond turning of large silicon optics [2].

The work of Oomen and Eisses [48] focuses on machining of non-ferrous materials using single crystal diamond tools. This trial tested a range of seventeen diamond tools, including some synthetic tools and various naturals with various nitrogen concentrations and identified imperfection types. The trial also used various non-ferrous materials; copper, aluminium and electroless nickel. The trial design does not consider that identical tools wear at vastly different rates, and therefore fails to ensure that there are multiples of each type of tool. This is a critical consideration when attempting to perform wear analysis of single point diamond turning tools. Despite the number of tools and the overall scale of the trial, the findings are limited. The most useful are the observations on tool wear when machining the various metals. Their results show that aluminium resulting in "severe tool edge rounding and clearance face wear". Wear resulting from copper is mostly confined to crater wear on the top-rake, while machining electroless nickel resulted in chipping of the tool-edge. When examining the other conclusions from the Oomen paper [48] the innate variability of diamond tools needs to be considered. As repeat trials with identical tools are not mentioned and considering the number of tools used this effect is likely to have arisen at some point during the trial. The material wear analysis displaying the trends of the wear patterns is of interest though, as these results are taken over various tools.

This work by Oomen and Eisses [48] used a 2D methodology for measuring wear (see figure 26).
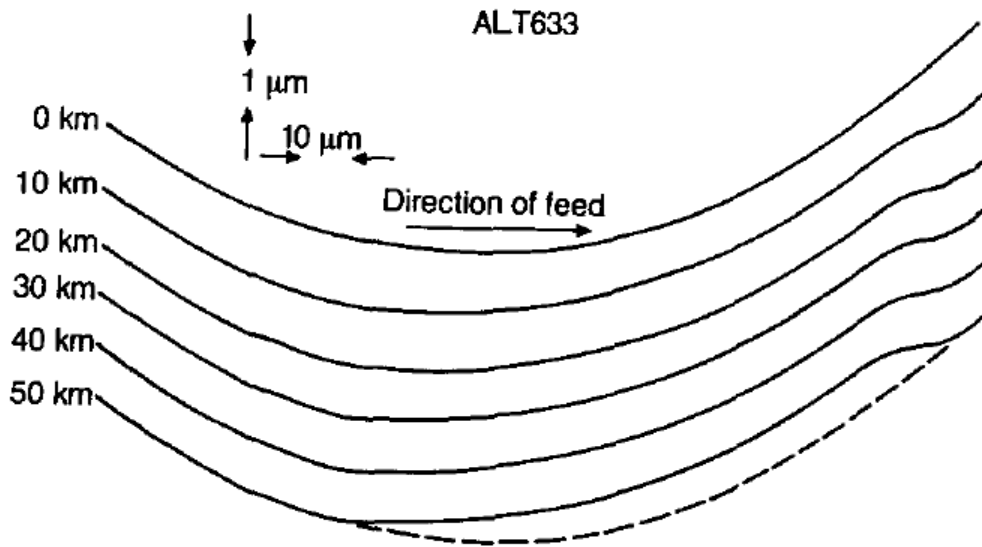
Figure 26: The wear progression of the tool edge while machining aluminium [48].

The tool-tip recession is measured by bringing the tool into contact with the spinning workpiece by only using the Z-axis. This plunging cut leaves a clear 2D cross-section within the tool material which can be clearly measured using a contact profiler. This work focused upon measuring wear in terms of the tool-tip recession and measuring crater wear. Because the tool-rake was zero for the tools used in this trial the above wear patterns could easily have been used to calculate the wear volume. However this raises further questions as there is no clear consensus on which metric is more suitable for describing diamond tool wear. Tool point recession, wear-area, wear-volume and wear on the top-rake (so called crater wear) are all measurable aspects of the diamond tool, though with different degrees of accuracy (volumetric wear analysis can be particularly demanding, see appendix A for details concerning a methodology developed but ultimately unused for the work within this thesis).

The tendency of electroless nickel to lead to chipping of the tool edge is confirmed in the work of Yamaguchi [46]. This paper examining potential methods of tool-life monitoring examines the cutting forces and records the acoustic emission from the tool. This machining process used a tool with a pointed profile. The use of a pointed tool edge might be to accentuate the wear (a relatively small cut distance would result in an

obvious wear pattern on such a tool). After a distance of just 0.6 Km the tool is said to be experiencing chipping of the tool edge. The typical tool-life of the tools examined in this paper was exceedingly short (less than 1 Km) however, leading to some concern about the suitability of the experiment and the applicability of the findings. The effort to monitor tool life rather than predict it is of limited application: in most cases the onset of failure makes the workpiece unsuitable for use.

Wear behaviour of diamond while machining electroless nickel is in strong contrast to the wear behaviour seen when machining copper. Shimada's work [53] details a very clear attempt to find a chemistry based explanation for the wear of diamond tools during diamond turning. The argument put forward in his work states that the copper workpiece can act as a catalyst, with oxygen initially forming an oxide with the copper before reacting with the diamond.
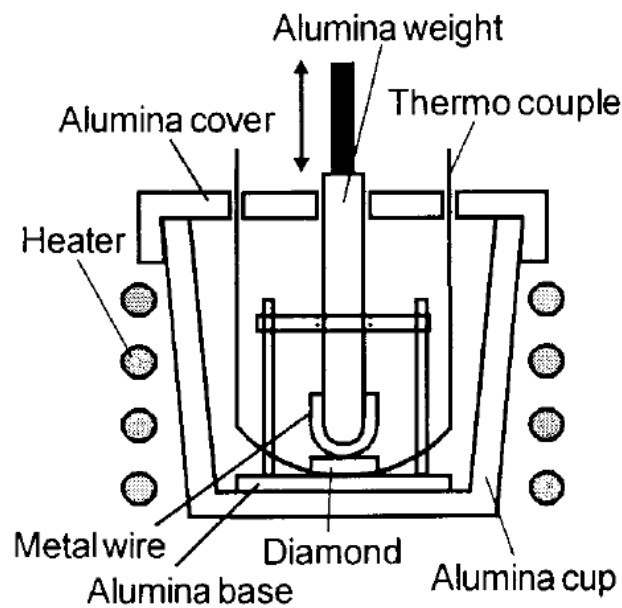
Figure 27: The experimental set-up used to examine the wear of diamond when in contact with copper. [53]

As can be seen from figure 27, the experiment is performed in a sealed container. This does allow the experiment to determine the effect of the quantity of oxygen in the chamber and the chambers temperature.
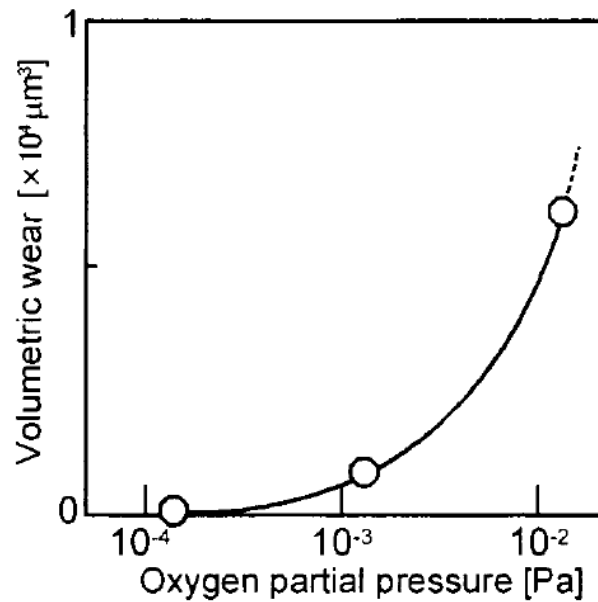
Figure 28: The wear result from the copper reaction chamber experiment [53].

The lack of any significant error bars in figure 28, and the very small volumetric wear that is recorded add doubt to the result, but the finding is an interesting one. The catalytic breakdown of diamond is an interesting idea and might help explain some wear behaviour. The results from the reaction chamber trial are supported somewhat with a diamond turning trial. During this trial nitrogen was passed over the tool and workpiece to reduce the quantity of oxygen in the tool engagement volume. Crater wear is clearly visible (in validation of Oomen's work [48]) during this turning experiment.

The body of work completed with non-ferrous metals allows an important conclusion about the behaviour of diamond turning to be drawn: different workpiece materials can cause varying wear behaviour upon the diamond tool. Some inspire chipping while others can promote large wear volumes via the continuous removal of carbon atoms in an almost atomic scale wear process. That some materials can act as a catalyst for oxidisation of the diamond tool is a finding of some interest and adds a chemistry based aspect to the already complex issue of diamond tool wear.

2.4.2 Tool-wear against IR materials

This thesis follows from the findings in an MSc thesis (by Tony Jacklin of Qioptiq [2]). In summary this work initially focused upon the effect of cutting fluids, the coolant flow-rate and the tool rake-angle. Though the experimental work was well planned all the findings were dominated by the effect of tool-life variability; (nominally identical) tools were displaying differences in tool-life that made interpreting the results more difficult. For some unknown reason, identical tools were being damaged by the machining process at very different rates. Though the thesis initially sought to perform process optimisation trials the findings were dominated by the tool variability. Though searching the literature has found evidence of similar tool variability findings dating from the 1970's [51], there are profound differences in the way the tool fails while machining non-ferrous metals than when machining brittle IR materials.

While there is a lot of literature detailing difficulties in achieving ductile machining with unworn-tools there is remarkably little literature on causes of a worn diamond tool to fail to machine a brittle material. What causes the onset of failure is too-often ignored in favour of testing machining factors like depth of cut.

A few of the things that are known are:

- Seemingly identical tools can display very different tool-lives
- Top-rake is a factor on tool-life
- Coolant is a factor on tool-life

Clearly a tools failure to machine in a ductile manner is related to wear of the tool, but no found literature links any of the wear-metrics (wear-recession, wear-area, wear-volume, crater-wear) to a failure mechanism that leads to brittle failure. Lacking this knowledge on any potential failure mechanisms makes predictions difficult.

2.4.3 Modelling cutting forces of worn diamond tools

Wear recession of tool edges is thought to be linearly proportional to the applied pressure and therefore accurately predicting tool-wear depends upon accurate predictions of the magnitude of force generated in the normal direction.

The turning process has received a lot of attention from researchers interested in developing cutting models. When modelling cutting forces during turning some have used a multiple regression analysis (for example Ravindra *et al*. [54]). This technique uses multiple linear or even nonlinear components to find the value of interest. From a scientific point of view this technique is problematic as it does not use any measurable parameters to determine the values sought and introduces many coefficients that can not be experimentally determined. This all makes multiple regression analysis a technique that appears to lack scientific rigor and was therefore not considered useful for the modelling within this work.

A paper from Huang and Liang [55], though focused on hard turning using CBN tools, indicates a link between contact area and thrust force, elaborating on Waldorf's wear force model (outlined in the appendix of that paper). This paper is extremely useful for several reasons:

- The similarity between the machining process studied (hard turning) and diamond turning. Similarities like low feed-rate, small depth of cut and moderate cutting speeds.

- Cutting forces generated are not significantly dependent upon cutting speed for many metal cutting situations. Assuming this is still correct for diamond turning, this makes predicting cutting forces for diamond turning simpler.

The Waldorf cutting force model provides a method for calculating cutting forces from a tool that is experiencing wear using values that can be calculated using the experimental data gathered. The validity of applying this method is extremely dependent on the accuracy of the method used for wear-area calculation. The accuracy of cutting force predictions (and therefore attritious wear calculations) are dependent on the accuracy of the wear-scar contact area.

2.5 Modelling wear of diamond

2.5.1 Molecular dynamics

Molecular dynamics is a computationally intensive technique that calculates the intermolecular potentials of a given volume and then adjusts the model accordingly. The

steps between calculations tend to be very small (Cheng used 10 femtosecond steps [56]) thus the total length of time successfully modelled tends to be very short. For example, the paper by Tanaka, Shimada and Ikawa [57] reports results from models lasting at most 250 picoseconds (0.25 nanoseconds). Similarly, the paper from Cheng et al. [56] runs a subnanosecond simulation (0.136 nanosecond). Small time-scale iterations are caused by the frequently required recalculations of the intermolecular potentials. The near constant recalculation is required as the forces are position dependent (and follow a nonlinear dependency making calculations further computationally demanding). Also the motion of a particular molecule is dependent upon all nearby potentials, making the final calculations a process of calculating all the potentials, moving the molecules and then recalculating the new potentials based upon the new positions. It should therefore be obvious that the number of molecules in the simulation greatly adds to the complexity and the computation time. Therefore the number of molecules acts as a further limitation. Both of the aforementioned papers deal with very small systems: the paper from Tanaka et al. [57] deals with indenter initiated crack phenomena within a two modelled bars of defect-free monocrystalline silicon of 24.4x2.7x1.09nm and 97.7x10.9x1.09nm (the first with 3802 atoms and the second with 58402 atoms).
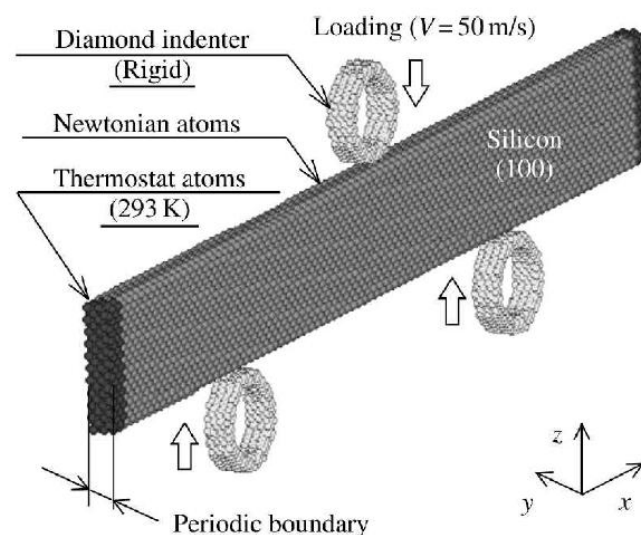
Figure 29: Model set-up used in Tanaka paper. [57]

The indenter geometry is similarly scaled, with a ring of diamond of only 0.53nm and 2.22nm for the two models. There are several problems with these model parameters. The interest into the how and when of the change from plastic deformation changes to brittle fracture is worthy of investigation, but results from experimental indentation testing can not be ignored. Lawn [6,8] has indicated that there is a scale issue and that silicon will deform plastically when the indented volume is small, this makes any claim of crack nucleation from their molecular dynamics paper difficult to believe but this exact claim is made.
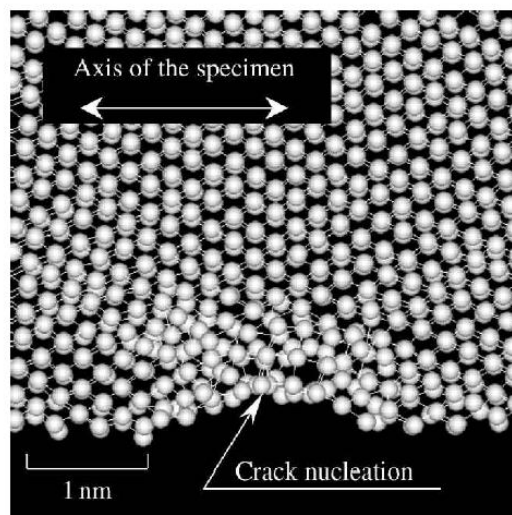
Figure 30: Crack nucleation for Tanaka's larger model, at t=231.5ps. [57]

The difference in findings between the model and experiment might be explainable through the differences in the substrates. The thin silicon layer is essentially an unreal situation. Few systems are ever going to be that slender. The difference could therefore be considered the difference between an almost 1D model and the behaviour of a 3D bulk. The velocity of the indenter (50m/s) is also considerable in an effort to "reduce the total computation time" [57]. Typical indentation testing uses a significantly lower indenter speed and the conclusion we are inevitably led to is that the set-up of the model is erroneous and that the findings are at best extremely specific or at worse meaningless.

The paper from Cheng et al. [56] deals with a similarly small volume of material. Here, the nanometric cutting is really a process of dragging a diamond AFM (atomic force

microscope) probe over a surface. The model deals with a limited volume of silicon (as shown in figure 31), just 5.99x1.18x3.64nm, again to limit the calculation time required.
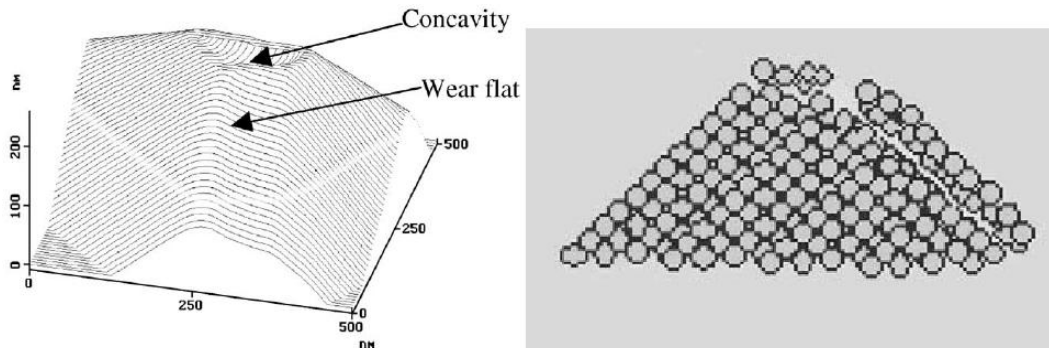
Figure 31: Images from reference 57. (Left) The AFM probe after machining and (right) the modelled AFM probe displaying some tip damage and some microdelamination damage.

The experimental validation for this paper is performed via machining of a 2x2 µm square of silicon (at an undisclosed feed step rate making working out the total distance machined impossible). The wear on the AFM probe is measured (presumably using AFM, due to the difficulties with measuring such a small sample) and compared against the models findings. Depth of cut is also unclear, as is the preparation method for the silicon workpiece surface. Though a simplification of diamond turning, this paper is looking at the attritious wear of diamond and is relevant. The experimental technique used by Cheng [56] is very similar to an experimental paper [15] that used a Vickers indenter to show that silicon behaves in a ductile manner when the removed volume is small, (see figure 32).
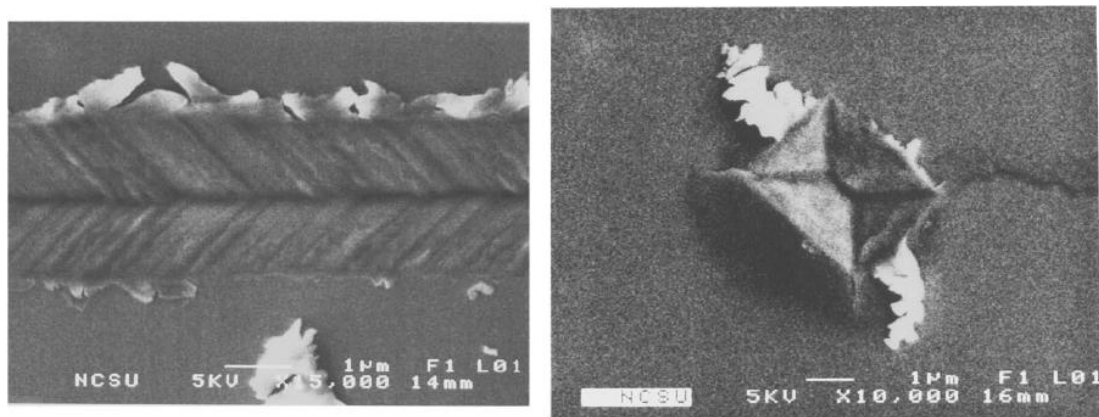
Figure 32: (Left) The trench left after ductile-type groove machining with a Vickers indenter. (Right) An indent in silicon displaying extruded material around the site. [15]

This is mentioned as it clearly demonstrates that the ductile regime is so much larger than the size of model frequently used. This is perhaps an unintuitive thought as the ductile mode of silicon is so often considered small, but it reinforces the small scale of the molecular dynamics models.

Looking more specifically at diamond turning we can start to appreciate the difficulties involved with a molecular dynamics approach. Depth of cut is significant when dealing with SPDT of brittle materials and this is a difficulty for molecular dynamics simulations. Within the literature molecular dynamics work on SPDT of silicon carbide uses very small depths of cut to draw quite bold conclusions about the suitability of diamond versus CBN as a SPDT tool material [60] or flank wear of a diamond tool [61]. Furthermore using the experimental set-up described in this project (machining at 1200rpm) a tool that lasts 20.1Km (25cuts) will require ~20,000 seconds of machining time. This would be a huge task for a model system containing very few molecules within it, but the number of atoms involved in SPDT is exceedingly high. We therefore get to a situation where if results on a sub-nanosecond simulation have any error, then that error is hugely magnified. Clearly molecular dynamics is a very suitable method for some extremely short timescale and small scale problems. Unfortunately the conclusion that those sort of boundary conditions are suitable for diamond turning problems can not be supported: diamond turning tools are large compared to molecular dynamics simulations and this problem can not be rationalized away easily. Neither can the huge disparity between timescales be ignored.

While all the above criticisms are valid the primary and most obvious reason to avoid molecular dynamics is cracking of the diamond tool. Cracks and chips along the tool-edge are large compared to the volumes a molecular dynamics model can simulate and their importance and effect can not be predicted.

A simulation that has a suitable scale was performed by Cai [58] and focuses on the stresses and temperature rises experienced by a silicon workpiece during turning. Again

with molecular dynamics the time-scale is very limited. This particular model focuses upon the silicon workpiece and has limited application to diamond tools.

Limited simulation times, limited model scales and ignoring cracks: for all these reasons molecular dynamics is considered an inappropriate methodology for the investigation of total cut-life. Though, for more isolated work dealing just with the fundamentals of attritious wear (a smaller sub-sect of the total problem) it would appear to be a suitable methodology. Indeed, any such work carried out in the future dealing with predicting attritious wear as a function of crystallographic orientation would be considered an important contribution to the field.

2.5.2 Finite element analysis

Finite element analysis (FEA) is a well established method for solving engineering problems. In general terms, FEA simulates the physical system by using a series of nodes which are linked using 1D calculations, the result is a mesh of calculable equations that model the bulk effects of the subject of the model. This simplification allows the extremely complex to be modelled within a reasonable degree of accuracy. Traditional uses of FEA are the loading behaviour of engineering components or systems, such as in the aeronautical industry where effort is put into modelling of wing flexing behaviour or in the automotive industry where deformation during crashing is modelled.

Another very successful area for FEA modelling is modelling heat flow. Temperature modelling becomes very difficult as so many properties are heat dependent. For example, thermal conductivity and thermal diffusivity (both very important for working out how heat travels through a material) are both temperature dependent. Potentially the most disruptive is the thermal expansion, which will require a quite complicated software package to successfully model the behaviour of a system that is being exposed to a thermal gradient.

There are numerous varieties of software that use FEA methods, many are highly specialised for the industry they are targeted towards. Metal cutting is difficult to model using FEA as any cutting process, by definition, will require the severing of some of the mesh strands. However the FEA software "Third Wave" is a package that is specifically designed for metal cutting industries.

"Third Wave" has an interesting approach to the modelling of problems. Specifically; meshes will, if put under sufficient pressure, form new nodes where the model is being deformed. Initially this seems quite sensible, giving the software the freedom to resize the mesh size to a more appropriate value, (mesh size is always something that needs to be carefully thought about when designing the simulation). However, (from discussions within the Precision Engineering Centre), the Third Wave software can give different answers when simulations are repeated. Third Wave is therefore not deterministic. The working assumption within the group is that method of determining the new mesh uses a random number generator to determine the new mesh size. From these small variations the changes grow and propagate throughout the model.

2.5.3 Other model methodologies
In previous work [59], the widely used program MATLAB (and the add-on simulink) was used to model the surface of a workpiece created through diamond turning. The great strength of MATLAB is the versatility it offers. The FEA and molecular dynamics modelling techniques would be suitable for modelling in 3D however the problem has historically been dealt with most successfully by using a 2D cross-sectional methodology (Blake and Scattergood's method [5]).

2.5.4 Thermal effects on diamond behaviour
Thermal effects are difficult to calculate as temperature changes so many of the qualities we would wish to remain constant [62]. For diamond the Youngs modulus displays a strong decline over a temperature range of 300 to 1400 Kelvin. The change

also varies with crystallographic orientation (with the [111] direction displaying the most noticeable decline) [62].
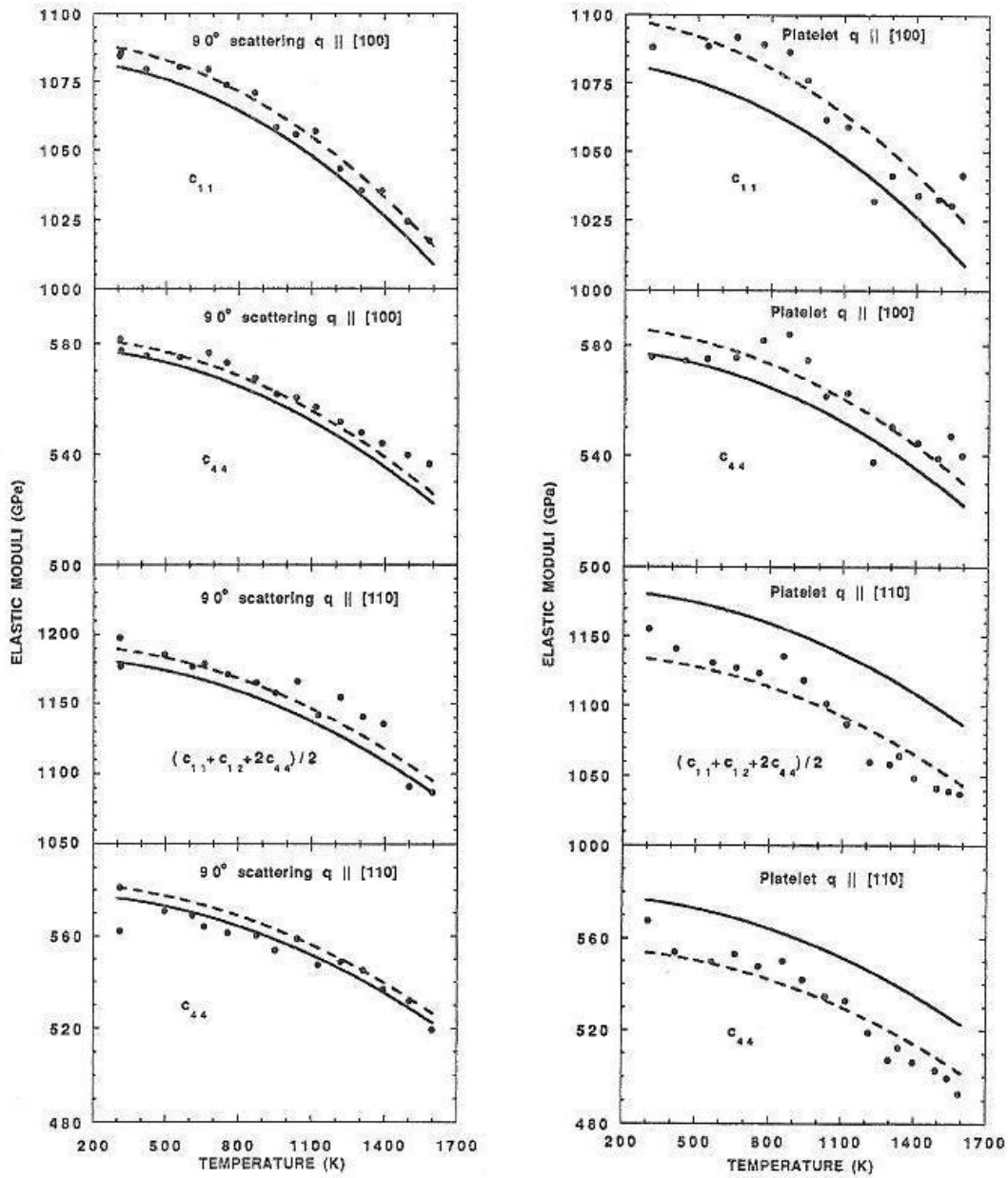
Figure 33: Brillouin scattering data from two scattering geometries at different crystallographic orientations. [62].

It is also worth noting that the heat capacity of diamond changes with temperature too. Thus even a simple calculation to discover the temperature difference between two different sized tools becomes complex very quickly. At higher temperatures chemical

effects can become significant [63] and at temperatures of 1800K [64] Diamond will change to graphite.

2.6 Wear processes

The field of tribology deals extensively with the damage occurring from surface interactions and has categorised several wear types. From reference [65] there are seven types of wear:

1. Adhesive
2. Abrasive
3. Corrosive
4. Erosive
5. Cavitation
6. Fatigue
7. Fretting

Of importance are the various situations that the different wear-methods are likely to create and what physical variables have the most effect on wear rates.

2.6.1 Adhesive wear

In adhesive wear, material moves from one surface and forms on the other contacting surface. Adhesive wear arises from bonding between surfaces. In the case of Van der Waals forces it is comparatively light, but for true covalent bonding this is extremely heavy. Loading of the surfaces increases contact and therefore can act to increase adhesive wear.

Considering the diamond turning case while cutting silicon a process will inevitably lead to severing silicon-silicon bonds and the very similar bonding structure of diamond and silicon, adhesive wear could be considered important for diamond turning silicon. However as adhesive wear tends to lead to the less strongly bonded material adhering to the more strongly bonded material, we would expect silicon to be adhering to the diamond. Wear of the diamond tool is perhaps because of another mechanism.

Aluminium is not bonded together in a way that is similar to diamond and therefore adhesion between such surfaces is unlikely to occur.

2.6.2 Abrasive wear

Abrasive wear occurs when hard asperities on a surface, or free particles rub against a surface, resulting in cutting or plastic deformation of the worn surface. From SEM images [2] it is known that small chips of diamond have been removed from some tools during the machining process, resulting in diamond particles free within the machining zone, along the clearance face. However when softer materials are machined tools display wear-scars that are free of chipping damage. Therefore for most diamond turning situations the effect of abrasive wear would appear to be limited.

Abrasive wear of diamond tools during diamond turning is considered a minor effect at best and unlikely to have much effect on generating the volumetric wear of the diamond tool that has been consistently visible. Abrasive wear requires abrasive particles (fixed as in grinding wheels or free as in polishing solutions), and during diamond turning they are not here in any serious quantity.

2.6.3 Corrosive wear

Corrosion or oxidisation wear is a chemical process and is therefore extremely dependent upon the constituent parts that are brought into contact. In the book (*surface effects in adhesion, friction, wear, and lubrication,* [65]) nickel is used as an example of a material that readily forms an oxide layer and therefore resists oxidisation attack. However, it is known that electroless nickel is a material that can strongly wear diamond tools during turning [48]. Though it is possible to speculate that this high wear is linked to the workpiece materials tendency to form an oxide layer and the diamond materials weakness to oxidisation.

If in some cases corrosive wear was the cause of diamond tool wear, then in those cases:

- The wear rate would depend upon workpiece oxygen adsorption.
- Wear would be pretty much independent of the depth of cut and any cutting forces (except for any associated thermal effects)

Silicon does not form a protective oxide layer, so this wear mechanism might not be applicable for this material. While aluminium tends to make very thin oxide layers and is unlikely to be corroding diamond in any traditional sense of the word.

2.6.4 Erosive wear

Erosive wear occurs through particulates bombarding a surface. This can occur using solid, liquid or even gases as the bombarding material (in the case of gases, an ionic gas is mentioned and chemical attack from a stream of gas could be considered possible). For the diamond turning case, this is not happening (there are no fast travelling particles travelling through a gas layer), our tool is within the deforming material, a gas layer separating workpiece and diamond tool is implausible. Speeds during turning also tend to be slow enough that this method appears unlikely.

2.6.5 Fatigue wear

Fatigue is a controversial topic for diamond. The concept of defect mobility within a crystal as hard as diamond is considered by some to be unlikely. However there are papers upon the subject [66,67]. Fatigue results in cracks and subsurface damage, which is very different from the sort of wear that is resulting in smooth wear-scars on diamond tools. Because of the controversy surrounding fatigue of diamond this wear mechanism is therefore not considered important to diamond turning at this time.

2.6.6 Fretting

Fretting is a two stage process, composed of initial adhesion and then chemical attack via corrosive wear. The corrosive wear works to liberate the material that had adhered from the worn surface. For example, Iron that adheres to another surface which is then given a chance to oxidise, the Fe_2O_3 then is free to form loose debris. Though interesting, this is not considered to be especially likely with diamond turning.

2.6.7 Cavitation

Wear of a surface from a stream of liquid containg trapped gas bubbles that impact with the surface. High stream velocities is a requirement for any considerable wear in this situation. High velocities jets of fluid are not typical when diamond turning and therefore the effect of this wear-type is ignorable.

2.6.8 Wear summary

As we see from looking at the various wear mechanisms and thinking about diamond turning there is no obvious candidate that explains all of the behaviour seen across various tool-workpiece combinations. This is a clear indicator that the subject is going to resist simple analysis.

As will be shown later, even if we were to know with complete certainty the type of wear that causes volumetric wear of diamond tools, the chipping damage to tool-edges will make the situation more complex.

2.7 Omissions within the available literature

Despite the extensive nature of the literature review some relevant facts remain unknown. For example it is worth noting that despite the significant number of wear studies against various workpiece materials, there is not a definitive wear metric for defining diamond turning tools. Previous work at Cranfield [52] examined both the flank-wear and the volume of material removed, though it is unclear if either are particularly relevant to the problem. Related to this problem is the lack of any literature detailing the method in which a worn tool is failing to cut in a ductile manner when machining brittle materials. These two unanswered questions will make experimental design more difficult as it is unclear which factors are important to measure.

Though the existence of the supertool phenomena mentioned in the available literature [51], causes of this behaviour are not given much of a theoretical basis. We therefore are no closer to discovering the root cause of supertool behaviour after the literature review. There is some evidence linking low nitrogen content with better resistance to

polishing [35] and to improved hardness [39] so it is likely the cause is related to nitrogen, but nothing within the literature definitively answers the supertool question. The literature review has helped to confirm that the three project aims described in Chapter 1 are going to lead towards an original contribution to knowledge.

2.8 Literature summary

Limited tool-life when diamond turning silicon exhibited by most (but not all [2,52]) diamond tools is a clear problem. It has been observed that some tools will exhibit extraordinary tool-life [52] and through an understanding of what makes these tools special it may be possible to either screen natural diamond for such gems or engineer a synthetic diamond that will display extraordinary tool-life.

During this chapter various causes for variation of diamond have been examined and the mechanical properties of diamond have been found to most strongly vary due to the following three properties:

♦ Crystallographic orientation

♦ Nitrogen and other impurities

♦ Crystallographic defects

The new MCC single-crystal CVD diamond is therefore an interesting test material as the growth conditions ensure consistent internal stresses and low nitrogen impurity content [22], eliminating two of the main influences on mechanical properties. Also explored within this Chapter were several minor causes of influence upon mechanical properties of diamond such as temperature [62], unusual growth history [19,28,29] and isotropic composition [49].

Looking at nitrogen content, there is indirect evidence from polishing trials that suggests high purity will be beneficial for tool-life when machining silicon [35] and more direct evidence of purity benefiting the machining of softer workpiece materials [43]. However the literature on the effect of nitrogen on the diamond turning properties of a tool can not be simply summarised as saying nitrogen is bad for tool-life. There is

considerable literature detailing the defects that nitrogen can form within the diamond. From simple inclusion within the structure of the diamond unit cell (as is common for the HPHT diamond material [21], ranging to large (in crystallographic terms) complexes that involve slow aggregation of many nitrogen atoms to form the platelet [24]. Some argue [43] that the form of nitrogen complex is more important to tool-life than low total nitrogen quantity, implying that a little nitrogen in specific arrangements is beneficial.

Previous cutting trials [48] have shown that silicon causes measurable volumetric-wear after short cutting distances and that brittle-failure can occur after a short distance [2]. None of the surveyed literature explains how diamond tools fail. The mechanism or mechanisms for inducing brittle damage into a brittle workpiece remain unknown, though there is an assumption that volumetric wear is related [52]. However, there is no confirmed mechanism linking the failure of a diamond-tool to any measurable wear behaviour (volumetric-wear, wear recession-distance, flank-wear, wear-area). Clearly tool-failure is related to the changes the tool experiences, but there is no literature reporting which metric is important and why, making explaining supertool phenomena perplexing: seeking tools that behave in unknown ways to unknown failure mechanism.

What little we know about the onset of brittle damage comes from the work of Lawn [6,7] and Scattergood [5] we know that geometry of the cutting regime can lead to brittle damage being introduced into the workpiece. Though the work of Blake and Scattergood is good, it focuses on the geometrically simple unworn diamond tool [5]. This is an approximation that does not stand over any sensible cutting distance while machining silicon (or to a lesser extent the other brittle IR materials).

While we know from the literature that machining of brittle-materials posses unique problems, machining soft non-ferrous metals is comparatively simple, with failure typically being defined by rising surface roughness (typically defined using either the R_a or P_a parameter [9]). Or alternatively the tool-geometry changes to the point at which it is unsuited for machining an intended complex workpiece geometry. Failure during

aluminium machining is highly application specific. Interestingly, while machining aluminium diamond tools can display supertool behaviour [51].

The hypothesis can therefore be summarised as: does high purity diamond, as exemplified by the new MCC material, make diamond turning tools that display longer achievable cutting distances when machining silicon and aluminium workpieces?

Chapter 3- Experimental procedures and equipment

3.1 Experimental design

In chapter 1 three research aims were decided and the eight objectives decided. The first aim is to "explore the effect of diamond quality on cutting tools during SPDT of silicon" and led to the first three objectives:

Objective 1: Test HPHT material against silicon workpieces
Objective 2: Test natural diamond tools against silicon workpieces
Objective 3: Test MCC material against silicon workpieces

The second aim "explore the effect of diamond quality on cutting tools during SPDT of aluminium" and led to the definition of objectives 4 and 5.

Objective 4: Test natural diamond tools against aluminium workpieces
Objective 5: Test MCC material against aluminium workpieces

These objectives were decided upon to fully explore the effect of diamond quality when machining silicon and aluminium workpieces. However as the findings from one workpiece material can not easily be claimed to be significant for another, designing different experiments for aluminium and silicon workpieces is therefore appropriate.

The third research aim described in chapter 1 was to explore the root origins of the "supertool" effect. As a previously identified "supertool" was available the experiments performed using silicon workpieces would also have to explore this phenomena and complete objectives 6 and 7:

Objective 6: investigate crystallographic orientation as a cause of supertool behaviour

Objective 7: Investigate impurity content of natural diamond as a cause of supertool behaviour

The design of the silicon machining experiment would therefore be investigating five of the eight objectives and require more testing of tools than the aluminium machining.

3.1.1 Design of aluminium workpiece cutting trial

Aluminium is commonly used as a diamond turned workpiece metal which can achieve very long cutting distances. A simple comparison between natural diamond and MCC tools was sufficient to gather meaningful information and complete objectives 4 and 5. A single natural diamond tool was tested and compared with two MCC tools. Aluminium machining lacks the clear failure point displayed by silicon workpieces, therefore the cutting distance was fixed at ~480Km. During the trial the workpiece would be cut using a total of 80 cuts over progressively shorter distances so that a small area was left uncut.
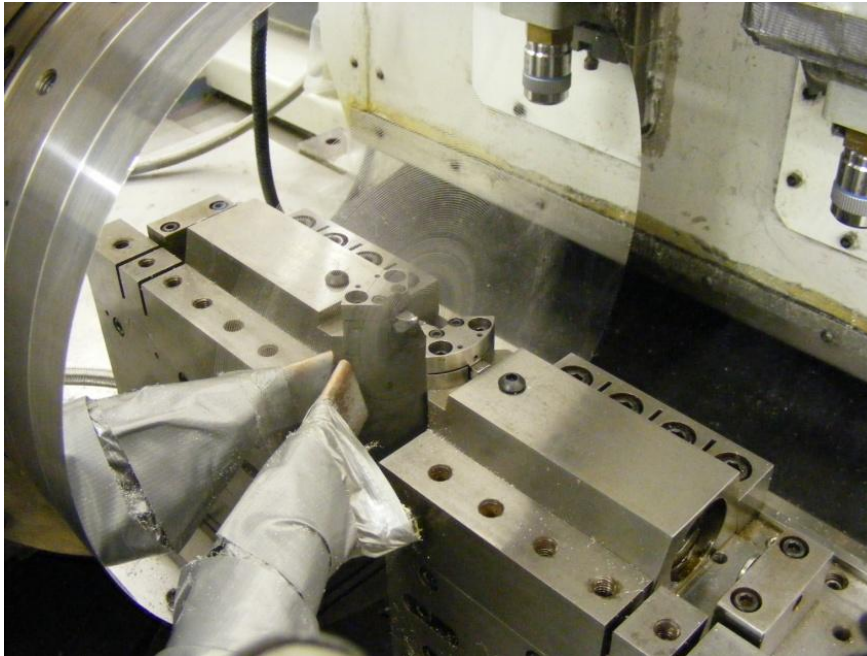
Figure 34: Experimental set-up of aluminium machining trials.

Leaving a section of uncut workpiece, as shown in figure 34, resulted in a region that was suitable for measuring surface roughness of the workpiece. Any supertool effect would not be expected over the distance of ~480Km, the design of experiment therefore eliminated this effect from the experiment. A total cut distance of ~480Km is a short tool-life in industry but represents a long distance for academic cutting trials where distances of 50Km are considered to give usable information [48].

Diamond tools with zero degree top-rake angle and a clearance of 10 degrees were used, and are typical values for machining aluminium. The tool radius was 500 μm, comparatively small for machining flat components, but this radius size allowed easier comparison with the tools for silicon. Aluminium 6061 alloy workpieces of 150mm radius dictated we use the NION machine for diamond turning. The feed-rate used was 10μm/rev, quicker than the feed-rate used for previous silicon machining [2,52] but appropriate for machining aluminium or other soft metals. The depth of cut for the machining of aluminium was 10 μm. The spindle speed was set at 600rpm. A white spirit cutting fluid was applied to the workpiece.

The metrology of the trial includes measuring surface finish of the workpiece, measuring cutting forces and taking SEM images at various points during the trial. Force was measured in the thrust direction using a Kistler (described in section 3.3.1). Surface roughness (using the R_a parameter) was measured. Combined with periodic SEM images of the tools this design ensured there was a great deal of data gathered over the cutting life of each tool.

3.1.2 Design of silicon workpiece cutting trials

Previous work at Cranfield [2,52] highlights the need for care when planning experiments when machining silicon workpieces using diamond tools. The extreme variability of natural diamond was shown to dominate any planned experiments. The presence of a supertool within the sample group makes any investigation of other parameters extremely difficult. Synthetic diamonds are grown under carefully controlled conditions the expectation was therefore that these diamond tools would be more consistent than natural diamond.

Two natural diamond tools (a previously identified normal tool and a supertool [2]) would be used, allowing comparison with previous work done at Cranfield. The MCC single crystal CVD tool material and the HPHT synthetic diamond will also be used within the trials. These two tool materials have different quantities of nitrogen [22] allowing the effect of this impurity material to be accurately determined.

Cost of diamond tools was a design consideration for the trials, as was the cost of machining time when using a diamond turning machine. A natural desire to minimise the cost of the trials and to maximise the findings from those trials made experimental design challenging. Design of experiments was therefore of critical importance. For the analysis of HPHT and MCC tool trials a statistical design (or Taguchi) methodology was selected.

The Taguchi methodology allows maximising results from small data groups and has been successfully used for designing tests aiming to improve industrial processes [66]. The plan is for a 2 factor two level experiment, testing the two synthetic diamond materials in two different crystallographic orientations. This experimental design is shown in table 1.

LEVEL	Tool material	Crystallographic orientation
1	HPHT	(100/100)
2	MCC	(100/110)

Table 1: Levels and factors of experimental design.

The Taguchi methodology allows a partial orthogonal experimental design in some cases, but due to the potential hidden factor that is giving rise to the supertool phenomena a full factorial design is required (with repetition of each factor-level combination required). The methodology allows all the results from one level to be averaged and then compared against the average results from the other level [68]. For example, all the results of the HPHT material, regardless of crystal orientation, can be averaged together and be compared with the similarly averaged MCC results to determine the effect of tool material. Testing levels against each other in this way allows broad conclusions to be made about the effect of tool-material and crystallographic orientation. Significantly, the most important factor on tool-life can be found, which is important for learning how to improve silicon machining.

The two design factors are tool material and crystallographic orientation of the tool. Tool material levels are HPHT and MCC, while crystallographic orientation levels are (100/100) orientation and (100/110) orientation.

Experimental responses for the silicon trial are:
- achieved cutting distance before onset of brittle-fracture

- thrust direction cutting forces

SEM images of the diamond tools are taken after failure.

As there is some unknown factor causing supertool phenomena in natural tools expanding the Taguchi part of the trial to include natural tools was not possible. Testing natural diamond tools, including a known supertool [2], allows comparison of the synthetic tool types against the current industry standard and with work done previously [2,52].

Silicon workpieces with diameters of 32mm were supplied lightly doped with an n-type dopant. Workpiece thickness was 2mm at the start of machining and both sides were polished by Qioptiq ltd before the trials. Each workpiece was cut repeatedly until the onset of brittle failure. Silicon workpieces were typically cut using a spindle speed of 1200rpm. For a few trials a 3000rpm spindle speed was used: these trials allowed better comparison between our work and industry. All silicon machining within this thesis was performed on a Moore Nanotech 350 UPL (detailed in section 3.2.1). Depth of cut has been shown to have little effect on the machining of silicon [5] so a depth of cut of 10μm was used, keeping this parameter the same as previous work at Cranfield [2,52]. The work of Blake and Scattergood set a definite limit on the maximum achievable feed-rate for silicon machining [5]. To keep this trial consistent with previous work [2,52] a feed-rate of 1 μm/rev was selected. The spindle speed was therefore constant and the option of using a constant surface speed was not used. Such a machining mode has difficulties with machining to the centre of turned objects: the required speed rises are greater than the capacity of the machines spindle. Also because changing spindle speed can cause changes in the machines dynamic behaviour; causing changes in vibration amplitudes if machining near resonances. Qioptiq also use constant spindle speeds, therefore results that were gathered in a way would be of more relevance to these industrial sponsors. The spindle speed was therefore kept constant and surface speed as a consequence tended to decay as the tool approached the workpiece centre of rotation.

Deionised water was applied as a coolant using a needle spray at a flow rate of 8-12 grams per minute. Using water as a coolant fluid for diamond machining of silicon was

established as superior in previous cutting trials [2]. In the literature released after those trails [52] the case is presented that the superiority of water over oil-based coolants is due to the higher thermal conductivity of water. This might not be the whole case, as it ignores many other factors. There is clearly a great deal of work that could be done testing different cutting fluids as the effect is quite considerable (tool-life increased approximately 200% when the fluid was changed from oil-based to water).

Testing using silicon workpieces requires different tool specifications than the aluminium work. There is compelling evidence that negative rake angles are better suited for machining silicon [5]. Previous trials used -25 degrees as the top-rake angle [2] so this was used as the typical value. Clearance angle was specified as 10 degrees, tool radius was kept constant at 500 microns. The MCC tool material would also be tested using a -45 degree top-rake trial against silicon (with results in section 6.3). The -45 top-rake angle tools required a special tool-insert to tilt forward the tool sufficiently. This resulted in a larger effective clearance angle than the 10 degrees nominally specified and changed which crystallographic orientation was normal to the workpiece.

Natural diamond turning tools for machining brittle materials are supplied with a (100/110) orientation, (see figure 35).
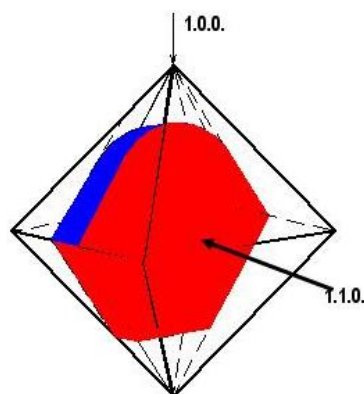
Figure 35: The orientation of natural diamond tools.

The (100/110) orientation description is defined as the point of the tool is aligned along the (100) crystallographic direction while the top-face of the tool is identifiable as the {110} crystal plane.

The HPHT tool-material is typically supplied with a [100] top-plane (shown in figure 36). However, because grinding a top-rake onto a tool with a [100] top-plane is not possible the HPHT tools were tilted to achieve the correct top-rake angle.
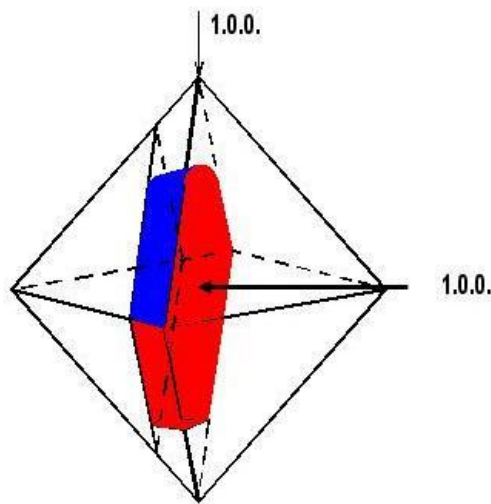
Figure 36: The orientation of HPHT diamond tools.

Most MCC diamond tools would be supplied in the (100/110) orientation but some would be supplied in the alternative (100/100) orientation, allowing clearer testing of the effect of crystallographic orientation on achievable cutting distance.

3.2 Diamond turning machines

The design of diamond turning machines should always comply with the guidelines for precision machine tools established by McKeown [1] in the 11 principles. These are a series of design considerations for precision machines. They are:

- Structural
- Kinematic/semi-kinematic design
- Abbe principle or options
- Bearing averaging
- 'Direct' displacement transducers

- Metrology frames

- Servo-drives and control

- Drives

- Carriages

- Thermal drift

- Error compensation

Each are large topics, any of which could have an entire thesis dedicated to them. However the intention behind all these points is remarkably simple. It is all done to keep the tool and workpiece as close to the intended position as possible. Clearly however, the design of the machine is just one part of the machining process, and other factors such as tool-wear can badly effect the accuracy of the machined workpiece.

For this project two diamond turning machines were used, each is described in some detail. Namely these are the; Moore Nanotech 350 UPL and the CUPE NION nanocentre. Both are high quality diamond turning machines suitable for producing parts to nanoscale tolerances.

3.2.1 Moore Nanotech 350 UPL

The Moore Nanotech 350 UPL (Or simply "Moore") is a commercially available and used single point diamond turning machine from Moore nanotech systems. The machine uses an airbearing spindle to rotate the workpiece; these bearings are particularly suitable for ultra-precision because of the very low error motion. The spindle has a programmable angular accuracy of 0.0001 degree [69]. The maximum spindle speed is 6000 rpm. Qioptiq (a project sponsor that produces IR equipment for defence applications), uses these machines to produce hybrid optics using IR materials at 3000rpm [70]. Due to the tool-wear problems when machining silicon these hybrid lenses are currently produced in germanium. Previous work at Cranfield University machined silicon at 1200rpm and 600rpm [2] using the Moore, and selected results from this work were published [52]. The use of the Moore machine therefore allows comparison with previous work.

Figure 37: The Moore machine.

The two axis slideways are made to precision ideals; using linear encoders and CNC control to achieve accuracy of less than 50nm [69]. These oil hydrostatic box-way slideways are designed to be stiff, ensuring the shape of the structure is maintained during machining; thus avoiding error motion. The Moore has a PID controlled chiller working to maintain the temperature of the spindle. Additionally the Moore machine is within a temperature controlled laboratory. This temperature control is necessary to minimise any thermal expansion that could affect machine tool accuracy. Depending upon the workpiece geometry that is being machined, a rotary B-axis can be used. This axis is removable and for the machining done as part of this thesis, the B-axis was not in place. Removing the B-axis improves the stiffness of the machine loop and eliminates any rotational error for the tool position.
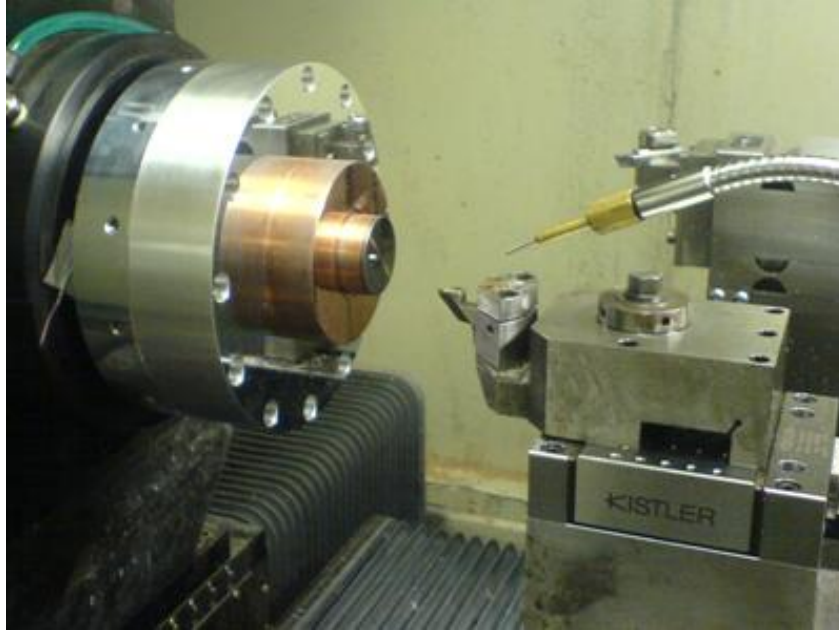
Figure 38: A 32mm diameter silicon workpiece upon the Moore Nanotech 350 UPL.

Tool position is determined using a removable optical tool-set. This is critically important for the accurate determination of tool position. The optical tool-set uses three points along the radius of the tool to accurately determine the centre of the tool's circumference. Control is then performed using the centre of the tools radius rather than the tool edge. Therefore during very long cuts it is possible for wear to result in inaccuracy of the form of the workpiece; regularly re-establishing "touch" with the worksurface can help reduce this error. Wear can clearly be problematic for determining the tool-centre if wear has changed the tool to a non-circular geometry.

3.2.2 CUPE NION nanocentre

The CUPE NION nanocentre (or just "NION") was developed by Cranfield Unit for Precision Engineering (CUPE) as a commercially available combined grinding or turning machine. Like the Moore the CUPE NION nanocentre has two hydrostatic linear axes and a hydrostatic spindle. However the spindle within the CUPE NION nanocentre has a lower maximum rotational speed of just 600rpm.

The NION has a smaller working volume than the Moore, but improved thermal stability. Another critical improvement is the fixed optical tool-set. This provides greater accuracy than the removable tool-set used, as any removable set introduces kinematic mounting type errors positional accuracy. The improved thermal stability and the fixed optical tool-set both contribute to an overall improvement of tool position accuracy for most machining when compared to the Moore.

Despite some disadvantages the NION was used as it could accommodate the larger workpieces that were used for the aluminium machining trials. These workpieces could not be fitted upon the Moore machine and for the trials to be of a manageable timescale the trial was performed using the NION.

A white spirit coolant/cutting fluid was used during the machining on the NION, and applied in a mist-spray arrangement. The coolant was applied as closely to the tool as practical. Due to the ductile nature of the workpiece material, long pieces of swarf were produced, and had a tendency to gather around the tool and act in an abrasive manner if not extracted. This could lead to surface damage and therefore misleadingly high surface roughness values so a simple vacuum extraction method was used to keep the worksurface as clear of swarf as possible while machining.

3.3 Other experimental apparatus

For precision engineering processes there are two clear stages that need to be performed; machining and metrology. Good quality metrology is essential for precision engineering. All but one of experimental apparatus described in the rest of this chapter are metrology devices. The great difficulty with metrology is the same as the great difficulty with precision engineering machine tools: no single machine is able to perform all the operations that are required for a given workpiece.

3.3.1 Kistler

The Kistler is a 3-axis dynamometer used for measuring cutting forces during the machining process. Forces are measured using three orthogonal piezoelectric sensors.

The piezoelectric effect arises in some crystals which lack symmetry centres. Applied forces across these crystals result in a proportional electric field. [71].

A problem with piezoelectric sensors is that charge tends to "leak" (dissipate through imperfect insulation). This results in values of specific readings for static forces decaying overtime. Attempts to compensate for this effect are often imperfect and therefore force measurements using piezoelectric methods tend to have a slow change (or "drift") of the zero value. Such drift needs to be compensated from the data as a first stage of accurate data processing.
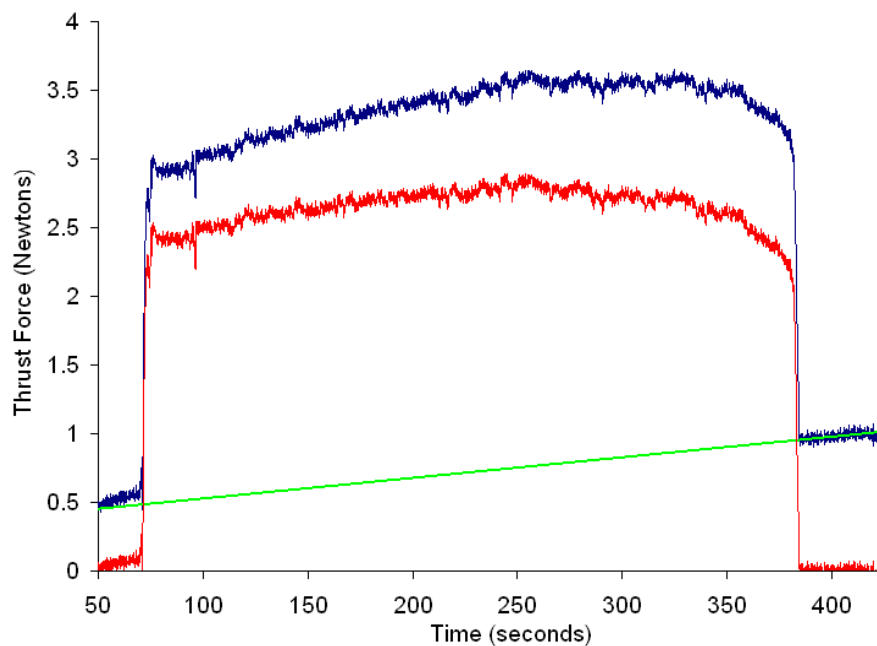
Figure 39: Cut force file with drift compensated (red) data and uncompensated (blue) data. Linear drift is shown in green.

Figure 39 shows the adjustment of the cut force files using a linear readjustment factor. Drift compensation is possible using the software provided by Kistler but was done using MATLAB. This added considerably to the data processing time, but ensures that the method used is known and that the compensation is done using a simple linear fit.

Figure 40: The 9256C2 model Kistler as used in this project [72].

The project used two models of Kistler, the smaller 9256C2 and the 9257BA. The force measurement range for the two Kistlers is different: 500 Newtons and 2000 Newtons (the 9257BA is more typically used for grinding where machining forces are higher). Understandably the first has a better force resolution compared to the second. This is the result of the digital-to-analogue converter causing a quantisation effect. However by using an average cutting force across the entire cutting time it is possible to reduce the effect of quantisation error.

Though the Kistler measures in three orthogonal directions, most commonly measured was the thrust force (the force component acting orthogonal from the workpiece). This component (acting along the z-axis on the Moore machine) gives the largest force signal. Using the largest force component helps reduce the quantisation effect from the digital-to-analogue converter, as cutting forces in all of the directions are typically very small, especially at the start of the cutting process.

3.3.2 Fisba

The Fisba µPhase interferometer is commercially available from Fisba Optik. The Fisba is a 5 phase interferometer working on a Twyman-Green interferometer principle; (similar to a Michelson interferometer).
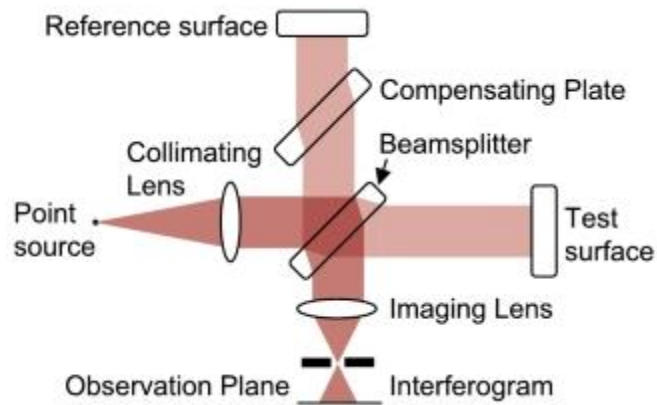
Figure 41: Schematic of the Twyman-green interferometer. [73]

A Twyman-Green interferometer schematic is shown above (figure 41). A beam from a collimated light source is split into two directions by a beam spliter. One beam is reflected from a flat reference mirror. The second beam is reflected from the test surface. The two reflected beams are recombined, to form the interference pattern.
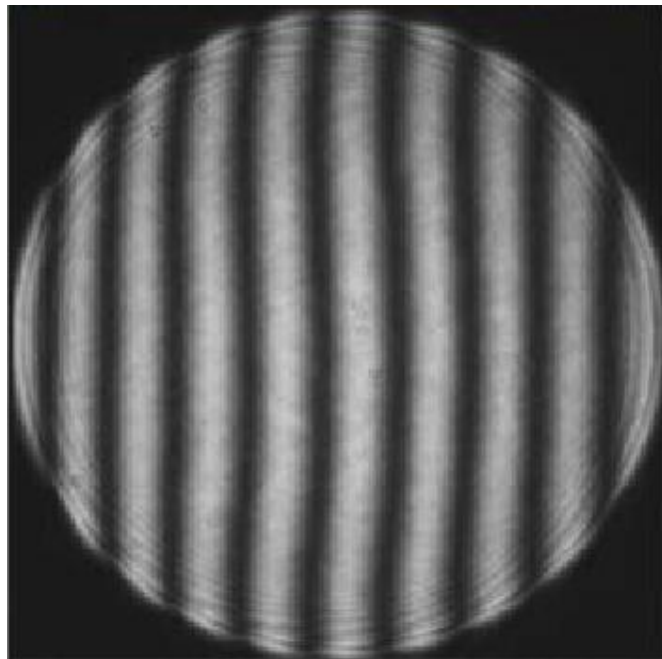
Figure 42: An interference pattern formed using a Fisba interferometer.

The difficulty with a static interference pattern is that though fringes are formed by a difference in height it is impossible to establish if the height change is from a rise or fall in the surface. A trench or a wall would both look identical to a static interferometer.

This problem is managed by the compensating plate which is moved through five different positions; the first and final positions are separated by one complete wavelength. A Helium neon laser is used as the source of coherent light required for the interference and works at a wavelength of 632.8nm. For the Fisba a CCD detector is placed at the observation plane, the phase information at each step is collected and analysed. This process allows calculation of the surface topography.

Lateral resolution of this instrument is 49µm and vertical resolution is 3.2nm [2]. Therefore this instrument is particular suited for measuring form accuracy of components. Form accuracy is critically important for optics when trying to reduce aberration effects. In this project the Fisba interferometer was primarily used to check the flatness of polished samples. (It was observed that the polished samples were often showing different curvatures on each surface). The side showing the smallest radius of concave curvature was placed in contact with the vacuum chuck.
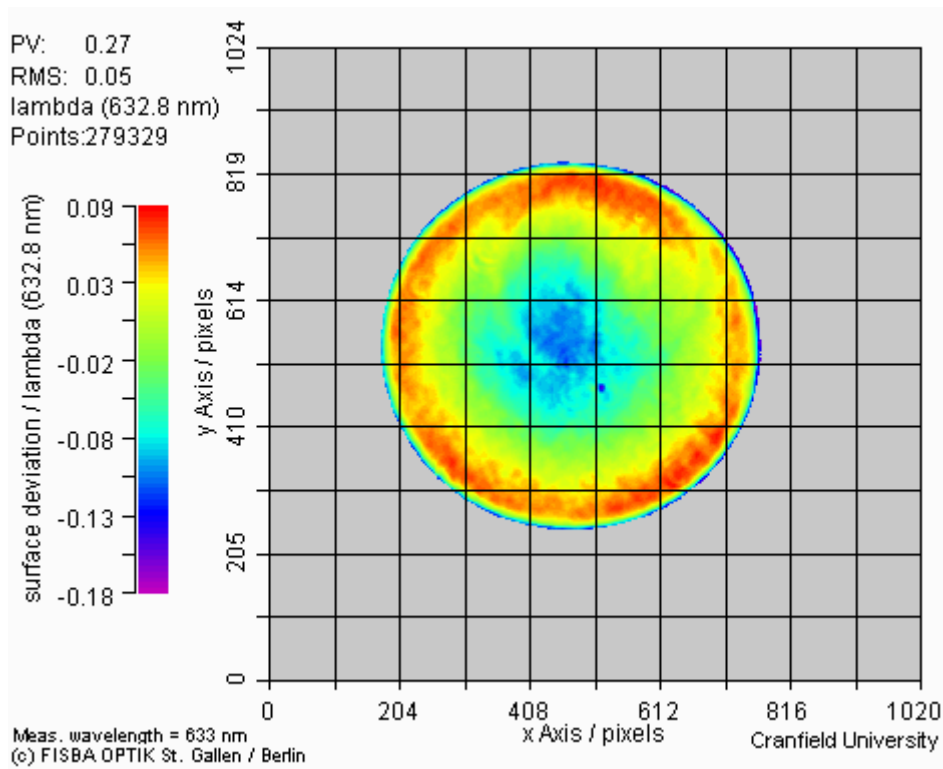
Figure 43: Contour information from the Fisba, showing the curvature of a typical 32 millimetre diameter silicon sample.

In figure 43 the back of a 32 millimetre silicon disc used within the trial is shown. The concave sides were chosen deliberately for a better seal on the vacuum chuck and to ensure that the curvature of workpiece was, as much as possible, kept consistent between tool assessments.

The resolution of the Fisba is insufficient to provide usable information on surface finish. Therefore, when machining optics the Fibsa must be used as part of a series of metrology steps if form and surface finish tolerances are to be measured.

3.3.3 Talysurf CCI 6000

The Talysurf CCI 6000 is a commercially available instrument that is used to accurately measure surfaces. The instrument works on the principle of Coherence correlation interferometry; a process where interference fringes are formed at a specific stand-off point from the imaging optics. In the CCI instrument this is achieved by using a Mirau interferometer. This focal point is then scanned across the surface by changing the height of the imaging objective (on this instrument the vertical range is 100μm). As the fringes form at a specific height above the surface accurately knowing the height of the microscope while it scans can be used to reconstruct the height across the scanned surface.

Performance of the CCI instrument is dependent upon the microscope objective used and pixel size, but for this work the x50 microscope objective was used exclusively. Lateral resolution was therefore 350nm, over a measurement area of 0.36mmx0.36mm.

A serious disadvantage of the CCI instrument is the maximum slope angle of the measured surface. The inability to gather information from surfaces that are angled too far from horizontal can result in significant numbers of lost data points when measuring complex surfaces. The CCI is therefore quite well suited for measuring low roughness surfaces with simple geometry such as a polished glass optic.

3.3.4 Scanning Electron Microscope

Scanning electron microscopy (or SEM) is an established technique for high resolution imagery, with the first commercially available apparatus becoming available in 1965 [74]. The SEM is widely used by both industry and universities to gather images at extremely small scales. The huge limitation of optical methods is the diffraction limit, which is limited by the wavelength of light used. Thus a very good optical microscope might have a resolution of approximately ~1 μm, but by using electrons rather than photons, the scale of the diffraction limit is dramatically reduced and resolution is greatly improved.

The SEM works on a very different principle to ordinary microscopy. The principal components of an SEM are the electron gun, electron optics and the electron detector. The electron gun used in the SEM at Cranfield (a Philips XL30 ESEM) is a tungsten filament cathode type gun. The tungsten filament produces electrons by thermionic emission, a process where electrons are given sufficient thermal energy (at 2650-2900K) to exceed the surface energy [74]. The free electrons can then be accelerated using electrostatic techniques. Electron optics uses electrical fields shape the electron beam in a way similar to glass optical components do in conventional microscopy, but make the beam raster-scan the target surface. Secondary electrons generated by the beams interaction with the surface are then detected.

Due to the strong insulating properties of diamond, electrical charge will tend to build-up on the diamond and cause distortions of the electron beam. Therefore environmental SEM (or ESEM) is used, which uses a low pressure atmosphere of water vapour. There are various applications for using this water vapour atmosphere over the vacuum normally used for SEM, but for this application it is the charge dissipation effect of the vapour that helps resolution.

3.3.5 FIB

Focused Ion Beam (FIB) is an apparatus that has found wide use in the electronics/semiconductor industry. It is limited by extremely small milling rates when

compared to other machining processes, but it has a number of advantages. Primarily the ability to machine very accurately at less than micrometre levels is important, however other advantages include the ability to construct nanostructures in 3D and some more niche applications such as ion implantation [75].

Similar to an SEM the FIB accelerates charged particles within a vacuum chamber. The critical difference though is that instead of electrons, metal ions are used to bombard the sample. The FIB at Cranfield uses a Gallium source (which is the most popular option), but there are many other options. Alternative sources used include such expensive options as gold or silver. Stranger options such as uranium or caesium have been used. Alloys are also possible, for changing melting point and for deliberate implantation for some semiconductor applications. [76].

As charged particles, ions are subject to strong electro-magnetic forces. These forces allow correcting lenses to correct the flight of ions and controls spot-sizes. (It should also be noted that the focusing optics is just one aspect of spot-size limits; there are material interactions that also have a strong effect). The electromagnetic force is also used to accelerate the ions to the required energy.

FIB milling is primarily a sputtering method [75]. Sputtering is a mechanism that uses bombarding ions to provide sufficient momentum for the atoms at the target surface to escape the surface energy.

As an energy beam type of material removal process, FIB will inevitably be compared to laser machining. It is worth drawing attention to the huge difference in scale between the two processes though; lasers have minimum spot sizes of approximately 1 μm while FIB can write minimum spot sizes of considerably smaller scale (typically on the 10's of nanometres scale) [77].
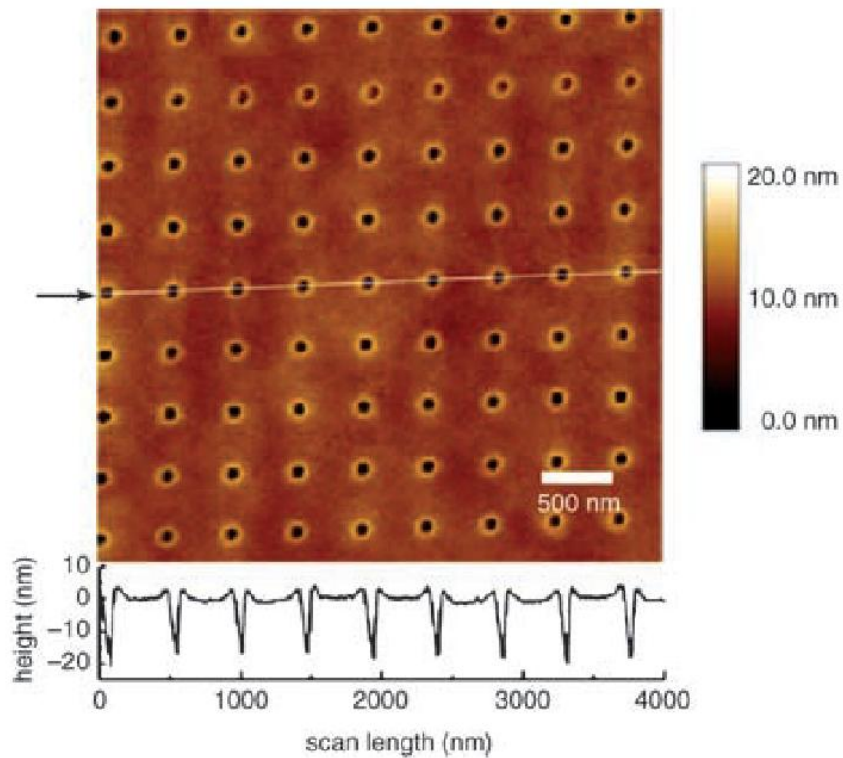
Figure 44: Array of nanoscale holes milled using FIB, and measured using AFM (atomic force microscopy) [78].

Cranfield has pursued FIB based activities for a range of different applications [79], in each case the ability to machine small scale features is critical. This capability is provided by an FEI 200 apparatus, (imaged below).

Figure 45: The FIB apparatus at Cranfield. [79].

An interest in machining complex forms, in particular sinusoidal wave patterns into metal surfaces led to the development of a novel polycrystalline CVD diamond tool.
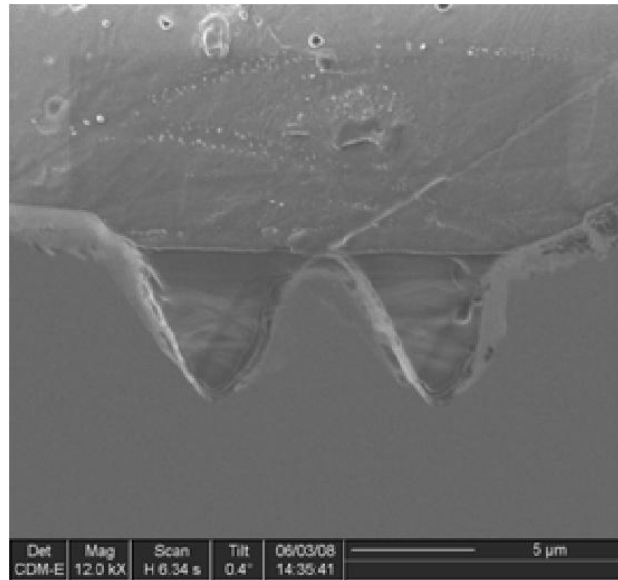
Figure 46: The polycrystalline CVD tool that has been reshaped using FIB [79].

The tool displayed in figure 46 was used to successfully cut sine-wave patterns into a soft metallic work-surface [80]. The change from polycrystalline to single crystal diamond produced some unique challenges for the FIB milling. For example, single crystal is more prone to charge build-up on the surface, and therefore causes greater electrostatic deflection of the ion beam.

In this thesis the FIB was used to re-shape a single-crystal diamond turning tool, to examine geometry effects on the diamond turning (results displayed in Chapter 5). In the FIB trial, a small section of the tool-edge was re-shaped to change an unworn tool to imitate chipping damage to the tool.

3.3.6 Fourier transform infra-red (FTIR) spectroscopy

Fourier transform infra-red spectroscopy is an analytical technique that can be used to identify the composition of materials. FTIR is an important non-destructive technique for analysis of diamond.

FTIR spectroscopy uses a tuneable IR light source to scan across different IR wavelengths and measure the optical response of the material. FTIR can be classified as either reflection or transmission depending on the experimental set-up. Obviously transmission FTIR spectroscopy is dependent on some of the IR light transmitting through the sample so the sample must be thin and/or a weak absorber of IR light. Once the raw data is gathered a Fourier transform is used to reveal the spectra.

FTIR spectra can be analysed to show both the presence of various impurities as well as the concentration of these impurities. There are several examples within the literature of diamond samples being tested using IR-spectroscopy to find either the nitrogen concentration [36] or the presence of specific nitrogen optical centres [21,37]. FTIR has also been used to identify impurities such as boron within diamond samples [37] or to examine the spectra of coloured diamonds [38]. As an optical technique FTIR is limited to testing the bulk properties of a sample and could not, for example, be used to precisely locate a platelet defect.

Chapter 4- Diamond turning results for aluminium using MCC and natural tools

Aluminium is a very useful material for many applications and is very suitable for diamond turning. The softness of the metal and the chemistry of the diamond-aluminium interaction all help to minimise tool-wear. Machining of the aluminium workpiece was performed using the NION machine (detailed in reference [81]). Cutting parameters are detailed in section 3.1.1. Workpieces were of 6061 aluminium and 300mm diameter. The composition of aluminium alloy 6061 is shown below:

Magnesium	1.0 %
Silicon	0.6 %
Copper	0.30%
Chromium	0.20%
Aluminium	The remaining %

Table 2: Composition of aluminium 6061 by weight [71]

In the above table the percentages are done by weight. Aluminium 6061 is an alloy that is used in a huge number of roles, from space-applications to furniture.

Each cut of the surface was made deliberately shorter than the previous cut. This left an area suitable for profile measurement and allows the R_a to be monitored against total cut length. In total three tools and three aluminium workpieces were used. Periodic plunges into the uncut area of the workpiece surface were later used to calculate wear volume. Contact profile measurements of the plunge combined with SEM images were used to establish wear volume of the diamond tools using a method established within the literature [52].

4.1 Natural tools machining aluminium

Natural tools are used widely for the machining of aluminium. For example, they were used in the MIRI instrument for the James Webb space telescope project [82]. Though total achievable cut distance is so long with aluminium that tool-life is not a limiting factor for most industrial applications, industry does find the unpredictable tool-life of natural tools undesirable.
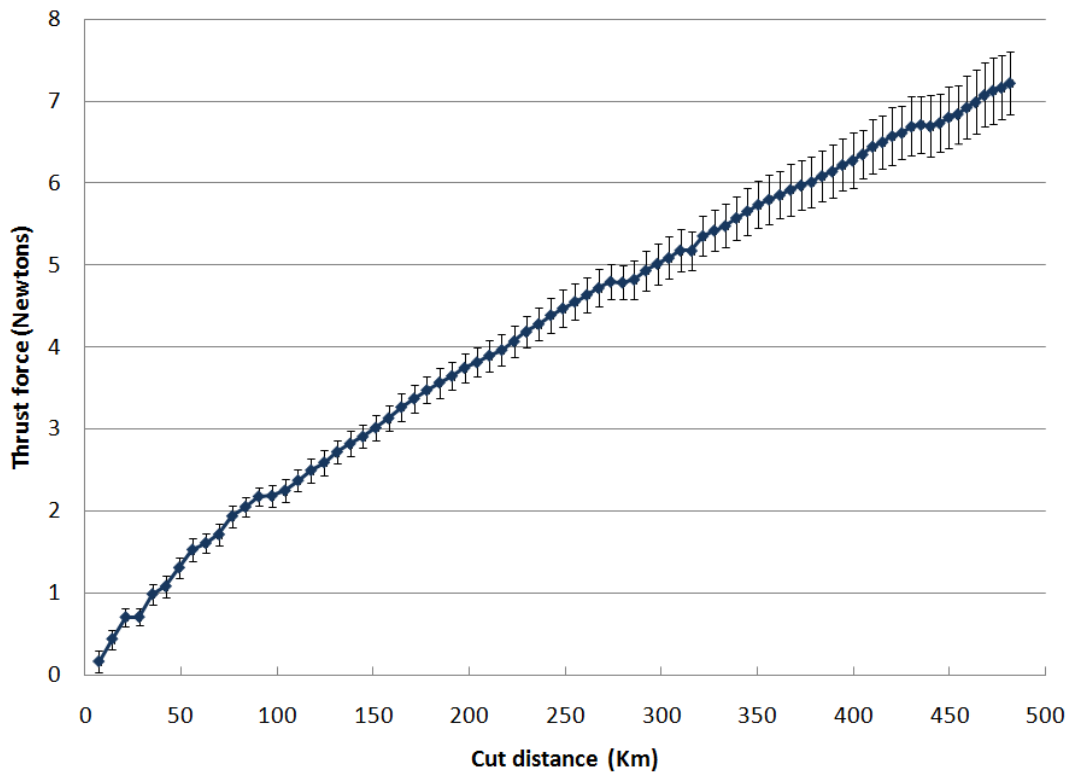
Figure 47: Cut force progression for natural tool while machining aluminium.

Testing the natural tool in this way provides the base-line for comparison with the MCC synthetic diamond tool. Differences in cutting forces, surface finish (measured using the Ra surface parameter) and analysis of the wear-scar all provide important metrics for the performance of the tool materials.

4.2 MCC tools machining aluminium

To the authors knowledge, this thesis is the first significant wear trial for the MCC single crystal CVD diamond material against aluminium. The MCC material is a synthetic material and therefore free from most of the issues associated with natural. MCC diamond has lower internal stress and lower concentrations of nitrogen and other trace impuries typical of natural diamonds. Crystallographic defects such as stacking faults area also found in much lower concentration within the MCC material [22]. The purity and the consistent quality of the MCC material makes it exciting as a possible tool material for single point diamond turning.
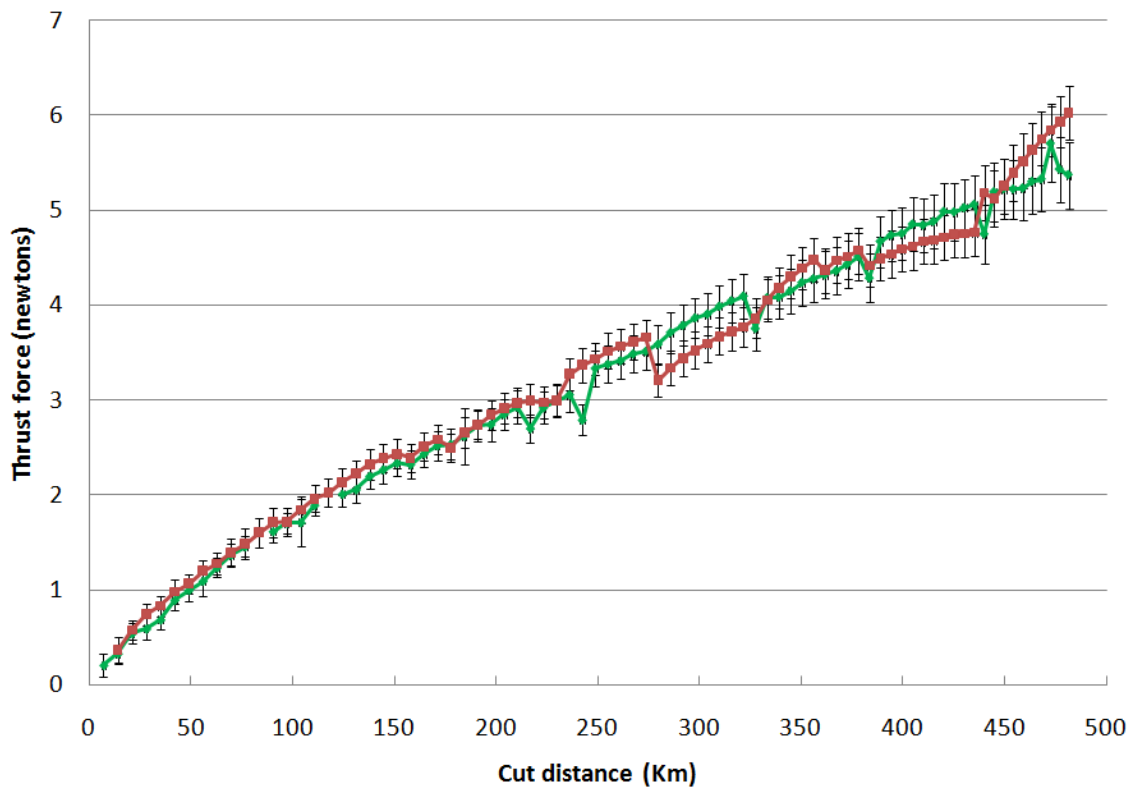
Figure 48: Cut force progression with increasing cut distance for the MCC synthetic diamond tools while machining aluminium.

MCC tools were tested twice. The results are consistent with each other and display a lower cut force is being generated when compared to natural tools. Graphing these two tool materials together aids this comparison.
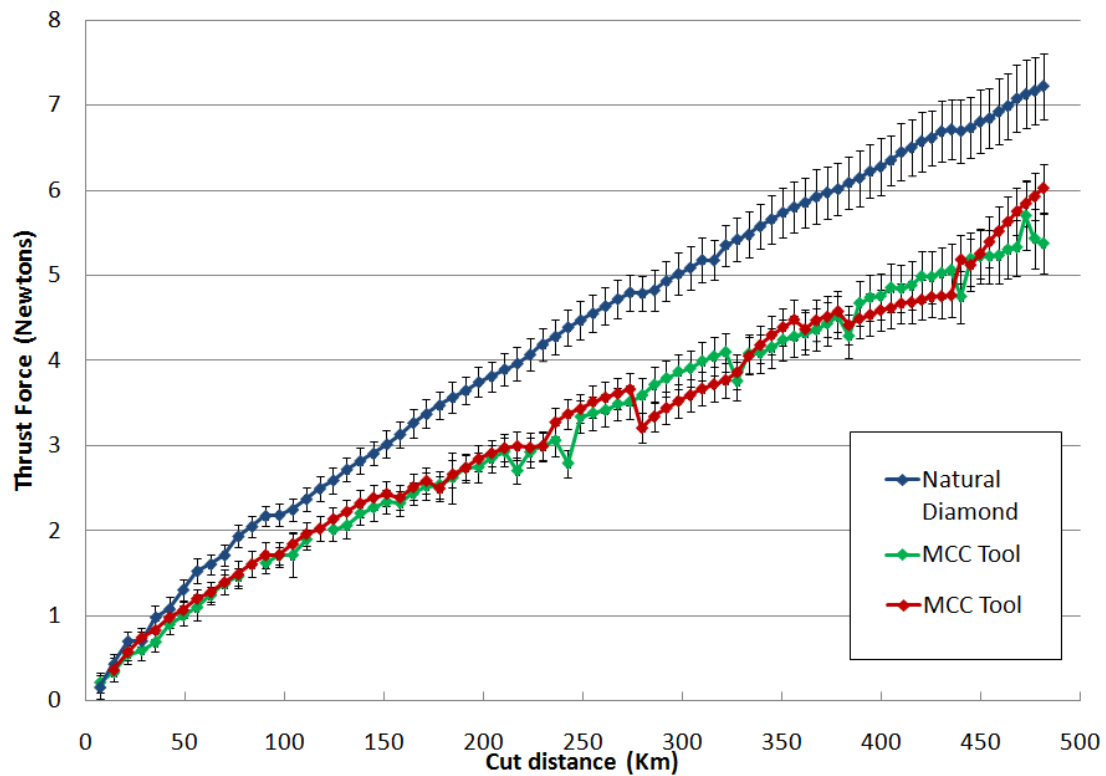
Figure 49: Comparison of cutting forces between natural tool and MCC tools.

From the above graph, it is clear that MCC tools are generating less force than a natural tool does over the same distance. A tool that generates lower cutting forces can be extremely useful when machining workpieces that easy distort. Regardless of workpiece geometry, the form accuracy can be compromised when forces rise to a level where they are causing a displacement of the axes or spindle. Cutting forces are not typically the deciding factor on the failure of a diamond tool. Most often, it is either the geometry of the tool changing due to volumetric wear or the surface roughness will rise to an unacceptable level.

4.3 Wear behaviour of MCC and natural tools against aluminium

The work of D.Keen [51] presents results on the wear of diamond tools when machining aluminium and is an early paper to observe the fluctuation of wear behaviour between tools: the earliest example of the supertool phenomena found for this project.

Oomen's paper [48] is another useful work that takes a broader interest in the different possible tools and a range of workpiece materials. This paper is relevant for the work on the synthetic diamond tools and because of the testing on the aluminium alloys T633 and T094. A more recent paper that machines aluminium 6061 [83] and which features a very similar machining methodology and shows a great interest in the removed chip.

990500 15KV X10.0K 3.0um
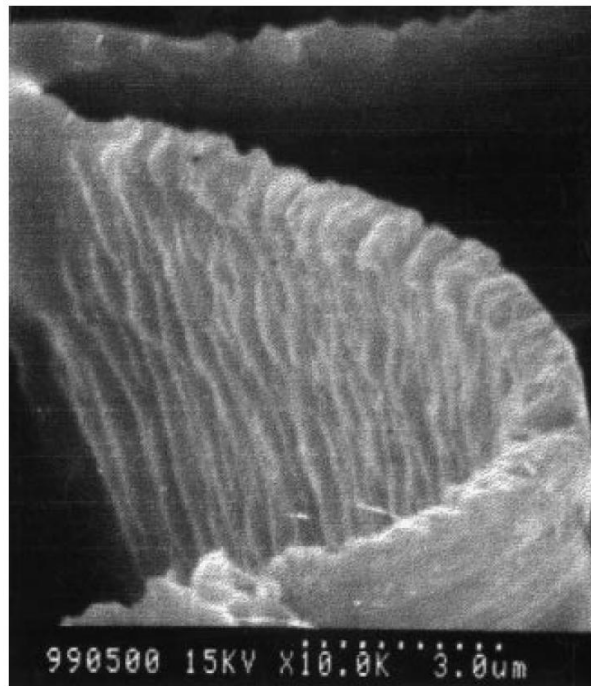
Figure 50: SEM image of a chip of aluminium swarf. [83]

All the references mentioned [48,52,83] note the variability of the wear characteristics of diamond tools but few agree on what is the most important cause of that variability. Composition of the diamond [48] and orientation [84] are both given as critical reasons. The work presented in this thesis is interesting as the impurity concentration is much lower for MCC than in natural diamond tools.

A difficulty that large wear volume brings is the error in tool position that occurs. The tool centre position is important for cutting radiuses or free-form optics. Excessive wear of the tool-tip can cause an offset error of the tool-centre and this error will propagate into the cutting surface if machining any surface more complex than a flat. Therefore with aluminium machining (and soft materials in general) the effect of wear upon surface finish is not the only effect of concern. Indeed a large volumetric wear can give

the diamond tools an effective tool radius that is much larger than the original value; therefore wear can imply an improvement of the cutting performance when for many applications the level of wear would be problematic in regards to form quality.
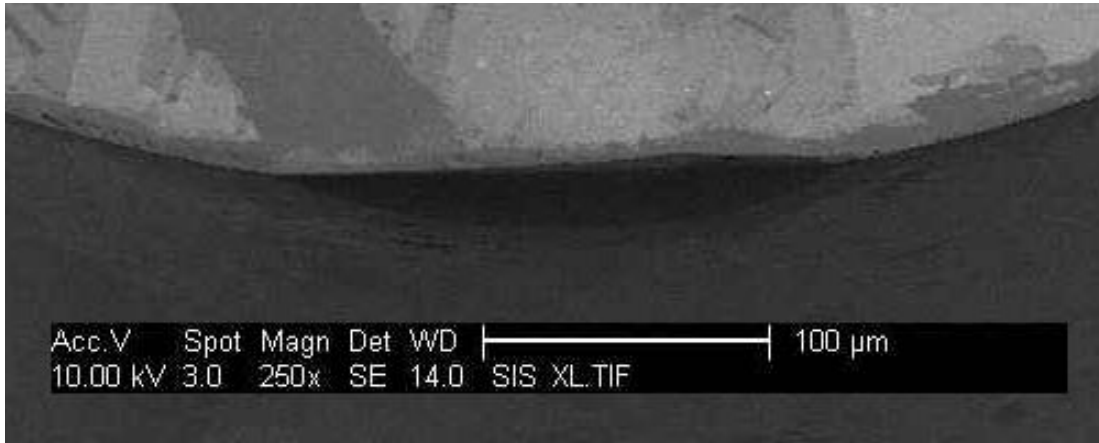
Figure 51: MCC tool (number S83781) after completion of cutting trial.

The above figure displaying the wear behaviour of the MCC, wear-scar length is 202µm and 24µm wide. The other MCC trial gave a wear-scar length of 198 µm and a width of 32 µm.

The wear behaviour of the MCC synthetic diamond material displays a very similar wear-scar to the natural diamond.
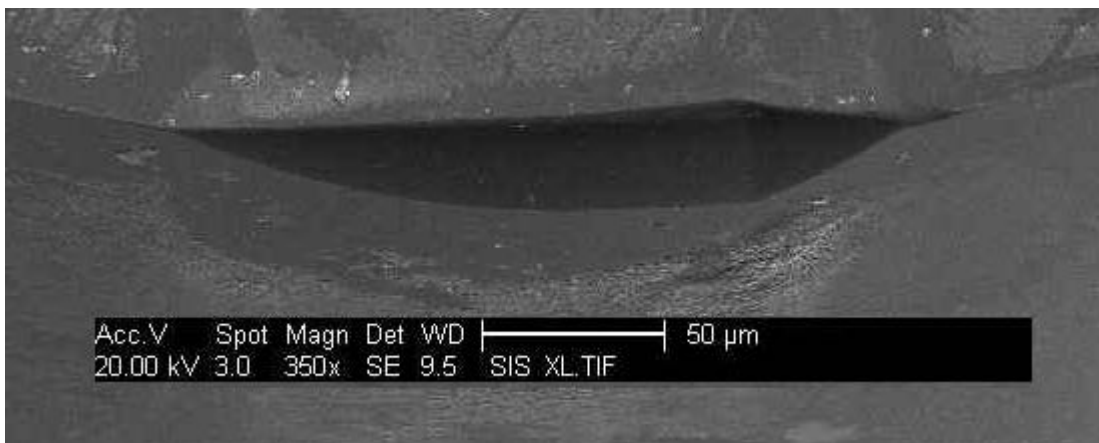
Figure 50: Natural diamond tool after completion of cutting trial.

SEM images of the natural diamond tool displayed a wear-scar length of 204 µm and a width of 28 µm: very similar dimensions to the MCC tools.

All wear-scars from the aluminium trial grew to large scales (large when compared to the wear-scar images taken during machining of silicon), however this did not have a negative effect on the machining being performed. Indeed the formation of a large wear-scar can be advantageous when cutting flats, though it can lead to form inaccuracies when machining more complex geometries.

Surface finish, often defined using the R_a parameter, is critical for many applications. The profile parameter R_a is often the main parameter used for defining if a surface is within tolerance. When machining soft materials this is most often the method to determine tool-life. Uncut flat areas on the aluminium workpiece were deliberately left for measuring R_a.
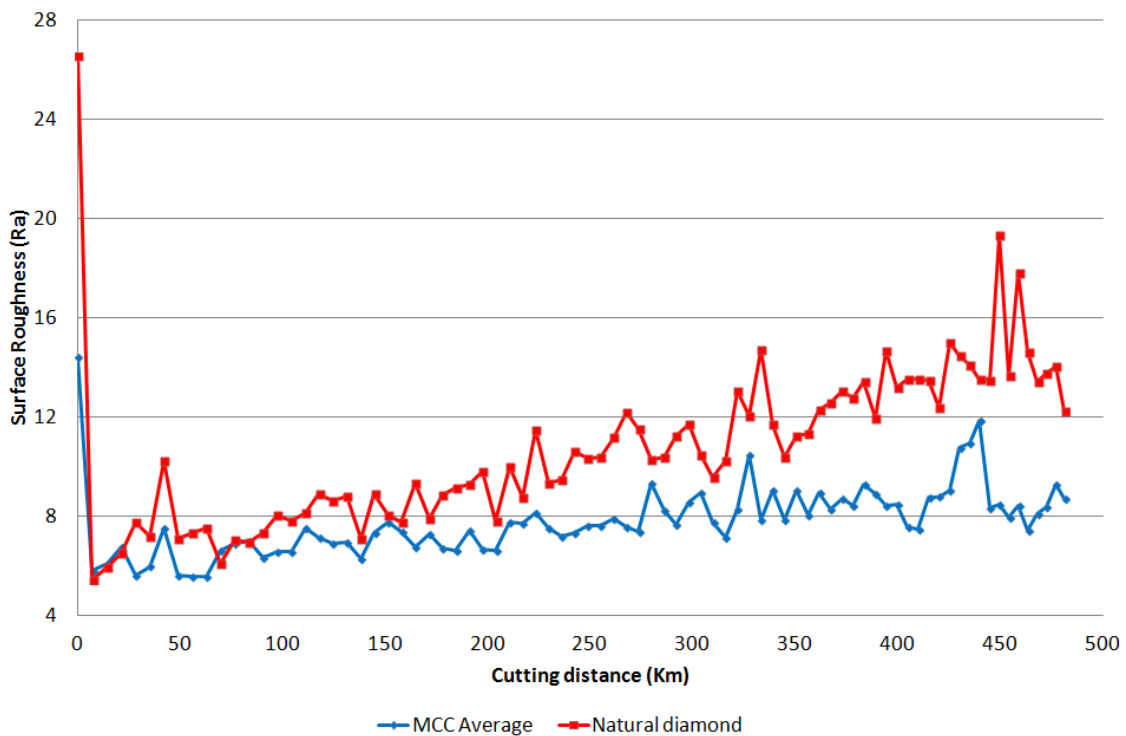
Figure 53: Roughness of the aluminium workpieces against tool cut-length

Roughness can be seen to generally rise as tool cut distance increases for all tools. Tools made from the MCC material display a generally lower increase in R_a when compared to the natural tool.

While turning silicon there is a clear transition of cutting mode from ductile to brittle. As aluminium does not display this behaviour the failure of a tool to cut satisfactorily is

almost entirely dependent upon the workpiece demands. For example a particularly small or thin workpiece could be distorted out of tolerance by rising cutting forces. A workpiece of higher geometrical complexity requiring high form quality could be cut out of tolerance by larger volumetric wear, or from higher cutting forces causing distortion of the machine axes. While cutting flats, large volumetric wear can have the result of increasing the effective tool radius. This effective increase of radius works to lower the theoretical P_t (a detailed derivation of this calculation method can be found in the paper by Blake and Scattergood [5]). However any small chips to the tool edge will likely cause roughness to rise as these defects are printed through into the workpiece. but this surface parameter is also highly dependent on the spindle error motion of the diamond turning machine that is being used. Therefore during cutting of flat workpieces, a tool that is experiencing a lot of wear is going to indicate that the surface is still of good quality (possibly even improving), making it a poor indicator for the condition of the tool on its own, and should be used with other metrics.

Tools made from the MCC CVD material were also used in industrial trials. These were performed at Qioptiq ltd, and though specific data was not forthcoming from these trials, the reported general impression was that these tools are a better performing alternative to natural tools for aluminium machining. The only possible disadvantage to be mentioned was a tendency for MCC to cut a rougher surface once the tool had failed, when compared to natural tools. This transition was found to be more sudden with the MCC and after a greater cut distance than the natural tools had machined. This sudden transition is going to be of more interest when discussing the results from the MCC machining of silicon, discussed in Chapter 6.

In summary of the aluminium trial results, the MCC tool material has been shown to be extremely well suited for this application. As machining aluminium is similar to electroless nickel and copper (and other non-ferrous metals) the MCC synthetic diamond material would appear to be particularly suitable for this application. Though machining trials to validate this would be a suitable future action. Regardless of which criteria the tool is tested against, when machining aluminium the MCC tool material is shown to be superior tool for machining aluminium.

Chapter 5- Diamond turning results for silicon against HPHT and natural tools

5.1 Natural tool trial

Testing of natural tools was required to provide a baseline comparison for the synthetic diamond materials that would be tested later. The natural diamond tools tested (tool serial numbers S65315 and S65317) had been previously tested as part of another trial at Cranfield [2,52], however that trial was primarily seeking to determine optimised cutting conditions though tools were tested until the onset of brittle fracture on the silicon workpieces. These previous results indicated one of tools (S65317) could achieve (consistently) superior cut distance, the other tool (S65315) is taken as a representative of normal tool-life tools. The previous work also confirmed that the refurbishment of the tool did not have any significant effect upon the tool life [2]. Therefore by including these tools the unusually long tool-life behaviour can be examined as well as normal tool behaviour. Testing these two tools gives the minimum number of trials required to examine normal tool behaviour and the unusual tool-life exhibited by some tools. Both tools were nominally identical: 0.5mm tool radius, -25 degree top-rake angle and 10 degree clearance angle, (the standard configuration for the tool trials in this work).

The total cut distance achieved by the normally performing natural diamond tool (S65315) was 32.17 Km (40 cuts). The superior tool (S65317) achieved a total cut distance of 64.34Km (80 cuts).
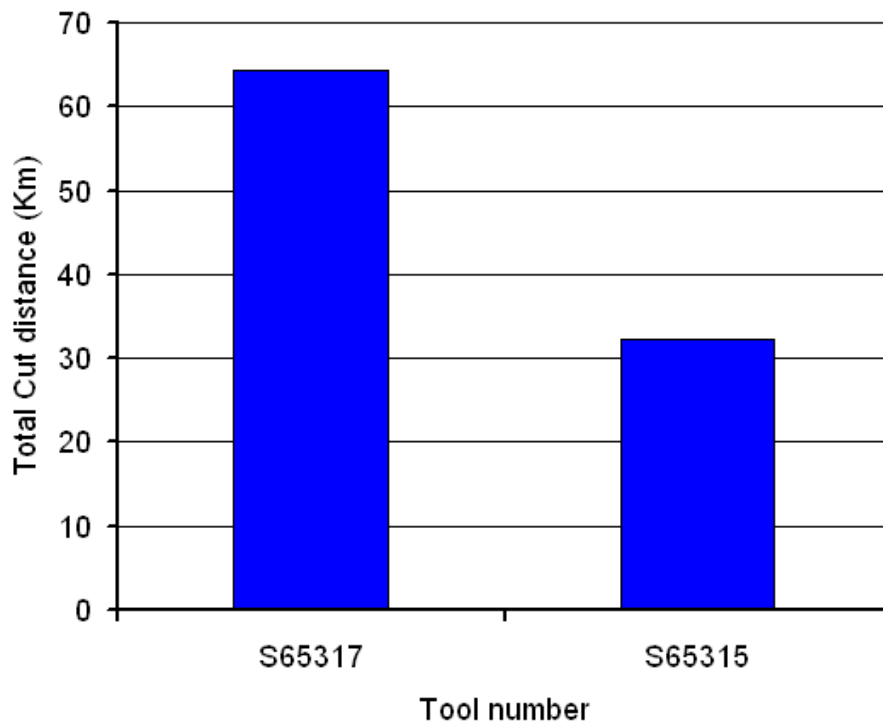
Figure 54: The comparison of results for tool S65317 and tool S65315.

During the trials the cutting forces were measured using a 9256C2 model Kistler dynamometer. The thrust force against cutting distance is shown in figure 55. (Each data point is the mean average of the thrust force during the length of the cut), while standard deviation of force is used as the error bar.
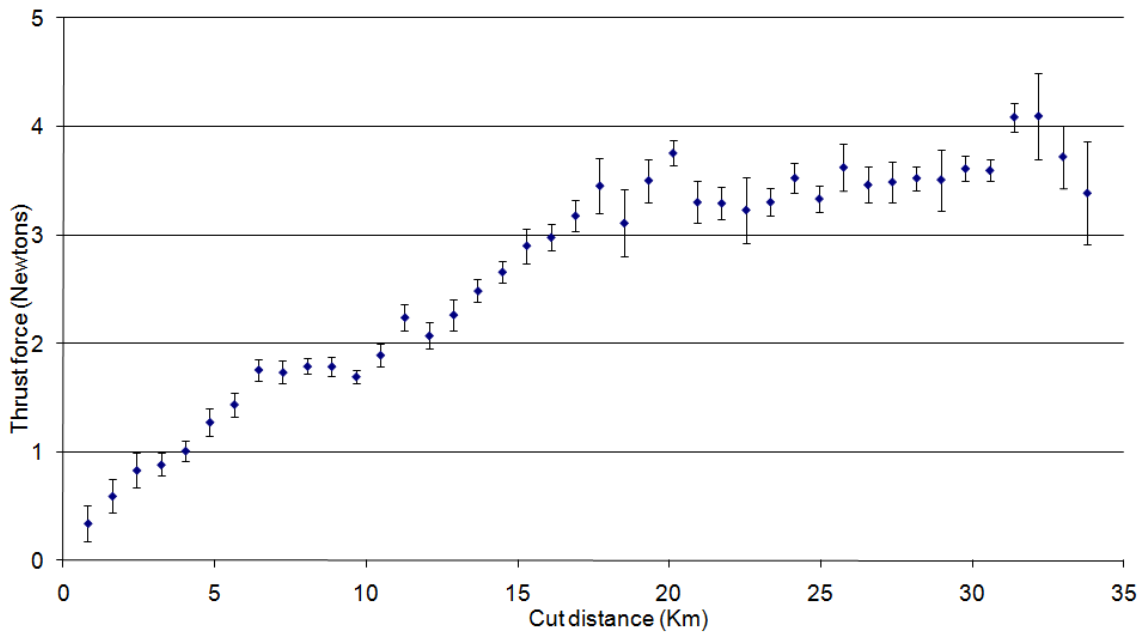
Figure 55: Mean average thrust force against cut distance for natural diamond tool S65315

In the above curve (figure 55) the forces rise to a higher final value than the mean average cutting forces achieve for tool S65317; as can be seen in the graph below (figure 56).
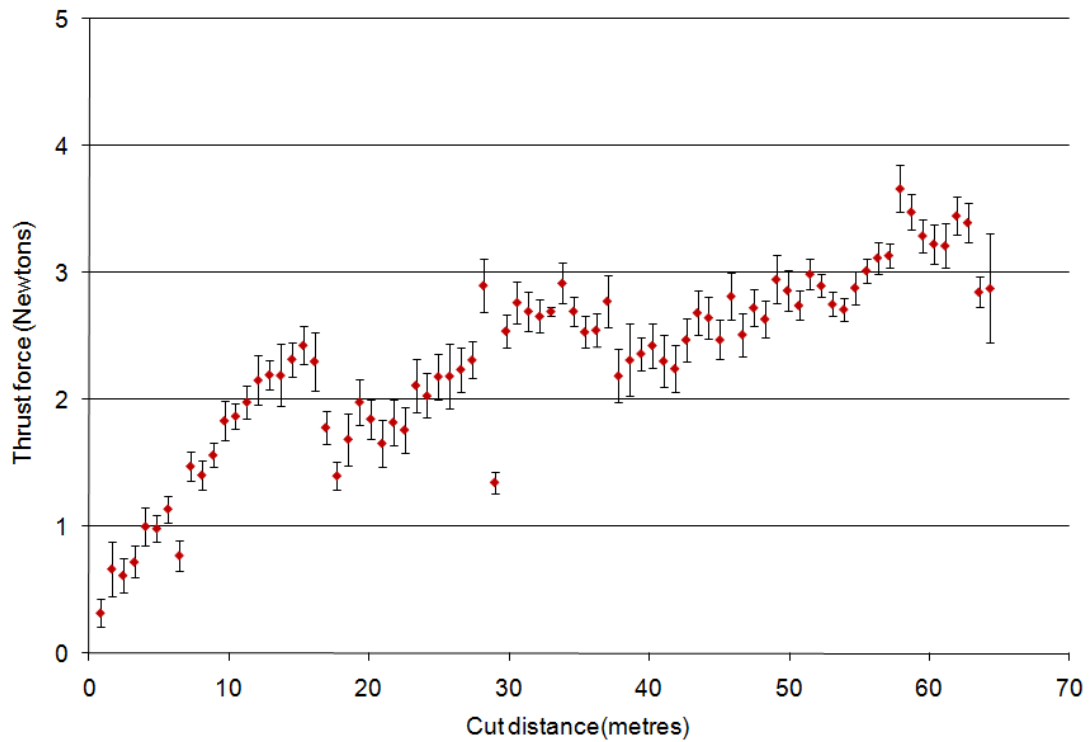
Figure 56: Cutting force progression of natural tool S65317.

It is notable that the cutting force progression of S65317 appears to have a strong linear trend initially. This is similar to S65315, which indicates that maybe this is common behaviour for all natural diamond tools. To better see the tool behaviour differences the two data sets are graphed on the following page (figure 57).
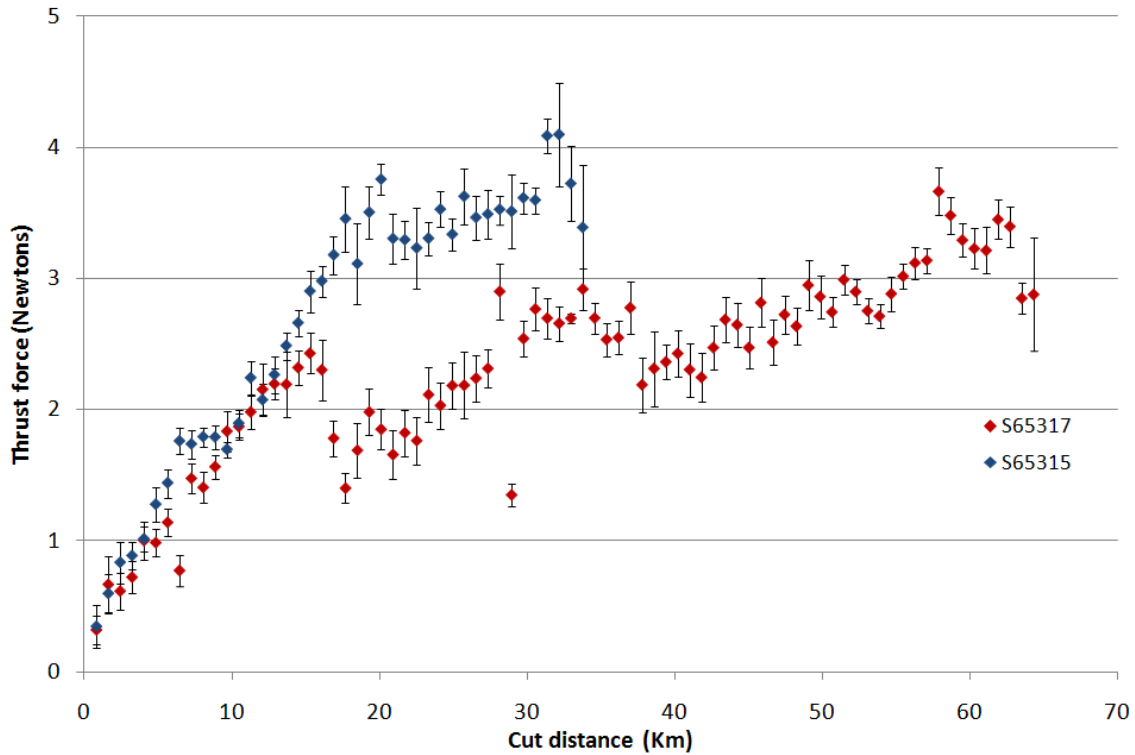
Figure 57: Comparison between natural tools S65315 and S65317.

The cutting force progressions appear similar, though there were two critical differences. First and most obvious, is the achieved total cut distance for tool S65317 is almost twice that of the S65315. Second, the mean average cutting forces at the end of the useful cutting life are different. During the final cut using tool S65315 3.4 Newtons was being generated, while tool S65317 was generating just 2.9 Newtons on its final cut.

Looking at the SEM images we see an interesting feature develop on the cutting edges of both natural tools.
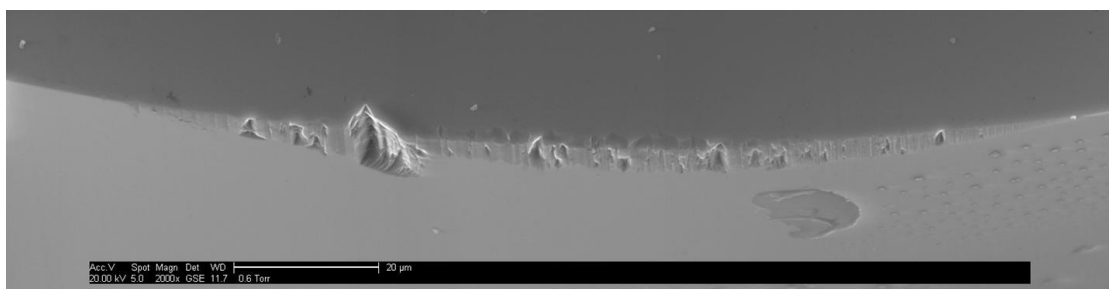
Figure 58: SEM image of tool S65317 taken after the onset of brittle failure.

The SEM image above in figure 58 is of tool S65317 (the superior performing tool). The tool engagement area is showing a narrow band of attritious wear, the so called "wear-scar". The wear-scar appears smooth on first inspection but after careful examination it can be seen that the wear-scar is marked by some regular vertical marks, (assumed to be at the same spacing as the feed rate of the machining process). This tool edge is also showing clear damage in the form of many small volumes of tool that have been removed by fracture (and not attritious means). These small areas of chipping damage along the tool edge are themselves less noticeable than the large volume of damage near the cut shoulder where a large section of the tool edge has been removed by some form of fracture removal.
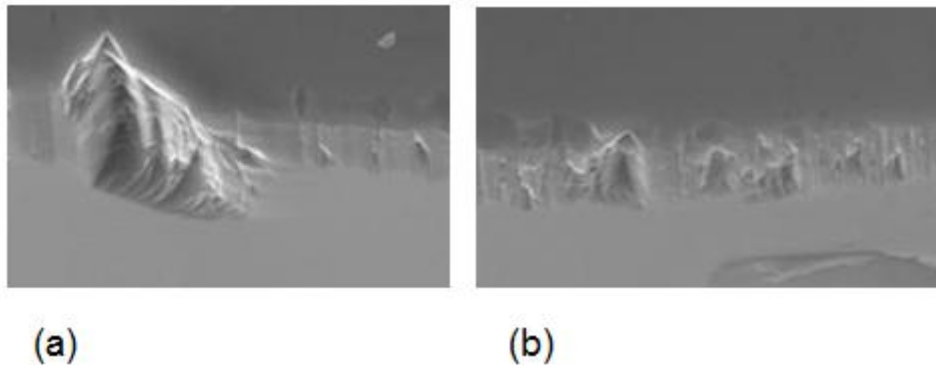
Figure 59: Closer images of (a) the large area of damage on the leading edge and (b) the area of many smaller fractures closer to the tip of the tool. (Tool S65317).

Note that the large fracture area shown in figure 59 (a) propagates entirely through the wear-scar generated by attritious wear. Also in image (b) the smaller chipping damage at the front of the tool which also propagates all through the wear- scar. When the chipping damage propagates all through the wear-scar the removed material per pass (or alternatively, the area that the tool removes with each revolution) is suddenly changed by this fracture. Furthermore from the work of Blake and Scattergood [5] we know that tool geometry, (in the form of the process constant Ψ), can have an influence on the machining process. Another important consideration arises from the work of B.R Lawn [6,8]; the geometry of removed material is important for predicting if the removal mechanism is going to be ductile or brittle.

If geometry changes are causing the failure of the tool to machine in a ductile manner at the generated surface, then many of the papers on the topic of tool wear, especially those focusing on attritious wear rates (such as J.Wilks [82]) are not of any use when trying to explain this failure mode.

Examining the SEM image of the other natural tool (S65315), the similarities to the SEM of S65317 are numerous.
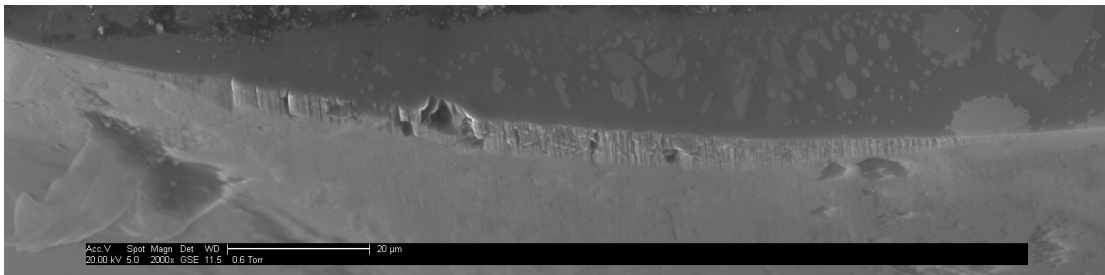
Figure 60: SEM image of the tool engagement area for tool S65315.

However, it is interesting to note that this tool achieved approximately half the cutting distance of S65317 and both have wear-scars of very similar thickness. Implying that the formation of the wear-scar is independent of the cutting distance after a sufficient initial cut distance. Note however that the large fracture damage on the leading edge of the tool does not propagate all the way through the wear-scar. Therefore the original geometry is effectively preserved, (at least in the 2D cross-section examination of the tool which is so important when considering the model proposed by Blake and Scattergood [5]).

The effect of crystallographic orientation was identified as a potential source of the variation in total achievable cutting distance early into the project. Within the literature there are many reports of the material properties of diamond type structures (including silicon and germanium) varying with orientation [3,7]. Links between the orientation of the crystal and the wear resistance ("wear" is used here in the sense of volumetric wear and not tool failure) have also been published [85].

X-ray diffraction is a commonly used method of determining crystal orientations. Measuring of several diamond tools (including tools used within this project and some

that were not) was outsourced to the Diamond Trading Company (DTC). The DTC are experts in analysing natural diamonds. The DTC is part of the De Beers group of companies [85].

One of the difficulties with making any firm conclusion with the XRD work done by DTC is the small sample group, especially considering the three angular degrees of freedom that can have an effect. A main problem is possible inconsistency of the machining situation (not all results were gained using the same coolants, coolant application method and size of the workpiece varied, etc. Not all results were gained as part of this work, and therefore may or may not have been subject to similar enough conditions to draw meaningful conclusions.
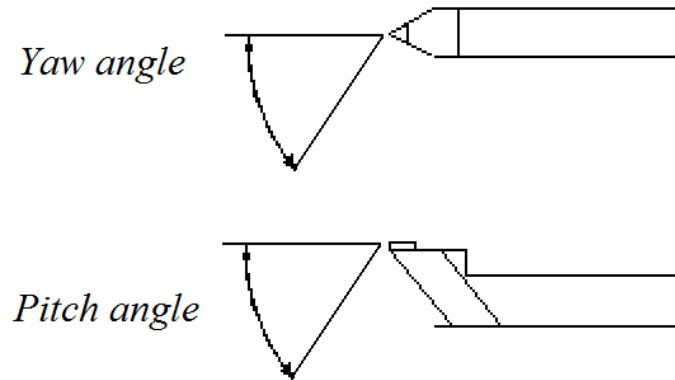
Figure 61: Yaw and pitch angles defined. Roll is clearly active in the third direction.

Each angular degree of freedom is described by yaw, pitch and roll, explained in the previous figure. Though the results were inconclusive, for completeness the results for S65317 and S65315 are given below.

	Tool 65315	Tool 65317
Pitch	4.5	-3
Roll	2	0
Yaw	-8.5	3.5

Table 3: Orientation angles of the two tested natural tools

As can be seen there is significant difference in both the pitch and yaw directions but not the roll direction. It has been mentioned previously that the Young's modulus of diamond (and structures using the same crystallographic unit cell, such as silicon or germanium) has an orientation dependency and that the polishing rate in different directions and orientations varies [86]. How (or even if) this relates to diamond turning tool-life is unclear.

5.2 Original orientation HPHT (100) top-face tools

HPHT is rarely used for machining of silicon. The HPHT tool-material is typically supplied with a [100] top-plane. HPHT does not have a good reputation for wear-resistance, but because it can be supplied in slightly larger sizes than natural diamonds it is possible to make HPHT tools with a very large tool-radius. The [100] top-plane is very resistant to grinding the top-rake onto a tool so the (100/100) orientation HPHT tools were tilted to achieve the correct top-rake angle. Three HPHT tools were tested: three was considered the minimum sensible number considering the variability in tool life known to be such a strong effect in natural tools.

The three tools, S82372, S82373 and S82374, achieved total cut distances of 19.3Km, 20.0Km and 21.7Km respectively. It should be noted that the spindle speed was changed from the standard 1200rpm to 3000rpm for tool S82373. This was done to see the difference between the typical machining speed used at Cranfield (1200rpm) and the machining speed used by Qioptiq (3000rpm) in their manufacturing of IR optics.
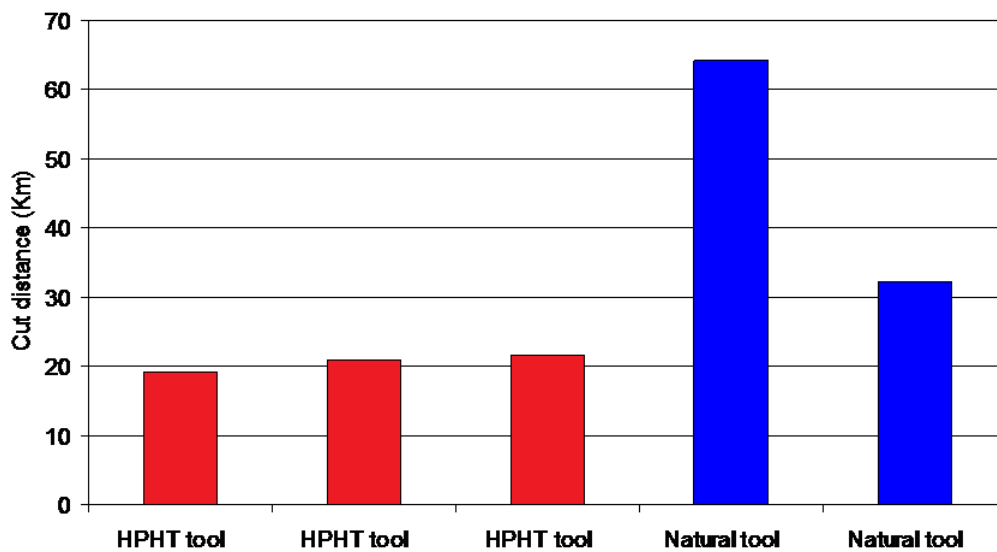
Figure 62: HPHT (100/100) orientation cutting distances compared to natural diamond tools.

It should be noted though that while machining a 32mm diameter part at 3000rpm did not show any excess wear, for larger parts thermal problems could start to manifest. This would originate from the surface speed increase associated with machining close to the edge of the larger workpiece.

The HPHT tool material was found to provide very consistent results, though achieving lower total cut distance than natural tools. It is worth noting that this difference could originate from orientation of the crystal, the HPHT (100) top-face tools have all had the [100] crystal direction tilted by 25 degrees. This idea would be tested when the (110) top-face HPHT tools were used.

The cut forces appear to develop in a different way to the natural tools. While the natural tools display a non-linear curve shape, the HPHT (100) orientation tools fit well to linear trends. This is shown in Figure 63.
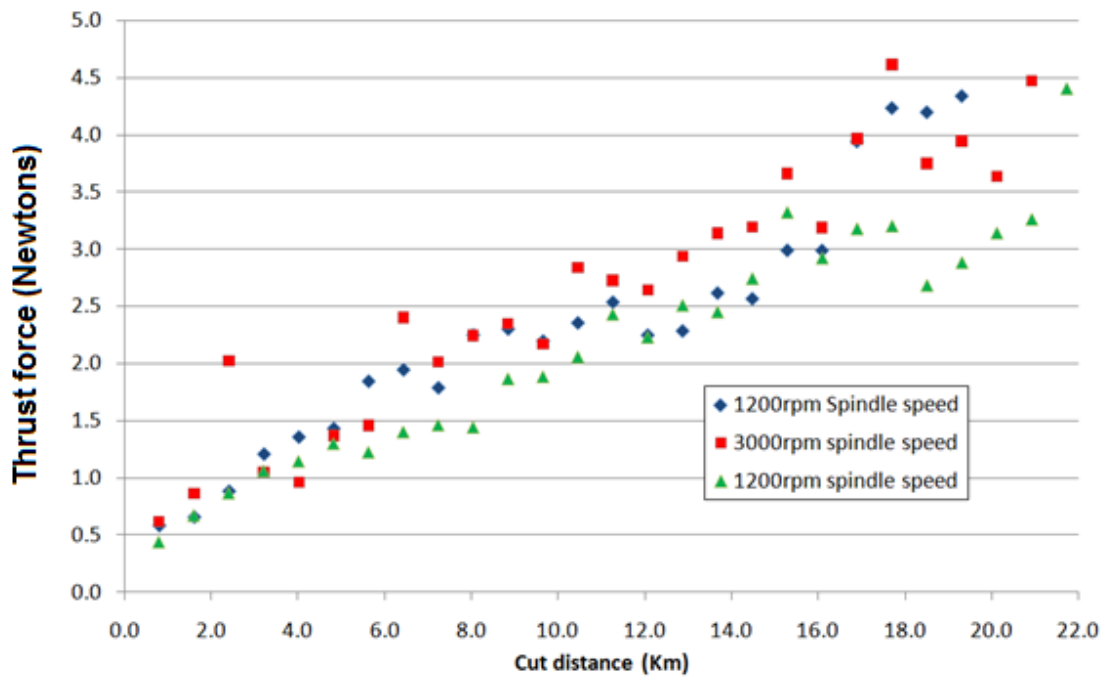
Figure 63: HPHT (100/100) orientation cutting forces.

An interesting point to note is the similar final cut force for each of the tools. The SEM images taken of the tools after failure help explain the difference in cutting forces between the HPHT (100) orientation tools and the natural tools.
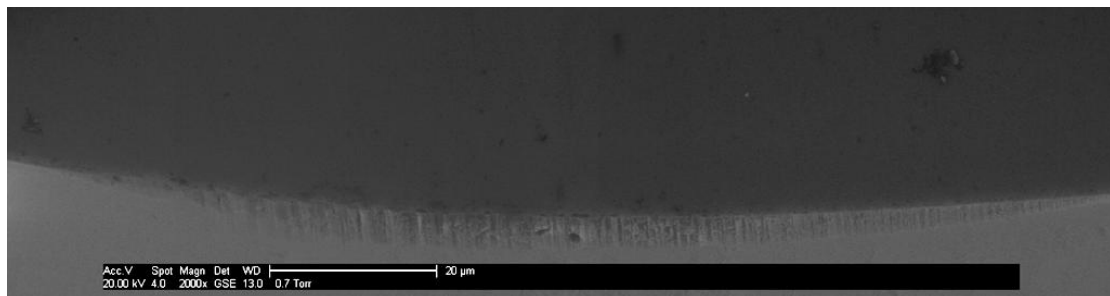
Figure 64: HPHT (100/100) orientation tool (number S82374).

The SEM image in the above figure is displaying a large wear-scar region that is mostly free of fracture damage.

5.3 Variant orientation HPHT (110) top-face tools

Due to the project's close links to Element 6 we were provided with diamond material that had been grown in the correct orientation for use in (110) top-face diamond tools; the same orientation as both the natural tools and the MCC tools. Results from HPHT (110) orientation tools are very important: comparison with the other HPHT (100) results allows analysis of the effect of a change in orientation, while comparing HPHT (110) with natural diamond allows direct comparison of the difference in composition of the diamond materials. The (110) HPHT tools are the best way of linking the results from the (100) HPHT and the natural tools (which are supplied in the (110) top-face orientation) and allowing some sort of determination of the effect of the two variables that are different between the first two tool types (specifically the orientation and the tool material).

Two tools were supplied in the (110) orientation, with three results gathered from them. This is considered the minimum number required for meaningful results. These tools were tested after the first HPHT (100) top-face tools. It was therefore known that the HPHT (100) orientation tools were known to perform consistently and therefore two tools in the HPHT (110) orientation was considered a suitable size of sample for this tool material.
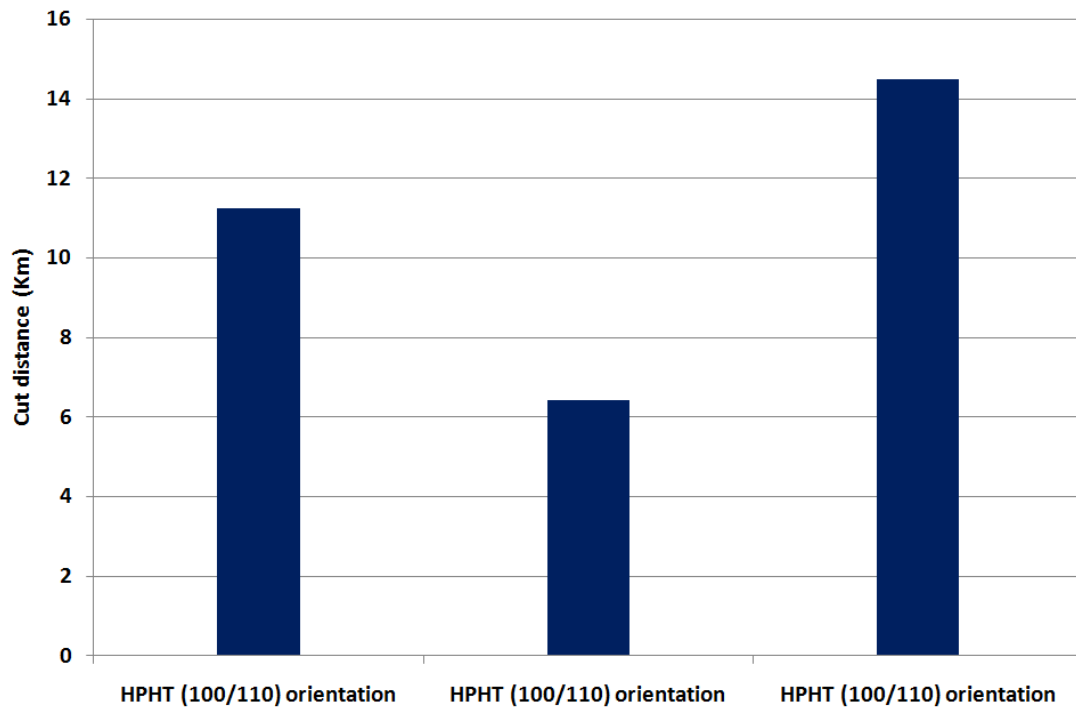
Figure 65: Cut distance achieved by (100/110) orientation HPHT tools.

HPHT in the (100/110) orientation results appear to be much less consistent than the HPHT (100/100) orientation results, implying innate variability in this crystallographic orientation. Also average achieved cut distance with this orientation is lower than the (100/100) orientation.

5.4 Discussion of observed wear-scar behaviour and failure modes

From the cutting force graphs displayed of the HPHT (100) orientation and natural diamond tools it can be seen that cutting forces evolve in different ways for the two tool materials. HPHT (100) tools fit closely to linear trends while natural diamond tools display non-linear trends.

From the SEM images of the tools, contact areas can be estimated and using the force measurements it is possible to calculate an estimate average contact pressure during the final cut. It should be noted that the calculated values are for average pressure over the entire tool engagement length, and that the peak pressure could be significantly higher than these values.

Tool	Contact area (m^2)	Force (Newtons)	Pressure (GPa)	Uncertainty (GPa)
S82372	9.42x10^{-10}	4.34	4.61	±0.58
S82373	9.37x10^{-10}	4.47	4.78	±0.21
S82374	9.62x10^{-10}	4.40	4.58	±0.38
S65317	8.22x10^{-10}	2.88	3.50	±0.52
S65315	8.92x10^{-10}	4.10	4.59	±0.44

Table 4: Contact and pressure information at tool failure [87] Natural tools are S65315 and S65317, remaining tools are HPHT (100) orientation tools.

In the above table, uncertainty values are calculated using standard deviation of measured cutting force and are not an exhaustive treatment of the uncertainty value.

Clearly each HPHT synthetic diamond tools exerted very similar pressure upon the workpiece on the final cut, indicating that there may be a pressure driven failure mechanism. Above a critical average pressure a tool will generate cracks of sufficient length that the generated work surface will have experienced some areas of brittle fracture. Blackley and Scattergood discussed pressure as a route cause of failure to ductile machine silicon [3]. These hints at a pressure failure mode are extremely interesting.

Pressure during diamond turning of silicon is very important, there is a growing body of literature that discusses the possible pressure related amorphisation of silicon (Shibata et al. [12], Jasinevicius et al. [14], Yan et al. [88]). The amorphisation transition for silicon requires significant pressure, 11.3-12.5 GPa has been reported [17] but that value can be lowered by using a shear force, to as low as 8 GPa. Conditions during diamond turning certainly contain a shear force component therefore lower amorphisation pressures will be relevant. There is evidence that the amorphous phase is preceded by a metallic phase [15].

The natural diamond tool S65315 reached a similar pressure to the HPHT synthetic diamonds. Interestingly the superior performing natural tool, S65317, despite cutting a greater distance does not generate as high an average pressure on the workpiece. The

failure of the natural diamond is not adequately described by any pressure threshold related failure and therefore needs another, more complex, description of tool failure.

Re-examining the SEM images taken after the onset of brittle fracture of the workpiece gives the most important clue to the failure modes at work for natural diamond tools.
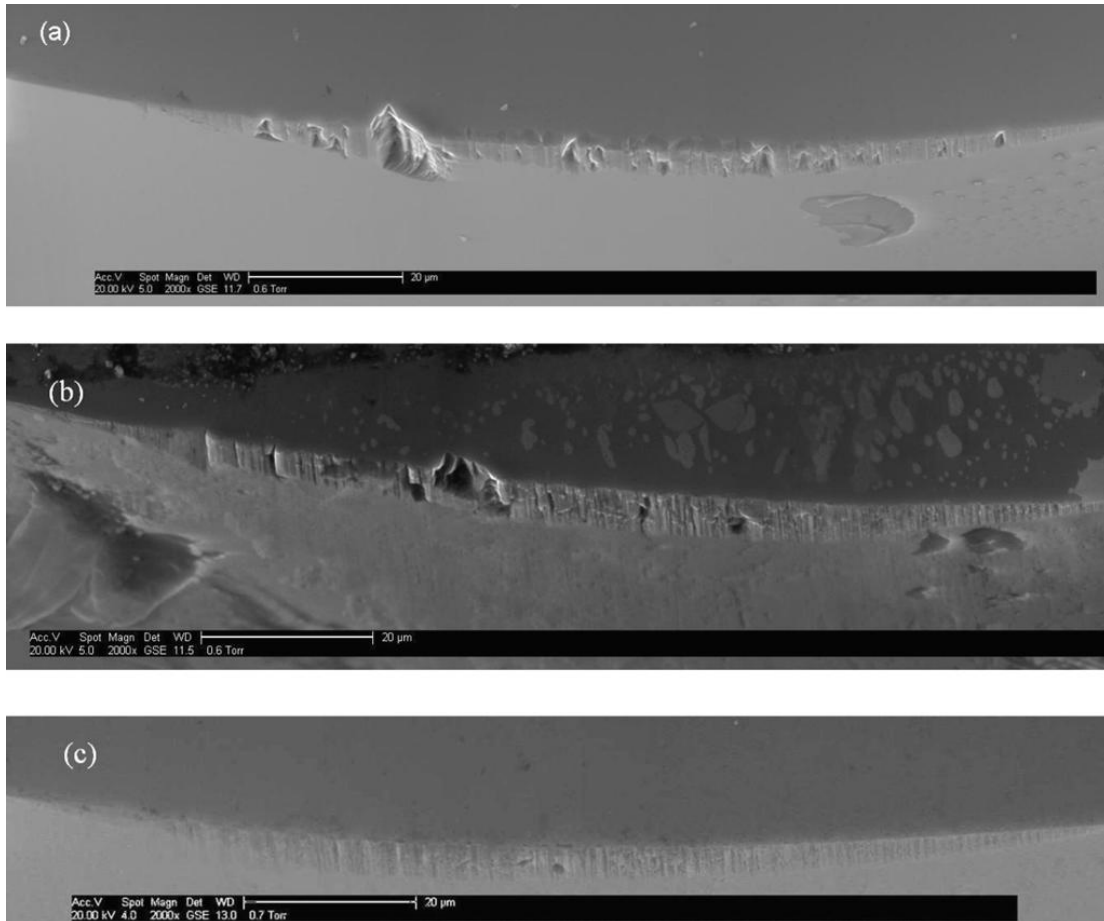
Figure 66: (a) SEM's of natural tool S65317 (b) natural tool S65315 (c) HPHT synthetic tool (Images reported in [87]). The leading edge is on the left of the image.

As can be seen from the images of the natural tools, by the onset of failure these tools have developed large damage areas on the leading edge. This is behaviour that was not displayed by any of the HPHT (100) synthetic tools.

This chipping damage can be seen to extend vertically throughout the wear-scar in the case of S65317 but in the case of S65315 the damage does not extend all the way through the wear-scar. The two natural tools therefore have very different tool-edge

geometries when looking at them from a top-down direction. The tool S65315 and the HPHT (100) synthetics are therefore of a similar tool-edge geometry despite the difference. It appears that tool S65315 and the HPHT (100) synthetic tools are all failing via a pressure related mechanism, while it is now thought tool S65317 is failing via a different mechanism: possibly due to the different tool geometry. Specifically, it is now thought that chipping on the leading edge of the tool changes the shape of the removed material and the result is to generate cracks of sufficient length to propagate into the generated worksurface.

When machining silicon (or other brittle) workpieces it appears that there are two possible failure modes, a pressure failure mode and a geometry failure mode. It would be hugely beneficial if the tool geometry can be experimentally proven to lead to a tools failure to machine in a ductile mode.

5.5 Simulated tool-edge chipping damage using FIB

From the fracture mechanics [6,8] we know that a tool that removes more than the critical thickness will result in cracks that will propagate to the minimum possible crack length. This was later used by Blake and Scattergood [5] clearly indicates that the critical chip phenomena is real. For silicon very small defects (the sort of defect that would remove a chip-thickness of approximately 57nm) produce cracks of 0.4 µm. Clearly if such a defect is less than 0.4 µm above the surface it will be damaged.

However there is an open question about if the cracks can propagate into the generated worksurface from specific geometric defect. Of particular interest was the damage being seen on the leading edge of the natural diamond tools and if they have been causing sufficiently long cracks to damage the workpiece. Can defects that develop on tool edges further above the generated worksurface than the minimum crack length lead to brittle damage of the workpiece. Clearly experimental testing would be needed to establish if such damage on tool-edges could lead to tool failure. It is clearly desirable during such an experiment to separate the effects of tool-edge chipping damage and the volumetric wear of the tool edge. The solution would be found by engineering artificial damage into an otherwise undamaged tool, by accurately removing some diamond from

the tool edge. FIB (focused ion beam) was selected as the method chosen to remove the section of diamond from a sharp diamond tool. This simulated chipping damage was designed to be similar to the large leading edge damage that was found on many of the diamond tools. To keep the damage simple the FIB pattern was formed from sharp edges at right angles to each other.
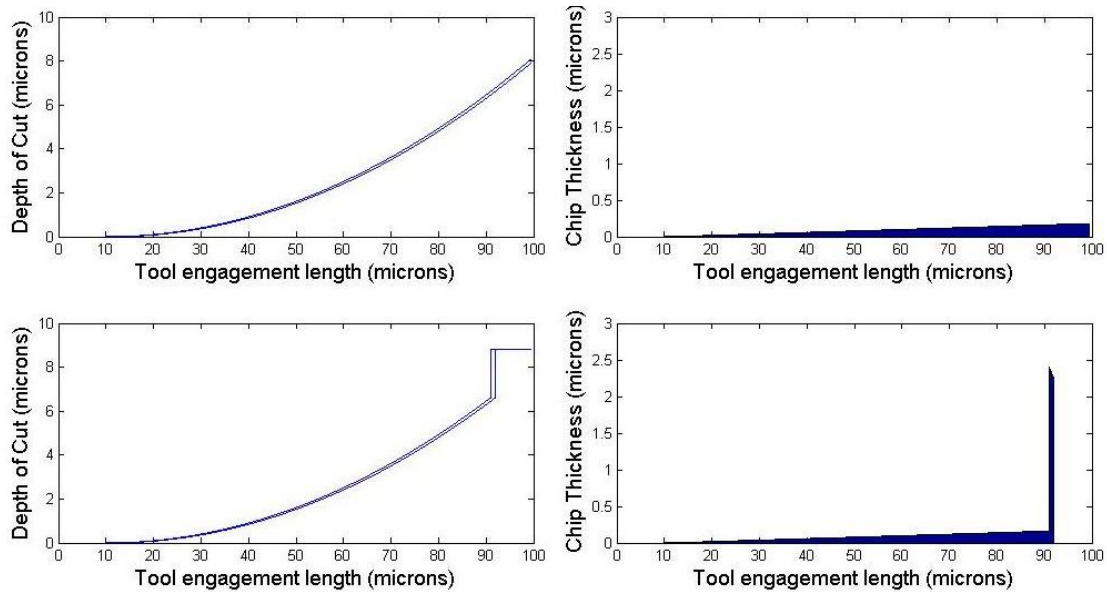
Figure 67: Top row- Tool profile and removed material from an undamaged tool. Lower row- FIB modified tool edge and resulting material removal.

As can be seen in figure 67 the inclusion of damage dramatically changes the distribution of damage across the tool-edge. The position of the FIB damage is extremely important. To ensure the tool was as similar to the damaged diamond tools as possible, the SEM images of the damage on the leading edges of various tools were examined. This simple analysis indicated that the position and size of these defects is consistent, and showed that the tool-experiences larger damage further from the generated surface.

A natural diamond tool (number S65316) was used for the FIB trial to try and reduce any effect from attritious wear on the experiment. Because the damage was positioned high up the tool when compared to the depth of cut two cuts were included in this experiment. The first cut used the side of the tool that had not been altered by the FIB, the second cut used the FIB altered edge of the tool. This ensured that the depth of cut

for the second pass of the tool was extremely accurate and eliminated any off-set error from positioning the tool. Though this added to the distance cut, the additional 800 metres was not considered to add greatly to the wear of the tool, and the need for accurately measuring the depth of cut was considered critical. Normal distilled water coolant was applied and the spindle speed was set at 1200 rpm.

The FIB has previously been used at Cranfield to machine complex shapes into polycrystalline diamond tools [79], but the change in tool material from polycrystalline to single crystal caused some processing difficulties. Specifically, single crystal diamond experiencing ion bombardment will start to gain electrical charge. A build-up of charge on the sample can lead to deflection of the ion beam, which makes imaging of the sample difficult and can cause machining of the sample to be extremely challenging. It was found that a coating of amorphous carbon onto the diamond tool dramatically reduced the problems and can be simply cleaned after the tool has been machined.
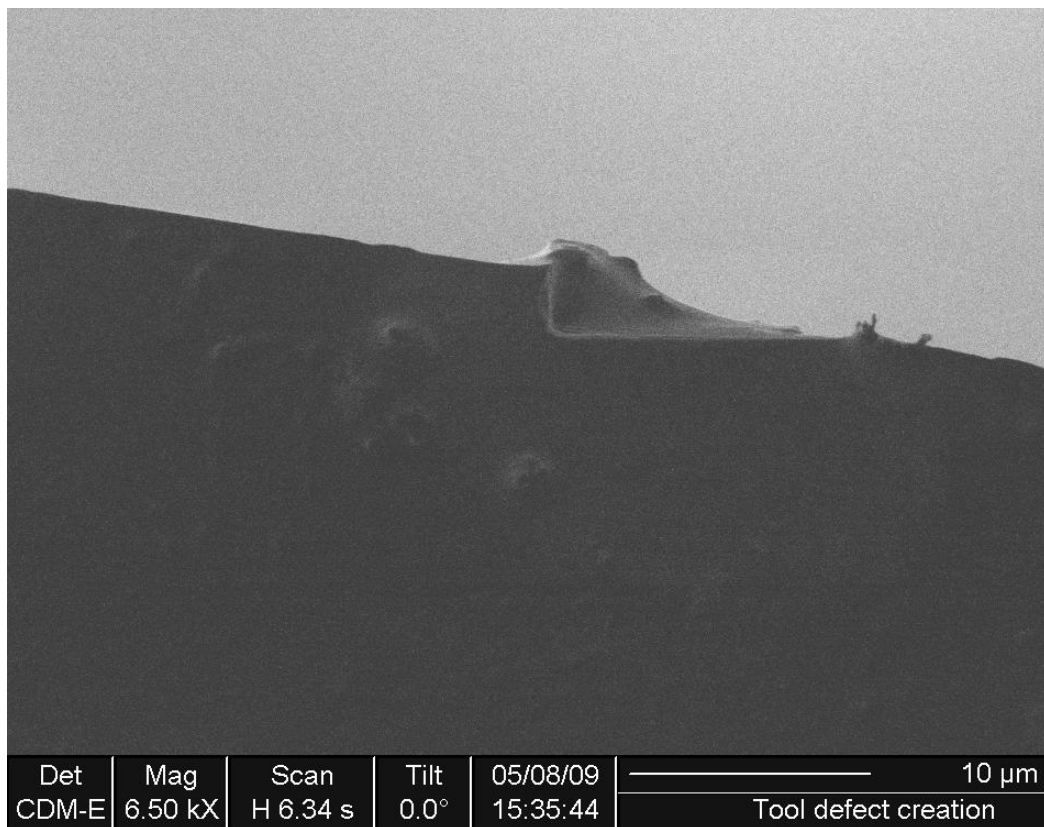
Figure 68: The diamond tool during FIB machining; viewed from directly above the tool using the FIB apparatus.

In figure 68 the damage placed on the tool edge is clearly seen. The image is taken from the FIB equipment. The ability to check the machining in-situ is valuable when machining natural diamond using FIB. The horizontal and vertical sides of the machined area are clearly visible. Also visible is the amorphous carbon, which is left after the ion bombardment. The bombardment of diamond with ions can result in an amorphous residue forming. Due to the softness of this amorphous material, it is expected that it will be easily removed when washed in ethanol or during cutting and will not contribute to the cutting edge during machining.
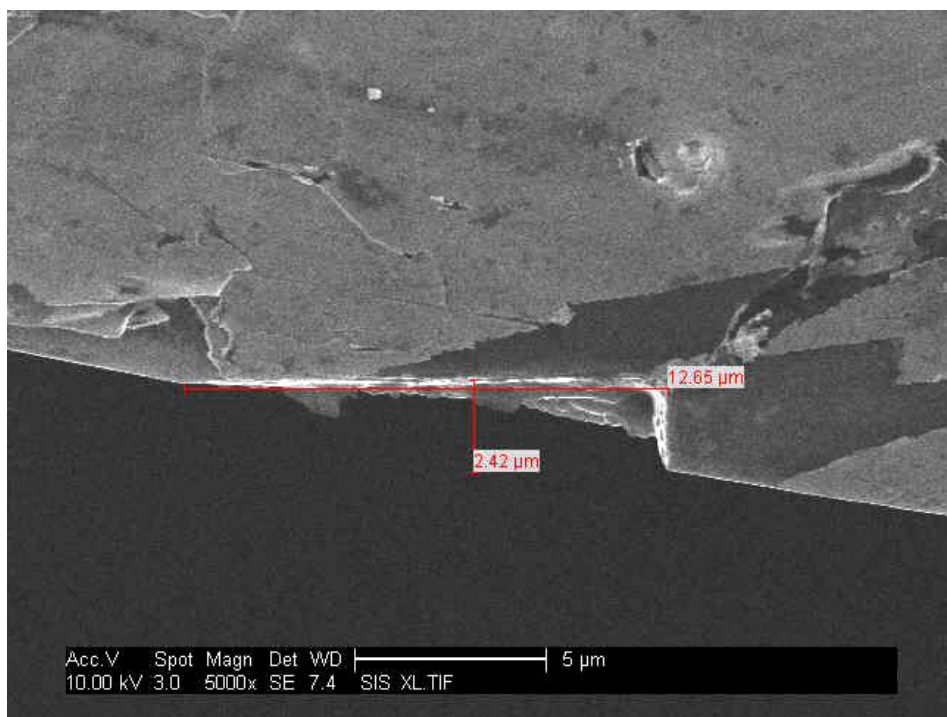
Figure 69: SEM image of natural tool S65316 with FIB damage size indicated.

The deliberate FIB damage is shown above (figure 69). While from the following SEM image, the removed section of diamond is shown to be extremely small.

It is surprising that such small damage on the tool-edge could have such dramatic effects on the workpiece during turning. Forces were monitored using the higher sensitivity Kistler, (the 9256C2 model), as forces of unworn tools had already been demonstrated to be very low. The effect of the FIB damage on the cutting forces was

unknown: the geometry of the tool is unique. However such a small volume of damage was expected to produce only a small rise in the generated cutting forces. This turned out to be exactly the case, as cutting force was found to remain extremely low through the machining of the workpiece.

The machining resulted in the familiar three-lobed brittle fracture pattern being observed on the workpiece. However, the damaged area did not cover the entire surface area and was limited to the outside edge of the workpiece.
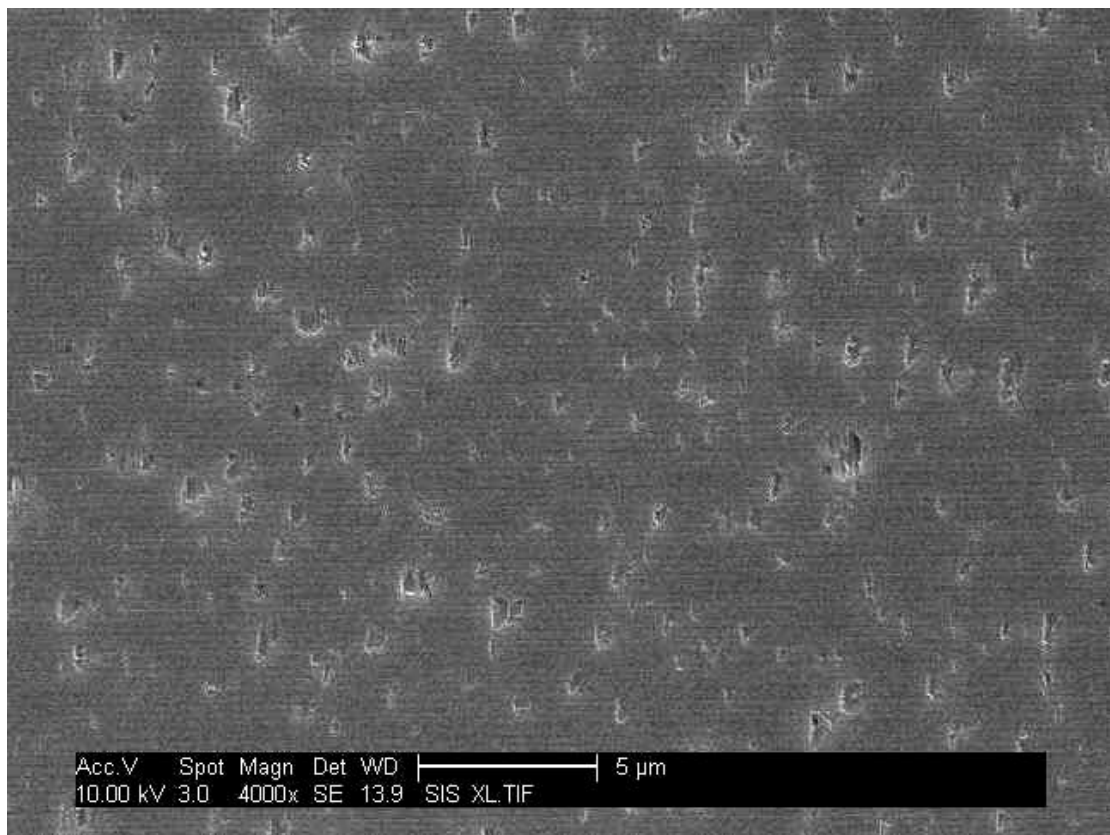
Figure 70: SEM image of damaged area of the silicon workpiece used during machining.

Above, the brittle fracture damage to the silicon workpiece is shown. This clearly shows both the feed-lines produced by the path of the tool and the areas where fracture damage has crossed into the generated worksurface. Despite the presence of brittle fracture though, the Ra values were found to be below the stated industry tolerance of 10nm. However as a contrast an SEM image of the same workpiece was taken at an

undamaged location closer to the centre of the workpeice. This clearly indicates the sort of finish that the diamond turning process can routinely achieve.
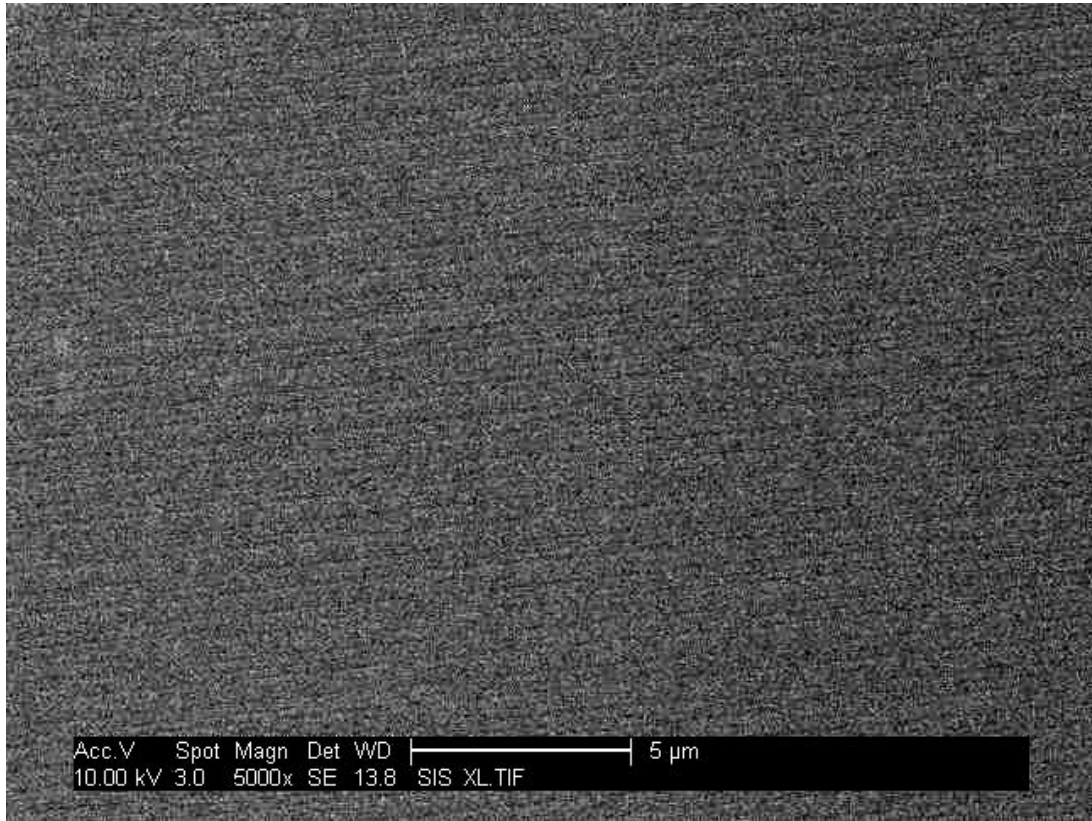
Figure 71: SEM image of a silicon workpiece that has been successfully machined in a ductile manner. Note that this image was taken at x5000 magnification (a greater magnification than the previous SEM) and still remains damage free.

Surface parameters were measured using contact Talysurf, AFM measurements and the non-contact CCI instrument. AFM data from an evaluation length of 25 μm found a P_a of 6.70nm in the areas that have experienced brittle damage and only 3.65nm in the areas that have been ductile machined.

Profile Parameter	Damaged workpiece area	Undamaged workpiece area
P_a	6.70nm	3.65nm
P_q	12.10nm	4.49nm
P_t	97.96nm	21.10nm

Table 5: Profile parameter comparisons of brittle damaged zone and ductile machined area. Values calculated from rough AFM data over a 25 μm evaluation length.

It is clear from the above AFM profile parameters that the brittle damaged area, though within tolerance, has had number of large cracks propagate into the surface. The P_t values in particular indicate that the damaged area has been subjected to deep cracking damage, images of the workpiece profile confirm this.
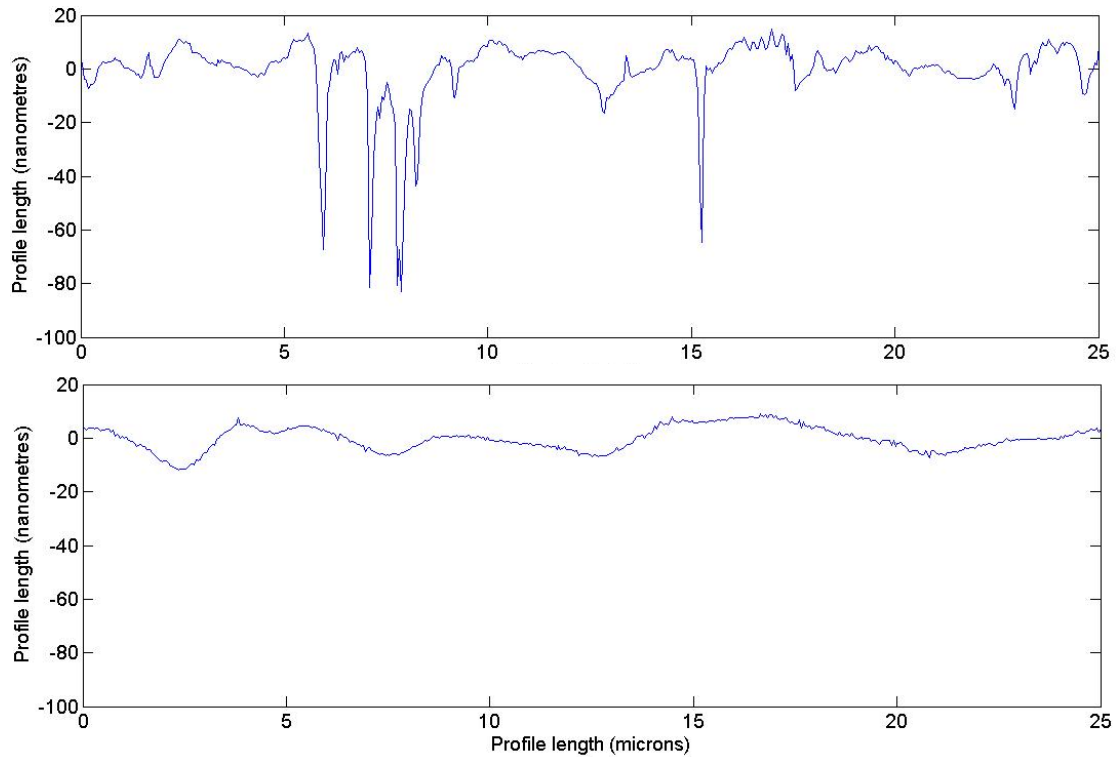
Figure 72: AFM profiles of two regions of the silicon workpiece after machining with the FIBed tool.

In the above figure, the AFM profiles are displayed. The two sets of data shown above are presented on identical scales. Brittle damage is leading to the large cracks into the surface of the workpiece and is responsible for the difference in P_a.
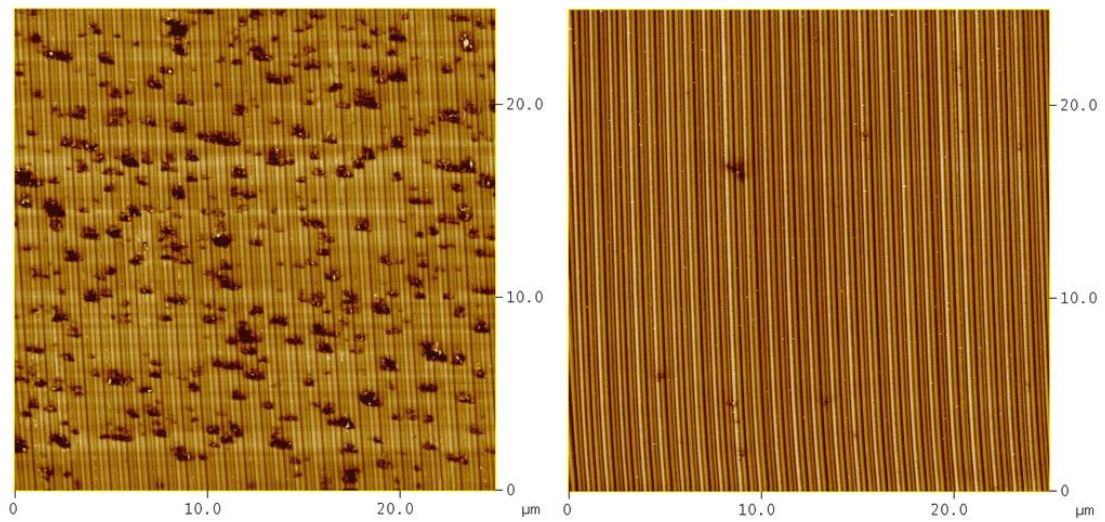
Figure 73: AFM images of the silicon workpiece, showing the difference in surface quality.

Above the AFM images of the workpiece machined in the FIB-induced damage trial is displayed. On the left is the image of the workpiece close to the outer edge of the silicon, the rightmost image is of a section of the workpiece further towards the centre of rotation (and therefore cut last).

Clearly something is causing a change in machining mode from brittle to ductile. As geometry is suspected to be so critical SEM images of before and after machining became important.
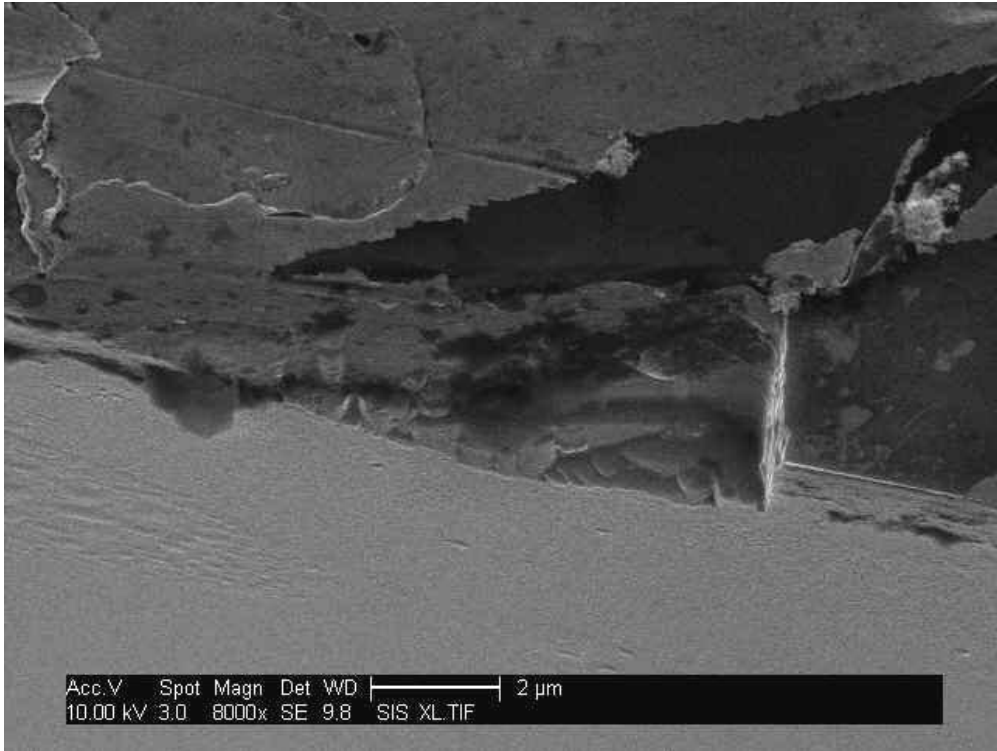
Figure 74: SEM image of the FIB damaged tool prior to machining. Note the sharp edge on the right side of the damage.

Above can be seen the FIB tool before machining and clearly showing the sharp edge to the right of the image.
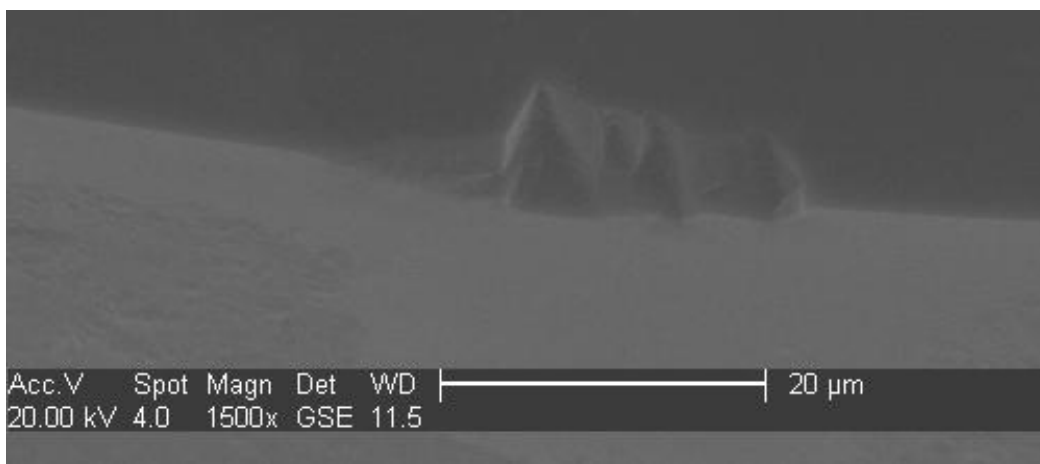
Figure 75: FIB tool after machining silicon.

The above SEM image of the tool after machining confirm that the tool suffered fracture damage during the machining process, appearing to fracture along the (111) cleavage

planes. Total "wear-volume" has increased in this new geometry, but is leading to ductile machining of the workpiece material.
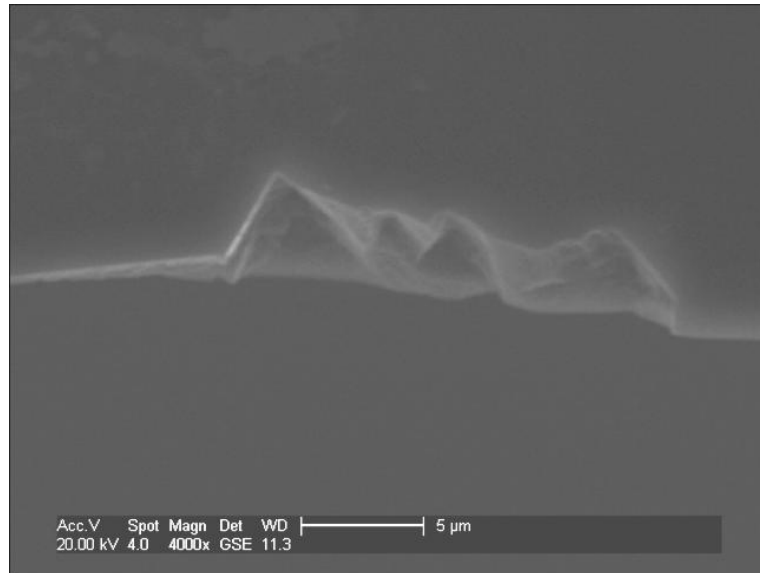
Figure 76: SEM of tool S65316 after machining, taken from a top down direction. Flat area on the left was a section of the original FIB design. The altered geometry from the failure, though unplanned, provides more evidence of the importance of the tools geometry.

This is much more revealing about the nature of the failure mechanisms at work during the diamond turning of brittle materials than the experimental plan anticipated. It shows that a tool that is in the original FIB damage geometry will fail to machine in a ductile manner, while the second image shows that total volumetric wear damage is not linked to failure to machine in a ductile mode.

It also shows how damage accumulated along the tool edge can act as a focus for gathering further damage, (as stated by Jacklin [2]). From the point of view of engineering complex diamond tool edges using FIB it is best to design the edge to run as close to parallel with the (111) plane as possible.

The most important finding from the FIB work was that brittle damage could be found at the generated worksurface using an unworn tool that had specific tool geometry. Failure in this small experiment was therefore solely a result of the geometry of the tool. This is proof that tool geometry is critical when machining brittle materials and is a strong indicator that the geometry failure mode is a real phenomena.

Chapter 6- Diamond turning results
for silicon using MCC tools

During this trial the MCC synthetic diamond material was used for the first time as a tool material for diamond turning of silicon. This chapter outlines the extensive results gathered (including (100/110) orientation the alternative (100/100) tool-orientation tools), the wear behaviour displayed by this new tool material and the work done on higher-negative rake angles.

The expectation at the start of the project was that the MCC material would display exceptional tool-life characteristics because of the extremely low nitrogen content. Consistency was also expected to be very good as the creation process of MCC is done in laboratory conditions and should not show the random growth histories that natural diamond is known to display [2]. Also, the defect concentration is expected to be consistent between MCC samples [22].

6.1 Original orientation MCC (110) top-face tools

Five MCC (110) top-face tools were prepared by Contour Fine Tooling to have 0.5mm tool radius, -25 degree top-rake angle and 10 degree clearance angle. The MCC tools were therefore in the same specifications as the natural diamond tools. The MCC (110) top-face tools were also in the same crystal orientation as the natural diamond tools. Variation of tool life found among natural tools made this large testing group a sensible precaution; the larger testing group makes finding tools with significant tool-life variations more likely; though the high variability shown in the natural diamond tools was not expected from the reportedly very consistent [22] MCC synthetic diamond material.

The tools had the following serial numbers; S83775, S83776, S83777, S83778 and S83779. The tool-life assessments were measured under the same cutting conditions as

those used for the natural and HPHT synthetic diamond tools detailed in Chapter 5. The total achieved cutting distances are shown in the following figure (figure 79).
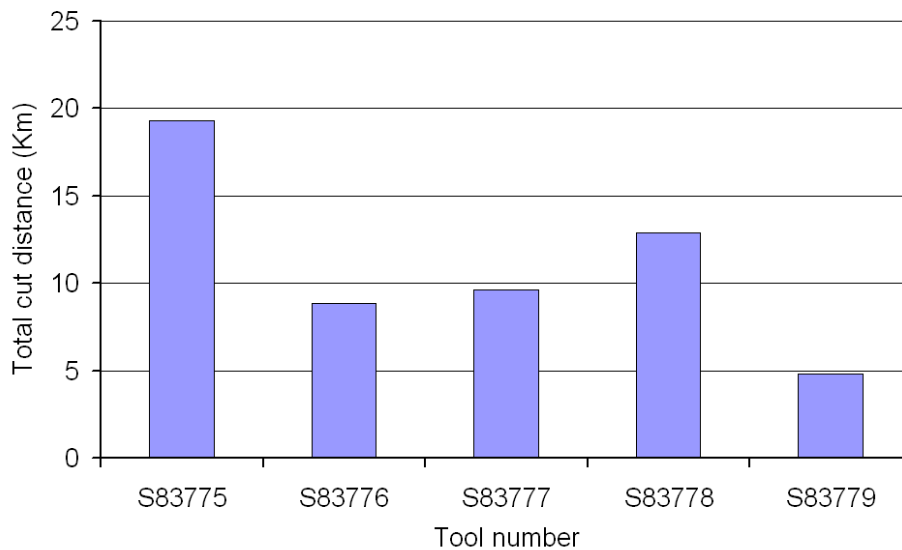
Figure 77: Total cut distance before the onset of brittle failure for the first set of MCC diamond tools.

The distance achieved by the MCC tools is disappointing from a silicon machining point of view. The two natural tools which were evaluated for tool-life performance using the same experimental set-up achieved cut distances of 32.17 Km and 64.34 Km. An MCC result showing a tool-life of less than 5 Km was particularly surprising from the tool material that was expected to supersede natural diamonds as a suitable single point diamond turning tool material.

Examination of the SEM images of the (100/110) orientation MCC tools proved interesting.
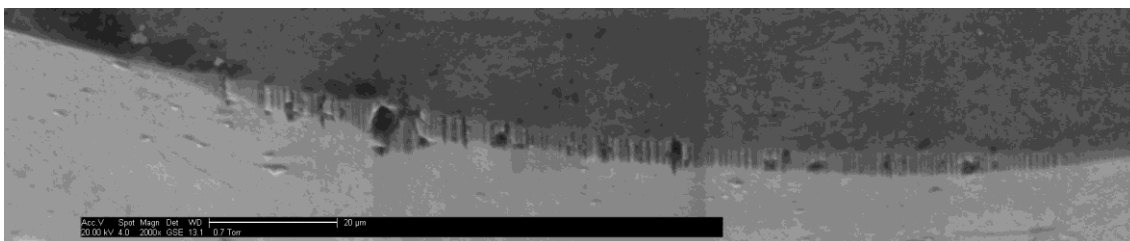
Figure 78: MCC tool (S83778) after cutting distance of 12.8Km and onset of brittle failure.

The above image is typical of all the MCC tools in the (100/110) orientation. All tools in this orientation display frequent small points of chipping damage along the tool edge. Testing using a spindle speed of 3000rpm was performed on the relapped tool S83778. This spindle speed was previously tested with a HPHT tool (see Chapter 5), and had no detectable influence (a result that helped to confirm that machining results at 1200rpm maintained their relevance to industrial practice).
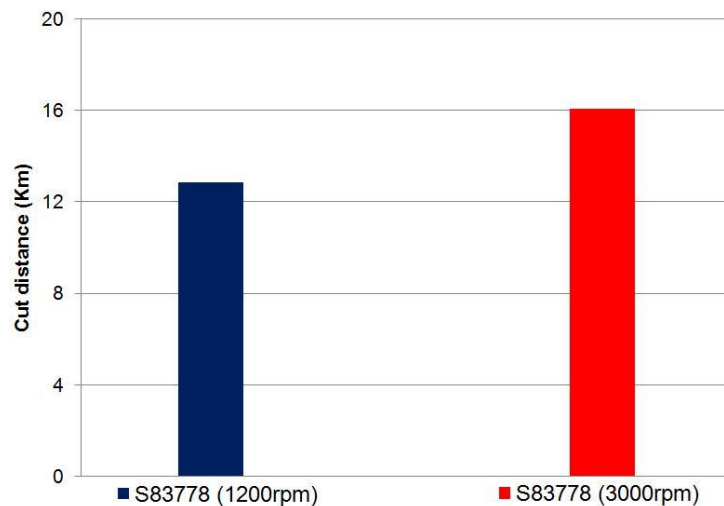
Figure 79: Difference between 1200rpm and 3000rpm spindle speeds for the MCC synthetic diamond tool S83778.

Cut distance results for MCC tool S83778 at the two spindle speeds are shown above in figure 79. Both results are within the previously found standard deviation: when taken with the results on HPHT tools there is a strong indication that industry is using a spindle speed that is not detrimental to total achievable cutting distance.

The best and worst performing tools (S83775 and S83779 respectively) were retested to check to see if the relative performance of these MCC results would repeat; in a similar manner to how natural diamond tools would expect to behave. Tool S83778 was also used for a repeat trial, give more complete repeat data.
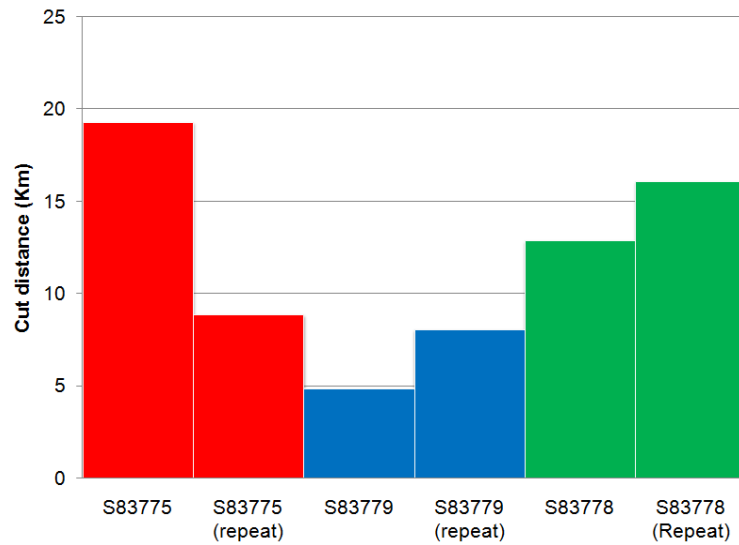
Figure 80: Original and repeat trial of tools S83775, S83778 and S83779.

As can be seen in the above figure, the MCC does not display the same repeatability that natural diamond tools do when repeat trials are performed. One tool displayed poorer performance on the second cut, while the other two displayed marginal improvements. An example natural diamond tools are consistent with themselves while MCC (100/110) clearly don't have that consistency. This inconsistency of achievable cut distance is a very interesting and important difference between natural diamond tools and MCC diamond tools when machining silicon. This strongly implies both that the failure mode is different for the MCC material and that the failure mode of the MCC material is less predictable.

6.2 Variant orientation MCC (100) top-face tools

MCC (100/100) orientation tools are important for comparison against the HPHT (100/100) orientation tools and the MCC (100/110) orientation. Clarifying if the consistent behaviour of the HPHT (100/100) orientation tools was a consequence of orientation or tool-material. Furthermore there was a desire from the industrial collaborators to find a way of using the MCC for machining silicon. The HPHT had proved surprisingly long lived in the (100) top-face orientation and it was hoped that MCC would also display a large improvement in cutting distance.

The MCC (100/100) orientation tools were subject to the same grinding problems during manufacture and were therefore made as 0 degree top-rake, 10 degree clearance angle tools and deliberately tilted the 25 degrees, just as with the original (100) top-face HPHT diamond tools.
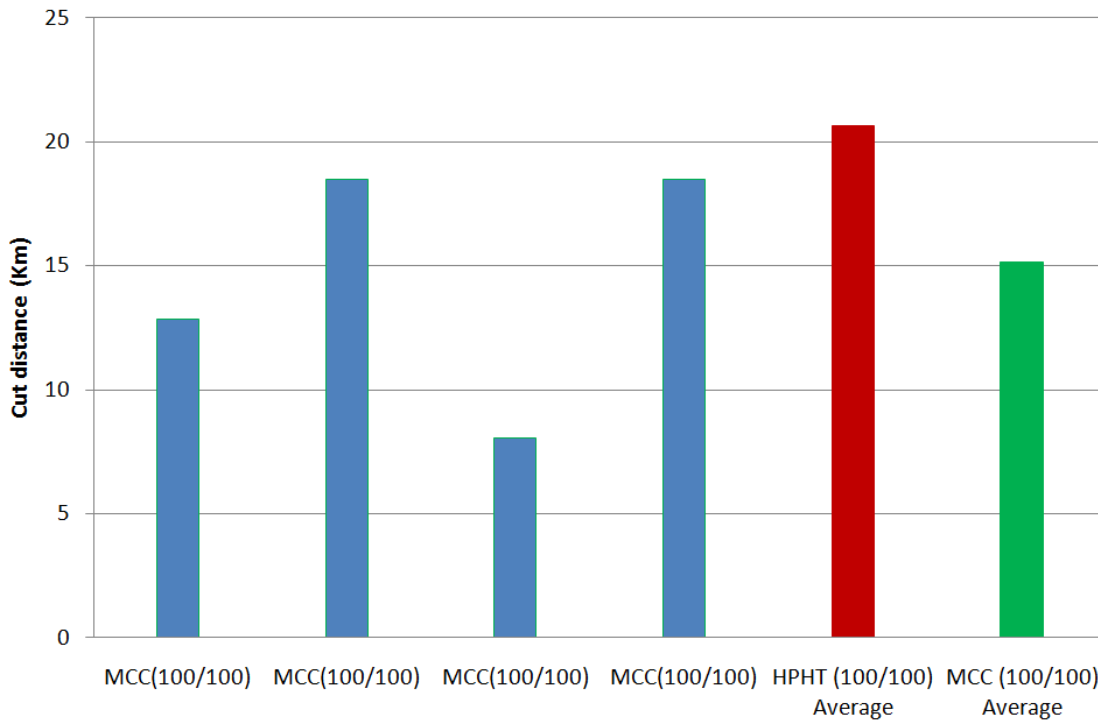
Figure 81: Individual MCC (100/100) results with average MCC and HPHT results.

From the above graph it is clear that the MCC (100/100) orientation results are less impressive than the HPHT (100/100) results: displaying poorer achieved cutting distance and a bigger standard deviation of results (MCC standard deviation 5.04Km, HPHT standard deviation 1.23Km).

Though disappointing this is a very interesting result that implies that HPHT is a better tool-material for machining silicon. An odd result considering the higher nitrogen content and the vast numbers of papers that tell us the wear resistance of diamond is inversely proportional to nitrogen content.

6.3 High negative rake work

The work of Blackley and Scattergood [3] indicates that pressure is important for the successful machining of brittle materials and proposed a model linking excess pressure to the generation of brittle fracture upon the generated worksurface. While Blake and Scattergood [5] confirm that top-rake angle has an effect on critical chip thickness. The work of Jacklin [2] also performed some trials upon various negative rake tools, including -45 degree tools. That work tested tools at -15, -25 and -45 degree top-rake tools. They found that the tool-life was highest for -25 top-rake tools. There is clearly a lot of work to be done on explaining the effect of rake angle upon the diamond turning process and finding optimum rake angles to extend tool-life against various workpiece materials.

For this thesis a principal reason for testing the high negative rake tools was to examine if different top-rake tools cause failure by different failure mechanisms. Furthermore, as the fracture damage on the tool-edge is causing failure finding a method for minimising it was assumed to be beneficial for tool-life for the MCC synthetic diamond material.

Two MCC synthetic diamond tools were set at -45 top-rake. This involved preparing the diamonds at the normal -25 top-rake angle and then brazing the tool stones on a specially manufactured tool insert, tilted by the remaining 20 degrees to achieve the -45 degrees. The machining process was kept at the standard testing parameters; 1200 rpm spindle speed, 10 μm depth of cut and 1 μm/revolution feed-rate. Deionised water was applied as coolant using the hypodermic set-up used previously in this trial. The workpieces used were single crystal silicon 32mm diameter discs. The tools used were S83776 and S83777 which had previously been used at -25 top-rake angle. While planning this trial, the fact that previous results did not reflect the performance that could be expected from repeat trials was known. Therefore the results gained while using the high negative rake angle of these tools would not be influenced by their previous results. The two extreme negative rake tools were reconditioned and re-tested: there are four total results at this rake angle. The results are shown in figure 82.
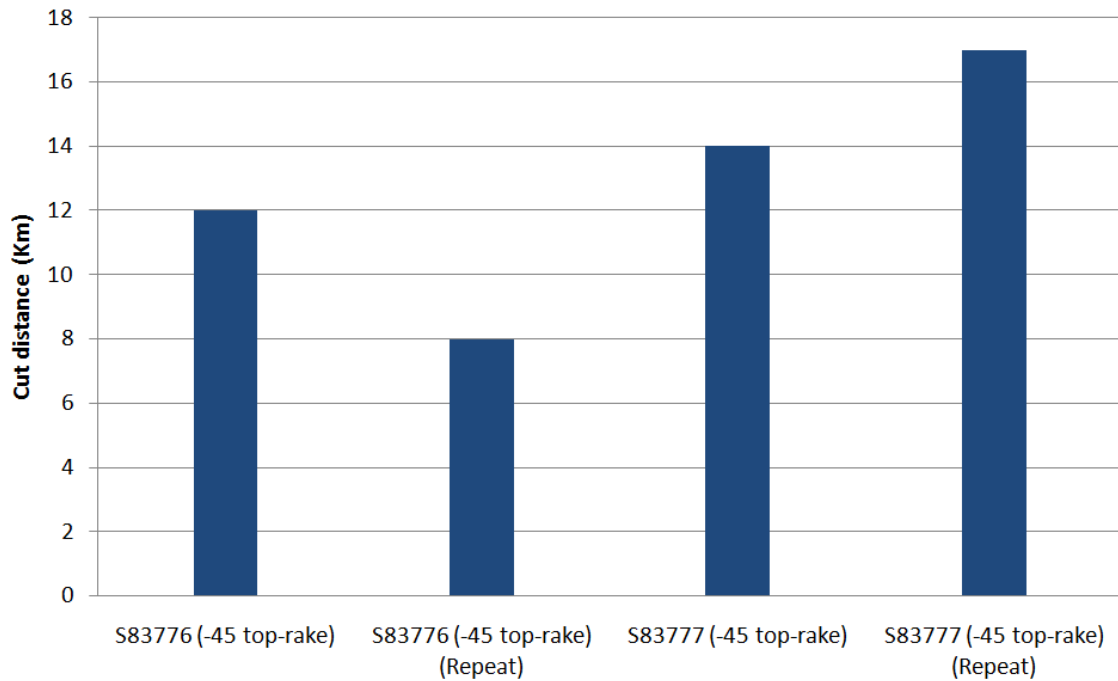
Figure 82: High negative rake angle results.

Normal top-rake MCC tools averaged 11.62Km before brittle failure while the -45 top-rake tools averaged 10.25Km. Changing the angle of the tool from the normal -25 to the high negative rake MCC tools displayed was found to lower the achievable cut distance, but in the case of the MCC tool material, neither top-rake angle would provide a suitable cut length to produce silicon optics of a sensible size. Of interest though is the insight these results give on the failure mechanism at work.

The measured cutting forces from the first high negative rake testing of tool S83776 are shown below (figure 83).
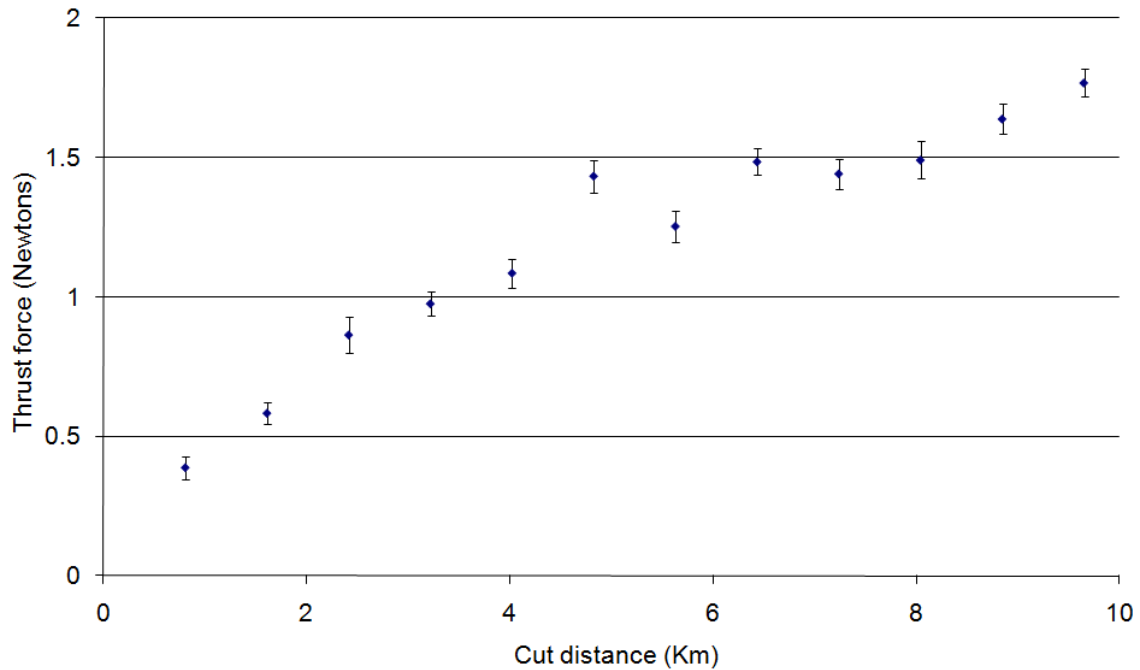
Figure 83: The progression of cutting forces during machining of S83776 (first trial at -45 degrees top-rake angle).

A -45 top-rake angle has the effect of raising cutting forces for the first cut when compared to the -25 top-rake tools. The final cut is generating a lower cutting force than expected. Final cutting force for -25 top-rake tools is typically in the range of approximately 3.5-4.5 Newtons. All -45 top-rake tools tested fail at significantly lower.

Another hint to the failure mode used is that all the -45 top-rake tools generated similar cutting force at failure. The consistency of the cutting force at failure indicate that there is a rake-angle dependency upon when the pressure failure mode is selected and that by tilting to -45 degrees the pressure failure transition is preferred. The generally lower cutting forces measured at failure of the high negative rake tools when compared to the -25 degrees top-rake are not an indication of the geometry failure mode. The high negative rake tools are known to focus greater pressure upon the workpiece than the -25 top-rake tools (as reported by Blackley and Scattergood [3]).

The SEM images help confirm that all the high negative rake tools displayed fracture free wear scars (therefore excluding fracture driven geometry changes as the cause of failure).

Figure 84: High negative rake tool after failure.

SEM images of the high negative rake tools all display small wear-scar areas and generally lack any regions of fracture damage, much like the HPHT (100/100) orientation tools. The assertion that the high negative rake tools are failing via a pressure driven mode is supported by the lack of any serious geometry change at the tool-edge due to fracture damage.

The change in wear behaviour is quite considerable when the rake angle is changed. This is due to the changed orientation of the diamond tools, arising from the tilting of the crystal. For tools at normal rake angles the [100] direction is aligned normal to the workpiece for diamond tools. Tilting therefore changes the wear behaviour experienced by the tool and changes the cause of the failure mode to a pressure driven failure.

Tilting the tool also results in a slightly different tool-profile.

Figure 85: Change in 2D tool geometry introduced by a 20 degree tilt of the tool.

From the above it can be clearly seen that tilting a tool by 20 degrees changes the geometry of the machining process. It should be clear that the tool engagement length can be made longer by tilting the tool, the removed chip of material therefore becomes wider in the horizontal direction, but also thinner in the vertical.

Tilting the tool also changes the orientation of the crystal cleavage plain (which lies along the {111} equivalent plains) and therefore changes the energy required for chipping damage to occur on the tool edge. Clearly from the lack of chipping damage to tool-edges when orientated in such a way, (as demonstrated by the HPHT tools and -45 top-rake tools), the energy required to cause chipping damage is not being efficiently coupled into the {111} cleavage plain.

6.4 SEM monitored tool trial

After examining all the SEM images of the MCC synthetic diamond tools there was considerable interest in the way that the fracture damage accumulated upon the tool edge. In particular, the distance along the tool cutting life at which these defects start to appear was unknown. The solution was to SEM the tool after each cut. The cut distance is only 0.8Km per cut, so a very detailed picture of how the wear scar develops could be gained using the SEM in this way.

This approach was considered as the initial methodology for all the tools tested as part of the project but was rejected for several reasons. Firstly, the time involved with removing the tool, measuring using the SEM and resetting the tool before finally finding the correct tool position is considerable. The time taken to successfully test a tool until the onset of brittle failure at the generated worksurface is already large. Secondly, this would likely introduce an error in the tool position between each cut, resulting in fluctuations in the depth of cut. This would have made the cutting force measurements significantly more difficult to interpret. As cutting forces were of interest from a model development point of view this was considered unhelpful. Therefore a single MCC diamond tool was selected as suitable for this sort of very detailed testing.

Of specific interest was if chipping damage formed on the tool edge during the initial stages of the machining process. A particularly interesting question that needed answering was if chipping occurred during the first few cuts, or happened later during the tool-life.
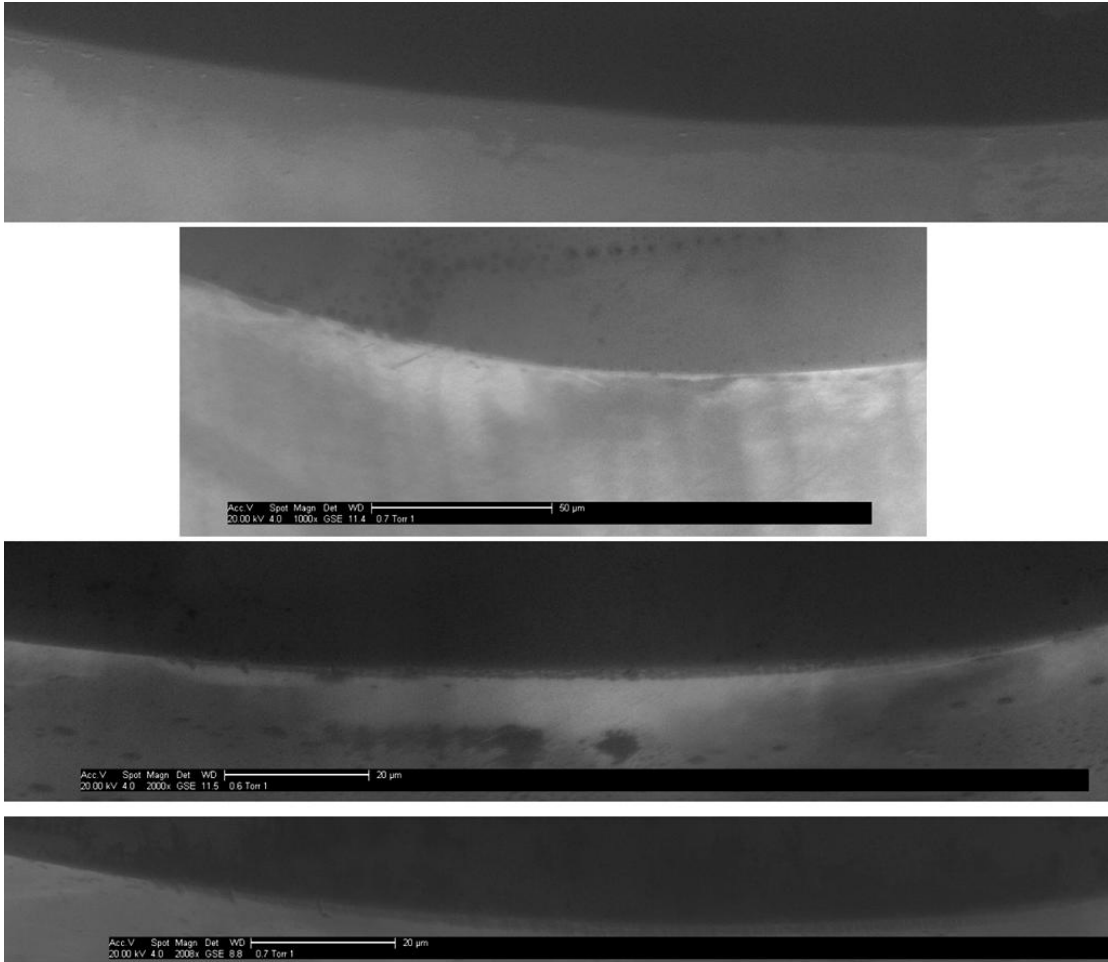
Figure 86: The first four cuts of MCC tool during the tool monitoring trial.

From the above SEM images, (figure 87) we can see that the wear scars are generally smooth and do not show any signs of significant chipping to the tool edge. Images shown above are of the tool after the first, second, third and fourth cut, (at which point the tool has cut 3.2 Km). These results help to confirm the (100/110) orientation MCC tools do not experience fracture when initially put into contact with the silicon workpieces.
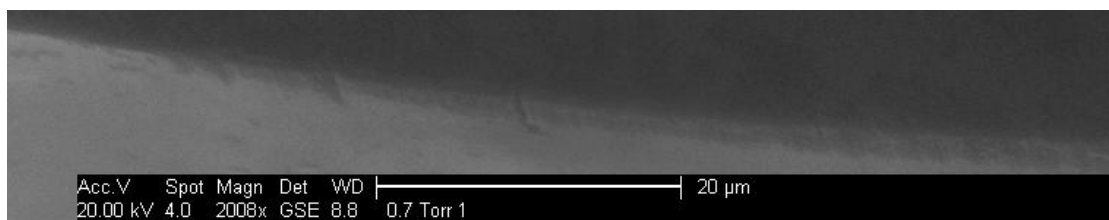
Figure 87: A close-up of the leading edge of the tool after the fourth cut.

From figure 87, an SEM taken after the fourth cut for this tool, it is clearer to see that the wear-scar does not have any chipping damage. There are features within the wear-scar on the leading edge of the tool, but this appears to be due to uneven wear of the tool, (possibly arising from slight variations in depth of cut) and not due to any fracturing of the edge. This result also helps to provide evidence that the onset of the chipping damage and the resulting change in tool geometry is the root cause for failure of the diamond tool.

6.5 Wear behaviour of MCC against silicon

As can be seen in the SEM images the wear behaviour of MCC is very orientation dependent. At a top-rake of -45 degrees the MCC synthetic material appears to adopt a pressure driven failure mode, while (100/110) orientation MCC tools seem to favour the geometry driven failure mode. It is suspected that orientation of the crystal causes a change in wear behaviour when moved from -45 top-rake to a -25 top-rake. This effect is not surprising, differing wear rates based upon crystal orientation has been noticed previously while diamond turning [48], and performing other wear experiments [33,34,35,89] .

Interesting though is how a relatively small orientation change of the diamond tool can result in a change in the way the tool will eventually fail to machine silicon in a ductile manner. It is clear that the (100/100) orientation MCC and the -45 top-rake MCC tools are both failing to machine silicon due to a common failure mode. This failure mode is clearly the same as the (100/100) orientation HPHT tools. The implication is that, like the HPHT (100/100), the pressure that is being applied by the tool onto the silicon workpiece is leading to brittle fracture reaching into the generated surface. The failure point appears quite consistent for these -45 top-rake tools and the threshold pressure for the pressure failure mode is lowered by the geometry change from -25 degrees to -45 degrees. It is interesting that such a relatively modest change of orientation (by only 20 degrees) can eliminate the obviously frequent chipping that was experienced by the -25 top-rake tool. The work on the two orientations of HPHT tools confirms that it is an orientation effect and not a tool material effect.

Tool material does however have a clear effect on tools in the (100/110) orientation. A notable feature of the MCC (110) top-plane tools was that wear-scar SEM images have a lot of fracture type damage. These wear-scars show more numerous examples of the small fracture damage. For MCC (100/110) orientation tools the geometry failure mode is much more likely as these tool edges experience significant issues with brittle-fracture. As hinted at in the literature review (Chapter 2), the MCC clearly has a tendency to fracture easily when directly compared to the natural diamond tool material. The cause of this brittle behaviour is due to the extreme purity of the material. It is known from the work of Shimada [43] that the higher nitrogen aggregates could well be helping limit crack formation. In particular small cracks that could be causing the small fracture areas are thought to be suppressed in diamonds that contain larger nitrogen aggregates. Also the work of Moore [47] indicates that the presence of nitrogen helped the crystalline structure to distort from the idealised structure.

When all the data on MCC is gathered, it is clear that the new MCC material is less desirable as a tool material than natural diamond tools for machining silicon.

Chapter 7- Modelling approach of diamond tool-wear

7.1 Tool-wear behaviour that requires modelling

A wear model for predicting tool failure while single point diamond turning is potentially useful to industry: allowing modification of cutting schedules with the aim of minimising wastage of tools, workpieces and machining time. From the SEM images of the tools used during machining trials it is clear however that there are two failure modes at work. First a geometry failure mode caused by edge chipping which effects most of the (100/110) orientation tools while machining silicon. There is also a failure mode that is caused by attritious wear of the tool which is linked to the thrust force and is the primary failure mode when using (100/100) orientation tools to cut silicon or when machining soft metals.

```
┌────────────────────────────────────────────────────────────────┐
│                    Diamond tool failure                         │
└────────────────────────────────────────────────────────────────┘

┌──────────────────────────────────────────────┐  ┌──────────────┐
│                  Attritious                  │  │   Geometry   │
└──────────────────────────────────────────────┘  └──────────────┘

┌───────────────┐ ┌───────────────┐ ┌───────────────┐ ┌───────────────┐
│ Machining non-│ │ -45 top-rake  │ │  (100/100)    │ │  (100/110)    │
│ ferrous metals│ │ tools         │ │ orientation   │ │ orientation   │
│               │ │ machining     │ │ tools         │ │ tools         │
│               │ │ silicon       │ │ machining     │ │ machining     │
│               │ │               │ │ silicon       │ │ silicon       │
└───────────────┘ └───────────────┘ └───────────────┘ └───────────────┘
```
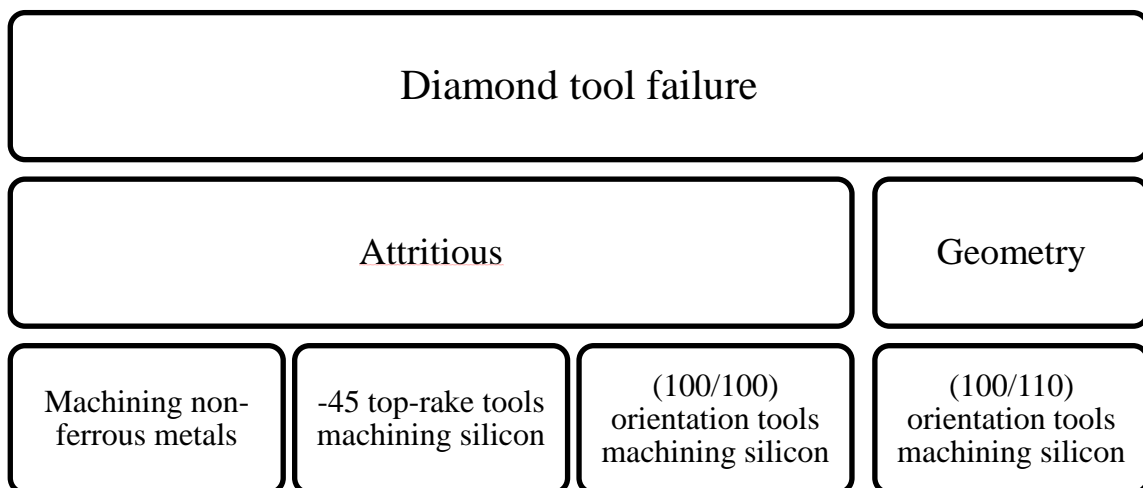
Figure 88: Diamond tool failure can be divided between the geometry and pressure failure mode. Specific diamond orientations and top-rakes will preferentially fail through a single failure mode.

With two failure modes possible during diamond turning it is logical to develop two models. A first model detailing attritious wear (the most widely applicable wear-situation) and a second model detailing brittle fracture. This Chapter details the development of the two models, details the structure of the models and the assumptions that have been made.

7.2 Attritious wear model

The tool-orientations and workpiece materials that are unlikely to result in brittle damage of the tool are best described using an attritious wear model. The majority of diamond tools do not experience significant brittle-damage when turning many workpiece materials such as non-ferrous metals or polymers. An attritous wear model is more significant in these cases where brittle-damage to the tool is less common. Attritious wear of diamond tools appears to be a deterministic process and is therefore well suited for modelling.

7.2.1 Initial planning of the attritious model

Wear is related to cutting distance therefore when structuring the model a decision had to be made concerning what resolution of distance to use. The decision was to enable the model operator to input the total number of cuts used and also allowing the user to define the length of each cut. The user therefore has control of the maximum distance used and the distance resolution. Rather than continuing until an output value is met (such as thrust force) the model is designed to perform a fixed number of cuts before stopping.

Cutting forces and wear is calculated separately for each cut, with the results influencing the following cut. Cutting forces are calculated using the Waldorf model [90] and wear is calculated using the Preston's equation [91].

At the start of the model some parameters need defining. Parameters such as clearance angle, top-rake angle, tool radius and feed-rate. Workpiece dimensions are also modifiable. The model also has a predefined horizontal resolution. The default resolution is set at 100nm, which over a 500 μm tool-radius gives more than 10,000 points to describe the tool-edge.

Assumptions

All models are an abstraction of a real system. The assumptions that are made are disclosed here and their effect on model accuracy is considered.

Principal assumptions are:

- Circular and flat workpiece geometry
- Uniform pressure distribution

- Wear is independent of contact sliding speed
- Thermal effects are not significant to attritious wear

Workpieces are assumed to be flat and circular. This assumption also has the effect of fixing the contact conditions between the tool and the workpiece.

Pressure is also assumed to be uniform across the tool-workpiece interface and assumed to result in uniform wear across the tool-workpiece contact. Pressure fluctuation caused by workpiece anisotropy (which is particular associated with brittle workpieces) is also considered unimportant.

The model ignores any non-linear effect on wear from sliding speed. This is deliberate as the non-linear wear dependency upon sliding velocity seen during polishing (by Hird & Field [33]) has not been seen in our experiments. This assumption within the model may lead towards inaccuracies: especially for larger workpieces and high spindle speeds. However few diamond turning machines have the capability of turning particularly large workpieces or have access to high spindle-speeds.

Ignoring thermal effects is considered a valid assumption based upon work done with FEA modelling software Thirdwave which was used to model thermal changes experienced by a diamond tool while machining 32mm diameter silicon workpieces at appropriate sliding velocities of 2.01m/s and 5.03m/s. These velocities correspond to spindle speeds of 1200rpm and 3000rpm respectively. The 2.01m/s simulation found tool temperatures peaked at 396.9K, while the 5.03m/s simulation found tool temperature peaked at 482.6K. It is known that high temperatures can cause change diamond into graphite at 1800K without catalytic help [63]. Therefore the assumption is that machining will not raise diamond tool temperatures above 1800K. As generated heat is related to sliding velocities between the two surfaces the assumption that thermal effects can be ignored may not be applicable for large workpieces or high spindle speeds.

Ignoring thermal effects is likely to be a poor choice for ferrous workpieces which are known to act as a catalyst for an oxidation reaction of the diamond-tool. The rate of this

reaction is shown to be related to temperature, as demonstrated by work on cryogenic cooling of diamond turning tools showing reduced wear [92].

7.2.2 Calculating Preston's Co-efficient values

The Preston's equation was developed to explain optics polishing. The Preston's coefficient (denoted using K_p) is the critical value for this equation. The Preston's coefficient is a value that must be found using direct experimentation. The recession depth must be found before the value of the Preston's coefficient can be calculated. The total recession value is dependent upon K_p, applied pressure and the total cut distance. Rearranging the Preston's equation into terms of K_p:

$$\frac{\Delta H}{\Delta s} \frac{A}{L} = K_P$$

To complete the calculation of K_p the wear area and applied load (in the direction normal to the cutting force) need to be established. As these values evolve during the process, average values need to be used.

Area is approximated by multiplying half the maximum wear-scar width by the total length of wear-scar. This creates a pair of triangles each with bases equal to the maximum width of the wear-scar and equal to half the length of the wear-scar. The average area was found by halving the final area, a method that assumes the wear-scar area grows linearly and that using a 2D quadrilateral to model the area of a much more complex 3D shape is a suitable method.

The cutting distance, Δs, is the total cutting distance achieved by the tool before the onset of failure. The value of the load, L, is an average of all measured force values over the life of the tool. Finding the maximum recession distance, ΔH, is not trivial on a diamond tool and requires use of an SEM to find the maximum width of the wear-scar and then using trigonometry to find the recession distance.

7.2.3 Structure of the attritous wear model

MATLAB was selected as the model development tool. This program was chosen because of its flexibility and to make it easier to add further features later on. Its use

within the literature also gave encouraging results [59, 93,94]. MATLAB has a number of advantages over other modelling methods. For example the scale of the model can be tailored to the problem faced: A molecular dynamics methodology would typically have extremely small spatial and time dimensions (nanometres and nanoseconds scales are usual). Applying molecular dynamics findings to diamond turning is questionable because of the very different scales involved. With the selection of MATLAB as the modelling program an initial structure can be decided (shown in Figure 89).

```
┌─────────────────────────┐
│   Establish tool-profile │
└─────────────────────────┘
            │
            ▼
┌─────────────────────────┐
│  Calculate cutting forces │◄──────┐
└─────────────────────────┘        │
            │                       │
            ▼                       │
┌─────────────────────────┐        │
│     Calculate wear       │        │
└─────────────────────────┘        │
            │                       │
            ▼                       │
┌─────────────────────────┐        │
│  Apply wear to tool-profile│      │
└─────────────────────────┘        │
            │                       │
            ▼                       │
┌─────────────────────────┐        │
│ Calculate wear-area, wear-│       │
│ volume and other parameters│      │
└─────────────────────────┘        │
            │                       │
            ▼                       │
┌─────────────────────────┐        │
│     Update distance      │───────┘
└─────────────────────────┘
            │
            ▼
┌─────────────────────────┐
│       End model          │
└─────────────────────────┘
```
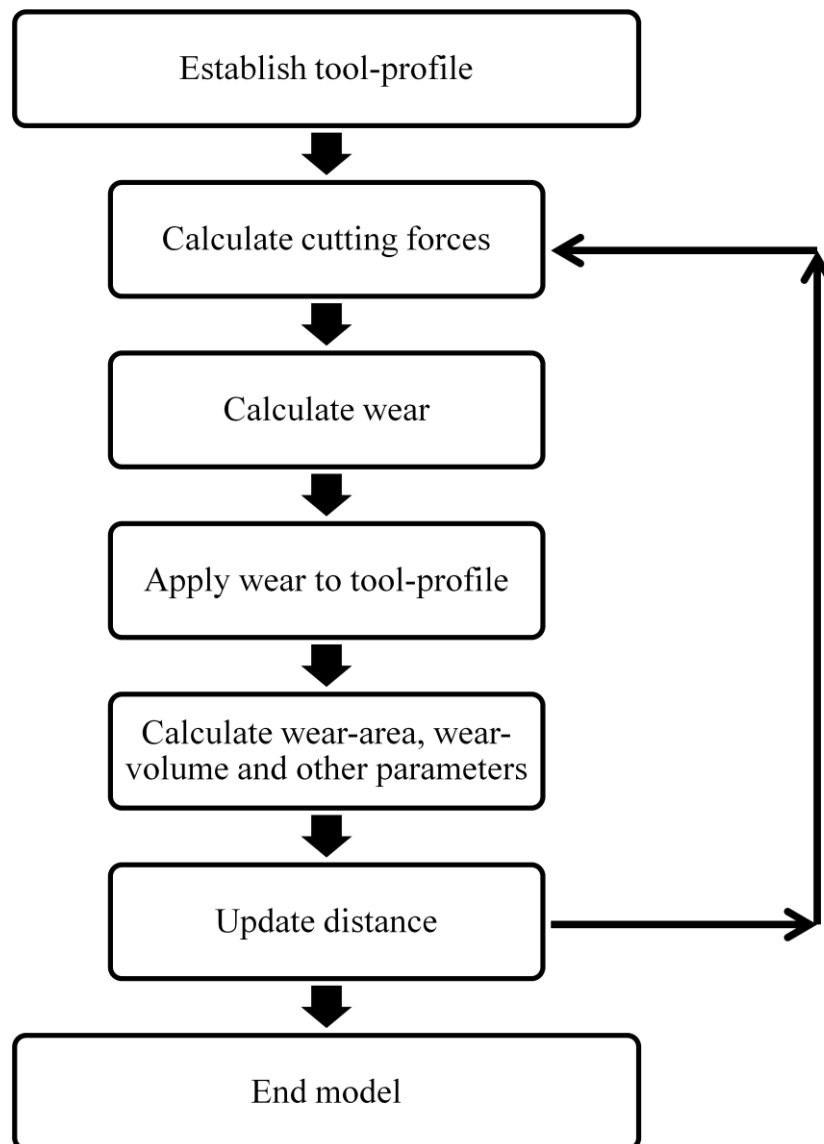
Figure 89: Initial flow of the attritious wear model. Each loop models a single cut.

For the silicon machining results presented in chapter 8 the total distance machined was ~32Km and distance per cut was ~0.8Km. For aluminium machining results, the total distance was ~490Km and distance per cut was ~7Km.

Establish tool profile

Using the circular cross-section approximation, the known radius of the tool and by limiting the tool to a 2D cross-section it is simple to establish the tool profile. Establishing a 2D tool-profile is simple when the majority of diamond tools are half or full radius tools that have the front clearance face following the cylindrical tool geometry.

Using an array (a single column of numbers representing the Z-axis measurement) for the 2D tool-profile rather than a matrix describing a full 3D shape may seem an excessive simplification, but is valid. From that 2D profile the full 3D values can be extrapolated, while keeping the required number of calculations low. For example the contact area can be established from the 2D profile and from the area calculate volume. Establishing the tool in full 3D would therefore add greater complexity to every subsequent operation without adding significant information.

Calculate cutting forces

Each cut is modelled individually and the results looped back to perform the calculations for the next cut. As cutting forces are influenced by the wear-state of the tool it is necessary to recalculate these forces after each simulated cut.

As discussed in section 2.4.3, the Waldorf force model uses the contact area between tool and workpiece to calculate thrust force. Using the Waldorf model causes problems for the first cut as contact area is extremely small. As thrust force will be linked to wear this could lead to artificially low wear for the first and every subsequent cut. We therefore need to define the initial value for thrust force. Thrust forces for second and subsequent cuts are calculated from the wear-area value calculated after wear is applied to the tool.

Calculate wear

In optics the Preston's equation has proven valuable in the low removal-rate application of polishing. Because both polishing and diamond turning wear are low removal rate processes applying this equation is considered an appropriate approximation. Here Preston's equation is shown (as taken from the work of L.M. Cook [91]).

$$\Delta H / \Delta t = K_p * (L / A) * (\Delta s / \Delta t)$$

Which can be simplified by the removing the time dependency, giving the following:

$$\Delta H = K_p * (L / A) * \Delta s$$

Where *ΔH* is recession distance, K_p the Preston's coefficient, *L* the load applied, *A* the contact area and *Δs* the distance the two surfaces have moved against each other. This makes the recession distance (measured normal to the workpiece) proportional to cut distance and the pressure being exerted upon the tool.

Apply wear to tool-profile

Following calculation of wear-recession the model needs to apply the wear-recession to the tool. As pressure and wear are both assumed to be evenly distributed along the tool, wear is applied evenly across the tool and workpiece contact.

Establishing where on the tool wear is applied is a process that needs repeating with each cut as tool-nose recession increases contact between the trailing edge of the tool and the workpiece.

Calculate wear-area wear-volume and other parameters

Wear on a diamond tool results in the tool forming a more complicated geometry than for an unworn tool. This very complex problem can be greatly simplified by breaking the complex 3D wear-volume into a series of smaller 3D shapes. This approach is used within the literature [52], where a wear-scar was broken into triangle-prisms.
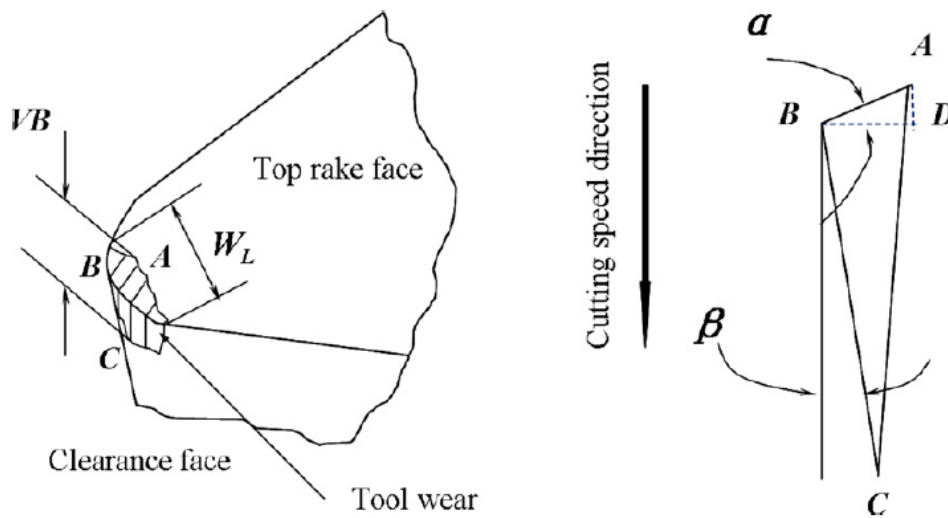
Figure 90: Geometrical approach to analysis of tool-wear within the literature [52].

It is possible to use the difference between the unworn tool profile and the worn tool profile to establish vertical recession distance at each point across the profile, giving the magnitude of the **BD** measurement on the previous figure.
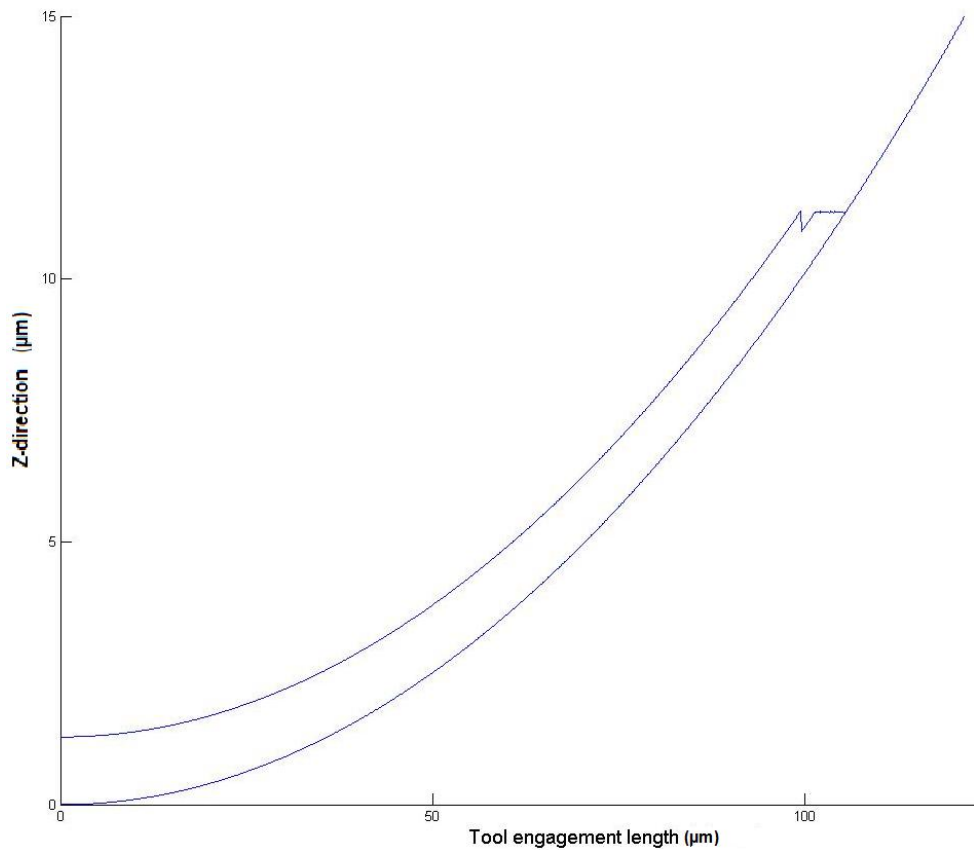
Figure 91: Difference in worn and unworn tool profiles. The recession distance is measured vertically between the curves and at 100nm intervals across the tool engagement length.

Contact area is found by comparing the worn tool profile with the unworn tool profile. The difference at each point across the tool is stored, giving a total recession distance at each point across the tool profile. The wear-area is geometrically related to the vertical recession value and the horizontal resolution. Wear-area at each point can be found by multiplying the length of the vector **AC** (shown in figure 90) by the horizontal resolution of the model (default is 100nm). Total wear-area is therefore easily found by calculating the contribution to wear-area from each point along the tool and summing together the resulting values.

Wear-volume at each point is also clearly found by finding the area of the triangle formed by points **ABC** and multiplying by the horizontal resolution of the model. Total wear-volume is found by summing each component of wear-volume.

End model

When the distance simulated matches the required cut distance the model ends. The predicted values for force in the thrust direction can be compared to the experimental data for this metric. Because of the thoroughness of the experimental measurements of force this comparison is the best guide to the performance of the model.

7.3 Modelling tool-edge geometry effects

Chipping damage on the tool edge leads to changes in the geometry of the tool edge. The experimental evidence from Chapter 5 indicates that these changes can lead to the failure of a single point diamond tool to machine in a ductile manner.

The tool-edge geometry code developed for the project was designed to examine the geometry failure mode, and was heavily influenced by the work of Blake and Scattergood [5]. By examining perfect tools and determining the thickness of removed material Blake and Scattergood [5] were able to link successfully machining of brittle materials to feed-rate. Perfect, unworn tools are an ideal situation clearly not present in many real situations due to attritious tool-wear and chipping damage geometry changes. The MATLAB based code is detailed in Appendix B, but the relevant findings are discussed here.
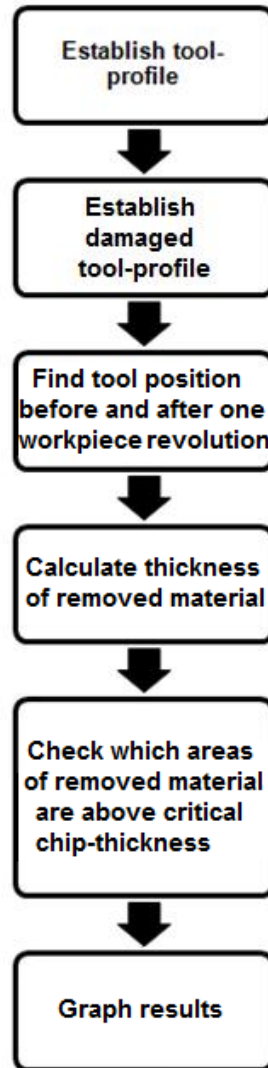
Figure 92: Flow of tool-edge geometry code

When tool-edge geometry changes the chip-thickness is the interesting parameter that is changed. Taking an undamaged 500 μm radius tool as a first example the calculated chip thickness using the developed code is shown below.
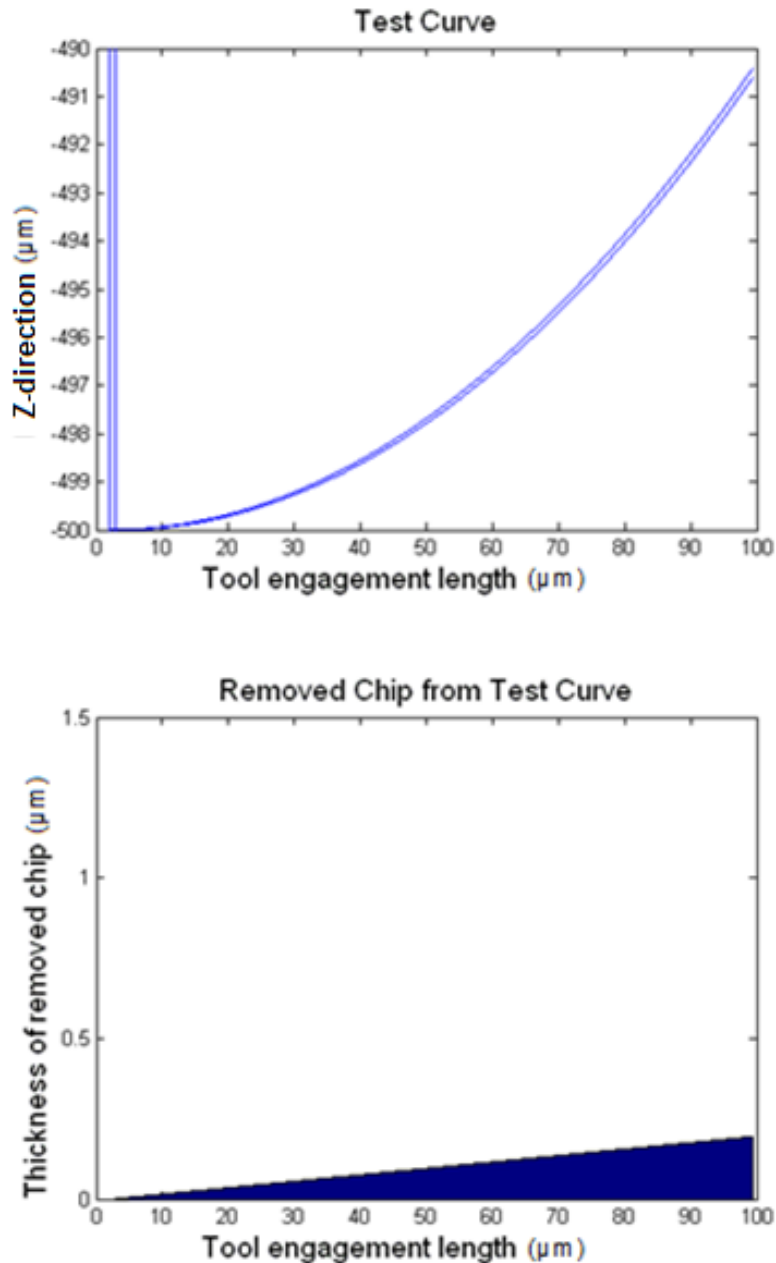
Figure 93: The top graph shows the tool-edge positions before and after a single revolution of the workpiece (a single feed in towards the centre of rotation). The lower graph displays the thickness of the removed material along the tool-engagement length.

Unworn tools produce uncomplicated chip-thickness graphs. From fracture mechanics it is known deformation of brittle materials will depend on energy scaling and that below a critical volume the material will preferentially deform. Above a critical thickness of chip a fracture mode of material removal is favourable. Clearly the point along the tool edge where the removed material chip is as thick as the critical chip thickness will be the transition line where removal of material is primarily a brittle cutting mode. With

148

the critical chip thickness for silicon being ~60nm we see that this transition of removal modes will occur close to the tip of the diamond tool.

Analysis of chip-thickness gets more interesting with damaged tool-profiles. A simple tool profile with a small vertical section is an abstraction of the true profile of a damaged tool, but can provide useful results. The damage section is 6.4 µm wide and 4.91 µm above the workpiece surface the vertical section of the damage, chip height as illustrated with the **h** notation, is only 0.9 µm high: this damage will be demonstrated to result in dramatic changes to the removed chip.
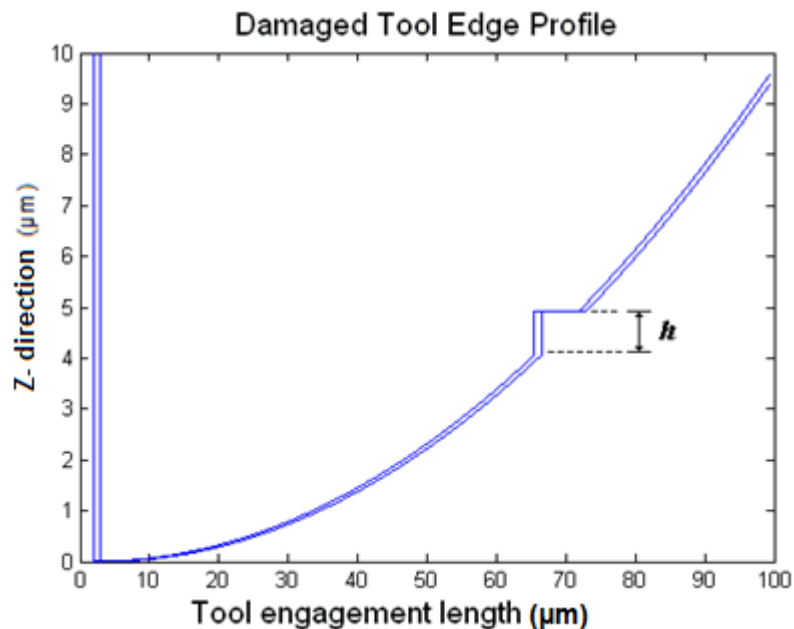
*Figure 94: The damaged tool edge profile at start and end of a feed. The distance **h** shows the chip height which will also be shown to be responsible for the thickest part of the removed material.*

Figure 94 shows the outlines of the tool-profile before and after a single revolution of the workpiece. The area contained within the boundary of these two lines is the removed material during that workpiece revolution. That removed material is shown in figure 95.
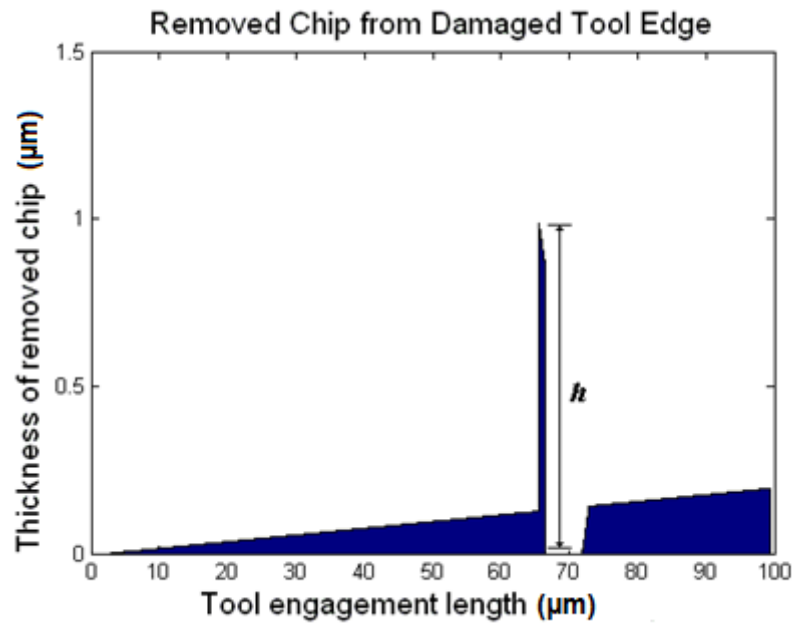
Figure 95: Calculated thickness of chip across the simplified tool damage models engagement length.

The large spike in the removed material is 0.9 µm high and 1µm wide (width is shown to be equal to feed-rate in this case). The height of the chip in the tool profile ***h*** is the origin of with this spike. As this chip is less than 5 µm from the generated-worksurface, cracks from this point do not have very far to propagate to result in a damaged workpiece surface, however predicting the length of cracks from this tool-edge damage is not possible. Such predictions would require detailed knowledge of the stress state of the material [71], information we do not have access to. This lack of knowledge about the pressures acting within the cutting zone causes other problems as it means despite knowing some criteria for causing damage to the tool-edge of a diamond tool we can not predict exact locations along the tool-edge which will fracture.

It is perhaps useful to note that damage to the tool profile does not change the volume of removed material, but redistributes which parts of the tool are removing the most material.
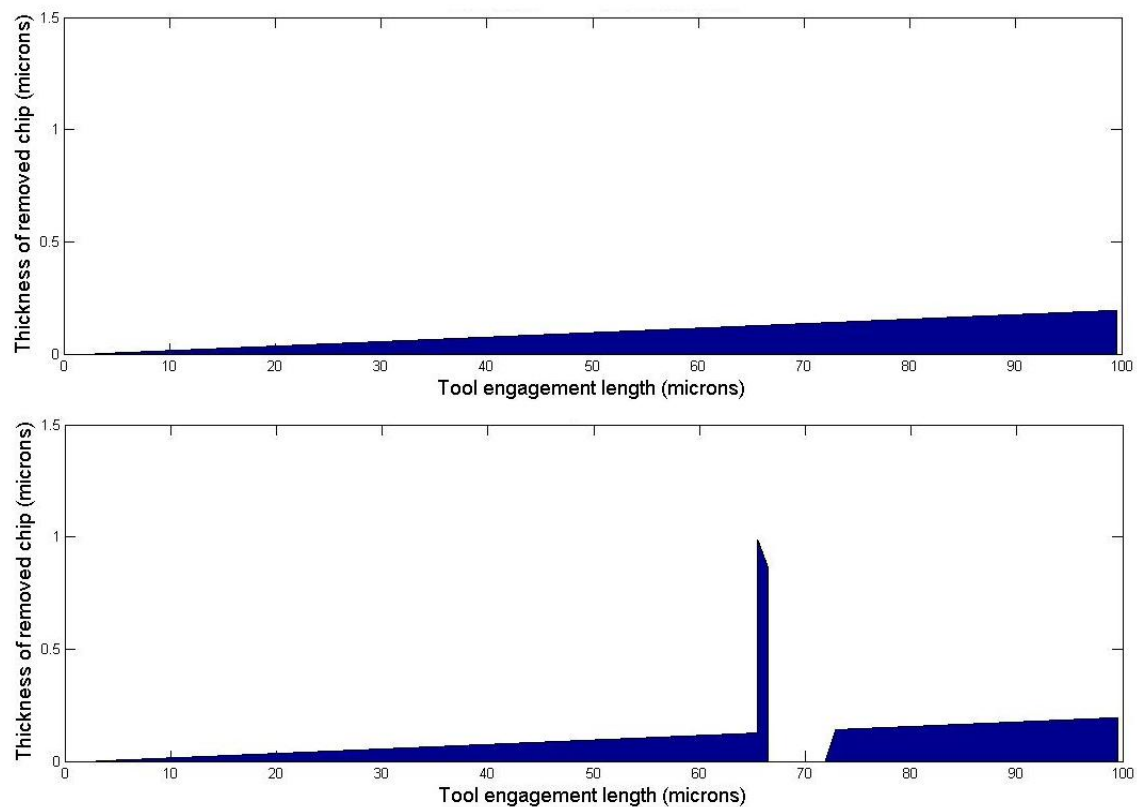
Figure 96: Material removal by a damage free tool and a chipped tool (the FIB tool from chapter 5).

Displayed in the above figure and confirmed by integrating the two areas, the chipping damage does not reduce the amount of workpiece material removed.

There are a few conclusions that can be drawn from this work:

- Firstly, that small chipping damage close to the front of the tool is very likely to introduce cracks into brittle workpieces. Location of damage is therefore very important.

- Secondly, the shape of damage is important. As the FIB trial in chapter 5 has shown, large chipping damage can lead to cracks in the workpiece but are dependent on the geometry of the damage.

- Thirdly, the size of a chipping damage location is not the most important aspect. It is perhaps unexpected but as the FIB trial in chapter 5 has demonstrated, a large area of damage can still result in a tool generating a damage free workpiece surface.

7.4 Summary of model development

Predicting which part of a diamond tool will experience damage is not possible. Fracture mechanics can predict the conditions required to initiate a fracture but not the location on an object where that fracture will initiate. Diamond is known to cleave along the (111) direction [95] and the mechanical properties relevant to fracture of diamond is also explored in the literature [23,96-99]. The calculation to establish the energy required to remove a small fragment of diamond from the tool edge is simple and primarily depends on the surface area of the removed fragment. However, there is no way of predicting the scale of the damage section removed from the tool edge as micro-cracks from subsurface damage, internal stresses and even crystallographic defects can all change the likely crack initiation site and the path of the crack. This is a big problem for SPDT as damage location on a tool is extremely important.

Constrained by a lack of detailed predictive theories about fracture of the tool-edge means model development will have to focus on modelling attritious wear. Fortunately attritious wear is the dominant wear mechanism for most diamond turning workpiece materials.

Chapter 8- Model results and refinement

During model development, several iterations of the model were constructed and tested. Presenting all the data gathered from all these tool-workpiece combinations and different models would be unclear. This chapter will be structured in the following way: results from the first model are shown here followed by a brief discussion of the changes made and finally the results from the very latest model.

8.1 First Model Results

The first model is detailed in chapter 7. Predictions were made for HPHT (100/100), natural diamond (100/110) and MCC (100/110) tools machining silicon. Further predictions were made for (100/110) orientation natural and MCC diamond tools while machining aluminium workpieces. To verify these models the predicted forces can be compared against experimentally measured forces. This is considered the primary method of testing accuracy, but as an additional verification check the predicted maximum wear-scar width can be checked against measurements from SEM images.

8.1.1 HPHT (100/100) machining silicon verification

Modelled cutting forces of the HPHT (100/100) tool correlated well with the experimental data gathered while machining silicon workpieces with this type of tool (see chapter 5 for details of machining results). Results are shown in the following graph (figure 97).
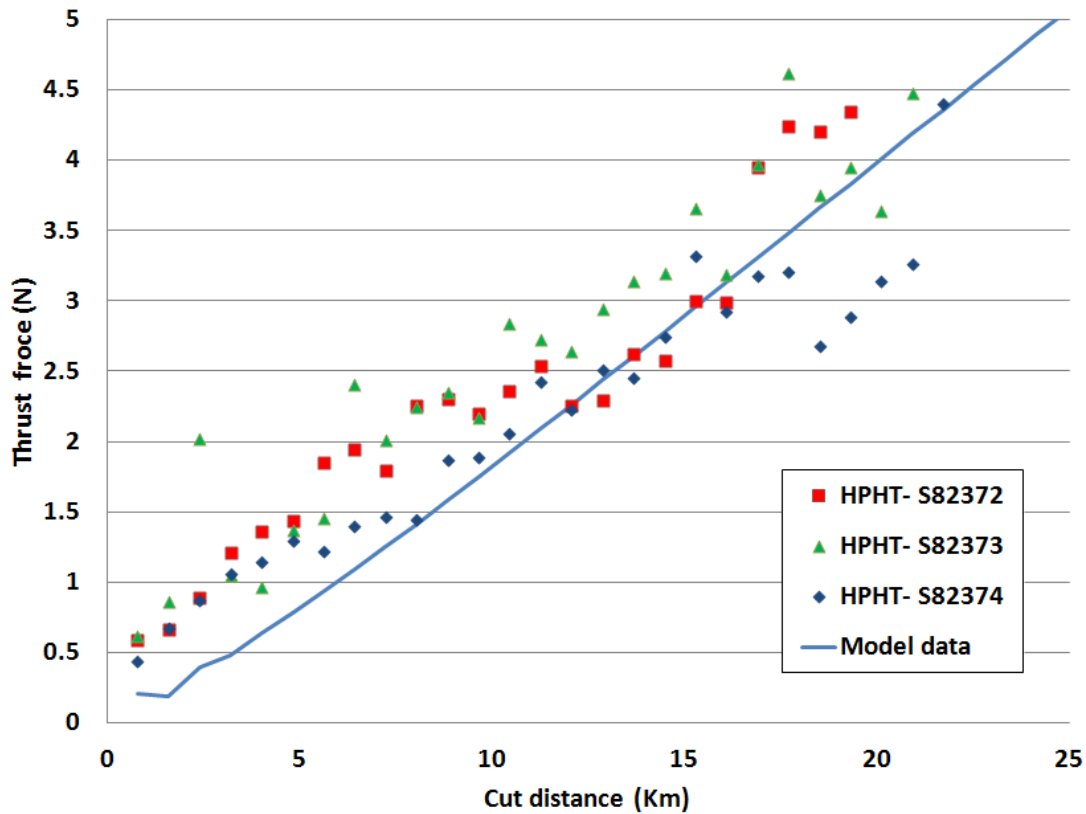
Figure 97: HPHT (100/100) cutting forces, model and experimental.

Cutting forces calculated by the model and gathered from the experiment are in good agreement however the model needs to accurately predict the size of wear-scar.

Tool	Cut distance (Km)	Model determined Width of Scar (µm)	Experimental Width of Scar (µm)	Percentage difference
S82372	19.3	3.41	4.81	70.9%
S82373	20.9	3.71	5.14	72.2%
S82374	21.7	3.87	4.02	96.2%

Table 6: Experimental and model wear-scar widths for HPHT (100/100) machining silicon.

From the above values in Table 6, the model is shown to have underestimated the true wear-scar width. For HPHT (100/100) tools the model was able to predict both the magnitude of the thrust force with increasing cut distance accurately but that the wear-scar was consistently too small. This clearly shows that the predicted wear is generating sensible force values but is not sufficiently changing the form of the tool.

8.1.2 Natural diamond (100/110) machining silicon verification

Natural tools exhibit interesting wear behaviour when machining silicon, showing some tool edge chipping, in addition to attritious wear. While it is not clear which failure mechanism is causing tool failure for these tools, geometry driven or pressure driven failure modes, it is suspected that geometry is the more important failure mode.
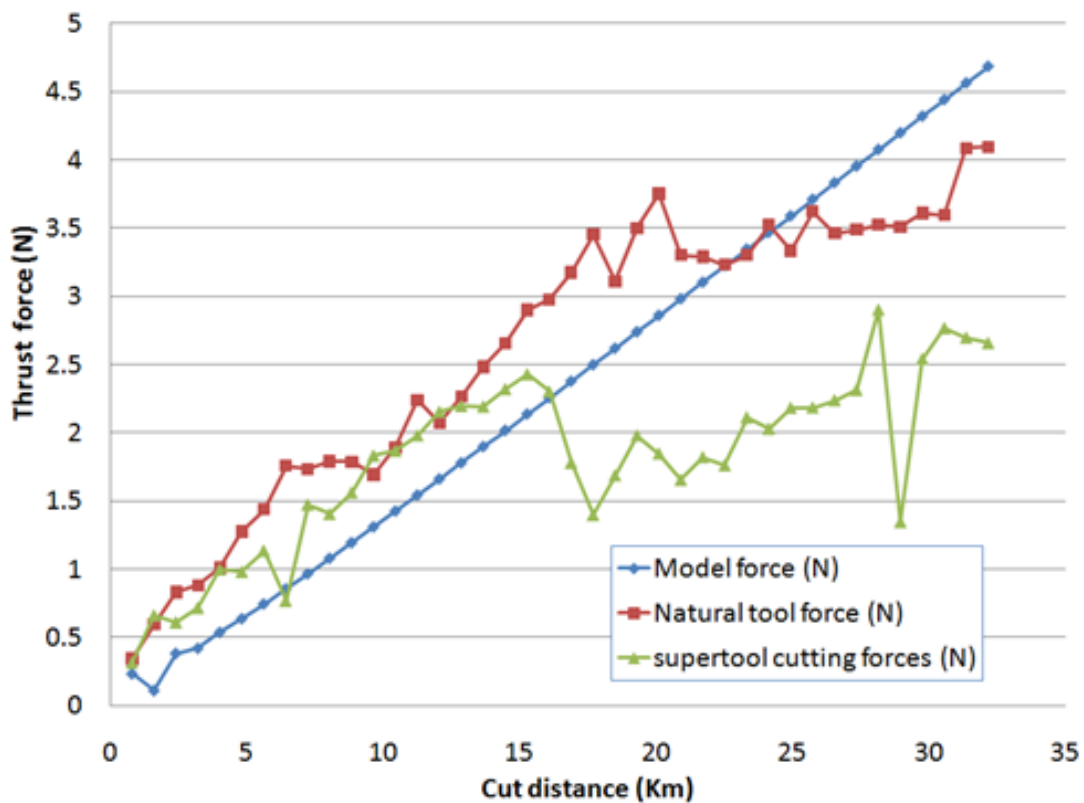
Figure 98: Model data and experimental results for natural (100/110) diamond tools cutting silicon.

Experimentally measured cutting forces for natural tools do not fit well to a linear form; with a simple linear stage preceding a change to a period where cutting forces do not substantially rise. This behaviour might be indicative of brittle damage on the tool-edge acting to reduce the contact between tool and workpiece and thus reduce generated forces. If this mechanism is working to reduce forces it would make predicting silicon machining with natural diamond tools almost impossible using any model that only calculates attrtious wear.

Examination of the SEM images and the model calculated recession depth allow further comparison between experiment and model. The model predicted a maximum wear-scar

width of 3.56 μm. From the SEM image of S65315 the maximum width of the wear-scar was found to be 4.64 μm. Therefore the model predicted a wear-scar that measures 76.8% of the actual wear-scar width.

8.1.3 MCC (100/110) machining silicon verification

Machining silicon with MCC (100/110) tools is dominated by the frequent and often large chips in the diamond tool edge. Modelling these tools is complicated by this behaviour.
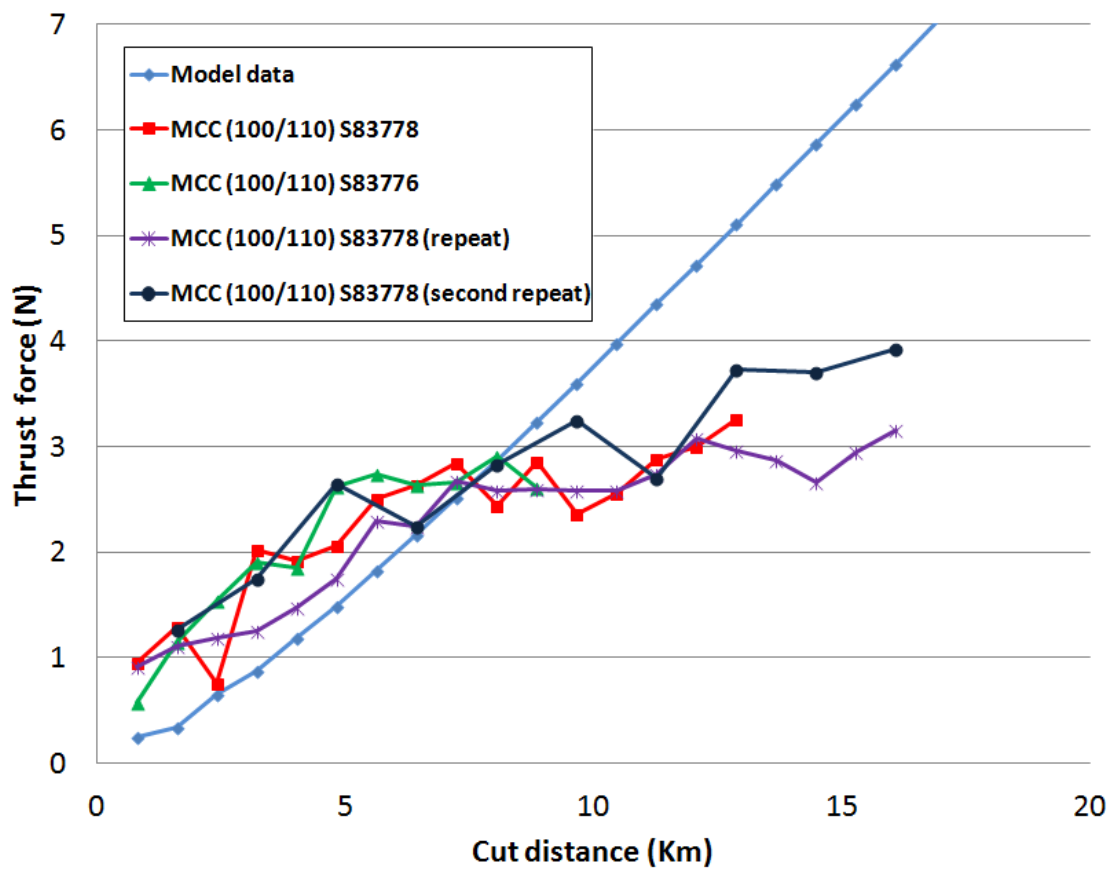
Figure 99: Model data and experimental results for MCC (100/110) tools cutting silicon.

As is clear from the above, the model can only successfully predict the first 7Km of cutting forces with any accuracy before predictions and experiment diverge wildly. It should be noted that the MCC (100/110) tools averaged only 12.1Km and so the scale of divergence is limited by this very short tool-life. Also note that the cutting data used above comes from some of the most successful tools.

Analysis of the predicted and measured wear-scar (at a distance of 12.1Km) showed the model predicted a maximum width of wear-scar of 3.57 μm, while analysis of the SEM image taken of tool S83777 after failure at a distance of 12.1Km the wear-scar was found to be 4.31 μm. The model therefore predicted 83% of the wear for MCC(100/110) orientation tools.
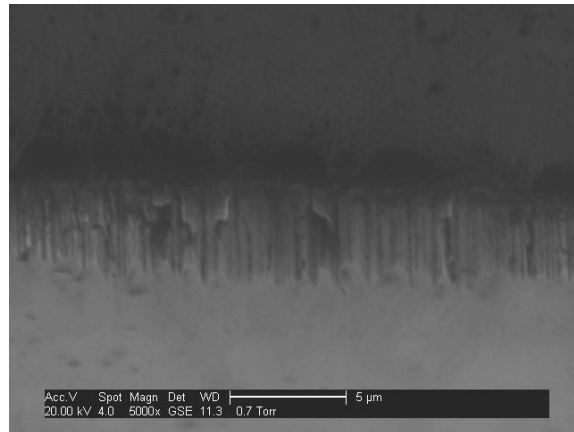
Figure 100: Wear-scar SEM of the MCC (100/110) tool S83777.

So despite the failure to predict cutting forces accurately for MCC tools while machining silicon, the initial model is just as accurate when determining the MCC wear-scar width as it is with HPHT or natural.

8.1.4 Modelling Aluminium machining: MCC (100/110) and natural tool (100/110)

During the machining of aluminium no tool experienced significant chipping damage therefore the expectation was that the attritious model would produce accurate results.
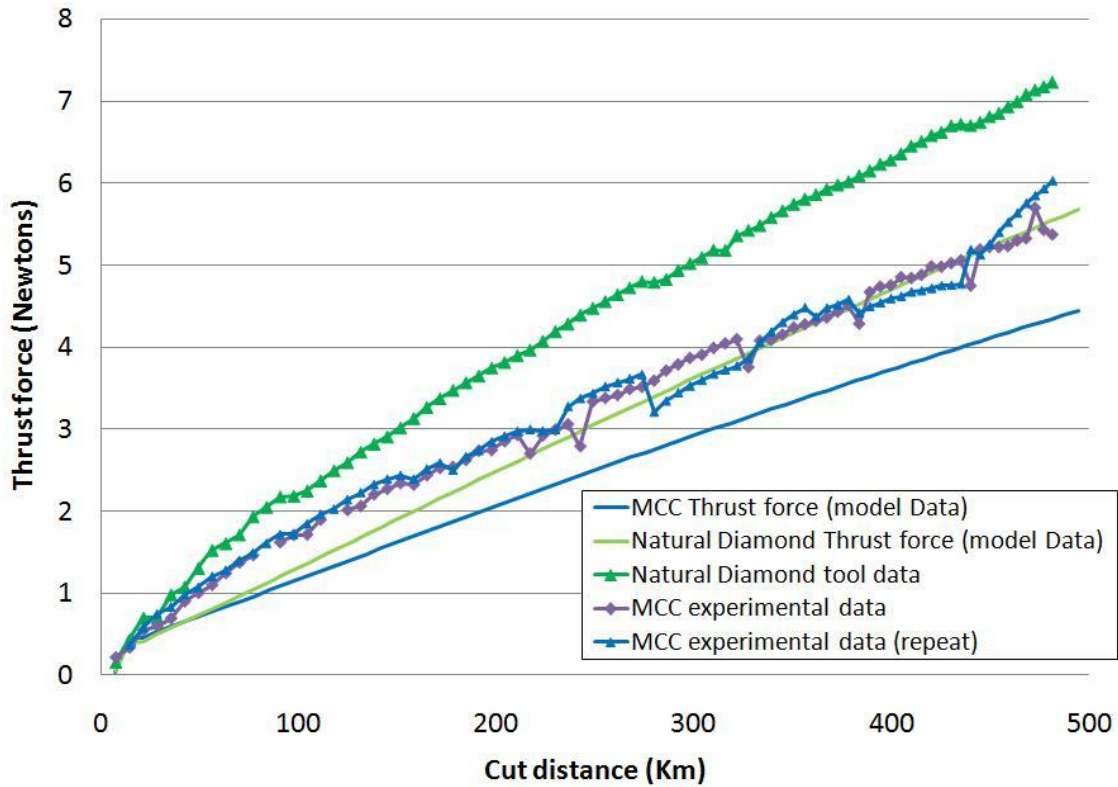
Figure 101: Model and experimental results of MCC (100/110) and natural (100/110) tools while machining aluminium.

Modelled forces are plotted with the experimental data for the MCC and natural tools. As with the silicon modelling, the model tends to predict values that are lower than the experimentally measured results.

	Natural	**MCC average**
Experiment Max. Wear-scar width (µm)	28.58	27.31
Model max. Wear-scar width (µm)	23.20	27.40
Percentage	81.20%	100.33%

Table 7: Wear-scar analysis of MCC and natural diamond tools machining aluminium.

Wear-scar analysis shows that despite problems with accurately establishing the forces, the width of the model wear-scar is quite accurate for aluminium machining.

8.1.5 Summary of initial model performance

Generally, the initial model predictions underestimated both thrust force and the wear-scar width. The model was therefore re-examined: looking at the basic assumptions and

looking for any oversimplifications that could be amended. As the magnitude of wear-scar and thrust force are related an effect that increases predicted values of either of these parameters will raise the other.

8.2 Refinements to the model

There were several refinements to the wear model as various simplifications in the basic model were re-examined and changed to closer resemble the physical situation. It is worth listing each amendment to the model and then detailing the effects these changes had.

Changes to the model:

- Addition of trailing edge
- Cutting force calculation method
- Updated force constants calculation method
- Clearance angle amendment to geometry

8.2.1 Addition of trailing edge

The initial model was consistently under-estimating the cutting forces for many tool-workpiece combinations. When the model was designed the contribution from the trailing edge was considered to be negligible as the contact area between the trailing edge of the tool is small.

Adding a trailing half of the tool and applying wear to it had the significant effect of raising the wear-scar area (and related thrust force) but also lowering pressure; making the effect on the model was difficult to predict. Generally the cutting forces rose very rapidly once the trailing edge was added, particularly for aluminium machining (as shown in following graph).
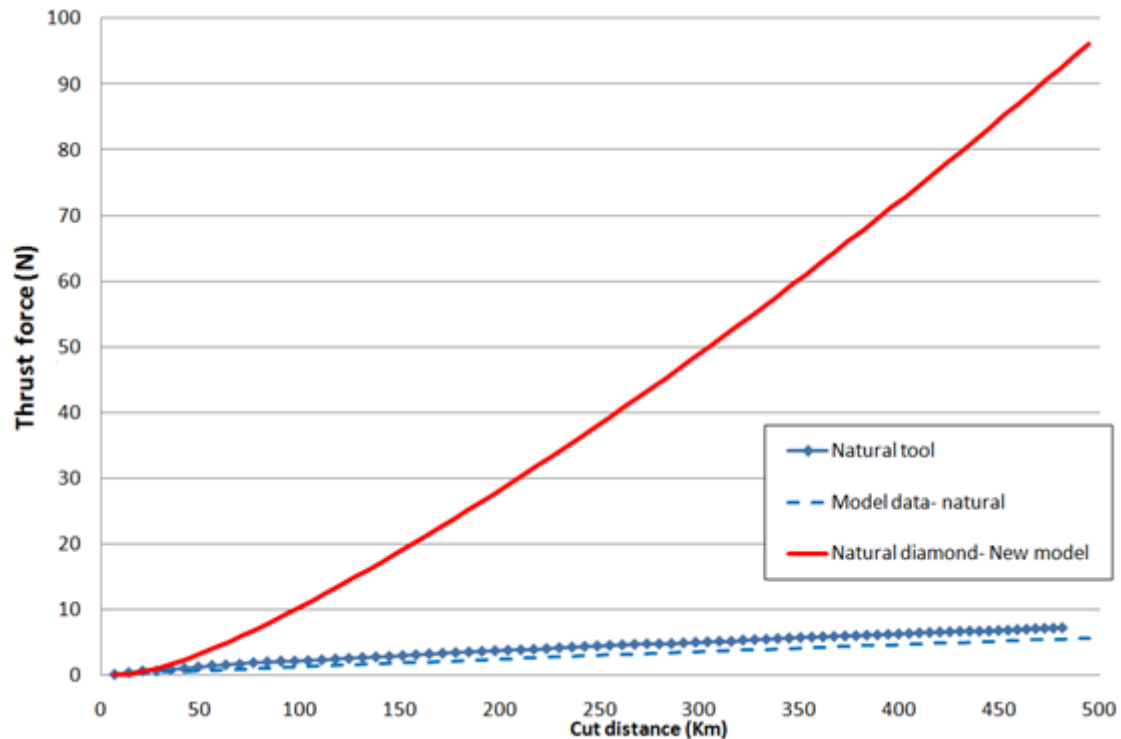
Figure 102: Natural diamond against the two models.

The addition of the trailing edge was therefore not a success. The implication from the results was that the method of calculating forces needed re-examining.

8.2.2 Cutting force calculation method

The cutting force calculation used to calculate the thrust forces of the initial model, can be represented as:

$$F_T = \ k.A$$

Where F_T is the total Force in the thrust direction, A is contact area between workpeice and tool and k is the constant of proportionality linking the two parameters. That equation is a simplified version of the following equation, (taken from Huang and Liang [55] but here using alternative notation):

$$F_T = F_{INITIAL} + k.A$$

The new addition is the initial force component $F_{INITIAL}$ which is the force acting in the thrust direction arising from the deformation of workpiece material at the front of the tool.

160

The $F_{INITIAL}$ element was initially excluded because estimating the magnitude of this $F_{INITIAL}$ component was seen as risky. Any error in that value will propagate through the model and start to affect every calculated quantity of the model. The addition of a small force component would not simply shift the cutting force curve upwards by the same value as the component. Pressure and therefore wear of each cut will be increased, resulting in greater contact areas which affects the wear experienced by further cuts and changes the contact areas. The pressures generated are quite different for the two models during the first few cuts where $F_{INITIAL}$ is contributing proportionately more of the total force and resulting in increased wear.

The only method determined as suitable for estimating the $F_{INITIAL}$ component was to examine the cutting force at the lead-on of the first cut. As it is solely related to the deformation of the material in front of the tool $F_{INITIAL}$ should only vary with tool-geometry or workpiece material (tool-material should have no effect).

Lead-on forces generated by various tools while machining silicon ranged from 0.04N to 0.12N. As the initial force component for each -25 top rake tool is independent of tool-material averaging over many results is possible and this greatly helps reduce any uncertainty in the result gathered: therefore an average value of 0.0736N was used. This value is likely a slight over estimate due to the very rapid wear expected for the first cut. Attempts to calculate the lead-on forces while machining aluminium proved frustrating, as the forces generated by this softer material were indistinguishable from experimental noise. This is due to the very small scale of cutting force when the tool starts cutting aluminium and made more difficult because the experiment used the lower sensitivity dynamometer (which was sensible considering the long cutting times and the tendency for the more accurate dynamometer to drift). Without a sensible experimental value to use, a range of potential values were tested to establish if the newer modelling approach would yield sensible predictions for aluminium machining. The test values were based upon the value used in the silicon machining modelling and ranged from 0.01N to 0.08N in 0.01N steps. From these tests it was shown that there is only a very small

effect among the selected range of values. Eventually, 0.01N was used as the force component from deformation of workpiece material as it was suitably low.

8.2.3 Updated force constants calculation method

The serious amendments resulted in a slight improvement of wear-scar predictions for the tools that were machining silicon. Cutting force accuracy was poor for silicon machining and extremely high for predictions of machining of the aluminium workpiece material. Wear-scar analysis for aluminium predictions was also disappointing, showing wear-scar predictions that were much larger than experimentally observed.

That the model over-estimated cutting forces and produced wear-scars that (for some tool materials) were far too large implies that the constant linking force to wear-scar area is too high (resulting in cut forces that are too high). As this was a problem affecting all the tools and workpiece combinations the problem was clearly with the method of calculating the constant. In particular the method for calculating wear-scar area from SEM images, leads to an error of the constant of proportionality between wear-area and cutting force (referred to as k-value). Low estimates of wear-area will produce a k-value that is too large.

Re-examination of the wear-area approximation used to find both constants was illuminating. To compare wear-area values calculated by the model against the wear-area method used to find the constants used in the model a simple MATLAB program (described in appendix D) was developed to efficiently perform these calculations.
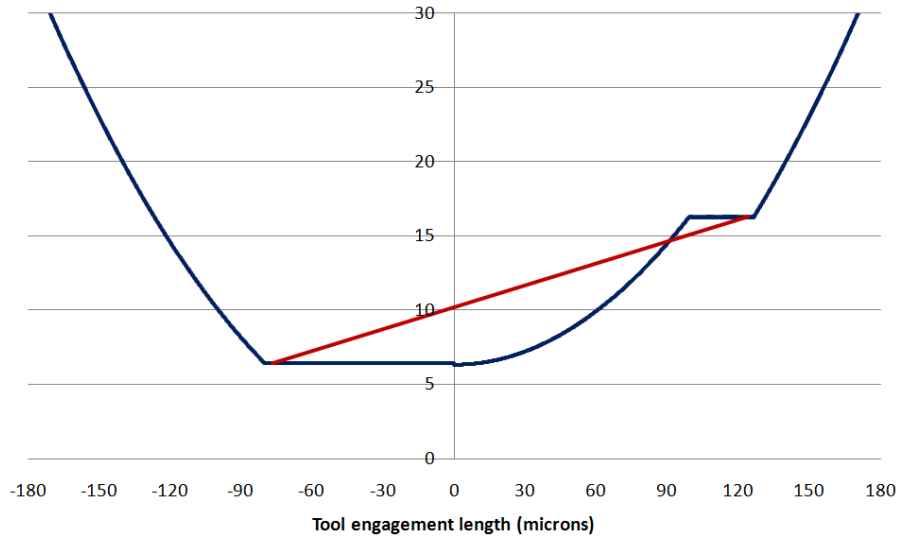
Figure 103: Wear-scar form along the tool edge and perceived length of war-scar when using the SEM (red line).

In figure 103 we see the difference in the perceived length of the wear-scar when using SEM and the real length of the scar. Clearly differences between these lines will result in differences when approximating the area.

In figure 104 the error percentage is graphed against the maximum width of the wear-scar. Where error value is defined as the value found by applying the method to determine the wear area from SEM as a percentage of the area determined by the model.
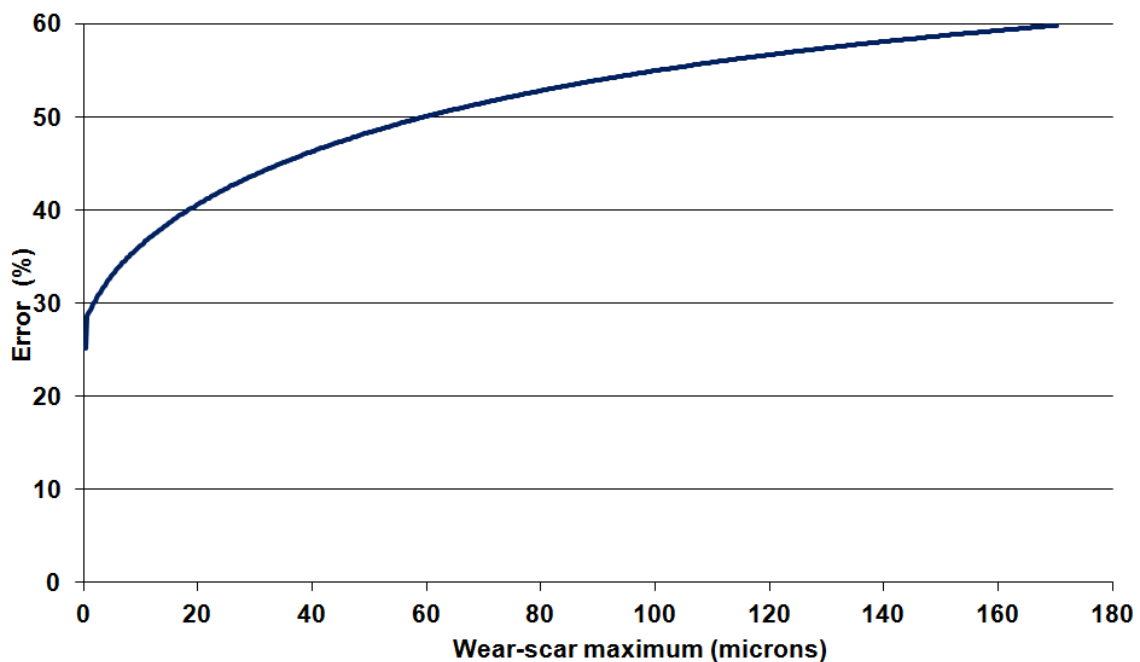
Figure 104: Comparison of wear-area calculation using tool with zero top-rake and 10 degree clearance.

163

The method of approximating wear-area from SEM images is clearly inaccurate, and also shown to vary considerably for different wear-scar maximums. In addition to changing with total wear experienced error was found to be a small influence from tool geometry. Using this information the wear constants were recalculated and the model re-tested. Applying more accurate wear-scar area values to recalculate k-values we get new values shown in Table 8.

Workpiece	Diamond tool Material	Old force constant	corrected force constant
Silicon	HPHT	1.198E+10	3.823E+09
Aluminium	Natural	3.307E+09	9.425E+08
Aluminium	MCC	2.586E+09	8.361E+08

Table 8: Old and corrected force constants for different workpiece/tool material combinations.

New k-values for machining aluminium were applied to the model.
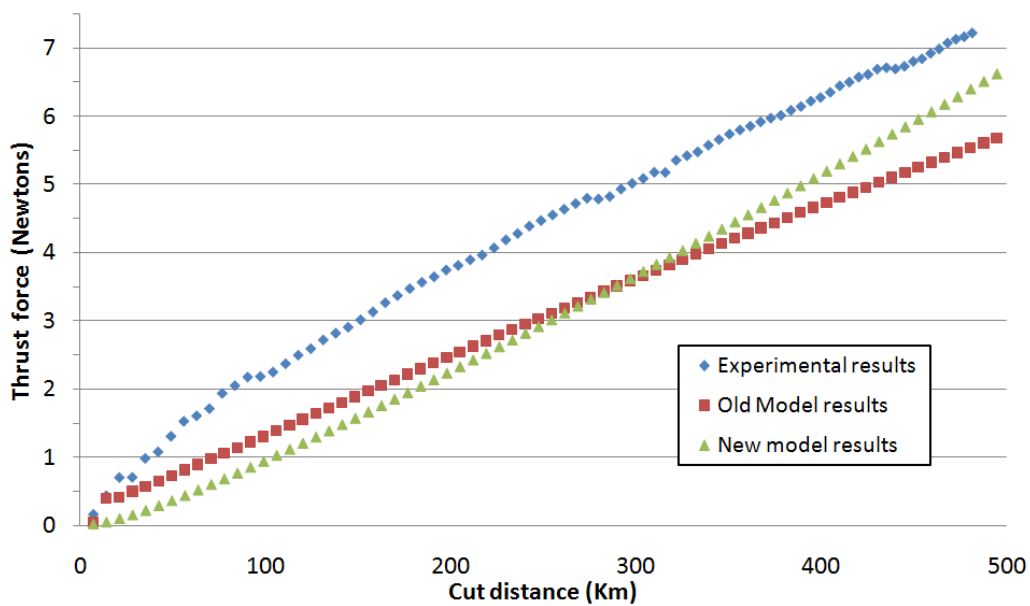
Figure 105: Natural diamond machining aluminium, comparison of experiment against model.

Though the updated force constant is worse at predicting the first 200Km of machining, after 200Km the model results start get closer to the experimental values. Examining the new values for MCC diamond tools machining aluminium are shown below.
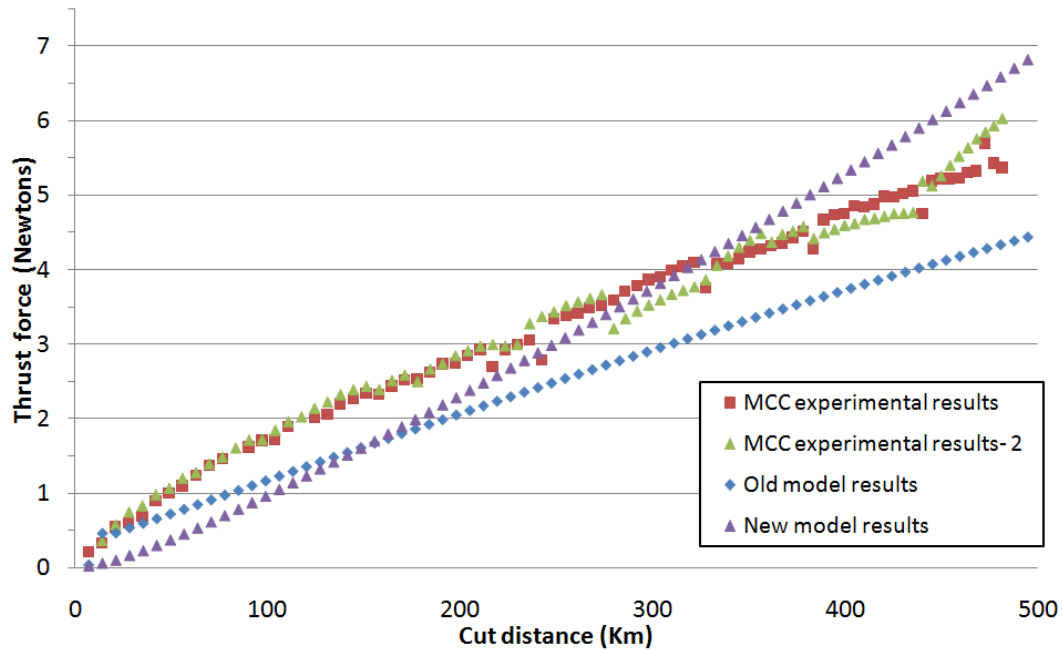
Figure 106: MCC diamond machining aluminium, comparison of experiment against model.

For machining of aluminium the model responded favourably to the adjustment of the force constant changes. However when applied to HPHT machining of silicon the model predicted very low force (achieving approximately 2 Newtons for the final cut).

8.2.4 Clearance angle amendment to geometry

At this time discussion of the tool form let to a final amendment. So far the cross-section form of the tool had been assumed to be circular, an approximation that is very close to the truth. However, the clearance angle introduces a form error by tilting the tool. Tool form is therefore a very subtle elliptical form rather than circular. Adjusting the model to change the form in this way increased contact area between tool and workpiece. Results from this final iteration of the model are presented in section 8.3.

8.3 Results of the final model

Comparison of the forces generated by the very first model described in 8.1 and the latest model incorporating all the changes in section 8.2, shows the comparative improvements gained.

Explaining how a tool fails to generate a ductile surface on a silicon workpiece is not going to be significantly explained by a model that only models attritious wear. A model attempting to model silicon machining would have to predict chipping damage to the tool-edge. This is further complicated, as the scale of the chipping damage and the location of the chipping damage are both important factors. A model predicting all these factors is clearly impossible. Because explaining the failure mode for SPDT machining of silicon can not be achieved using an exclusively attritious method, modelling of silicon machining was removed from the modelling work during the final model.
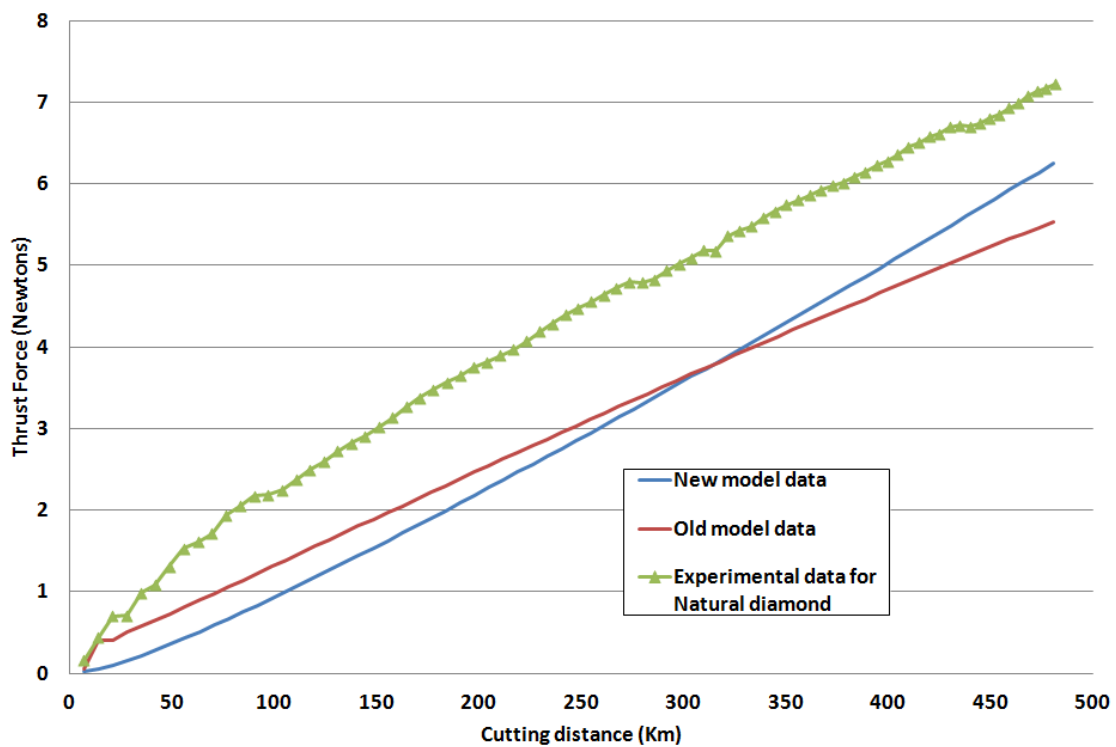
Figure 107: Natural diamond machining aluminium, model predictions against experimental data

The many adjustments have the effect of reducing accuracy before the ~300Km point but after this the final model performs better. For the final cut predicted cutting forces are within 0.98 Newton of the force measured during the experiment. To maintain

clarity the standard deviation of the experimental data is not shown, but the standard deviation of force measured at this distance in the experiment was 0.39 Newton.

The results for the final model were better for the MCC tools, as shown on figure 110.
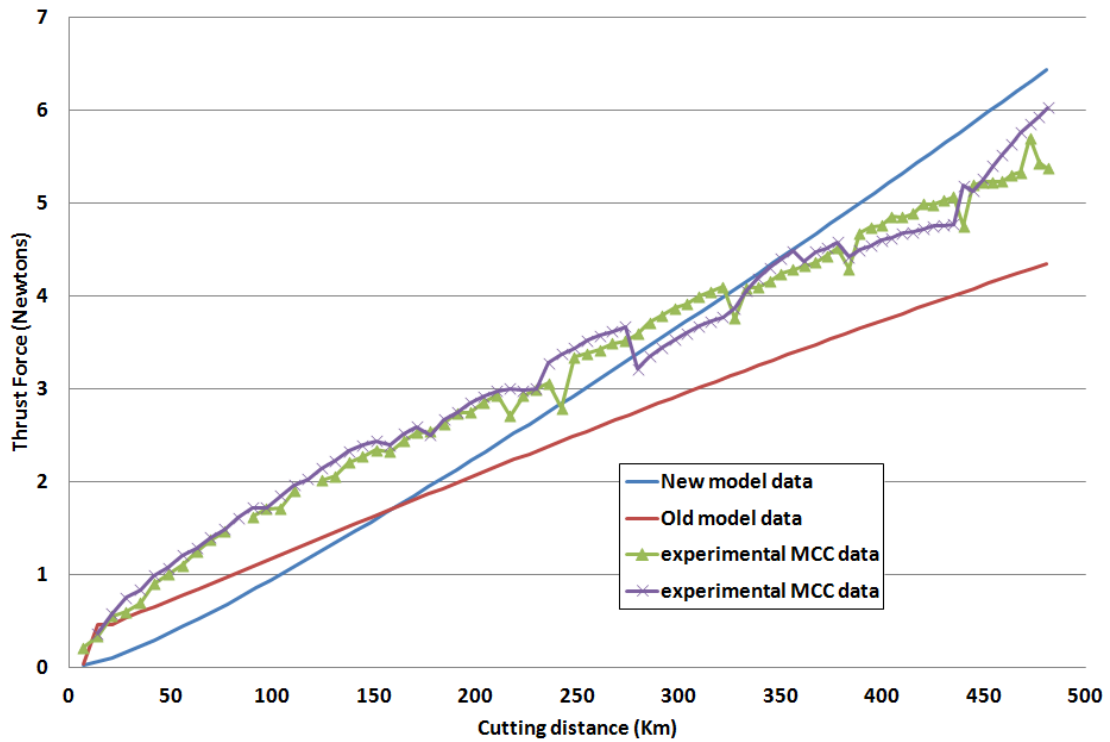
Figure 108: MCC tool machining aluminium, model predictions against experimental data

In the above figure the predicted force closely matches experimental work from ~240Km onwards. The standard deviation of the experimental work is not shown here but will be discussed.

At the final cut the model prediction is at closest 0.4 Newton away from experimentally measured average force (this experimental data had a standard deviation of 0.28 Newton). The model prediction is 1.05 Newton above the lower experimental data set at the end of the curve, (standard deviation on that data point was 0.35 Newton).

Chapter 9- Discussion

The discussion aims to clarify the contributions to knowledge gained from this work. The supertool phenomena is discussed first and the likely cause explained. Following this is the work on synthetic diamond tools which allows the effect of crystallographic orientation and the tool material to be analysed, each has a section dedicated to these issues. This leads to section 9.4 which is a discussion of the failure modes of diamond tools while machining brittle materials. Finally, the developed model is discussed in section 9.5 with a focus on the Preston's equation and the Waldorf wear-force model.

9.1 Explanation of the Supertool phenomena

Early during this work three possible causes of the supertool phenomena were identified:

- Nitrogen content
- Crystallographic orientation
- Crystallographic defects

Experimental methods were used to analyse the properties of a group of diamond tools. A supertool had previously been identified [2] and confirmed by the results in chapter 5. Tools from the work of Jacklin [2] that had previously been identified as normal diamond tools were able to provide a control group for comparison against the supertool.

9.1.1 Fourier transform infra-red spectroscopy

Using FTIR spectroscopy different impurity elements can be identified and even bonding structures between impurity atoms can be found. Tools S65317 (supertool) and tools S65314, S65315 and S65319 were sent to the Diamond Trading Company (DTC) for independent FTIR testing.
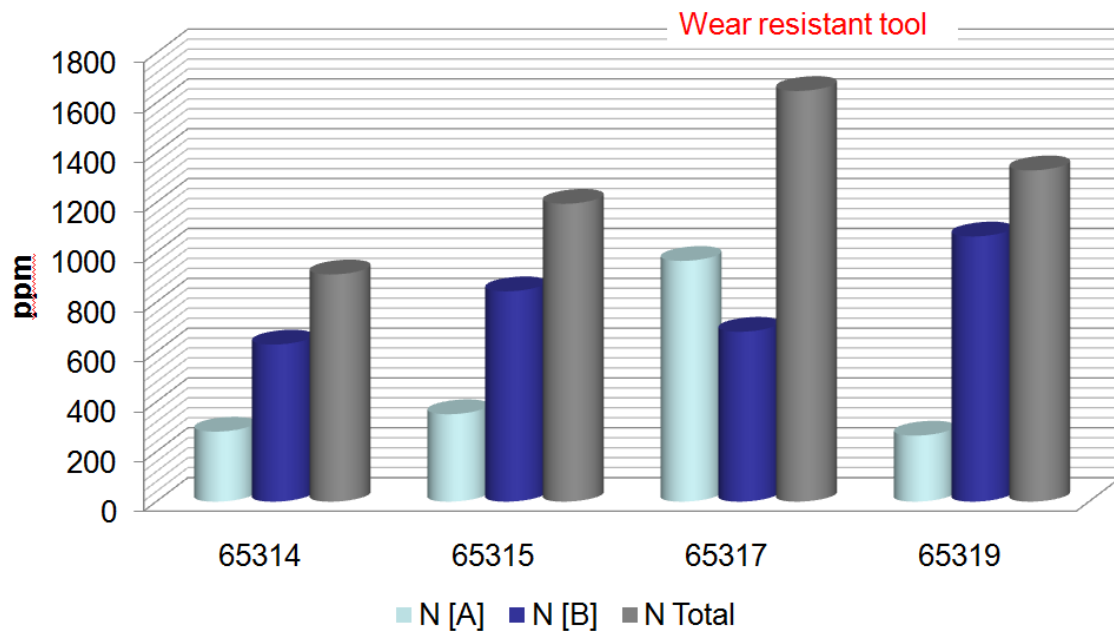
Figure 109: Concentrations of different impurity types with natural diamond tools.

Of interest in the above figure is the N[A] type of defect, a combination of two bonded nitrogen atoms within the structure of the diamond. Tool S65317 shows a high concentration of this defect type. The presence of this defect type could be linked to the extraordinary tool-life displayed by S65317. It should be noted that the supertool S65317 has the highest concentration of total nitrogen, a fact that puts it contrary to the widely held belief that nitrogen content is bad for a diamond tool. This apparent contradiction is likely the result of ignorance about the different failure mechanisms at work: researchers often assume that volumetric wear of the diamond tool leads to failure. For machining of aluminium (or other soft materials) this may be correct but this thesis has demonstrated that while machining silicon with diamond tools crystal properties that affect brittle fracture behaviour of the tools edge will be important.

That purer diamond crystals experience lower volumetric wear is intuitive. Reasons for the link between a high concentration of N[A]-type nitrogen and a diamond tools resistance to the likely change in tool-geometry that leads to a failure to machine in a ductile way are not intuitive. One possible explanation is that the presence of the B-type nitrogen defect helps slow the progress of fracture along the {111} orientation cleavage planes by forcing energy to couple across into other planes. Similar theories have been

suggested previously [43] but for different defects. This new application of the recent platelet-hypothesis does not agree with the findings from this project, primarily because the S65314 and S65317 tools we have examined using SEM do not have significant differences in the number of chipped damage sites, chipping size or distribution of chipping damage. This knowledge about the composition of the supertool could be used to screen for diamonds with the relevant properties (as attempted previously [43]). Alternatively, engineering the tool-material for specific applications may be possible using the range of natural and synthetic diamonds available. One method is annealing, which has been performed on various grades of diamond [36,41,100] and has been shown to be able to alter the composition of diamond.

9.1.2 X-ray topography and cross-polariser strain measurement of tools

Another experimental technique used to investigate the possible origins of the supertool phenomena was X-ray topography (XRT). XRT is a technique that has been used successfully to investigate crystallographic properties of diamonds, and has high resolution. For example, M.Moore has used XRT to examine the more unusual diamonds that have been found, such as those showing twinning behaviour [28,29] or the extraordinary single crystal that displayed two different coloured sections [47]. Time was booked at the Daresbury synchrotron radiation source with the aim of seeing appreciable differences between normally performing natural diamond tools and the previously identified supertool. Specifically, station 16.3 was used (described in the literature [101]).

Nothing significant was found while testing for crystallographic defects in the tool-edge of the tools tested. However, looking for a cause of supertool behaviour in an analysis of the crystallographic perfection of the tool-edge was a mistake. It was previously established that tools maintain their relative performance after re-lapping [2], a process that removes about 20-30 µm of material from the top-rake face. Knowing that supertool behaviour is preserved during this process it is possible to conclude that the origin of the supertool behaviour has to be related to one of the bulk properties of the diamond tool.

XRT can provide information on the crystallographic perfection of the diamond and via rocking curves examine the distortion of the crystallographic structure within the diamond, as shown in the literature [26,47]. As it is known that a bulk property that is of interest, using XRT to measure distortion within the crystal was excessively complex. A simple cross-polariser experiment would show the samples to have different internal strain behaviour, as used previously for diamond within the literature [102].
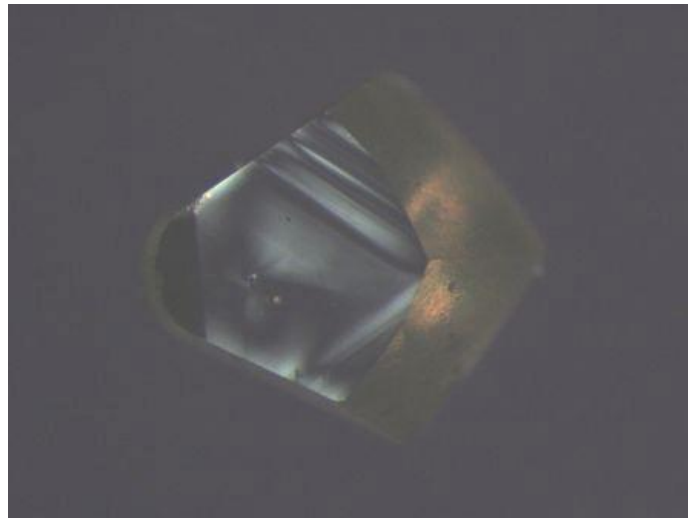
Figure 110: Cross-polariser image of diamond tool S65315.

Cross-polar images were taken, but the results were not decisive. Diamond tool S65315 displays a higher internal strain than tool S65317.
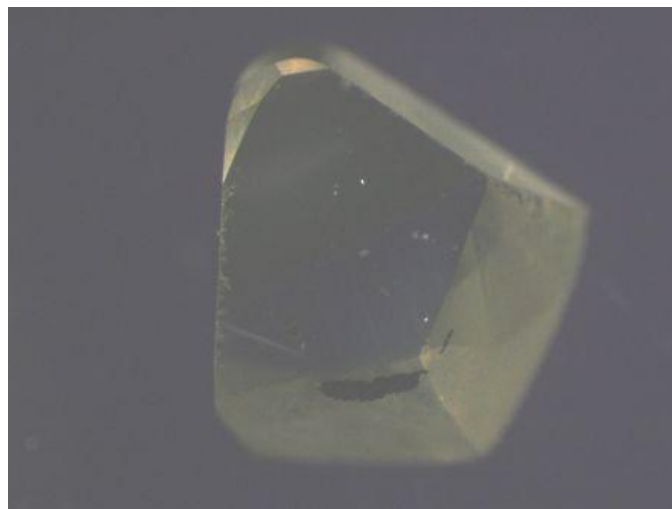
Figure 111: Cross-polariser image of diamond tool S65317.

The identified supertool therefore has less strain than the normal tool. Internal strain is an artefact from the diamond crystals growth conditions [19,47] and is not significantly affected by the tool making process.

9.1.3 Summary of the supertool phenomena

At the start of section 9.1, three hypotheses for supertool behaviour were proposed; nitrogen content, crystallographic orientation and finally crystallographic defects. Each has been examined, using the supertool identified in previous work [2].

Purity of diamond appears to be of very limited importance. Certainly the high purity MCC (100/110) diamond tools have shown poor performance during cutting trials against silicon. Nitrogen content of natural diamond tools was examined using FTIR and by examining the concentrations of various different defects the supertool was shown to have an unusual concentration of N[A]-type nitrogen. It is now believed that this type of defect is very significant for supertool behaviour.

As detailed in chapter 5, diamond tools were sent to the DTC for x-ray diffraction analysis to determine the orientations of the tools. Each tool was made to the (100/110) orientation but displayed slight offsets in pitch, roll and yaw degrees of freedom. The analysis did not reveal any unusual properties of the supertool and proved to be inconclusive. Orientation of the diamond tool is therefore considered unlikely to give rise to supertool phenomena. Crystallographic defects are also eliminated as a potential cause of supertool behaviour. If an unusual defect was causing supertool behaviour it would be removed during the re-lapping process and the cutting performance of the tool would change, but it is known that tool behaviour is unaffected by the re-lapping process.

Many different analytical techniques were used to investigate different aspects of the supertool. Combined, these different investigative techniques show that N[A]-type nitrogen is the likely cause of the supertool phenomena, while other tool-life factors are less important. It is important to be clear that while many sources claim higher purity diamond is better for diamond turning tools, the ideal tool for diamond turning does

seem to be dependent on the workpiece material to be turned. For aluminium cutting the high purity MCC is clearly superior to natural diamond tools. For silicon the MCC material is much worse as a tool-material.

9.2 Effect of tool material

It is important to understand the effect that changing tool material has upon tool-wear during the SPDT process so that the correct material can be used for cutting a workpiece. Using an MCC tool will produce lower cutting forces and a smoother finish while cutting aluminium (as demonstrated by the thrust force data and lower R_a shown in chapter 4). For aluminium the requirements for choosing tool material is clear: a higher purity diamond is preferable and now with the availability of MCC the choice is clear.

For the machining of silicon the criteria appears to be more complex and involve at least two possible failure modes. However, a comparison between MCC and HPHT is possible and gives clues to the effect of nitrogen content on tool-life.
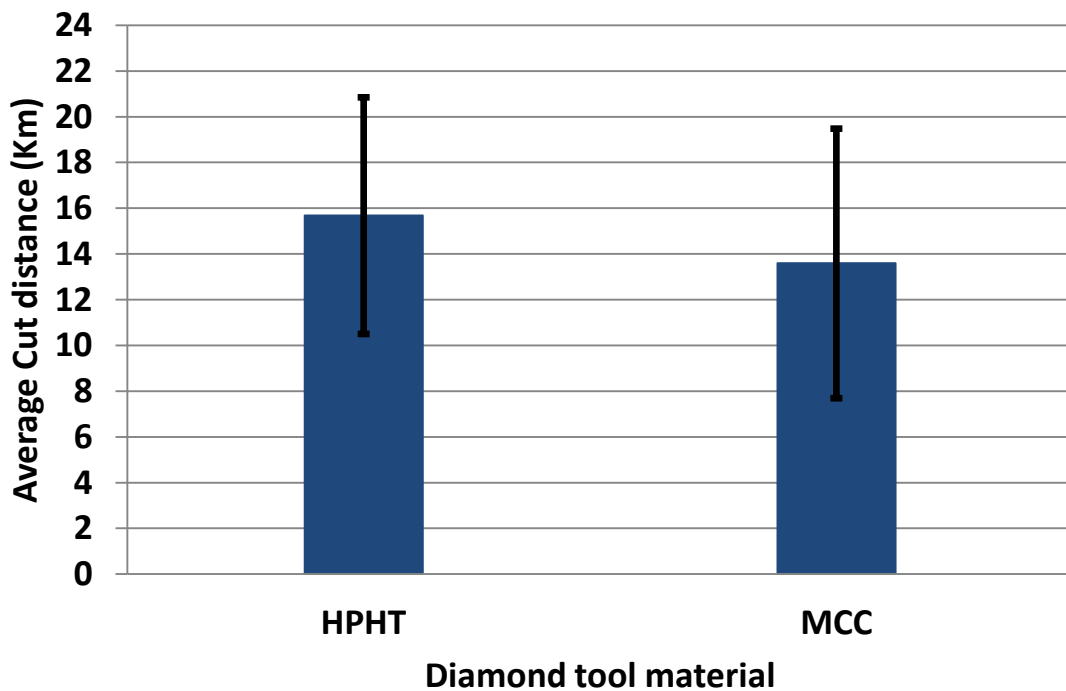
Figure 112: Average achieved cut distance for HPHT and MCC tools when machining silicon.

This graph implies that regardless of tool orientation the HPHT diamond is better suited for machining of silicon. However considering the very poor result of both synthetic diamond types compared to natural diamond clearly the composition of an ideal diamond material for silicon machining is more complex.

It is sensible from the work performed in this thesis to conclude that MCC would be superior for machining all workpieces below a threshold hardness. This threshold may be much higher than expected, as tools machining silicon have a very limited tool-life even when compared with germanium or other workpiece materials used for IR-applications.

9.3 Effect of crystallographic orientation

From the literature it is known that diamonds polish at different rates in different crystallographic orientations [33,34,35], a natural result of the strong anisotropic material parameters. When the natural variation of tool life was found during the work of Jacklin [2] a possible explanation was variance in the crystallographic orientation of the diamond tool. Using the data from both HPHT and MCC synthetic materials and both the (100/100) and (100/110) crystallographic orientations gave enough data to establish the effect of crystallographic orientation upon the attritious wear of diamond tools during SPDT.
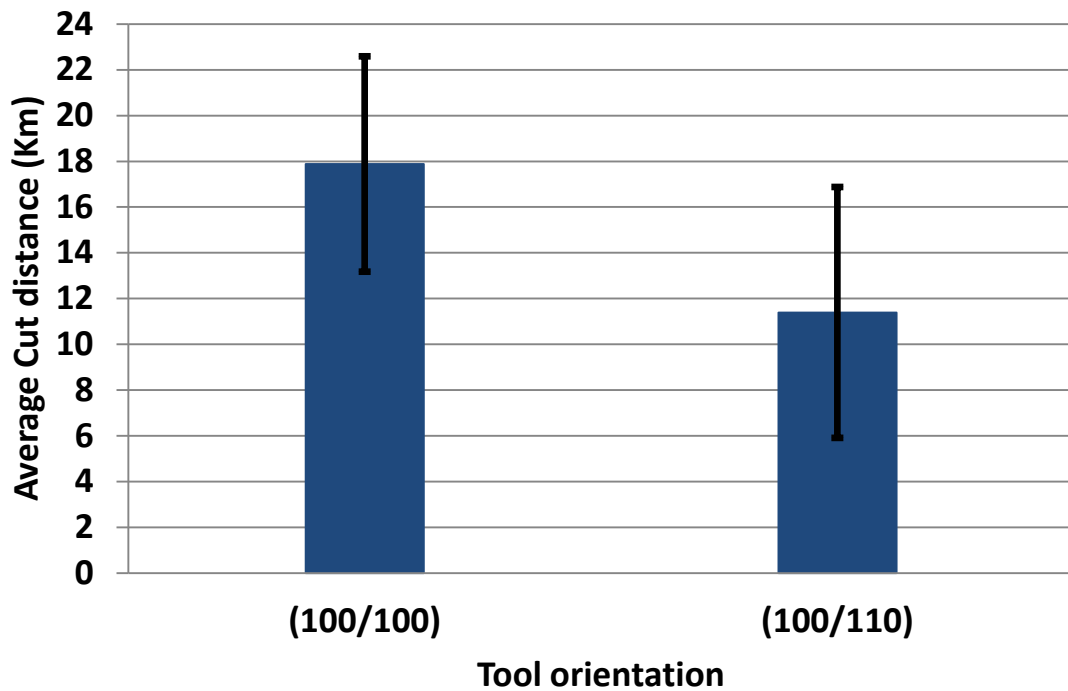
Figure 113: Average (100/100) and (100/110) orientation tool cut distances.

This finding is unusual as industry prefers to use (100/110) orientation tools for most roles. Generally the (100/100) orientation tools displayed linear cutting force progression (particularly the HPHT tools in this orientation) while the (100/110) orientation tools generally adopted a non-linear trend. Comparison of the SEM images gave the clearest indication of the reasons for this difference in cutting force progression with the frequent chipping damage seen on the tool-edge of the (100/110) orientation tools. All the (100/110) orientation tools displayed such damage, and would work to lower the contact area of the tool-workpiece interface. Therefore this damage type works to effectively lower the area and lower resulting cutting forces, however the attritious wear that is experienced will constantly drive cutting forces upwards and we therefore see the non-linear relationship develop.

It is interesting that a change in crystallographic orientation of the tool from (100/110) to (100/100) eliminates any chipping of the tool-edge. Clearly the orientation of the tool results in the {111} equivalent planes being easier or harder to couple energy into. Related to the discussion about the (100/110) and (100/100) orientation tools is the effect of tilting the tool through the additional 20 degrees required for the -45 top-rake

angle work. This changed the orientation of the tool with respect to the workpiece, influencing the wear-behaviour seen and suppressed any chipping of the tool-edge.

9.4 Failure mode of diamond tools

A persistent theme during this thesis is the failure of diamond tools. With silicon the failure is clearly visible on the workpiece but the cause of this failure has never really been well defined in the available literature. There was a general assumption that volumetric wear of the diamond tool was linked to failure [52], but the work presented here clearly puts a case for that assumption to be rejected. Indeed, this work has shown that there are at least two failure modes possible when machining brittle workpiece materials. Here is a discussion of these failure modes, attempts to characterise and explain their origin.

9.4.1 Discussion on the geometry failure mode

Discovering that geometry changes of the tool can lead to failing to machine silicon in a ductile manner is a new finding generated by this project. This finding was reported at the Lamdamap conference [87] but to remain within the non-disclosure agreement the results from the MCC tools were withheld and the comparison between natural tools and HPHT tools was used to illustrate the failure mode.

The basis of this failure mode is in the fracture mechanics demonstrated in the work of Lawn [6,8] while the MATLAB code that was used to calculate the thickness of removed material is an expansion of the work by Blake and Scattergood [5], and is similar to work done on grinding of brittle materials [103]. Though this thesis has focused upon silicon and may have given the impression that silicon is the only material which is affected by this failure mode when diamond turned. However all brittle materials will be susceptible to this failure mode. Many of the IR-materials used in optics are brittle and would have values of critical thickness of removed material similar to that of germanium or silicon. The minimum crack length of silicon is approximately

0.4 µm [8], while germanium has a lower minimum crack length (which allows germanium to be more easily diamond turned).

It should be clear that for all brittle materials a detailed look at the thickness of removed material for a given tool geometry is important. Particularly as complicated tool geometries begin to be developed using sub-micrometre machining methods (such as FIB machining methods [80]). As shown in this thesis a FIB tool with a deliberately machined defect far from the generated cut plane was able to lead to fractures within the generated surface. This result illustrates the problem with trying to make predictions of crack length from a tool with any given geometry: because fracture mechanics can not predict crack lengths accurately (due to the geometry dependencies in existing equations). We are therefore limited to making predictions using minimum crack lengths of materials. For example, we now know that while generating minimum crack lengths a small chipping damage type defect at the front of the tool will almost certainly induce cracks into the workpiece.

An interesting attempt to reduce tool-wear issues when machining silicon is the work of Marsh et al. [104] which used a rotating tool. Their experimental design is very similar to the traditional diamond turning arrangement but is intended to distribute wear across a much larger tool-edge than normal by rotating a rotationally symmetrical tool. Knowing about the geometry failure mode and the critical effect having even small areas of chipping damage close to the generated surface clearly means this methodology is unsuited for turning of brittle materials. There are problems with rotating tool methodologies when turning softer materials too. Such as the machining set-up introducing a second spindle which has the effect of reducing stiffness and increasing spindle error motion [104]. Furthermore, tools using this approach are also likely to experience uneven wear as a result of the effect of orientation on wear, with the likely effect that tool geometry will stop being circularly symmetric. For all these reasons future work should not focus upon this rotating tool method.

9.4.2 Discussion on the pressure failure mode

Tools that are free of chipping damage have been shown to induce cracks into brittle workpieces. The cause of these failures is not clear, but pressure is considered related (details are in Chapter 5 and were presented [87]). A paper that discusses issues related to the pressure failure mode is the recent work of Yan et al. [105]. This paper extensively discusses pressure effects during an increasingly deep cut, (a cutting arrangement much like the work of O'Connor [7], but drawing very different conclusions).
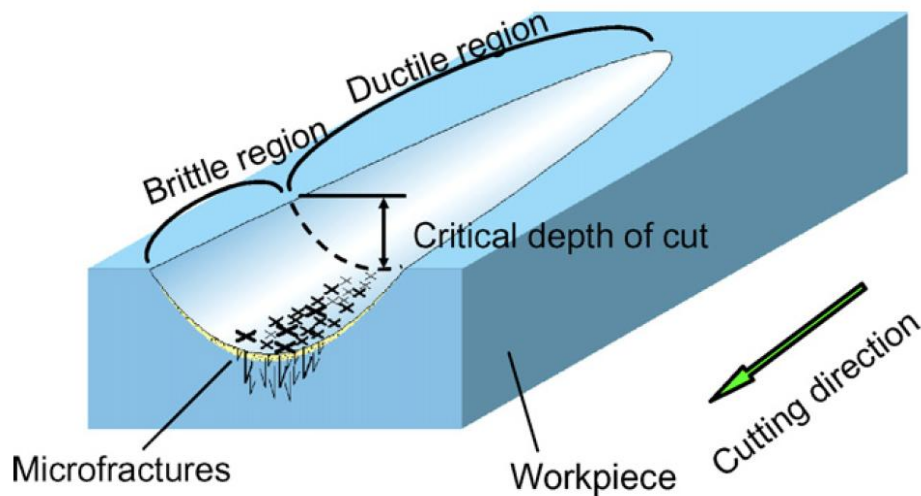
Figure 114: Cutting scheme used by Yan et al 2009 [105]

The methodology shown above displays an ignorance of the work of either Blake and Scattergood [5] or Lawn [6] as both these papers would show that the increasing thickness of removed chip has lead to this brittle fracture: it was not caused by excessive pressure. Cutting forces presented within this paper also appear to be unusually high considering the extremely shallow depth of cut and the presumably sharp status of the tool. Calculated pressures offers the clearest comparison of the discrepancy between the data presented by Yan and the work within this thesis. The work of Yan [105] reported pressures regularly in excess of 10GPa while the work on HPHT in chapter 5 indicates that HPHT calculations of pressure gave values of approximately 4.6GPa [87]. From the error analysis of the model in Chapter 8 it is known that the simple method used to calculate wear-area is estimating approximately 35% of the true wear-scar area value, therefore a closer estimate for pressure during the

final HPHT cuts is closer to 1.6GPa. Whatever the true pressures generated during diamond turning of silicon, it is clear that they are large. From examination of a diamond turned silicon workpiece Shibata et al. [16] was able to discover a thin layer of amorphous silicon and was verified by Tanikella et al. [15] and Jasinevicius et al. [14,16]. This is strong evidence that successful ductile machining of silicon requires sufficient pressure to change the workpiece material from the crystalline phase into the amorphous phase, possibly via a metallic phase [18].
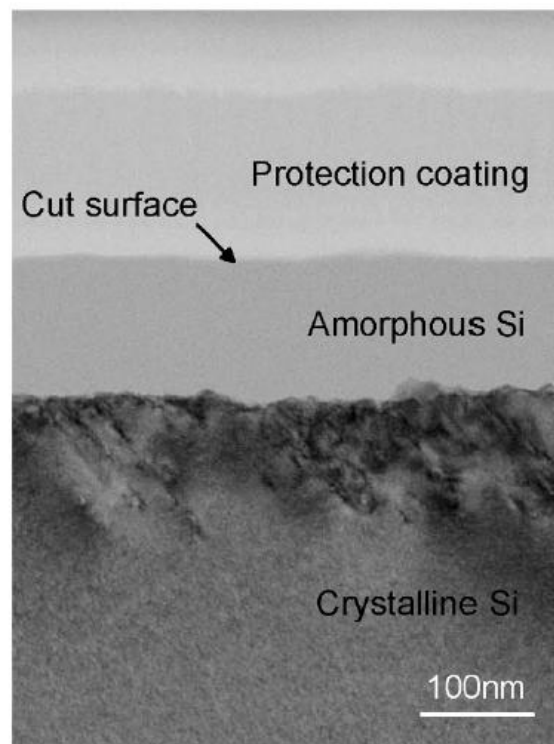
Figure 115: Cross-sectional TEM micrograph from reference [4]

From the above and the previous work of Puttick [4] we can assume that much of the removed material from a workpiece is in an amorphous phase. It should be noted that for many models attempting to predict thermal behaviour, the thermal properties of the chip is a required variable. Amorphous silicon is reported as having a thermal conductivity of 1.5W/mK and heat capacity of 992J/Kg K [106]. The same source makes it clear that the thermal conductivity of amorphous silicon is approximately 100 times lower than the crystalline phase, and therefore this is clearly an important factor to consider for thermal modelling of diamond turning of silicon.

Knowing that there is a pressure threshold below which silicon will not undergo phase-transformations it could be argued that the pressure failure mode arises not from a rise in pressure above a threshold limit, but from pressure dropping lower than the phase-transformation threshold. Essentially a tool that is not causing sufficient pressure to initiate the phase-transformation could be causing initiation of cracks. It is known that wear-scars get bigger as cut distance is increased, so pressure may be lowered through this mechanism. However from the modelling work there is reason to believe that is not the cause.
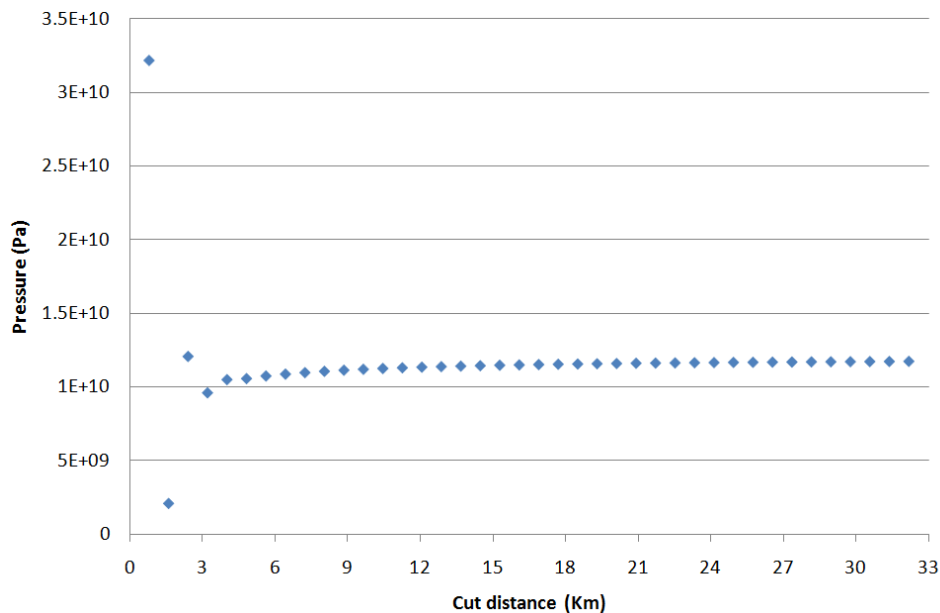
Figure 116: Pressure calculated from HPHT model results.

Pressure values calculated from the amended model results do not show any significant drop in pressure. It is important to note that these calculations of pressure are average values across the tool-engagement length. With brittle materials we would expect fracture to occur high up the cut shoulder reducing pressure there and therefore greater force to be focused through the nose of the tool. Peak pressure within the tool-workpiece interface can be reasonably assumed to be higher than average values calculated.

Much about the pressure failure mode remains unclear and the true failure mechanism could well be only indirectly linked to pressure. The exact method in which the brittle fracture of the workpiece material is being caused in the failure mode here termed the "pressure failure mode" is unclear. From the pressure calculations from the developed model it could be argued that it is not related very strongly to pressure. Not knowing the full origin of this failure mode would be a bigger concern if this failure mode was more widely applicable but so far it seems to be limited to the (100/100) orientation tools, which are not widely used for machining brittle materials.

A case could be made that there is no pressure failure mode and this failure mode is actually a misdiagnosis of the geometry failure mode. Checking worn tool-edges and calculating the thickness of removed material using the technique described in appendix B would quickly determine if this is happening. Using the wear model to generate a worn tool edge (using HPHT tool material constants and a cut distance of ~32Km) and then analysing that curve using the chip-thickness code used to explain the geometry failure mode. From this examination we know that the removed material remains very similar to that of an unworn tool. As always it is the way material is removed closest to the generated worksurface that is of most importance. This examination of removed material, when combined with the evidence from the FIB modified tool-edge trial shows that the pressure failure mode and the geometry failure mode are not re-iterations of each other and are separate methods for diamond tools to fail.

9.5 Discussion of the modelling methodology

To the authors knowledge applying the Preston's equation to diamond tool-wear is a new application of an old equation. The Preston's equation is fairly simple, depending as it does upon force in the thrust direction, contact area and the Preston's coefficient. Using a Preston's equation method can generate worn tool shapes but despite many small revisions the data from the model thrust force predictions are not satisfactory.

One of the amendments made during the model updates was the inclusion of a small permanent force component from the deformation of workpiece material on the top-rake face of the diamond tool. This change moved the model closer to the cutting model it was based upon [83] and disposed of the previous estimated cutting force value used for the first cut. On its own the cutting force adjustment made only a small difference to the models outputs. However when wear of the lead-off tool-edge was combined with the adjusted cutting force calculation method the results were dramatically changed. Cutting forces were suddenly predicted to be extremely high, while wear-volume on the tool edge was adjusted down a significant amount. As noted in Chapter 8, this is a result of problems with estimating the constants and originates in the problems with estimating contact area. Better methods of estimating wear-area from SEM images would be extremely helpful to improve the accuracy of the values used to determine wear. The model appears to be describing the wear of a diamond tool quite well despite these difficulties. The final model predicted forces fit well to a straight line but many of the experimental data sets appear to be non-linear. A Preston's treatment of tool-wear therefore appears appropriate; but the Waldorf cutting force model could be argued to be over simplified.

9.5.1 The Waldorf wear force model

The developed model used a version of the Waldorf wear force model simplified by ignoring the force in the fed direction and limited to the force component in the thrust direction. This greatly simplified calculations however it may have been an over simplification that adversely influenced model accuracy.

By only calculating forces in the thrust direction the contribution to tool-wear from force acting in the feed direction was ignored. This is a sensible assumption when looking at the end of a tools life as the force in the feed direction is small compared to the thrust force. The assumption is much less accurate while modelling an unworn tool when the forces in the feed and thrust directions are of similar magnitudes. The first few cuts are extremely important for the tools further development and therefore force in the feed-direction may be more important to include than originally thought.

Implementing this second force component would get extremely complex very quickly and would be a significant technical challenge however we can anticipate some of the effects this would have and evaluate if this would be beneficial to the model accuracy.

- Over the first few cuts we would expect calculated wear to be higher, resulting in greater contact area and therefore a quicker rise in thrust force. All would help the accuracy of the model.

- Slight non-linearity would be expected. Initially the model would predict higher wear but once the contribution to total force becomes low the wear will change. This would likely change the linear thrust force progressions that the model currently produces and should help model predictions.

Introducing a force component in the feed direction would subtly change the way that damage is applied to the modelled tool. Wear recession is parallel with force, so by introducing a second force component wear will also act across the tool profile in the feed direction.
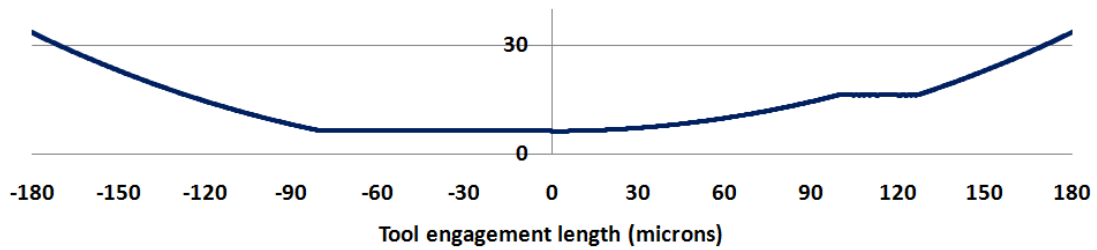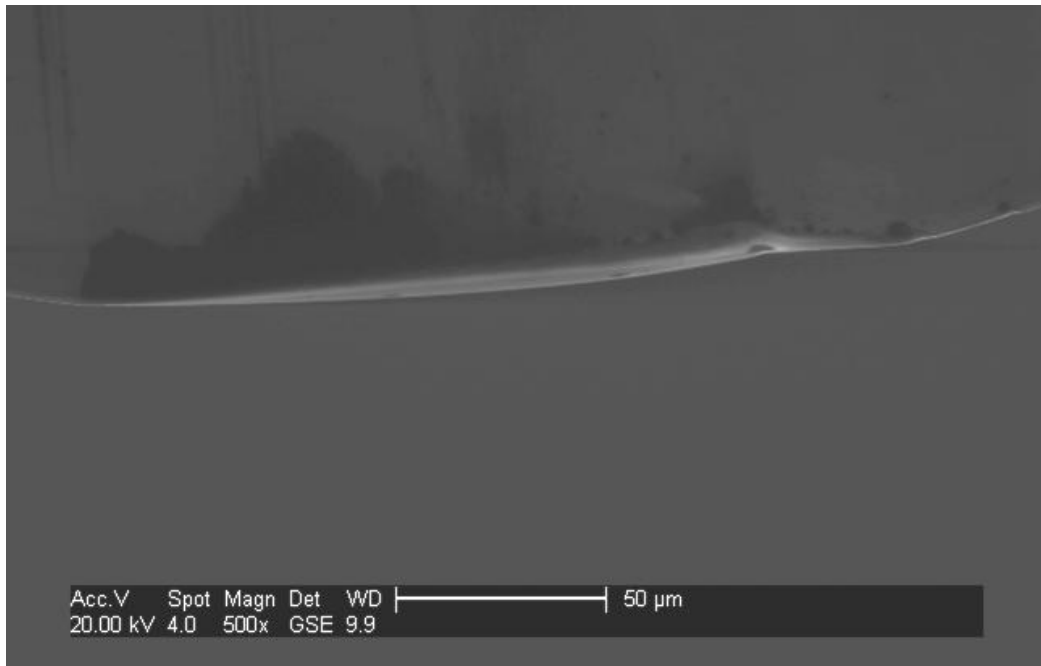
Figure 117: Comparison of tool wear form. Top image: an MCC tool used to machine aluminium. Lower image: the tool profile predicted by model.

As the above image shows the simplified wear direction used in the model provides suitable form predictions with a single component. It is therefore expected that the inclusion of the second force component would have only a very minor effect on geometry. If wear from multiple components need to be considered the anisotropic wear-resistance of diamond [84,85] will also need to be considered. If wear is applied in different directions at the workpiece-tool interface the problem quickly becomes extremely complex.

9.5.2 Application of Preston's equation to wear of diamond tools

The Preston's equation can be arranged into the following form:

$$\Delta H = K_p * (L/A) * \Delta s$$

Which links the wear-recession distance to pressure (load L divided area A) and distance traversed (in the case of diamond turning, the cut distance). Preston's equation is therefore not dependent on the sliding velocity and agrees that wear should be independent of velocity considerations, which agrees with our work at 3000rpm and 1200rpm. This finding contrasts with the work of Hird and Wilks [33], which looked specifically at diamond polishing upon a scaife type apparatus.
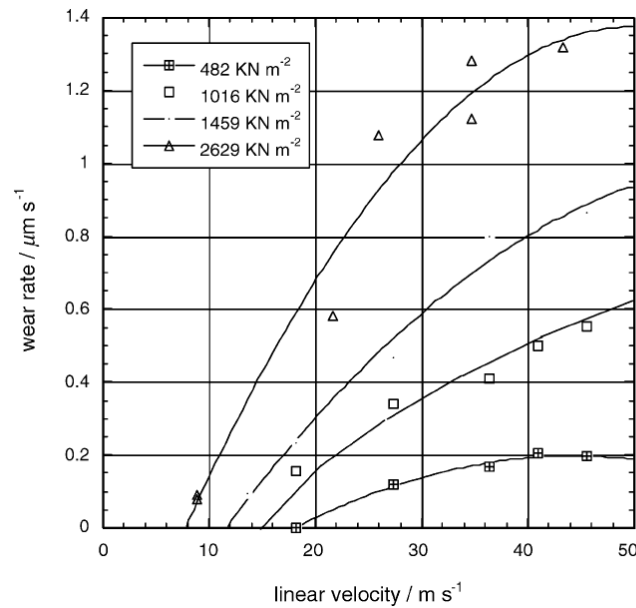
Figure 118: Non-linearity of wear rate with linear velocity [33]

It is not clear if this is particularly applicable to diamond turning, as the sliding velocities used during diamond turning tend to be quite low due to a combination of small component size and limited spindle speeds (for example the spindle on the Moore machine is limited to 6000rpm).

Looking at the slightly earlier work of Hird and Field [34] we see their later claims of a non-linear dependency might not be real as the uncertainty of the experimental work is large.
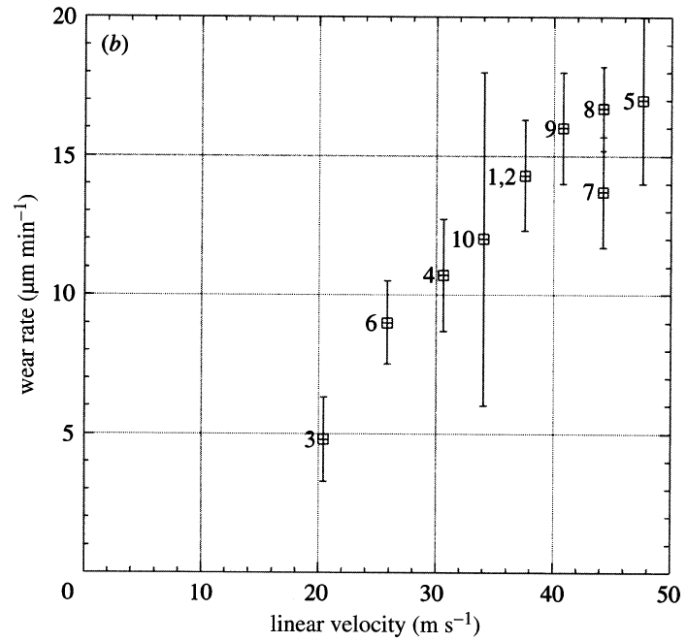
Figure 119: Earlier scaife experiments from Hird and Wilks [34].

As the paper explains, there were issues with experiments 7 and 10 that raise questions about their validity. Particularly experiment 7 where the diamond sample was reportedly set incorrectly. The maximum sliding velocity during turning a 32mm diameter workpiece at 3000rpm is only 5.03m/s. Even the extreme situation of a 200mm diameter workpiece being turned at 3,000rpm will produce maximum sliding speeds of 31.4m/s. It is therefore clear that most diamond turning of brittle materials will happen at sliding velocities not well described by the scaife polishing work of Hird and Wilks [34].
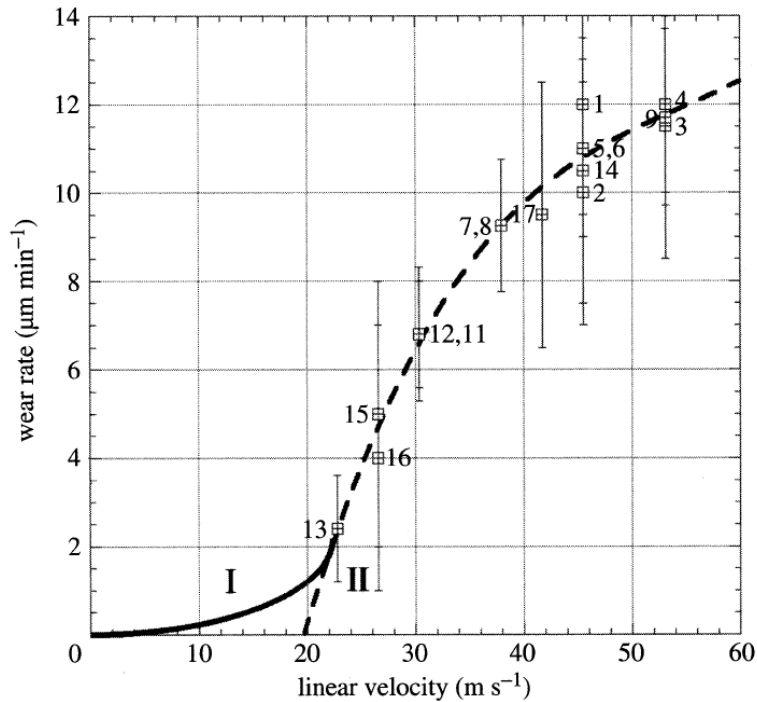
Figure 120: Hird and Wilks attempt various fits to the data, (fits labelled I and II) [34].

The scaife work is not ignorant of the data gap at 0-20 m/s, and considers the idea that wear-rate should probably be zero at 0m/s. Hird and Field speculate that the wear-rate of diamond would be small at first before *"an activation energy has to be reached before significant wear can begin"* [34] and also speculate that the "tail-off" type of non-linearity at higher sliding velocities is due to the softening of the scaife surface, an effect we would not expect to see while diamond turning brittle materials.

From the findings of Hird and Wilks it would be reasonable to assume that diamond tools during diamond turning will experience an accelerated wear-rate when the surface speed is sufficiently high. Due to differences in the materials involved it is difficult to say at what speed this effect will start to have any measurable influence.

Further evidence in support of the Preston's equation comes from the more recent work of Scattergood [107] where the Archard model was used to predict wear of diamond tools while machining 6061 aluminium. Equation 1 of that paper states:

$$V = k_A.F_f.d_s$$

Where V is the wear volume, d_s is the slide distance and F_f is the flank force. The force F_f acts along the face of the tool in the direction of the sliding motion. The term k_A is refered to as the Archard constant. Looking at Preston's Equation once again:

$$\Delta H = K_p.(L/A).\Delta s$$

And multiplying both sides of that equation by contact area:

$$\Delta H.A = K_p * L * \Delta s$$

Logically $\Delta H.A$ must equal wear-volume. Therefore the above equation is stating that the wear volume is equal to Prestons constant multiplied by load and slide distance.

$$k_A.F_f.d_s = V = K_p.L.\Delta s$$

The Archard and Preston's equations both link wear-volume to force and distance, the difference between the two is simply which force component is used and the value of the constants.

$$k_A.d_s / K_p = L.\Delta s / F_f.$$

Which can be simplified to:

$$k_A / K_p. = L / F_f$$

So the ratio of loading force to frictional force is the same as the ratio of the Archard and Preston's constants. As all the components of cutting force are linkable the implication is that the Archard wear model and the Preston's equation are both the same phenomena but previously used to describe different phenomena. Preston's equation is primarily used to explain polishing, while Archard's equation is typically used to explain wear of two surfaces in frictional contact. As polishing involves suspensions of fine but hard grits and the Archard equation describes wear caused by surface asperities maybe it is not surprising these are linked.

9.6 Summary of Research Aims

It is useful to re-examine these aims decided in Chapter 1. The first Aim was to "explore the effect of diamond quality on cutting tools during SPDT of silicon". The experimental trials performed using various tool materials and tool-gem crystallographic orientation were able to show that the high quality MCC material proved to be a poor substitute for the natural diamond tool, an unexpected result that led to the discovery of the two-failure modes.

The second aim, "explore the effect of diamond quality on cutting tools during SPDT of aluminium", was a greater success for the MCC tool-material. The clear implication is that high-quality diamonds that contain smaller quantities of impurities are superior to other diamond. This was expected, based on the available literature reviewed in Chapter 2, but could not be assumed to be true once the MCC was demonstrated to be worse than the other tool materials for machining silicon.

The third aim, "explore the origins of the "supertool" effect" was the broadest aim. The literature review was able to narrow the possible causes down to crystallographic orientation or nitrogen content. The XRT work performed at Daresbury looking at crystallographic defects was not particularly successful and from the knowledge gathered by Jacklin [2] it was possible to eliminate this as a possible cause. XRD techniques were deployed to examine the effect of orientation but the available results imply that this factor is not a dominant one for predicting "supertool" behaviour. Finally it was an examination of the nitrogen content via the FTIR method that gave the strongest indication of causality between a measurable quantity of the diamond material and the presence of supertool behaviour.

While the cause of the supertool behaviour is a significant contribution to knowledge there are other findings that have been discovered which might be important. This thesis the first to test the new MCC CVD diamond material as a tool for SPDT. These results demonstrated that the popular belief that purity was significant to tool-life was only partially correct. This belief has been demonstrated to be wrong for harder workpiece materials, but appears correct for softer non-ferrous materials.

This work is also notable for the extensive work on different orientations of diamond tool. There are other works looking at the effect of orientation upon the tool-behaviour

(for example Uddin's 2004 work [85]) but because this trial tested to the failure of the tool rather than to a fixed cut distance the conclusions were reached without having to extrapolate the flank wear progression of a diamond tool to the final tool failure. Testing to the point of tool-failure led to the discovery of two failure modes while machining silicon. Before this work the wear problem appeared to have a simple explanation and could be summarised as "volumetric wear of tools during SPDT lead to failure". It is now clear that this was an over simplification.

Chapter 10- Conclusions and recommendations for further work

10.1 Conclusions

From the wok presented in Chapter 4 it is clear that the MCC tool material is a significant improvement when machining aluminium workpieces and it is reasonable to assume that it will perform well against other non-ferrous metals. Contour Fine Tooling have been quick to establish this tool-material as a replacement for natural diamond tools. Unfortunately while machining silicon workpieces the MCC tool material proved to have a very poor cutting life when compared to natural tools, so a dependency on natural diamond material remains for some applications.

The identification of the geometry failure mode for diamond tools machining brittle materials is an important advancement in understanding tool failure. Before this project understanding the failure of diamond tools to successfully machine brittle materials was limited to sharp tools, as described in the work of Blake and Scattergood [5] and Blackley and Scattergood [3]. In particular the work with Blake [5] linked a critical feed-rate to the failure to machine in a ductile way, and made clear that geometry of tool is important for causing or avoiding brittle fracture of the workpiece. This statement is backed not only by the experimental results from their paper but the field of fracture mechanics, specifically the work of Lawn [6,8]. This thesis is very much a continuation of these works. Having access to SEM images of the tools at failure proved important for identifying the geometry failure mode experienced by diamond tools while machining brittle materials.

Using the FIB to modify the tool-edge geometry of a diamond tool and investigate failure modes was a novel trial. Though efforts have been made previously to modify the edge of diamond tools using FIB, these efforts were aiming to achieve "print through" of the FIB modification features onto the surface of the softer workpiece materials. These attempts to create specific geometry of the workpiece surfaces are a very different application to the more fundamental cutting theory research performed in this trial. The FIB trial was accidently able to prove more than intended, as the FIB

damage to the tool-edge proved unstable and the vertical edge was lost through chipping damage during machining. Despite increased damage the tool was able to achieve ductile removal of silicon. It was the vertical side of the FIB machined tool-edge damage that led to the damaging shape of the removed material and therefore the brittle damage of the workpiece. Evidence for the geometry failure mode exists in several forms: the FIB modified tool-edge trial, the analysis of the material removed from such a tool and the fracture mechanics. Together these make a convincing case for the presence of the geometry failure mode when diamond turning brittle materials.

The geometry failure mode does not explain why some wear-scar images were free of chipping damage. Clearly the geometry failure mode for diamond tools does not apply to every tool that is machining silicon. Therefore there must be a minimum of two possible failure modes while machining brittle materials. Using the HPHT (100/100) results presented at Lamdamap [87], an argument was presented for a significant threshold pressure value. However it is not clear why there is a pressure threshold, or why machining with a very sharp tool does not cause fracture of the workpiece. The "pressure failure mode" is therefore a title that may bear little resemblance to the failure mechanism it currently describes.

Probably the most significant finding is the FTIR spectroscopy results that imply a possible cause of the supertool phenomena. This vital clue is significant for the firms within the diamond turning industry which turn brittle materials. Finding a predictable method for improving the cutting life of tools while machining of brittle materials would enable larger and more valuable optics to be machined. This finding is of significance to the diamond turning industry and could have a significant inpact on the IR optics that are now possible to manufacture.

10.2 Recommendations for further work

To develop upon the work done in this thesis several further modelling tasks and outlines of experimental trials are given as ideas for potential work. Building upon the work presented here could give deeper understanding of the tool-wear process and help

industry to design relevant machining schemes that minimise wear of the tool and either reduce the number of wasted workpieces or allow machining of larger scale workpieces. The obvious continuation project needs to screen a batch of diamond tools for the presence of the N[A] nitrogen defect and confirm this is a predictor of supertool phenomena. As the concentration of the N[A] nitrogen defect is a likely factor the effect of this will also need quantifying. Unfortunately such a trial is likely to be time consuming as the work within this thesis has demonstrated that tool-life while machining silicon can not be predicted based upon the volumetric wear experienced over a limited cutting distance. The potential supertools will therefore need to be machined until the tool fails to produce a ductile surface.

10.2.1 Finding more applications for MCC

As MCC behaves so differently when machining silicon and aluminium it is thought that there is a transition point where the hardness of workpiece is low enough for MCC to be superior to natural diamond for SPDT applications. Unfortunately because of time constraints finding this transition point was not possible as part of this work. As total achievable cutting distance for germanium is much higher than silicon, (experiments with cut distances of 1000+Km are expected [108]), MCC could be suitable for even this hard wearing IR-material. A future trial looking at the wear behaviour of MCC while machining germanium could be a success for the MCC material.

10.2.2 Improving cutting distance when diamond turning silicon

Improving achievable cut-distance of SPDT of silicon workpieces through the process now appears to be a more approachable challenge than before. The work of Jacklin [2] was dominated by the variability within the natural diamond gem. However HPHT (100/100) tools appear to be very suitable as research tools for improving the silicon machining process as this tool material has the consistency between results that are needed to minimise the required number of trials. Also important is the ~20Km tool-life against silicon which allows quicker completion of trials. As a previous project has demonstrated a huge improvement by moving from an oil-based cutting fluid to a water-based cutting fluid [2], further experimentation with cutting fluids could be considered.

An experiment similar to the one proposed here was conducted by Patten and Mumford [109], which uses both acid and alkali chemical machining slurry in addition to deionised water and air as cutting mediums. Here a diamond profilometer stylus was used to scratch the surface of a (100) plane n-doped crystalline silicon sample and measured using AFM. This work found that using alkali polishing slurry increased the load that was required to initiate brittle fracture. Therefore experimenting with alkali cutting fluids might reasonably provide an improvement to the current cutting fluids for silicon (and due to the very similar chemistry, germanium).

Another interesting experiment to perform would be testing different compositions of silicon. Silicon is frequently used for electronics applications in a doped state (with deliberately added impurities). If silicon can be doped without significantly changing the optical properties, using such a material would likely make machining easier as the hardness is lower for such materials [110]. Exploring cutting fluids and silicon dopant effects in this way would be likely to significantly improve tool-life for non-HPHT tools while machining silicon IR-optics.

10.2.3 Recommendations for aiding further model development

Non-linear wear dependencies such as the reported pressure non-linearity reported in work on polishing with soft-pads [111] and other possible non-linearities need examining to improve model accuracy. The model was forced to use fixed values of the Preston's equation and the force-constant, calculated from the data gathered during the last cut of the tool. This assumes these values remain constant despite the following:

- cutting speed
- orientation of the workpiece
- changing tool geometry

Further experimental trials could help to establish how the constants are influenced by the above variables and lead to more accurate model predictions and a better understanding of the wear process.

Cutting speed

The effect of cutting speed on wear is perhaps the easiest of the identified variables to start investigating. Cutting speeds are very predictable and easily calculated, but decay as the tool feeds towards the centre of the workpiece. Not cutting the entire workpiece would appear to be a sensible experiment design to measure wear as a factor of cut speed. From Hird and Wilks' polishing results [33] (discussed in Chapter 9) we know that there is an expected non-linearity of polishing speed with velocity. Additionally there is some literature discussing non-linearity of the Preston's equation in relation to sliding speed [34]. A test designed to machine a cylindrical boule type workpiece in an oblique type orientation (as used by Born [112]) would reduce variation of cutting speed, so a comparison trial between oblique and transverse cutting might be sensible. From the cutting trials done during this work we expect cutting forces to be relatively unchanged as the tool feeds across the workpiece: therefore the force constant is likely to be only weakly influenced by cutting speed.

Orientation of workpiece

Unless the workpiece material is completely isotropic there will be variation of workpiece properties as the workpiece is rotated. This is likely to add an angular dependency to both constants and require recalculating the wear at least six times per revolution of a {111} orientated workpiece. This will result in many more calculations required to make the model predictions. Gathering experimental data to base the recalculation of both constants will be challenging and will take considerable thought to separate the affect of the Preston's constant and the force constant on the wear rate.

Changing tool geometry

Separating the affect of tool geometry on the constants used within the model is going to be an extremely difficult. One possible method would be to use a range of cut distances and examine the tool for wear at each distance. It is not clear if both constants will change as tool-geometry changes. Designing an experiment to separate the effect of geometry on these constants would be challenging, but as this work has shown, the FIB can be a useful tool during such tests.

Though exploring the three outlined parameters would help model development it could also increase knowledge of the qualitative affect of these variables and aid practical machining.

References

[1] *The development of high precision CNC machine tools.* P.A. McKeown. Journal of Mechanical Working Technology. **17** 225-236 (1988)

[2] *Single Point Diamond Turning of Silicon Optics.* Tony Jacklin. Cranfield University. (2005)

[3] *Crystal orientation dependence of machining damage- A stress model.* W.S. Blackley and R.O. Scattergood. Journal of the American Ceramic Society. **73** [10] 3113-3115 (1990)

[4] *Energy scaling transitions in machining of silicon by diamond.* K.E. Puttick, L.C. Whitmore, P. Zhdan, A.E. Gee and C.L. Chao. Tribology Internnational. **28** [6] 349-355. (1995)

[5] *Ductile-regime machining of germanium and silicon.* P.N. Blake, R. Scattergood. Journal of the American Ceramic Society. **73** [4] 949-57 (1990)

[6] *A model for crack initiation in elastic/plastic indentation fields.* B.R. Lawn and A.G. Evans. Journal of Materials Science. **12** 2195-2199 (1977)

[7] *On the effect of crystallographic orientation on ductile material removal in silicon.* B.P O'Connor, E.R. Marsh and J.A. Couey. Precision Engineering. **29** 124-132 (2005)

[8] *Hardness, Toughness and Brittleness: An indentation Analysis.* B.R. Lawn and D.B. Marshall. Journal of the American Ceramic Society. **62** [6-7] 347-350 (1979)

[9] ISO 4287:2000

[10] ISO 230-7:2000

[11] *Diamond turning of silicon substrates in ductile-regime.* T.P. Leung, W.B. Lee, X.M. Lu. Journal of Materials Processing Technology **73** 42-48 (1998)

[12] *Cross-section transmission electron microscope observations of diamond-turned single-crystal Si surfaces.* T. Shibata, A. Ono, K. Kurihara, E. Makino and M. Ikeda. Applied Physics Letters. **65** [20] 2553-2555 (1994)

[13] *Ductile-regime turning mechanism of single-crystal silicon.* T. Shibata, S, Fuji, E. Makino, M. Ikeda. Ductile-regime turning mechanism of single-crystal silicon. Precision Engineering. **18** 129-137 (1996)

[14] *Structure evaluation of submicrometre silicon chips removed by diamond turning.* R.G. Jasinevicius, J.G. Duduch and P.S. Pizani. Semicond. Sci. Technol. **22** 561-573 (2007)

[15] *Phase transformations during microcutting tests on silicon.* B.V Tanikella, A.H. Somasekhar, A.T.Sowers, R.J. Nemanich and R.O.Scattergood. Appl. Phys. Lett. **69** 2870-2872 (1996)

[16] *In-situ Raman spectroscopy analysis of re-crystallization annealing of diamond turned silicon crystal.* R.G. Jasinevicius, J.G. Duduch and P.S. Pizani. J. of the Braz. Soc. of Mech. Sci. & Eng. **29** [1] 49-54 (2007)

[17] *Brittle to ductile transition dependence upon the transition pressure value of semiconductors in micromachining.* R.G Jasinevicius, P.S. Pizani, and J.G. Duduch. Journal of Materials Research. **15** (8), 1688-1692, (2000)

[18] *Load effects on the phase transformation of single-crystal silicon during nanoindentation tests.* J. Yan, H. Takahashi, X. Gai, H. Harada, J. Tamaki and T. Kuriyagawa. Materials Science and Engineering A. **423** 19-23 (2006)

[19] *Diamond Morphology.* M. Moore. Industrial Diamond Review. **45** 67-71. (1985)

[20] *Spectroscopy of defects and transition metals in diamond.* A.T. Collins. Diamond and Related Materials. **9** 417-423 (2000)

[21] *Aggregate nitrogen in synthetic diamond*. K.M. McNamara. Appl. Phys. Lett. **83** (7) 2003.

[22] *Chemical vapour deposition synthetic diamond: materials, technology and applications.* R.S. Balmer, J.R. Brandon, S.L. Clewes, H.K. Dhillon, J.M. Dodson, I. Friel, P.N. Inglis, T.D. Madgwick, M.L. Markham, T.P. Mollart, N. Perkins, G.A. Scarsbrook, D.J. Twitchen, A.J. Whitehead, J.J. Wilman and S.M. Woollard. J. Phys.: Condens. Matter. **21** (2009)

[23] *Measuring strain in polycrystalline CVD diamond films.* M. Golshan, D. Laundy, P.F. Fewster, M. Moore, A. Whitehead, J.E. Butler and O. Konovalov. Journal of Physics D: Applied Physics. **36** 153-156 (2003)

[24] *Things we still don't know about optical centres in diamond.* A.T. Collins. Diamond and Related Materials. **8** 1455-1462 (1999)

[25] *Double-crystal diffractometric and topographic studies of (111) oriented synthetic diamonds*. G. Kowalski, M. Moore, G. Gledhill and Z. Maricic. Journal of Physics D: Applied Physics. **29** 793-800 (1996)

[26] *Synchrotron X-ray studies of strain in (100)-orientated high pressure-high temperature (HP-HT) synthetic diamonds.* G. Kowalski, M. Moore, G. Glenhill, Z. Maricic. Diamond and Related Materials. **5** 1254-1263 (1996)

[27] *X-ray topographic studies and measurement of lattic parameter differences within synthetic diamonds grown by the reconstitution technique.* W. Wierzchowski, M. Moore, A.P.W. Makepeace, A. Yacoot. Journal of Crystal Growth. **114** 209-227 (1991)

[28] *Twinning in natural diamond. I. Contact Twins.* A.Yacoot, M. Moore, W.G. Machado. Journal Applied Crystallography. **31** 767-776 (1998)

[29] *Twinning in natural diamond. II. Interpenetrant cubes.* W.G. Machado, M. Moore, A.Yacoot. Journal Applied Crystallography. **31** 777-782 (1998)

[30] *Synchrotron X-ray topography.* M. Moore. Radiat. Phys. Chem. **45** [3] 427-444 (1995)

[31] *X-ray studies of the growth of natural diamond.* M. Moore. Industrial Diamond Review. **48** 59-64 (1988)

[32] Communications with Contour Fine Tooling Ltd.

[33] *A wear mechanism map for the diamond polishing process*. J.R. Hird and J.E. Field. Wear. **258** 18-25 (2005)

[34] *Diamond polishing.* J.R. Hird & J.E. Field. Proceedings: Mathematical, Physical and Engineering Sciences. **460** 3547-3568 (2004)

[35] *The abrasion resistance of natural and synthetic diamond.* E.M. Wilks and J.Wilks. Wear. **81** 329-346 (1982)

[36] *The annealing of interstitial-related optical centres in type Ib diamond*. A.T. Collins, A. Dahwich. Diamond and Related Materials. **13** 1959-1962 (2004)

[37] P*roperties of large single crystal diamond.* R Linares, P. Doering. Diamond and Related Materials. **8** 909-915 (1999)

[38] *Defects in coloured natural diamonds*. F. De Weerdt, J. Van Royen. Diamond and Related Materials. **10** 474-479 (2001)

[39] *Mechanical properties of synthetic type IIa diamond crystal*. H. Sumiya, N. Toda, S. Satoh. Diamond and Related Materials. **6** 1841-1846 (1997)

[40] *Aggregation of nitrogen in diamond, including platelet formation*. B.P Allen, T. Evans. Proceedings of the Royal Society of London. Series A, Mathematical and Physical Sciences. **375** 1760 93-104 (1981)

[41] *High-temperature annealing of optical centres in type-I diamond.* A.T. Collins. A. Connor, C. Ly, A. Shareef and P.M. Spear. Journal of Applied Physics. **97** (2005)

[42] *A new proposal for the structure of platelets in diamond.* J.M. Baker. Diamond and Related Materials. **7** 1282-1290 (1998)

[43] *Scientific screening of raw diamond for an ultraprecision cutting tool with high durability*. T. Yamaguchi, M. Higuchi, S. Shimada, H. Tanaka and K. Obata. Annals of the CIRP. **55** 1 (2006)

[44] *Non-destructive strength evaluation of diamond for ultra-precision cutting tool*. N. Ikawa, S. Shimada and H. Tsuwa. Annals of the CIRP. **34** 1 (1985) 117-120

[45] *Qualification of raw diamond from a viewpoint of chipping and wear resistance for ultraprecision cutting tool*. S. Shimada, H. Tanaka, M. Higuchi, T. Yamaguchi and M. Yoshinaga. Proceedings of the 7th euspen International Conference. **1** 103-106 (2007)

[46] *Tool life monitoring during the diamond turning of electroless Ni-P*. T. Yamaguchi, M. Higuchi, S. Shimada, T. Kaneeda. Precision Engineering. **31** 196-201 (2007)

[47] *On the role of nitrogen in stiffening the diamond structure*. S.G. Nailer, M. Moore, J. Chapman and G. Kowalski. Journal of Applied Crystallography. **40** 1146-1152 (2007)

[48] *Wear of monocrystalline diamond tools during ultraprecision machining of nonferrous metals*. J.M. Oomen and J. Eisses. Precision Engineering. **14** [4] 206-217 (1992)

[49] *Effect of Isotropic Constitution of diamond on its elastic constants: 13C Diamond, the hardest known material*. A.K. Ramdas, S.Rodriguez, M. Grimsditch, T.R. Anthony and W.F. Banholzer. Physical Review Letters. **71** [1] 189-192 (1993)

[50] *X-ray Topography*. D.R. Black, G.G. Long. NIST special publication 960-10. (2004)

[51] *Some observations on the wear of diamond tools used in piston machining*. D. Keen. Wear. **17** 195-208 (1971)

[52] *3D characterisation of tool wear whilst diamond turning silicon*. I. Durazo-Cardenas, P. Shore, X. Luo, T. Jacklin, S. Impey and A. Cox. Wear. **262** [3-4] 340-349 (2007)

[53] *Suppression of tool-wear in diamond turning of copper under reduced oxygen atmosphere*. S.Shimada, T.Inamura, M.Higuchi, H.Tanaka, N.Ikawa. Annals of the CIRP **49** [1] 21-24 (2000)

[54] *Modelling of tool wear based on cutting forces in turning*. H.V. Ravindra, Y.G. Srinivasa, R. Krishnamurthy. Wear. **169** 25-32 (1993)

[55] *Modeling of cutting forces under hard turning conditions considering tool wear effect*. Y. Huang & S.Y. Liang. Transactions of the ASME. **127** 262-270 (2005)

[56] *Modeling and simulation of the tool wear in nanometric cutting.* K. Cheng, X. Luo, R. Ward, R. Holt. Wear. **255** 1427-1432 (2003)

[57] *Brittle-ductile transition in monocrystalline silicon analysed by molecular dynamics simulation.* H. Tanaka, S.Shimada, N. Ikawa. Proc. Instn. Mech. Engrs. Part C. J. Mechanical Engineering Science. **218** 583-590 (2004)

[58] *Study of the temperature and stress in nanoscale ductile mode cutting of silicon using molecular dynamics simulation.* M.B. Cai, X.P. Li, M. Rahman. Journal of Materials Processing Technology. 607-612 (2007)

[59] *High Precision surfaces generation: Modelling, simulation and machining verification.* X. Luo. PhD Thesis. Leeds Metropolitan University. (2004)

[60] *Replacing diamond cutting tools with CBN for efficient nanometric cutting of silicon.* S. Goel, X. Luo, R.L. Reuben, W.B. Rashid. Materials Letters. **68** 507-509 (2012)

[61] *Molecular dynamics simulation model for the quantitative assessment of tool wear during single point diamond turning of cubic silicon carbide.* S. Goel, X. Luo, R.L. Reuben. Computational Materials science **51** 402-408 (2011)

[62] *Temperature dependence of the elastic moduli of diamond: A Brillouin-scattering study.* E.S. Zouboulis and K. Grimsditch. Physics Review B. **57** [5] 2889-2896 (1998)

[63] *Thermo-chemical wear mechanism of diamond tool in machining of ferrous metals.* S. Shimada, H. Tanaka, M. Higuchi, T. Yamaguchi, S. Honda, K. Obata. CIRP annals-Manufacturing Technology. **53** [1] 57-60 (2007)

[64] *Chemical aspects of tool wear in single point diamond turning.* E. Paul, C.J. Evans, A. Mangamelli, M.L. McGlauflin, R.S. Polvani. Precision Engineering. **18** 4-19 (1996)

[65] *Surface effects in adhesion, friction, wear, and lubrication (Tribology series 5).* D.H. Buckley. Elsevier. (1981)

[66] *The cracking and fatigue of diamond.* J.G. Bell, M.E.C. Stuivinga, A.G. Thornton, J.Wilks. J. Phys. D: Appl. Phys. **10** 1379-1387 (1977)

[67] *Cumulative deformation and fatigue of diamond- new developments.* C.A. Brookes, L.Y. Zhang. Diamond and Related Materials. **8** 1515-1521 (1998)

[68] *A Primer on the Taguchi Method.* R. Roy. Van Nostrand Reinhold. New York. (1990)

[69] Moore Nanotech 350 UPL. Specification Overview (2003).

[70] Discussion with Qioptiq.

[71] *Materials Science and Engineering: 7th Edition.* W.D. Callister. John Wiley & sons, inc. (2007)

[72] Kistler dynometer technical specifications:
http://www.kistler.com/mediaaccess/en-ex/000-484e-08.10.pdf

[73] *http://spie.org/x32483.xml*

[74] *Practical Scanning Electron Microscopy*: J.I. Goldstein and H. Yakowitz. Plenum Press. New York (1975)

[75] *A review of focused ion beam applications in microsystems technology.* S.Reyntjens, R. Puers. Journal of Micromechanics and Microengineering. **11** 287-300 (2001)

[76] *Recent developments in micromilling using focused ion beam technology.* A.A.Tseng. Journal of Micromechanics and Microengineering. **14** 15-34 (2004)

[77] *Application of a focused ion beam system to micro and nanoengineering.* R.M. Langford, A.K. Petford-Long, M. Rommeswinkle, S. Egelkamp. Materials Science and Technology. **18** 743-748 (2002)

[78] *Recent developments in nanofabrication using focused ion beams*. A.A. Tseng. Small. **10** 924-939 (2005)

[79] *Focused ion beam machining of hard materials for micro engineering applications.* R.Evans. PhD Thesis. Cranfield University. (2009)

[80] *PCD tooling made by combined laser beam machining and focused ion beam machining.* R.W.Evans, I.S.Durazo-Cardenas, D.M.Allen. Proceedings of the Euspen International Conference. (2009)

[81] *Machining of Optical surfaces in Brittle Materials.* P. Shore. PhD Thesis. Cranfield University. (1995)

[82] *Manufacturing and measurement of the MIRI spectrometer optics for the James Webb space telescope*. P. Shore, P. Morantz, D. Lee. Annals of the CIRP. **55** (2006)

[83] *Tool-wear in ultra-precision diamond cutting of non-ferrous metals with a round-nose tool.* M. Zhou, B.K.A. Ngoi, X.J. Wang. Tribology Letters. **15** [3] 211-216 (2003)

[84] *Performance of diamonds as cutting tools for precision machining.* J. Wilks. Precision Engineering. **2** [2] 57-72 (1980)

[85] *Effect of crystallographic orientation on wear of diamond tools for nano-scale ductile cutting of silicon.* M.S. Uddin, K.H.W. Seah, X.P. Li, M. Rahman, K. Liu. Wear. **257** 751-759 (2004)

[86] http://www.debeersgroup.com/diamond-trading-company/

[87] *Tool failure mechanisms while single point diamond turning silicon*. L. Kirkwood, I. Durazo-Cardenas, P. Shore. Laser Metrology and Machine Performance (LAMDAMAP) IX. 337-347 (2009)

[88] *Nondestructive measurement of machining-induced amorphous layers in single-crystal silicon by laser micro-Raman spectroscopy.* J. Yan, T. Asami, T. Kuriyagawa. Precision Engineering. **32** 186-195 (2008)

[89] *The resistance of diamond to abrasion.* E.M. Wilks, J. Wilks. J. Phys. D: Appl. Phys. **5** 1902-1919 (1972)

[90] *A worn tool force model for three-dimensional cutting operations.* D.W. Smithey, S.G. Kapoor, R.E. DeVor. International Journal of Machine Tools & Manufacture. **40** 1929-1950 (2000)

[91] *Chemical processes in glass polishing.* L.M. Cook. Journal of Non-crystalline Solids. **120** 152-171 (1990)

[92] *Cryogenic diamond turning of stainless steel*. C.Evans, J.B. Bryan. Annals of the CIRP. 40 1 571-575 (1991)

[93] *Modeling flank wear of carbide tool insert in metal cutting.* X. Luo, K. Cheng, R. Holt, X. Liu. Wear **259** 1235-1240 (2005)

[94] *The effects of machining process variables and tooling characterisation on the surface generation.* X.Luo, K.Cheng, R.Ward. International Journal of Advanced Manufacturing Technology. **25** 1089-1097 (2005)

[95] *An examination of polished diamond surfaces in the electron microscope.* A.G. Thornton, J. Wilks. J. Phys. D: Appl. Phys. **9** 27-35 (1976)

[96] *The fracture stress of chemical vapour deposited diamond.* C.S.J. Pickles. Diamond and Related Materials. **11** 1913-1922 (2002)

[97] *Strength, fracture and friction properties of diamond.* J.E. Field, C.S.J. Pickles. Diamond and Related Materials. **5** 625-634 (1996)

[98] *Mechanical properties of different types of diamond.* V.Blank, M.Popov, G.Pivovarov, N.Lvova, S.Terentev. Diamond and Related Materials. **8** 1531-1535 (1999)

[99] *Encyclopedia of Materials science and technology*. Elsevier 2133-2143 (2001)

[100] *The annealing of interstitial-related optical centres in type II natural and CVD diamond.* L. Allers, A.T. Collins, J. Hiscock. Diamond and Related Materials. 7 228-232 (1998)

[101] *SRS station 16.3: description and utilization of a high-resolution diffraction facility.* S.P Collins, B.M. Murphy, C.C. Tang, M.C. Miller and G. Oszlanyi. J. Phys. D: Appl. Phys. **32** 81-83 (1999)

[102] *Measurement of stress in a synthetic diamond substrate using the photoelastic method.* H. Liang, A. Vescan, E. Kohn, K.K. Chin. Diamond and Related Materials. **5** 664-668 (1996)

[103] *Ductile-regime grinding: A new technology for machining brittle materials.* T.G. Bifano, T.A. Dow, R.O. Scattergood. Transactions of the ASME. **113** 184-189 (1991)

[104] *Detection of orientation-dependent, single-crystal diamond tool edge wear using cutting force sensors, while spin-turning silicon.* E.R. Marsh, E.J. Sommer, T.R.S. Deakyne, G.A. Kim, J.A. Simonson. Precision Engineering. **34** [2] 253-258 (2010)

[105] *Fundamental investigation of subsurface damage in single crystalline silicon caused by diamond machining.* J. Yan, T. Asami, H. Harada, T. Kuriyagawa. Precision Engineering. **33** 378-386 (2009)

[106] *Thermal conductivity of amorphous silicon.* H. Wada, T. Kamijoh. Jpn. J. Appl. Phys. **35** 648-650 (1996)

[107] *Diamond tool wear when machining Al6061 and 1215 steel.* B.M. Lane, M. Shi, T.A. Dow, R. Scattergood. Wear. **268** 1434-1441 (2010)

[108] *High-efficiency machining of single-crystal germanium using large-radius diamond tools.* T. Ohta, J. Yan, S. Yajima, Y. Takahashi, N. Horikawa, T. Kuriyagawa. Int. J. Surface Science and Engineering. **1** [4] 374-392 (2007)

[109] *The effects of fluid on the deformation and ductile to brittle transition of silicon.* J.A. Patten, S.V. Mumford. Proceedings ASPE 2000 Annual meeting. **22** 604-607 (2000)

[110] *Micromechanical and tribological characterization of doped single-crystal silicon and polysilicon films for microelectromechanical systems devices.* B. Bhushan, X. Li. Journal of Materials Science. **12** [1] 54-63 (1997)

[111] *Modeling of chemical-mechanical polishing with soft pads.* F.G. Shi, B. Zhao. Applied Physics A. **67** 249-252 (1998)

[112] *An empirical survey on the influence of machining parameters on tool wear in diamond turning of large single-crystal silicon optics.* D. Krulewich Born, W.A. Goodman. Precision Engineering. **25** 247-257 (2001)

Appendix A- Volumetric wear analysis: a 3D methodology

At Cranfield there has previously been work done on characterising wear damage to the tools during diamond turning using a 2D series of geometric arguments to reach an understanding of the 3D wear. An example of how wear is defined is shown in figure A1.
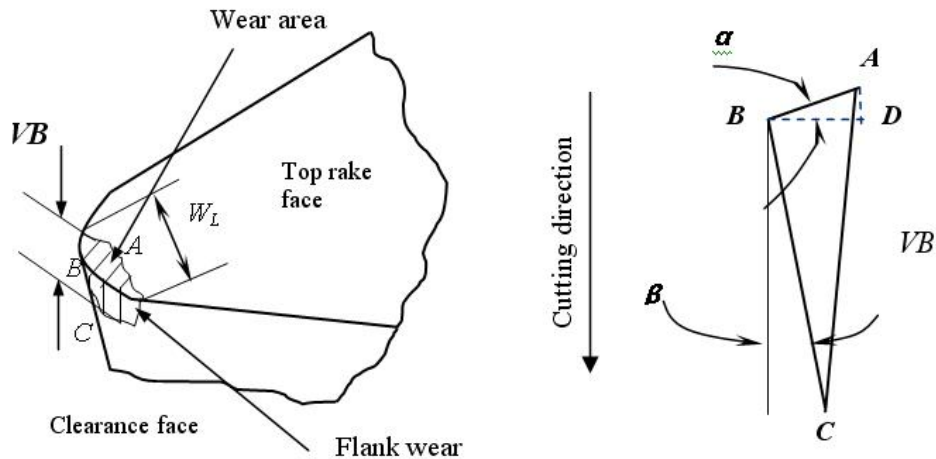
Figure A1: The 3D wear-scar is abstracted into a triangular geometry.

The calculated wear-volumes from the work of Durazo-Cardenas et al. are displayed in figure A2. The origin of the uncertainty bars used in this methodology is not explained in the original text. It is also worth noting the range of calculated values, the highest wear-volume being only 500 cubic micrometres. Such a small volume is extremely sensitive to any error sources.
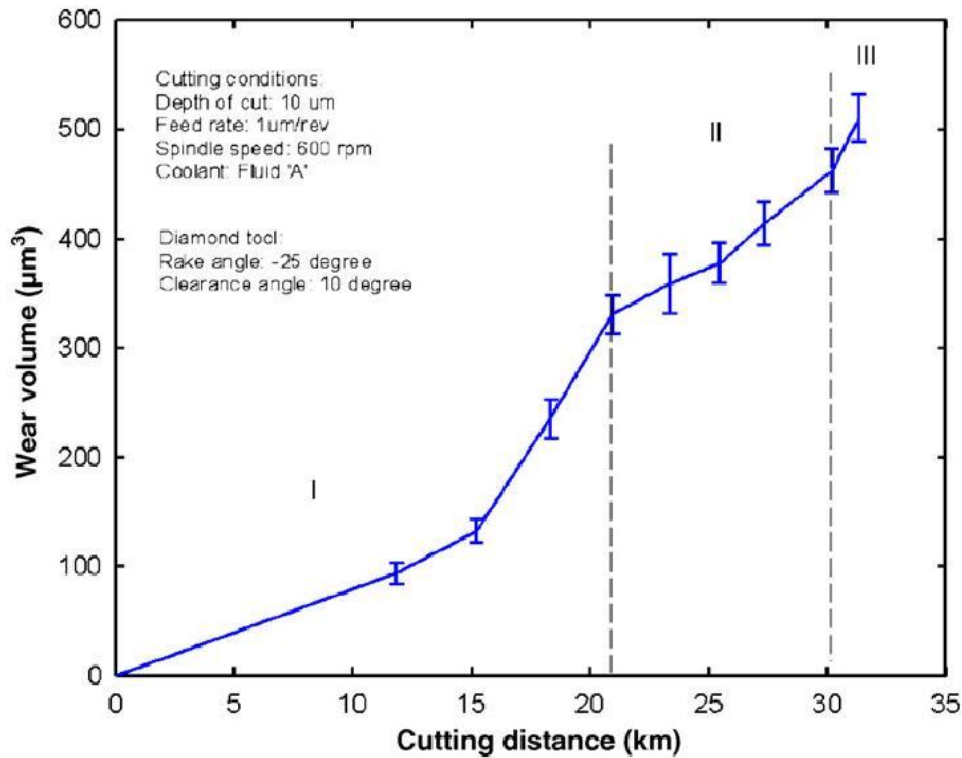
Figure A2: The previous reported results for diamond tool wear-volume.

In the described method 3D wear is found by using a series of triangles to approximate the wear volume (in the work done previous to this project 10 such triangles were used). Defining the total 3D volume removed via wear in such a manner is an approximation (based upon ten previous approximations). Adding more accuracy to the process was considered a valuable activity at the start of the project, when the volumetric wear was considered strongly related to tool failure.

The measuring methodology developed uses an indentation technique, by forcing the worn tool into a surface of oxygen free copper. The C-axis is locked to eliminate roll of the spindle (which could result in damage to the tool-edge) and the tool is very slowly pushed in the Z-axis towards the workpiece 15 μm into a diamond turned copper surface. This depth was selected to allow a definite positive capture of the parts of the tool that are worn by the 10 μm depth of cut and to allow for any error in the Z-axis. A series of indents are performed at the start of a trial and after each cut. This scheme allows averaging over the indent sites at a given cut-distance and gives the option to

discard a particular indent if any doubts exist about the quality of the print-through from the indent process or damage has occurred to the copper workpiece.

Measuring the copper indents is done ex-situ on the Talysurf CCI. This white-light interferometer instrument works on a Coherence Correlation Interferometer technique (hence the name CCI). The CCI uses a combination of a short correlation length light and a focusing microscope objective to create interference fringes at a very specific point in the vertical. By moving the focusing objective in the Z-axis, the interferometer fringes scan through the height of the workpiece and a detailed surface measurement is performed. The CCI instrument has a 1 megapixel detector. The sampled area (a square of approximately 350 μm in each direction) is divided between these pixels. Individual pixels therefore measure the Z-axis (height) for an area of approximately 350nm x 350nm. The newer methodology developed as part of this work uses the idea of summing each of the measured data points to find the total volume of an indent into copper. This task is accomplished by exporting the data from the CCI using an ASCII format. This format is importable into MATLAB, where it is easily manipulated.
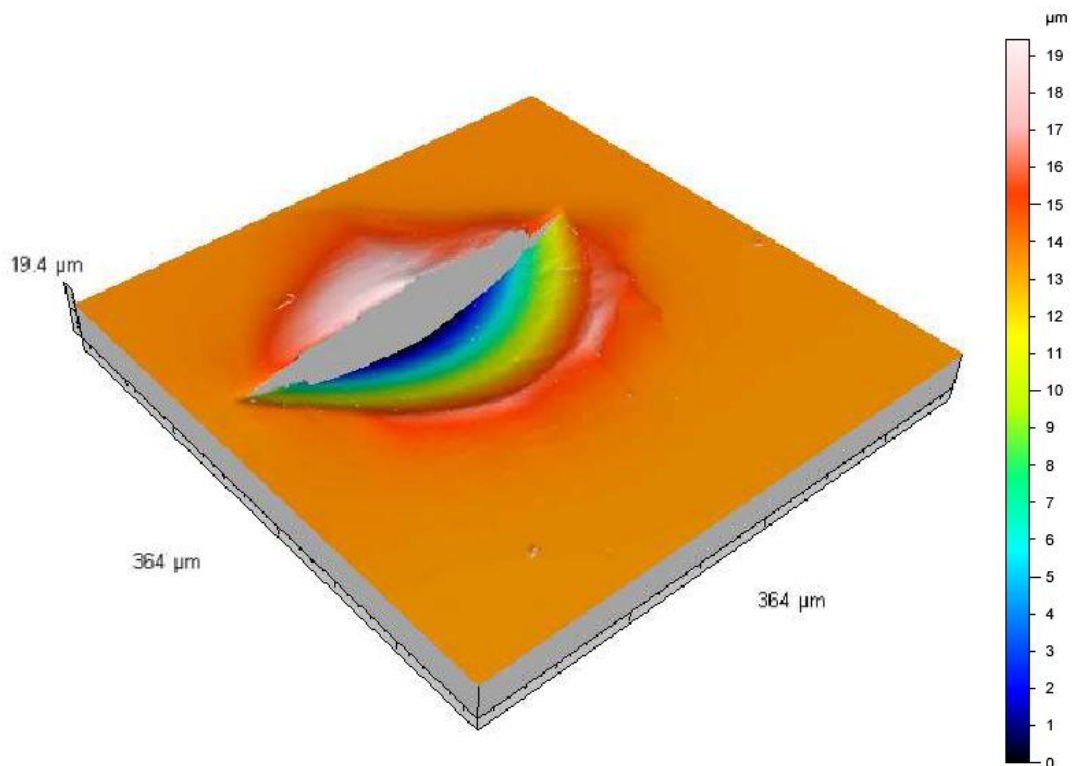

Figure A3: Image of an indent site as measured on the CCI instrument.

Figure A3 shows a surface measured by CCI. This indent site shows clear plastic deformation of the copper material (red and white areas) and the indentation of the clearance angle face of the tool (yellow, green and blue). The large grey area is an area of missing data, arising from the extreme angle of the top-rake face (this effect is covered in more detail later). With this data in MATLAB the volume component from each pixel could be found and all these small volume components summed to find total volume. Comparison of this total volume against the volume measurement of the unworn tool allows the determining of the difference which should only be caused by the wear-volume of the tool.

There are three serious issues with this technique that have caused it to be discussed here as an appendix. These are covered in detail so as to aid future researchers to avoid repeating the failures made in this work. Primarily there is an issue with depth uncertainty. Any inaccuracy of tool position (in the Z-axis) means there is an error in the planned indentation to a depth of 15 µm. For a tool performing 10 µm depth of cut much of the resulting 15 µm indent does not need to be considered. The data can be put through a deliberate threshold: where the data below the 12 µm level is kept and the data above this point is set equal to zero. Once the thresholding has been done (and data above the 12 µm depth is discarded) the remaining data-points can be summed to find a total volume for the indent.

The greatest difficulty with this method is establishing where to set the threshold. There is no reliable datum to take this depth from. A sensible datum for an unworn tool is the tool-tip, but as wear-mechanisms work on the tool this datum would move. Moving the threshold causes two sources of error, the number of data-points that make the indent changes and the value of each data-point is altered. As there are so many data points that are summed to find the total volume and the expected volume is so small that the cumulative effect of setting the threshold at the wrong level leads to an unacceptable error on the final calculation.

Another critical problem with the new methodology is the extreme sensitivity to the angle of the copper indentation surface and the subsequent CCI measurement. The CCI

has an angular limit, any slope of more than 22.5 degrees measured from horizontal (an objective dependent value: the value quoted is for the highest resolution x50 magnification objective) will result in a point of missing data. Due to the angle of the diamond tool top-rake during silicon machining, there is guaranteed to be a large section of missing data. Furthermore, the wear-scar region is extremely rough and often has small regions of missing data due to this angular requirement.

The third issue is that with the wear-scar development, parts of the tool which previously were the top-rake face are now nearly parallel with the workpiece. Areas that were previously missing data (and not contributing to the volume calculation) are therefore contributing towards the final volume. Oddly enough, because of this effect the calculated indent volume can appear to get larger, with the implication that the tool is starting to grow as total cut distance increases. Because the data points that appear with increased wear appear at the lowest point of the indent, each pixel that appears will be affecting the volume by about 1.47 cubic micrometres (a 12 µm depth multiplied by 0.35 µm pixel length multiplied by 0.35 µm pixel width).

All these problems became apparent while trying to collect data from the indents. Below is a graph of results (figure A4) collected via this method as part of the project.
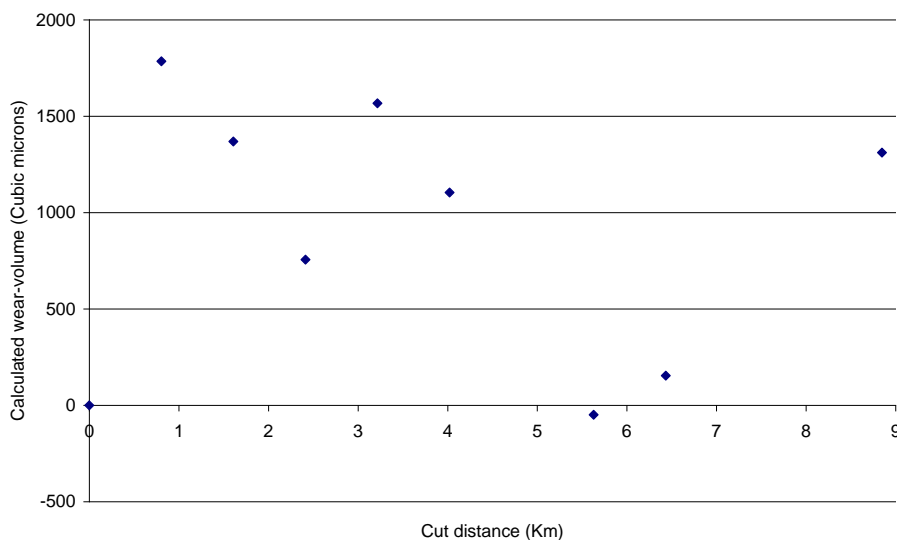
Figure A4: Data calculated from the indents for tool S83776

The above graph clearly shows the scale of the issue with this methodology. No conclusions could be made from this graph. Particularly odd is the data point at 5.6Km, which indicates that the tool has experienced a modest growth of the diamond tool since the start of the trial. Despite repeated efforts to make the data work (in particular experimenting with different methods of finding the thresholding calibration was tried extensively), no believable data was ever gathered.

Though the CCI based method of measuring wear-volume proved to be unworkable, the method the model uses to calculate volume is similar and certainly originated within the work done with the CCI.

To conclude this appendix it is clear that the developed methodology did not work satisfactorily. The three reasons have been outlined but it is clear that together they can lead to errors in the final calculated volume of several hundred cubic micrometres. The uncertainty therefore exceeds any sensibly calculated value. The failure of this methodology should raise questions concerning any other researchers measurements of wear-volume using CCI instruments or other optical methods.

When calculating the extremely small volumes that are removed from a diamond tool during diamond turning great care must be taken with any source of errors.

Appendix B- Program for examining thickness of removed material from a given tool edge

During the work done for this thesis a program was developed to calculate the thickness of removed material from a test curve. This helped initial work towards exploring the geometry failure mode and later helped to design the FIB modified tool-edge trial.

Though it was at one stage though that this code would be included into the tool-wear model, the difficulties with predicting chipping damage (particularly where on a tool-edge chipping damage would occur and what scale the damage would be) and the difficulties in calculating the length of a crack generated from a given defect on the tool edge. A further difficulty lies with predicting if a crack once initiated could be further expanded in later passes of the tool. With such clear problems this code was considered unsuitable for fitting into the wear model. It remains as a useful method for visually seeing how a given tool will remove material and can be used to examine hypothetical tool designs.

When the crack-initiation length is known for a given material (for example it is approximately 57nm for silicon) and the minimum crack length is also known (approximately 0.4 μm for silicon) some predictions can be made. Any defect on the tool that is removing more than the crack-initiation thickness and is less than the minimum crack length above the generated worksurface plane the result will be a damaged worksurface. The fracture mechanics in this case dictates that cracks will be initiated and some will reach the generated surface.

This code basically performs the same analysis as the technique used by Blake and Scattergood in their analysis on ductile machining. However while they used the geometry of an unworn tool their approach struggles with more complex geometries and therefore a simple MATLAB program is needed. It should be noted that they measured thickness of chip in the radial direction and not the vertical direction that this code has used. The developed technique therefore assumes that the differences in the chip thickness when measured in the vertical and radial directions are small. This is an

approximation that applies differently at different points along the tool engagement; it is a very good approximation towards the front of the tool and fits less well further around the tool edge. A brief analysis on the significance of this problem was performed using a calculated chip from an ideal tool profile and then compared against the Blake and Scattergood results. The profile was of a tool with a 500 μm radius and a 10 μm depth of cut. The results agreed to within 3% at the very edge of the profile (the error is more extreme towards the edges). We can therefore conclude that where the tool radius is large and the depth of cut is small then this is an approximation that fits well. However, should the chosen tool have a very small radius or the depth of cut become large the validity of that approximation breaks down. Furthermore, B.P O'Connor took the vertical direction as the critical chip-thickness when performing silicon experiments to determine the effect crystallographic orientation has upon critical chip-thicknesses: raising the valid question of whether Blake and Scattergood were correct to use the radial direction.

Calculation of removed material code:

```
ToolRadius=500;
DoC=10;
Dmax=0.057;
% DoC equals Depth of Cut.
% Dmax=critical chip thickness.

RminusDoC= ToolRadius -DoC;
CosTheta= RminusDoC/ ToolRadius;
Theta=acosd(CosTheta);
% Theta is the ANGLE between lowest point and edge of cut shoulder.
% (not the angle  across the entire width).
AngleARRAY=linspace(0,Theta,10001);
% Makes it into an array of angles.
AngleRadians=(-0.5*pi)+2*pi*(AngleARRAY./360);
% Converts from Degrees to Radians, which is Very important!
[X,Y]=pol2cart(AngleRadians,ToolRadius);
% Converts to cartesian co-ordinates

TestCurve(:,2)=[X];
```

```
TestCurve(:,1)=[Y];
% Sets up the TestCurve matrix.
% This is the damage free case for the tool


TestCurve2(:,2)=[X];
TestCurve2(:,1)=[Y];
TestCurve2(6358:7003,1)= TestCurve2(7003,1);
% TestCurve2 is the curve with the damage added.


B(1:10302,1:4)=[0];
% Sets up the right size of array for checking over 4 curves.
B(1:10001,1)=TestCurve(:,1);
B(101:10101,2)= TestCurve(:,1);
B(201:10201,3)= TestCurve(:,1);
B(301:10301,4)= TestCurve(:,1);
B=B+500;
% Which places the correct data on the right columns.
% This allows graphing of "B"
% which should prove interesting viewing for how the tool progresses
% and how much material is removed per pass.


B2(1:10302,1:4)=[0];
% Sets up the right size of array for checking 4 curves.
% B2 is the chip-damaged tool
B2(1:10001,1)=TestCurve2(:,1);
B2(101:10101,2)= TestCurve2(:,1);
B2(201:10201,3)= TestCurve2(:,1);
B2(301:10301,4)= TestCurve2(:,1);
B2=B2+500;
% Which places the correct data on the right columns.
% Graph of B2 which should prove interesting viewing for % how the
tool progresses and how much material is
% removed per pass.


% The plan is to use N as the way to find the chip removed by the last
pass of the tool
% in B. This is achieved by looking at the lowest point
% of the last three passes of the tool.
N=B(1:10151,1:3);
```

```
for i=1:1:length(N)
MIN(i)=min(N(i,:));
end
MIN=MIN';
% Excellent! Min is the lowest point on all three of the first three
curves.
Chip=MIN-B(1:10151,4);
MIN=MIN';
Chip(10102:10151,1)=0;
Chip(1:50,1)=0;
LOGIC=Chip>0;
CHIP2=LOGIC.*Chip;


N2=B2(1:10151,1:3);
for i2=1:1:length(N2)
MIN2(i2)=min(N2(i2,:));
end
MIN2=MIN2';
% Min is the lowest point on all three of the first three curves.
Chip2=MIN2-B2(1:10151,4);
MIN2=MIN2';
Chip2(10102:10151,1)=0;
Chip2(1:50,1)=0;
LOGIC4=Chip2>0;
CHIP4=LOGIC4.*Chip2;


LOGIC2=CHIP2>Dmax;
BRITTLE=LOGIC2.*CHIP2;
%Brittle is used to show the parts of the tool curve that are causing
brittle fracture
% Displays the troublesome bits of the curve
LOGIC4=CHIP4>Dmax;
BRITTLE2=LOGIC4.*CHIP4;
%Brittle2 is used to show the parts of the tool curve that are causing
brittle fracture
% Displays the troublesome bits of the curve


problem=LOGIC2(1:10001,1).*B(301:10301,4);
% Problem is the variable that graphs the sections of the curve that
```

```matlab
% are causing brittle fracture.
% NOTE; crack lengths from these trouble sections are not indicated
problem2=LOGIC4(1:10001,1).*B2(301:10301,4);
% Problem is the variable that graphs the sections of the curve that
% are causing brittle fracture.


subplot(2,2,1), plot(TestCurve(:,2), B(1:10001,3), 'b',
TestCurve(:,2), B(1:10001,4), 'b')
axis([0 100 0 10])
xlabel('Tool engagement length (microns)', 'FontSize',14)
ylabel('Depth of Cut (microns)', 'FontSize',14)
title('Test Curve', 'FontSize',14)
subplot(2,2,2), area(TestCurve(1:10001,2), CHIP2(1:10001,:))
axis([0 100 -0 1.5])
xlabel('Tool engagement length (microns)', 'FontSize',14)
ylabel('Thickness of removed chip (microns)', 'FontSize',14)
title('Removed Chip from Test Curve', 'FontSize',14)
subplot(2,2,3), plot(TestCurve(1:10001,2), B2(1:10001,3), 'b',
TestCurve(1:10001,2), B2(1:10001,4), 'b')
axis([0 100 0 10])
xlabel('Tool engagement length (microns)', 'FontSize',14)
ylabel('Depth of Cut (microns)', 'FontSize',14)
title('Damaged Tool Edge Profile', 'FontSize',14)
subplot(2,2,4), area(TestCurve(1:10001,2), CHIP4(1:10001,:))
axis([0 100 0 1.5])
xlabel('Tool engagement length (microns)', 'FontSize',14)
ylabel('Thickness of removed chip (microns)', 'FontSize',14)
title('Removed Chip from Damaged Tool Edge', 'FontSize',14)
% substituting "problem" for "CHIP2" and "problem2" for "CHIP4" in the
% subplot lines looks at areas of the curve causing brittle fracture.
```

Appendix C- Diamond tool wear model

Included for completeness is the full wear model, results from this version of the model are presented in Chapter 8. Within the models code are the Prestons coefficients and force-constants used within the thesis.

Wear model code:

```
%%%%%%%%%%%%%%%%%%%%%%%%%%%%%%%%%%%%%%%%%%%%%%%%%%%%%%%%%%%%%%%%%%%%%%
%                    Initial information
%%%%%%%%%%%%%%%%%%%%%%%%%%%%%%%%%%%%%%%%%%%%%%%%%%%%%%%%%%%%%%%%%%%%%%

f = input('Enter feed-rate in microns-');  ;
% f is the tool feed-rate in microns.
 DoC=10;
% Depth of Cut.
 ToolRadius=  input('Enter Tool radius (in microns)-')  ;
% Tool radius in microns. This work assumes circular profile tools.
  rMM = input('Enter radius of workpiece (in mm)-') ;
  r=rMM/1000 ;
% r=radius of workpiece, in *metres*.
 NUMBER_OF_CUTS = input('Enter number of cuts-');
% NUMBER_OF_CUTS=number of times that each modelled cut is repeated.
 ClearanceAngle = input('Enter clearance Angle of the tool (degrees)-
') ;
% Tool clearance angle.
 top_rake = input('Enter top-rake angle of the tool (degrees). i.e -25
for silicon, or 0 for aluminium work-') ;
% Tool top rake angle.


 Kp=  2.69175836E-21       ;
% HPHT vs silicon
% Kp=  1.38494411E-21        ;
% Natural vs silicon
% Kp=  4.04111470E-21        ;
% MCC vs silicon

% Kp=1.291689629E-20         ;
% Natural (100/110) against aluminium
% Kp= 1.664861505E-20   ;
% MCC (100/110) against aluminium
% Kp is the Preston coefficient. Traditionally measured in cm^2/dyne.
% A dyne is 1E-5 of a Newton.
% This model works using SI units.

  k=    1.19751853E10    ;
% HPHT vs silicon
% k=    1.37499114E10    ;
% Natural vs silicon
%  k=    1.45842828E10    ;
% MCC vs silicon
```

216

```
% k= 3.307154906E9      ;
% Natural (100/110) against aluminium
% k= 2.586430755E9    ;
% MCC (100/110) against aluminium
% k is the constant of proportionality linking cutting force with wear
area

%%%%%%%%%%
% Using modified k-values: from work on wear-area issues.

% k=    3.823494E9     ;
% HPHT vs silicon

%  k=9.424793E8    ;
 % Natural against Aluminium

% k=8.360975E8      ;
 % MCC against Aluminium
%%%%%%%%

 X_spacing= 0.1 ;
% X_spacing is the horizontal resolution of the model (in microns)
% Currently, =100nm array spacing.
%%%%%%%%%%%%%%%%%%%%%%%%%%%%%%%%%%%%%%%%%%%%%%%%%%%%%%%%%%%%%%%%%%%%%%%%


feed_rate=f*1E-6;
% feed_rate is measured in *metres* per revolution


 Load(1:NUMBER_OF_CUTS+1,1)=(0);
 % Preallocating Load array.
%Load(1,1)= 0.01  ;
Load(1,1)= 0.073632879 ;
% Use 0.073632879 N for silicon. 0.01N against aluminium ;
% Here load is the force required to distort and cut the workpiece
material infront of the tool rake-face.
% Later, this load value is added to a componentfrom the contact area

Area(1:NUMBER_OF_CUTS+1,1)=(0);
 % Preallocating area array.
Area(1,1)= 2e-11;

 sliding_distance=(pi*r^2)/feed_rate;
% Sliding Velocity was the original value, but we are not interested
in the time dependent for of height.

Total_Distance= NUMBER_OF_CUTS*sliding_distance ;
% Total_Distance= distance cut over all simulated cut.


%%%%%%%%%%%%%%%%%%%%%%%%%%%%%%%%%%%%%%%%%%%%%%%%%%%%%%%%%%%%%%%%%%%%%%%%%
% END OF INITIAL INFORMATION
%%%%%%%%%%%%%%%%%%%%%%%%%%%%%%%%%%%%%%%%%%%%%%%%%%%%%%%%%%%%%%%%%%%%%%%%%


%%%%%%%%%%%%%%%%%%%%%%%%%%%%%%%%%%%%%%%%%%%%
%   Tool profile
%%%%%%%%%%%%%%%%%%%%%%%%%%%%%%%%%%%%%%%%%%%%
```

```matlab
 % For the first time this is done a little differently
% than when calculated later in the model.
 X_spacing= 0.1 ;
 ToolRadiusPrime= ToolRadius* cosd(ClearanceAngle) ;
 Model_dimensions=(100+ToolRadius/2);
% "Model_dimenions" is how far along the tool radius we will model
% (measured in microns).

X2=linspace(0,(Model_dimensions),((Model_dimensions*(1/X_spacing))+1))
';

Y2=sqrt((ToolRadiusPrime^2)-((ToolRadiusPrime^2)*((X2.^2)/
ToolRadius^2)));
 Y2=-1.*Y2;
 TestCurve2(length(X2),2) = 0;
TestCurve2(:,1)=X2;
TestCurve2(:,2)=Y2 - Y2(1);

%%%%%%%%%%%%%%%%%%%%%%%%%%%%%%%%%%%%%%%%%%%%%%%%%%%%%%%%%%%%%%%%%%%%%



%%%%%%%%%%%%%%%%%%%%%%%%%%%%%%%%%%%%%%%%%%%%%%%%%%%%%%%%%%%%%%%%
% Calculating toolprofile of lead off edge
%%%%%%%%%%%%%%%%%%%%%%%%%%%%%%%%%%%%%%%%%%%%%%%%%%%%%%%%%%%%%%%%
TestCurve_lead_off(length(X2),NUMBER_OF_CUTS)= 0;
TestCurve_lead_off(:,1)= X2;
TestCurve_lead_off(:,2)= TestCurve2(:,2);
% "TestCurve_lead_off" is the array that models the "lead-off"
% (trailing edge) half of the tool



%%%%%%%%%%%%%%%%%%%%%%%%%%%%%%%%%%%%%%%%%%%%%%%%%%%%%%%%%%%%%%%%%%%%%%
% Pre-allocating important matrices
%%%%%%%%%%%%%%%%%%%%%%%%%%%%%%%%%%%%%%%%%%%%%%%%%%%%%%%%%%%%%%%%%%%%%%

 Ty(1:length(X2'),1)=0;
% Gives us the size of the Ty matrix before we start

 WEAR_TOTAL=0;
% The WEAR_TOTAL will be calculated cumulatively, but needs an initial
% value.

Pressure(NUMBER_OF_CUTS+1,1)=0;

WEAR(1:NUMBER_OF_CUTS,1)=0;

WEAR_metres(1:NUMBER_OF_CUTS,1)=0;

Wear_volume(1:NUMBER_OF_CUTS,1)=0;

worn_curve_unadjusted(1:length(X2),1:NUMBER_OF_CUTS)=0;
Depth_adjusted_Curve(1:length(X2),NUMBER_OF_CUTS)=0 ;
Depth_adjusted_Curve(1:length(X2),1)=TestCurve2(:,2) ;
```

```matlab
%%%%%%%%%%%%%%%%%%%%%%%%%%%%%%%%%%%%%%%%%%%%%%%%%%%%%%%%%%%%%%%%%%%%%%%%
% Pre-allocating important matrices- END OF
%%%%%%%%%%%%%%%%%%%%%%%%%%%%%%%%%%%%%%%%%%%%%%%%%%%%%%%%%%%%%%%%%%%%%%%%


%%%%%%%%%%%%%%%%%%%%%%%%%%%%%%%%%%%%%%%%%%%%%%%%%%%%%%%%%%%%%%%%%%%%%%%%
%  Loop - Doing the advancing cut distance work
%%%%%%%%%%%%%%%%%%%%%%%%%%%%%%%%%%%%%%%%%%%%%%%%%%%%%%%%%%%%%%%%%%%%%%%%

for CUTS=1:NUMBER_OF_CUTS;

% First "for" loop here. Using "CUTS" as the array name.
% This is rather than a typical M, M2, M3 looping method.

% Loop jobs are- Kp-eqns, wear calculation, profile array saving, area
calculations, force calculations

 Distance(1:CUTS)= CUTS* r/ feed_rate ;
 % Calculates distance with each cut. Assumes face cutting geometry of
the part

%%%%%%%%%%%%%%%%%%%%%%%%%%%%%%%%%%%%%%%%%%%%%%%%%%%%%%%%%%%%%%%%%%%%%%%%
%            ****    PRESTONS CALCULATIONS  ****
%%%%%%%%%%%%%%%%%%%%%%%%%%%%%%%%%%%%%%%%%%%%%%%%%%%%%%%%%%%%%%%%%%%%%%%%
% Traditionally measured in cm^2/dyne. A dyne is 1E-5 of a Newton.
% This model works using SI units.


Pressure(CUTS,1)= Load(CUTS,1)/Area(CUTS,1);
% Pressure= Load/Area.

WEAR_metres(CUTS,1)=Kp*Pressure(CUTS,1)*sliding_distance;
% Assuming uniform wear in Y direction.

WEAR(CUTS,1)=WEAR_metres(CUTS,1)*1E6;
% Converts from metres to microns. Important to keep the graphs
accurate

 TEL_LOGIC(1,1:length(X2)) =
Depth_adjusted_Curve(1:length(X2),CUTS)<DoC    ;

% "TEL_LOGIC" is finding parts of the curve lower than DoC. The sum of
these data points are proportional to the total Tool Engagement
Length, "TEL".
 TEL_LOGIC_RECORD(CUTS,1:length(X2))= TEL_LOGIC(1,1:length(X2));

WEAR_ARRAY=WEAR(CUTS,1).* TEL_LOGIC_RECORD(CUTS,:) ;

TestCurve2(:,[CUTS+2])=TestCurve2(:,[CUTS+1])+WEAR_ARRAY';
% Applies damage to old curve to find the new curve.

Ylow=min(TestCurve2(:,CUTS+2));

Depth_adjusted_Curve(:,CUTS+1)=TestCurve2(:,CUTS+2)-Ylow;

% "Ylow" is the numerical value for the lowest point on the tool edge
% here we're using (TestCurve2) array as the tool edge. For an unworn
tool
```

```
% it should be 0 (ZERO). Wear increases it, therefore tool profiles
need adjusting
% down to the correct Depth of Cut.

WEAR_TOTAL=WEAR_TOTAL+WEAR(CUTS,1);
% WEAR_TOTAL is designed to give the sum total wear experienced by the
% tool.

WEAR_TOTAL2=sum(WEAR(1:CUTS))  ;
% WEAR_TOTAL2 is the alternative method for calculating WEAR_TOTAL
% Sums the amount of wear over the various cuts.

 worn_curve_unadjusted(:,CUTS)= TestCurve2(:,CUTS+2)  ;
% A profile curve, that is unadjusted for depth of cut.
% This will give a truer indication of the change in the tool
appearance.

Ylow=0;
% Re-sets Ylow back to zero. Shouldn't be strictly needed, but will
lower
% the chances of any minor errors creeping into the model.

%%%%%%%%%%%%%%%%%%%%%%%%%%%%%%%%%%%%%%%%%%%%%%%%%%%%%%%%%%%%%%%%%%%%
% END OF WEAR CALCULATION & DAMAGE APPLICATION
%%%%%%%%%%%%%%%%%%%%%%%%%%%%%%%%%%%%%%%%%%%%%%%%%%%%%%%%%%%%%%%%%%%%


%%%%%%%%%%%%%%%%%%%%%%%%%%%%%%%%%%%%%%%%%%%%%%%%%%%%%%%%%%%%%%%%%%%%%
% DAMAGE APPLICATION- Trailing edge tool half
%%%%%%%%%%%%%%%%%%%%%%%%%%%%%%%%%%%%%%%%%%%%%%%%%%%%%%%%%%%%%%%%%%%%%
Lead_off_logic = TestCurve_lead_off(1:length(X2),CUTS) < WEAR_TOTAL;

Transition = sum(Lead_off_logic');

TestCurve_lead_off(:,CUTS+2)=TestCurve_lead_off(:,2);
TestCurve_lead_off(1:Transition,CUTS)=WEAR_TOTAL ;
%%%%%%%%%%%%%%%%%%%%%%%%%%%%%%%%%%%%%%%%%%%%%%%%%%%%%%%%%%%%%%%%%
%%%%%%%%%%%%%%%%%%%%%%%%%%%%%%%%%%%%%%%%%%%%%%%%%%%%%%%%%%%%


%%%%%%%%%%%%%%%%%%%%%%%%%%%%%%%%%%%%%%%%%%%%%%%%%%%%%%%%%%%%%%%%%%%%%
% AREA CALCULATIONS
%%%%%%%%%%%%%%%%%%%%%%%%%%%%%%%%%%%%%%%%%%%%%%%%%%%%%%%%%%%%%%%%%%%%%
% CALCULATING WEAR AREA AND VOLUME
% Using triangles to calculate the contact area, wear volume and plot
wear
% in the recession direction.

Ty= worn_curve_unadjusted(:,CUTS)- TestCurve2(:,2)  ;
% Recession depth = worn curve – original curve
Ty=Ty.*1E-6;
% And converted to microns.

Tz= Ty*(1/tand(ClearanceAngle)) - Ty*tand(top_rake+ClearanceAngle);
% Tz is the direction of the triangle in the contact plane.

contact_AREA_element(CUTS,:)=Tz(:,:)*X_spacing*1E-6;
% Area calculations first. (working in m^2 not microns squared)
```

```
Area1(CUTS+1,1)=sum(contact_AREA_element(CUTS,:));

%%%%%%%%%%%%%%%%%%%%%%%%%%%%%%%%%%%%%%%%%%%%%%%%%%%%%%%%%%%%
% END OF AREA CALCULATIONS
%%%%%%%%%%%%%%%%%%%%%%%%%%%%%%%%%%%%%%%%%%%%%%%%%%%%%%%%%%%%


%%%%%%%%%%%%%%%%%%%%%%%%%%%%%%%%%%%%%%%%%%%%%%%%%%%%%%%%%%%%
% AREA CALCULATIONS- trailing edge part of tool section
%%%%%%%%%%%%%%%%%%%%%%%%%%%%%%%%%%%%%%%%%%%%%%%%%%%%%%%%%%%%
% CALCULATING WEAR AREA AND VOLUME
% Using triangles to calculate the contact area and wear-volume
Ty2= worn_curve_unadjusted(:,CUTS)- TestCurve_lead_off(:,2)   ;
% Ty established. Ty= Recession depth.
% Recession depth = worn curve – original curve
Ty2=Ty2.*1E-6;
% And converted to microns.
Tz2= Ty2*(1/tand(ClearanceAngle)) - Ty2*tand(top_rake+ClearanceAngle);
% Tz is the direction of the triangle in the contact plane.
contact_AREA_element2(CUTS,:)=Tz2(:,:)*X_spacing*1E-6;
% Area calculations first. (working in m^2 not microns squared)
Area2(CUTS+1,1)=sum(contact_AREA_element2(CUTS,:));
Triangle_AREA2(CUTS,:)=1/2*Ty2.*Tz2;
% Area of each of the small volume elements.

VOLUME_of_TRIANGLE2(CUTS,:)=X_spacing*1E-6*Triangle_AREA2(CUTS,:);
% Volume calculations. Done by arrays.

 TOTAL_VOLUME2(CUTS,:) =sum(VOLUME_of_TRIANGLE2(:,CUTS));
% The above lines work out contact area *if* top-rake/workpiece
contact
% can be ignored. Contact_AREA is more correctly, wear-area.
%%%%%%%%%%%%%%%%%%%%%%%%%%%%%%%%%%%%%%%%%%%%%%%%%%%%%%%%%%%%
% END OF AREA CALCULATIONS
%%%%%%%%%%%%%%%%%%%%%%%%%%%%%%%%%%%%%%%%%%%%%%%%%%%%%%%%%%%%


%%%%%%%%%%%%%%%%%%%%%%%%%%%%%%%%%%%%%%%%%%%%%%%%%%%%%%%%%%%
% Total AREA
%%%%%%%%%%%%%%%%%%%%%%%%%%%%%%%%%%%%%%%%%%%%%%%%%%%%%%%%%%%
Area(CUTS+1,1)= Area1(CUTS+1,1)+ Area2(CUTS+1,1)  ;
% Total of lead-on and lead-off halves of the tool.
%%%%%%%%%%%%%%%%%%%%%%%%%%%%%%%%%%%%%%%%%%%%%%%%%%%%%%%%%%%


%%%%%%%%%%%%%%%%%%%%%%%%%%%%%%%%%%%%%%%%%%%%%%%%%%%%%%%%%%%%
% Wear Volume calculation (both tool halves)
%%%%%%%%%%%%%%%%%%%%%%%%%%%%%%%%%%%%%%%%%%%%%%%%%%%%%%%%%%%%

 Triangle_AREA(CUTS,:)=1/2*Ty.*Tz;
% Area of each of the small volume elements.
VOLUME_of_TRIANGLE(CUTS,:)=X_spacing*1E-6*Triangle_AREA(CUTS,:);
% Volume calculations. Done by arrays.
TOTAL_VOLUME1(CUTS,:) =sum(VOLUME_of_TRIANGLE(:,CUTS));
TOTAL_VOLUME(CUTS,:)= TOTAL_VOLUME1(CUTS,:) + TOTAL_VOLUME2(CUTS,:);
Wear_volume(CUTS,1)=sum(TOTAL_VOLUME(1:CUTS));
% Gives the volume worn in metres cubed.
Wear_volume_microns(CUTS,1)=Wear_volume(CUTS,1)/1E-18;
% Wear_volume_microns is the wear volume in cubic microns.
```

```
%%%%%%%%%%%%%%%%%%%%%%%%%%%%%%%%%%%%%%%%%%%%%%%%%%%%%%%%%%%%%%%%%%%%
% END OF VOLUME CALCULATIONS
%%%%%%%%%%%%%%%%%%%%%%%%%%%%%%%%%%%%%%%%%%%%%%%%%%%%%%%%%%%%%%%%%%%%


%%%%%%%%%%%%%%%%%%%%%%%%%%%%%%%%%%%%%%%%%%%%%%%%%%%%%%%%%%%%%%%%%%%%
% FORCE CALCULATIONS
%%%%%%%%%%%%%%%%%%%%%%%%%%%%%%%%%%%%%%%%%%%%%%%%%%%%%%%%%%%%%%%%%%%%
Force_Normal_direction(CUTS,1)= k.*Area(CUTS,1);
%  force in the normal direction is proportional to wear area.

Load(CUTS+1,1)= Load(1,1)+ Force_Normal_direction(CUTS,1);

%%%%%%%%%%%%%%%%%%%%%%%%%%%%%%%%%%%%%%%%%%%%%%%%%%%%%%%%%%%%%%%%%%%
% End of FORCE CALCULATIONS
%%%%%%%%%%%%%%%%%%%%%%%%%%%%%%%%%%%%%%%%%%%%%%%%%%%%%%%%%%%%%%%%%%%

 end
% The end of the loop (advancing cutting distance loop).
%%%%%%%%%%%%%%%%%%%%%%%%%%%%%%%%%%%%%%%%%%%%%%%%%%%%%%%%%%%%%%%%%%%%%

 Total_Distance
%Outputs the distance cut. (In metres)
WEAR_TOTAL
% Should out-put WEAR_TOTAL (Measured in vertical recession).
Wear_Volume_cubic_microns=Wear_volume_microns(NUMBER_OF_CUTS,1);
% Outputs the wear volume in microns
Wear_Volume_cubic_microns

%%%%%%%%%%%%%%%%%%%%%%%%%%%%%%%%%%%%%%%%%%%%%%%%%%%%%%%%%%%%%%%%%%%
```

Appendix D- Wear-area calculation method comparison code

While analysing the model it became clear that there was a need to check the assumption that the rough area calculation method was accurate. The rough area calculation method used SEM images of wear-scars, with area found by multiplying the wear-scar length, by the maximum wear-scar width and then multiplying by a half. Area was therefore assumed to be roughly the same as that of an irregular four-sided polygon. However this is a 2D method which is being applied to a 3D problem.

The area calculation code worked by calculating the wear-area using the approximation method and compared it with the wear-models calculated value of wear-area. The wear-model uses a very accurate method of calculating area; breaking the wear-scar into a series of 100nm wide strips and determining how long those strips are. By summing all the area components area can be accurately calculated. When this code was used the approximate methodology was comprehensively shown to be inaccurate.

This code was designed to be run immediately after the model (indeed the model code was briefly automatically running this program after either completing a single cut or after all cuts had been calculated). In section 8.5 a fixed amount of wear-recession was applied to the tool instead of calculated amounts of wear with the aim of providing information at different wear-scar widths, this worked well and was able to find that area error changed with increasing wear-recession and that there was a difference in error progression with different tool geometry.

Wear-area error calculation code:

```
% Code for finding the error in area calculation

% Part 1: Finding the tool-workpiece contact length
L1=Transition*X_spacing;


L2(CUTS,1)=sum(TEL_LOGIC(1,1:length(X2)))'  ;
L2(CUTS,1)=X_spacing.*L2(CUTS,1)   ;

Ltot = L1 + L2(CUTS,1) ;


% Part 2: Finding the approx length visible on SEM images

z=DoC- WEAR_TOTAL ;

d= sqrt ( Ltot^2  +  z^2 )    ;

% Part 3: Maximum wear-scar calculations


Wear_scar_max = WEAR_TOTAL*( tand(90-(clearance_angle)) -
tand(top_rake)  ) ;


% Part 4: Area calculation

Area_approx= 0.5 * d * Wear_scar_max   ;


% Part 5: Comparisons

Wear_scar_max        ;
Area_approx               ;
Area_microns= Area(CUTS+1)/1E-12   ;

Area_error= (Area_approx./Area_microns)*100

% END
```